

République Algérienne Démocratique et Populaire
Ministère de l'Enseignement Supérieure et de la Recherche Scientifique

UNIVERSITE HASSIBA BENBOUALI DE CHLEF



Faculté de Technologie
Département de Génie Mécanique



Pour l'obtention du diplôme de Doctorat en Science

Spécialité : Génie Mécanique

Par Mr. MISSOUM MOHAMMED

Intitulé de la Thèse

Contribution of high-energy performance housing using solar energy in the sustainable development: case of Chlef district

Soutenue le : **01 Décembre 2015**

Devant le Jury

Zahloul Hamou	Professeur	UHBC Chlef	Président
Tahar-Abbès Miloud	Professeur	UHBC Chlef	Examineur
Hadj-arab Amar	Directeur de Recherche	CDER Alger	Examineur
Bachari Nour El-Islam	Professeur	USTHB Alger	Examineur
Hamidat Abderrahmane	Directeur de Recherche	CDER Alger	Directeur de Thèse
Loukarfi Larbi	Professeur	UHBC Chlef	Co-Encadreur de Thèse

Année scolaire 2015/2016

Remerciements

En premier lieu, je tiens à remercier Monsieur A.Hamidat, mon directeur de thèse et je lui exprime particulièrement toutes mes reconnaissances pour m'avoir fait bénéficier de ses compétences scientifiques, ses qualités humaines et sa constante disponibilité. Mes vifs remerciements à Monsieur L. Loukarfi, professeur à l'université de Chlef qui m'a initié à assurer ma future tâche, ainsi pour ses conseils fructueux et ses encouragements. Je remercie aussi Monsieur, H. Zahloul, maître de conférence à l'université de Chlef d'avoir accepté la présidence du jury. Je remercie sincèrement Monsieur Hadj-arab, Directeur de recherche au CDER d'avoir accepté de faire partie du jury. Je remercie Monsieur, N.E.I. Bachari d'avoir accepté d'examiner ce travail. Mes remerciements à Monsieur, M. Tahar-Abbès, professeur à l'université de Chlef d'avoir accepté de juger ce travail. Je saisis cette occasion pour remercier tous les enseignants de l'université de Chlef et à tous ceux qui ont contribué à notre bonne formation. Je remercie infiniment Monsieur K. Abdeladim pour son aide durant toute la période de préparation de ce travail. Je remercie tous mes amis et toutes les personnes qui m'ont soutenu durant ces années de recherche.

Enfin, merci à ma famille, à vous qui m'avez soutenu et avez su être mon inspiration quand j'avais des baisses de régime. Merci à mes chers parents qui sans eux je ne serais parvenu là où je suis. Un grand merci à mon frère et toutes mes sœurs, à ma chère femme qui était toujours à mes côtés et surtout mon cher fils Larbi et ma chère fille Safaa.

Abstract

Nowadays, it is well recognized that the residential sector is responsible of a great part of final energy consumption. Recent statistics indicate that forty-two percent (42%) of Algerian primary energy is consumed by the building sector and it is still in expansion, due to mainly on an exceptional growth of population and urbanism. During the last few years, the Algerian authorities have made development of rural housing one of their priorities by launching a program for the construction of more than 450000 units in rural areas in order to keep rural populations in place and to encourage their return from urban areas. However, the construction of these houses whose level of energy performance is very bad, surely leads to a significant increase in energy consumption.

The present thesis aims to study the contribution of high-energy performance rural housing using solar energy in the reduction of global energy consumption and greenhouse gas mitigation. To reach this goal, a TRNSYS model of a multi-zone house coupled with a solar heating system was developed and validated with experimental data. The experimental study, which was realized on a bioclimatic house located in Algiers, served also to investigate the contribution of the solar heating system in the improvement of the indoor air temperature in cold period of year. In addition, a model of grid-connected PV system was developed in order to investigate the contribution of solar photovoltaic in the production of the electricity needed for the house.

These developed models were applied on a case study single-family house located in rural area of Chlef district. The model of solar heating system was used to estimate the heating, cooling and DHW loads and the model of grid-connected PV

system was used to estimate the electrical energy load of the reference house. Furthermore, a parametrical study was conducted in order to improve the energy performance of the house and reach the level of high-energy performance house. The energy performance of the reference house was improved by passive mean through the integration of a set of energy efficiency measures in the house envelope and by active mean with the application of solar heating system and grid connected PV system.

Based on the energy balance of the reference house, the potential energy savings and the associated CO₂ emissions reduction resulting from the improvement of energy performance of rural housing built during last rural housing programs in Chlef district was investigated. The results show that more than 131 GWh and 1480257 cylinders of butane gas can be saved annually. In addition, the annual CO₂ reduction associated to these energy savings was estimated at 71540 tons for butane gas and at 85374 tons for electricity.

Résumé

Aujourd'hui, il est bien reconnu que le secteur résidentiel est responsable d'une grande part de la consommation d'énergie finale. Selon des statistiques récentes, quarante-deux pour cent (42%) de l'énergie primaire en Algérie est consommée par le secteur du bâtiment et il est encore en pleine expansion, en raison principalement d'une croissance exceptionnelle de la population et de l'urbanisme. Au cours des dernières années, les autorités algériennes ont fait du développement de l'habitat rural une de ses priorités en lançant un grand programme pour la construction de plus de 450 000 de logements dans les zones rurales afin de maintenir les populations rurales à leurs terres et les inciter à quitter les zones urbaines. Cependant, la construction de ces maisons dont le niveau de performance énergétique est très mauvais, sûrement conduit à une augmentation significative de la consommation d'énergie.

La présente thèse vise à étudier la contribution de l'habitat à haute performances énergétiques utilisant l'énergie solaire dans la réduction de la consommation global d'énergie et la réduction des gaz à effet de serre. Pour atteindre cet objectif, un modèle d'une maison multizone couplé à un système de chauffage solaire a été développé sous le logiciel TRNSYS et validé avec des données expérimentales. L'étude expérimentale, qui a été réalisée sur une maison bioclimatique située à Alger, a également servi à étudier la contribution du système de chauffage solaire dans l'amélioration de la température de l'air intérieur de la maison en période froide de l'année. En outre, un modèle de système photovoltaïque raccordé au réseau a été développé afin d'évaluer la contribution de l'énergie solaire photovoltaïque dans la production de l'électricité nécessaire à la maison.

Ces modèles développés ont été appliqués sur maison individuelle située en zone rurale de la wilaya de Chlef. Le modèle de système de chauffage solaire a été utilisé pour estimer les charges de chauffage, de rafraîchissement et d'eau chaude sanitaire et le modèle de système photovoltaïque raccordé au réseau a été utilisé pour estimer la charge de l'énergie électrique de la maison de référence. En outre, une étude paramétrique a été réalisée afin d'améliorer la performance énergétique de la maison étudiée et atteindre le concept d'une maison à haute performance énergétique. La performance énergétique de la maison de référence a été améliorée par moyen passive grâce à l'intégration d'un ensemble de mesures d'efficacité énergétique dans l'enveloppe de la maison et par moyenne active avec l'application du système de chauffage solaire et du système photovoltaïque.

Basé sur le bilan énergétique de la maison de référence, le potentiel d'économies d'énergie et la réduction associée des émissions de CO₂ résultant de l'amélioration de la performance énergétique de l'habitat rural construit au cours des dernières programmes de construction de l'habitat rural dans le district de Chlef a été étudiée. Les résultats montrent que plus de 131 GWh et 1.480.257 bouteilles de gaz butane peuvent être sauvées chaque année. En outre, la réduction annuelle des émissions de CO₂ associées à ces économies d'énergie a été estimée à 71 540 tonnes pour le gaz butane et à 85 374 tonnes pour l'électricité.

ملخص

من المعروف اليوم أن قطاع السكن مسؤول عن حصة كبيرة من الاستهلاك النهائي للطاقة في العالم. وفقا للإحصاءات الأخيرة، اثنين وأربعين في المئة (42%) من الطاقة الأولية في الجزائر يتم استهلاكها من قبل قطاع البناء والتشييد وهذه الزيادة في الاستهلاك في ارتفاع مستمر، ويرجع ذلك أساسا إلى النمو السريع لعدد السكان وتطور العمران.

في السنوات الأخيرة، جعلت السلطات الجزائرية تطوير السكن الريفي من بين الأولويات من خلال إطلاق برنامج ضخم لبناء أكثر من 450 ألف وحدة سكنية في المناطق الريفية من أجل حث سكان الريف على الاستقرار في أراضيهم وتشجيعهم على مغادرة المناطق الحضرية. ولكن بناء هذه المنازل دون مراعات قوانين النجاعة الطاقية للبناءات، سيؤدي بلا شك إلى زيادة كبيرة في الاستهلاك العام للطاقة. تهدف هذه الأطروحة إلى دراسة مساهمة السكان التي تتميز بنجاعة طاقية عالية والتي تستخدم الطاقة الشمسية في الحد من الاستهلاك العالم للطاقة وكذا الحد من انبعاث الغازات المسببة للاحتباس الحراري. ولتحقيق ذلك، تم تطوير نموذج بواسطة برنامج TRNSYS لمنزل متعدد الغرف مزود بنظام التدفئة بالطاقة الشمسية والتحقق من صحة النتائج عن طريق الدراسة التجريبية. تم إجراء الدراسة التجريبية على منزل عالي النجاعة الطاقية يقع في الجزائر العاصمة. تم استعمال النظام الشمسي الحراري أيضا لدراسة درجة حرارة الهواء داخل المنزل في الفترة الباردة من السنة. وبالإضافة إلى ذلك، تم تطوير نموذج للنظام الضوئية المتصلة بالشبكة لتقييم مساهمة الطاقة الشمسية الكهروضوئية في إنتاج الكهرباء.

تم تطبيق النماذج المذكورة سابقا على منزل يقع في منطقة ريفية من ولاية الشلف. تم استخدام نموذج النظام الشمسي الحراري لتقدير تكاليف تدفئة المنزل وتسخين الماء الصحي والنظام الشمسي الفوطوضوي المتصلة بالشبكة لتقدير المنزل تكاليف تزويد المنزل بالطاقة الكهربائية. بالإضافة إلى ذلك، تم إجراء دراسة من أجل تحسين النجاعة الطاقية للمنزل والذي تم بطريقتين عن طريق دمج مجموعة من التدابير والتي تتمثل في الاستخدام المباشر للطاقة في المنزل والطريقة الثانية تتمثل في استعمال النظامين الشمسيين السابقين في إنتاج الطاقة الحرارية والكهرو بائية.

بناء على النتائج المحصل عليها من خلال دراسة كمية الطاقة المقتصدة من طرف منزل يأوي عائلة واحدة في منطقة الشلف، تمت دراسة كمية الطاقة الاجمالية التي يمكن اقتصادها وخفض الانبعاثات المرتبطة بها الناتجة عن تحسين النجاعة الطاقية في المساكن الريفية التي تم بناءها في إطار برامج بناء المساكن الريفية في منطقة الشلف في السنوات الأخيرة. وأظهرت النتائج أن أكثر من 131 جيجاوات ساعي و1480257 أسطوانة غاز البوتان يمكن اقتصادها كل عام. وبالإضافة إلى ذلك، قدرت الانخفاض السنوي في انبعاثات غاز ثاني اوكسيد الكربون المرتبطة بتوفير هذه الطاقة ب 71540 طن ناتج عن خفض استهلاك غاز البوتان و85374 طن عن خفض استهلاك الكهرباء.

Contents

Acknowledges.....	i
Abstract.....	ii
Contents	vi
Nomenclature.....	xii
List of figures.....	xx
List of tables.....	xxv
<u>General introduction</u>	1
<u>Chapter 1: Bibliographical study</u>	
1.1 Introduction.....	6
1.2 Passive solar systems.....	6
1.3 Active solar systems.....	13
1.4 Conclusion.....	16
<u>Chapter 2: Energy situation in Algeria</u>	
2.1 Introduction.....	17
2.2 Conventional energy.....	17
2.2.1 Energy consumption.....	20
2.3 Renewable energy.....	21
2.3.1 Potentials.....	21
2.3.1.1 Solar energy.....	22
2.3.1.2 Wind energy.....	23
2.3.1.3 Hydroelectricity.....	24

2.3.1.4 Geothermic energy.....	24
2.3.1.5 Biomass energy.....	25
2.3.2 Renewable energies applications.....	26
2.4 Conclusion.....	29

Chapter 3: Solar energy applications in rural housing

3.1 Introduction.....	30
3.2 Passive solar design.....	31
3.2.1 Principal of passive solar design.....	31
3.2.2 Elements of passive solar design.....	33
3.2.2.1 Orientation of the house.....	33
3.2.2.2 Room placement inside building.....	36
3.2.2.3 Thermal mass.....	37
3.2.2.4 Thermal insulation.....	38
3.2.2.5 Glazing type.....	39
3.2.3 Nocturnal ventilation.....	40
3.3. Active solar systems.....	41
3.3.1 Solar heating systems.....	41
3.3.1.1 Solar thermal collectors.....	42
3.3.1.2 Storage tank.....	44
3.3.1.3 Heating floor system.....	45
3.3.2 Photovoltaic systems.....	46
3.3.2.1 Off-grid PV system.....	46
3.3.2.2 Grid-connected PV system.....	47
3.4 Conclusion.....	49

Chapter 4: Modelling of a residential house coupled with solar systems

4.1 Introduction.....	50
4.2 Presentation of TRNSYS software.....	50
4.3 Description of the model.....	51
4.4 Modelling of solar radiation.....	53
4.4.1 Solar angles.....	53
4.4.2 Solar radiation on horizontal surface.....	55
4.4.3 Solar radiation on tilted surface.....	56
4.5 Mathematical description of the house model.....	58
4.5.1 Energy balance of a thermal zone.....	58
4.5.2 Modelling of heat conduction through house envelope.....	59
4.5.3 Heat fluxes at surfaces of an exterior wall.....	61
4.5.4 Heat gain from inside surface of an exterior wall.....	64
4.5.5 Heat gains from internal and adjacent walls.....	65
4.5.6 Total gains from surfaces in a zone.....	65
4.5.7 Infiltration and convective coupling.....	65
4.5.8 Free-floating temperature.....	66
4.5.9 Heating and cooling loads.....	69
4.5.10 Thermal window model.....	72
4.6 Model of the heating floor.....	74
4.6.1 Heats flow on the slab surfaces.....	75
4.6.2 The Resistance R_x	76
4.6.3 Thermal transmittance through pipe.....	78

4.6.4 Mean water temperature in a pipe coil.....	79
4.6.5 Total resistance.....	80
4.7 Modelling of the solar collector.....	82
4.7.1 Absorbed solar radiation.....	83
4.7.2 Collector energy losses.....	87
4.7.3 Useful energy.....	88
4.8 Modelling of Water storage tank.....	89
4.8.1. Energy balance of the tank.....	91
4.8.2. Average tank temperature.....	94
4.9 Complete model of solar heating system.....	95
4.9.1. Valves.....	95
4.9.2. Controllers.....	98
4.9.3. Temperatures.....	99
4.9.4. Pumps.....	101
4.10 Modelling of grid connected PV system.....	102
4.10.1 PV array output.....	102
4.10.2 Module operating temperature.....	103
4.10.3 Energy interchange between PV system and grid.....	104
4.11. Conclusion.....	105

**Chapter 5: Experimental study and validation of the solar heating
system model**

5.1 Introduction.....	106
5.2 Description of the model.....	106
5.2.1 Bioclimatic house characteristics.....	106

5.2.2 Description of the solar heating system.....	107
5.3 TRNSYS model.....	111
5.4 Experimental study.....	113
5.4.1 Data acquisition system.....	113
5.4.2 Experimental results.....	114
5.4.3 Validation of the model.....	117
5.5 Conclusion.....	121

**Chapter 6: Solar energy integration in rural housing and their impact
on the sustainable development of Chlef district.**

6.1 Introduction.....	122
6.2 Energy situation of Chlef district.....	123
6.3 Rural housing programs.....	125
6.4 Improvement of energy performance of a rural house.....	127
6.4.1 Reference house characteristics.....	127
6.4.2 Weather data.....	129
6.4.3 Energy efficiency measures.....	130
6.4.4 Impact of energy efficiency measures.....	132
6.4.4.1 Effect of house orientation.....	132
6.4.4.2 Effect of windows size and shading device.....	133
6.4.4.3 Effect of thermal insulation.....	135
6.4.4.4 Effect of glazing type.....	136
6.4.4.5 Effect of the combination.....	137
6.4.5 Thermal comfort.....	140
6.4.6 Solar heating system.....	142

6.4.6.1 Description of the system.....	142
6.4.6.2. Household hot water consumption.....	143
6.4.6.3 Optimization of system parameters.....	143
6.4.6.4 Performance of optimized solar heating system.....	146
6.4.7 Grid-connected PV system.....	150
6.4.7.1 Electrical consumption profile.....	151
6.4.7.2 Optimization of the PV system size.....	154
6.4.7.3 Contribution of PV energy.....	155
6.4.8 Energy balance of the HEP house.....	159
6.5 Overall energy saving and CO2 mitigation.....	161
6.6 Economic analysis.....	164
6.6.1. Yearly income.....	165
6.6.2. Investment cost.....	166
6.6.3. Return on investment.....	168
6.7 Conclusion.....	170
<u>General conclusion</u>	172
References.....	175
Appendix.....	186

List of Figures

2.1	Evolution of final energy consumption by sectors between 1980 and 2013..	18
2.2	Evolution of final energy consumption by product between 1980 and 2013..	18
2.3	Distribution of final energy consumption by sector in 2013.....	19
2.4	Distribution of final energy consumption by product in 2013.....	20
2.5	Evolution of energy consumption in the residential sector between 2010 and 2013.....	20
2.6	Distribution of energy consumption in residential sector in 2007.....	21
2.7	Example of the overall exposure received in Algeria.....	22
2.8	Wind chart in Algeria.....	24
2.9	Albian platform situation.....	26
3.1	Concept for application of a passive solar system.....	32
3.2	Heating energy saving, depending on shape factor and orientation.....	33
3.3	Effect of overhang on incident radiation through window.....	34
3.4	Effect of deciduous trees.....	35
3.5	Evolution of the heating requirement with window size.....	35
3.6	Placement of rooms inside a house.....	36
3.7	Effect of the thermal mass on energy requirement in winter.....	37
3.8	Effect of the thermal mass on energy requirement in summer.....	38
3.9	Difference between an insulated room and no insulated room.....	38
3.10	Different types of thermal insulation.....	39
3.11	Thermal quality of glass.....	40
3.12	Nocturnal ventilation strategies.....	41
3.13	Main components of a solar combi-system.....	42

3.14	Flat-plate collector.....	43
3.15	Evacuated tube collector.....	44
3.16	Schematic of the stratified storage tank.....	44
3.17	Tubing configuration in a concrete floor slabs.....	46
3.18	Stand-alone PV system.....	47
3.19	Grid-connected PV system.....	48
4.1	The black box model in the TRNSYS program.....	51
4.2	The house, its heating system, and PV system under investigation.....	52
4.3	TRNSYS simulation process.....	53
4.4	Input and output of house model (Type 56).....	58
4.5	Heat transfer at an external wall.....	61
4.6	Star network for a zone with three surfaces.....	62
4.7	Power output versus temperature.....	70
4.8	Resistance network between window panes.....	73
4.9	Heat flow in a cross section of a thermos-active construction element.....	75
4.10	Network of resistances, star arrangement.....	77
4.11	Thermal resistances inside a water tube.....	79
4.12	Change in temperature along the pipe coil.....	80
4.13	Resistance between water inlet temperature and core temperature.....	80
4.14	Parameters, input and output of the thermal collector.....	82
4.15	Multiple reflections between the solar collector cover and absorber plate....	84
4.16	Thermal network for a single cover collector in term of resistance between plates.....	86
4.17	Parameters, input and output of the storage tank.....	90
4.18	Fully mixed storage tank.....	91

4.19	Overview of solar heating system model in the TRNSYS studio.....	94
4.20	Flow diverter.....	95
4.21	Tee piece.....	97
4.22	Tempering valve.....	97
4.23	Grid-connected PV system.....	102
5.1	The prototype bioclimatic house.....	107
5.2	Plan view of the prototype house.....	108
5.3	Scheme of the solar heating system.....	109
5.4	TRNSYS model of the direct solar floor system.....	112
5.5	Control strategy of the solar heating system.....	112
5.6	Data acquisition system.....	113
5.7	Computer and a Keithley digital multi-meter2700.....	113
5.8	Pyrometer.....	113
5.9	Testo.....	113
5.10	Evolution of the outdoor temperature and solar radiation.....	114
5.11	Wall surfaces temperatures.....	115
5.12	Measured temperature of interior air of the house.....	116
5.13	Effect of the heating floor on the interior air temperature.....	117
5.14	Average tank temperature during the monitored period.....	118
5.15	Measured and simulated temperatures of the outlet collector fluid.....	119
5.16	Measured and simulated temperatures of the interior air of the living room..	120
5.17	Measured and simulated temperatures of air of Room1 and Room2.....	121
6.1	Evolution of the number of electricity and natural gas subscriber's in Chlef..	123
6.2	Evolution of the electricity consumption in the residential sector in Chlef.....	124
6.3	Evolution of the butane gas consumption in Chlef.....	125

6.4	Housing construction programs in Chlef district.....	126
6.5	Typical rural houses in Chlef with flat roof.....	127
6.6	Typical rural house plan.....	128
6.7	Average daily monthly irradiance and temperature of Chlef district.....	130
6.8	Annual heating and cooling needs at different orientations.....	132
6.9	Annual heating energy at different windows sizes.....	134
6.10	Annual cooling energy at different windows size.....	135
6.11	Energy saving at different insulation thickness for ceiling and walls.....	136
6.12	Annual energy reduction rate.....	138
6.13	Annually energy requirement comparisons between two houses with and without EEM.....	138
6.14	Monthly energy requirement comparisons between two houses without and with EEM.....	139
6.15	Frequency of indoor temperatures without and without EEM.....	141
6.16	Scheme of the solar heating system under study.....	142
6.17	Daily hot water consumption profile (200 l/day).....	143
6.18	Variation of the annual solar fraction for different collector areas.....	144
6.19	Variation of the annual solar fraction for different collector's mass flow rate.....	145
6.20	Variation of the annual solar fraction for different tank volume.....	146
6.21	Monthly thermal energy loads.....	147
6.22	Annual thermal energy loads.....	148
6.23	Monthly heat production of the solar heating system.....	149
6.24	Annual heat production of the solar heating system.....	149
6.25	Daily home electricity consumption profile.....	154
6.26	Annual electricity production with different PV array sizes.....	155

6.27	Electrical simulation results.....	156
6.28	Monthly average electrical produced by the grid and PV system.....	157
6.29	Monthly net electricity purchases from the grid.....	158
6.30	Hourly electrical simulation results of a sunny day.....	159
6.31	Hourly electrical simulation results of a cloudy day.....	160
6.32	Comparison between annual energy demand and energy production.....	161
6.33	Overall energy saving and CO ₂ reduction.....	165
6.34	The capital cost of the grid-connected PV system and EEM and the yearly income.....	169

List of Tables

2.1	Solar potential in Algeria.....	23
2.2	Distribution of installed power per resources.....	25
2.3	Distribution of installed power by application.....	27
2.4	Hydroelectric production park.....	28
4.1	Mathematical description of Tempering Valve	97
5.1	U-values of the building envelope.....	109
5.2	Characteristics of the thermal collector.....	110
5.3	Characteristics of the heating floor system.....	110
5.4	Characteristics of the storage tank.....	111
5.5	Mean relative error.....	119
6.1	Wall characteristics of the reference house.....	129
6.2	Energy saving measures and their combination.....	131
6.3	Effect of the glazing type.....	137
6.4	Difference between RH with and without EEM.....	140
6.5	Indoor thermal comfort in the RH with and without EEM.....	140
6.6	Electrical specifications of module ET-M660250WW.....	150
6.7	Electricity consumption of the sample.....	151
6.8	Annual electrical equipment consumption of the reference house....	153
6.9	Energy production and energy demand of HEP.....	160
6.10	Electrical energy and gas butane saving.....	163
6.11	Overall CO2 emissions reduction.....	164
6.12	Cost of thermal insulation and SS components.....	167

Acronyms

<i>HEP</i>	High Energy Performance
<i>RH</i>	Reference House
<i>EEMs</i>	Energy Efficiency Measures
<i>DHW</i>	Domestic Hot Water
<i>SH</i>	Space heating
<i>PV</i>	Photovoltaic
<i>GHG</i>	Greenhouse Gas
<i>SS</i>	Solar system
<i>PVS</i>	Photovoltaic system
<i>SHS</i>	Solar Heating System

Solar radiation

δ	Solar declination	(°)
ω	Hour angle	(°)
<i>AST</i>	Apparent solar time	(h)
θ_z	Zenith angle	(°)
Y_s	<i>Solar azimuth angle</i>	(°)
θ	Solar incidence angle	(°)
β	Tilt angle of solar collector	(°)
γ	Surface azimuth	(°)
h	Solar altitude angle	(°)

K_T	Clearness index	-
I	Global horizontal radiation	(kJ/hr.m ²)
I_b	Beam horizontal radiation	(kJ/hr.m ²)
I_{bT}	Beam radiation incident on the solar collector	(kJ/hr.m ²)
I_d	Diffuse horizontal radiation	(kJ/hr.m ²)
I_T	Global radiation incident on the solar collector	(kJ/hr.m ²)
R_b	Ratio of beam radiation on a tilted surface to that on a horizontal surface	-
R_r	Ratio of reflected radiation on a tilted surface to the total radiation on a horizontal surface	-
R_d	Ratio of diffuse radiation on a tilted surface to that on a horizontal	-

Dynamic modelling of the house

C_a	Specific heat of air	KJ / kg K
ρ_a	Volume mass of air	kg/m ³
k	Thermal conductivity of material	KJ/hr.m.K
m_{inf}	Mass flow rate of infiltration air	kg/s
\dot{m}_{vent}	Mass flow rate of ventilation air	kg/s
h_c	Convective heat transfer coefficient	KJ/hr.m ² .K
$S_{s,i}$	Radiation heat flux absorbed at the inside surface (solar and radiative gains)	kJ/hr
$S_{s,o}$	Radiation heat flux absorbed at the outside surface (solar gains)	kJ/hr
$q_{r,s,i}$	Net radiative heat transfer with all other surfaces within the	

	zone	kJ/hr
$q_{r,s,o}$	Net radiative heat transfer with all surfaces in view of the outside surface	kJ/hr
$q_{w,g,i}$	User defined heat flux to the wall or window surface	kJ/hr
$q_{s,i}$	Conduction heat flux from the wall at the inside surface	kJ/hr
$q_{s,o}$	Conduction heat flux into the wall at the outside surface	kJ/hr
$q_{c,s,i}$	Convection heat flux from the inside surface to the zone air	kJ/hr
$q_{c,s,o}$	Convection heat flux to the outside surface from the boundary/ambient	kJ/hr
$T_{s,i}$	Inside surface temperature	°C
$T_{s,o}$	Outside surface temperature	°C
T_{sa}	Air-soil temperature	°C
f_{sky}	Fraction of the sky seen by the outside surface	-
T_{sky}	Fictive sky temperature used for long-wave radiation exchange (°)	°C
$\varepsilon_{s,o}$	Long-wave emissivity of outside surface	-
σ	Stephan-Boltzmann constant	-
T_i	Inside zone air temperature (°)	°C
T_o	Outside zone air temperature (°)	°C

Heating floor system

R_w	Thermal resistance between the center of the water tube and inside surface of tube mantle.	$m^2 K / W$
R_r	Thermal resistance through the pipe shell.	$m^2 K / W$

R_z	Thermal resistance along the tubing.	$m^2 K / W$
R_x	Resistance originated from the transformation of the triangular arrangement into the star arrangement.	$m^2 K / W$
R_1	Concrete's thermal resistance of the upper part of the slab.	$m^2 K / W$
R_2	Concrete's thermal resistance of the lower part of the slab.	$m^2 K / W$
T_w	Water supply temperature at the center of the water tube.	$^{\circ}C$
T_3	Temperature at the outer side of the tube mantle.	$^{\circ}C$
T_c	Mean temperature at the water tubing plane or equivalent concrete core temperature	$^{\circ}C$

Thermal collector

N_s	Number of module in series	-
A_c	Collector area	m^2
β	Collector tilt angle	$(^{\circ})$
C_p	Fluid specific heat	$KJ/Kg K$
α	Absorptivity of the absorber plate	-
α_n	Absorptance at normal incident angle	-
τ	Transmittance of the collector cover	-
\dot{m}	Mass flow rate	kg/hr
Q_u	Useful energy gain	kJ/hr
U_L	Total heat transfer coefficient	$KJ/hr.m^2.K$
δ_p	Plate thickness	m
k_p	Thermal conductivity of plate material	$KJ/hr.m.K$
D	Outside diameter of the pipe	m

D_i	Inside diameter pipe	m
W	Tube spacing	m
h_{fi}	Heat transfer coefficient between the fluid and the tube wall	KJ/hr.m ² .K
F'	Fin collector's efficiency	-
FR	Heat removal factor	-
t_e	Thickness of edge insulation	m
k_e	Conductivity of edge insulation	KJ/hr.m.K
$h_{c,e-a}$	Convection heat loss coefficient from back of collector to ambient	KJ/hr.m ² .K
t_b	Thickness of back insulation	m
k_b	Conductivity of back insulation	KJ/hr.m.K
$h_{c,b-a}$	Convection heat loss coefficient from back to ambient	KJ/hr.m ² .K
U_t	Overall heat loss coefficient	KJ/hr.m ² .K
U_b	Bottom heat loss coefficient	KJ/hr.m ² .K
U_e	Heat loss coefficient from the collector edges	KJ/hr.m ² .K
T_a	Ambient temperature	°C
T_P	Collector plate temperature	°C
T_g	Cover glass temperature	°C
T_b	Collector back temperature	°C
T_{av}	Average collector fluid temperature	°C
$T_{coll,in}$	Inlet temperature of fluid to collector	°C
$T_{coll,out}$	Outlet temperature of fluid from collector	°C
S	Solar radiation absorbed by the absorber plate	KJ/hr.m ²
$(\tau\alpha)$	Product of the cover transmittance and the absorber	-
$(\tau\alpha)_b$	$(\tau\alpha)$ for beam radiation (depends on the incidence angle θ)	-

$(\tau\alpha)_d$	$(\tau\alpha)$ for sky diffuse radiation	-
$(\tau\alpha)_g$	$(\tau\alpha)$ for ground reflected radiation	-
r_{\perp}	perpendicular component of unpolarized irradiation	-
r_{\parallel}	parallel component of unpolarized radiation	-
ρ_g	Ground reflectance	-
ε_p	Infrared emissivity of absorber plate	-
ε_g	Infrared emissivity of glass cover	-
N_g	Number of glass covers	-
C_b	Bon conductance	-

Thermal storage tank

V_{tank}	Tank volume	m^3
A_{tank}	Surface area of tank	m^2
A_{HX}	Surface area of heat exchanger	m^2
C_p	Tank fluid specific heat	kJ/kgK
$M_{DHW,in}$	Mass flowrate entering at inlet DHW	kg/hr
$m_{DHW,out}$	Mass flowrate leaving at outlet DHW	kg/hr
$M_{SH,in}$	Mass flowrate entering at inlet SH	kg/hr
$m_{SH,out}$	Mass flowrate leaving at outlet SH	kg/hr
$m_{HX,in}$	Mass flowrate entering at heat exchanger	kg/hr
$m_{HX,out}$	Mass flowrate leaving at heat exchanger	kg/hr
d_i, d_o	Inside and outside diameters of heat exchanger tubes	m
L	Total tube length	m
h_o	Outside convection coefficient for internal heat exchanger	$\text{KJ/hr.m}^2.\text{K}$

λ_{tank}	Tank fluid thermal conductivity	KJ/hr.m.K
k_{wall}	Conductance of the tube wall	KJ/hr.m ² .K
λ_{wall}	Conductivity of the tube wall	KJ/hr.m.K
Nu_o	Nusselt number for external flow around a tube	-
Nu_i	Nusselt number for internal flow around a tube	-
Ra	Rayleigh number	-
Re	Reynolds number	-
Pr	Prandtl number	-
Gr	Graetz number	-
$T_{DHW,in}$	Temperature at inlet DHW	°C
T_{DHWout}	Temperature at outlet DHW	°C
$T_{SH,in}$	Temperature at inlet SH	°C
$T_{SH,out}$	Temperature at outlet SH	°C
T_{env}	Environment temperature	°C
T_{tank}	Average temperature tank	°C
T_{set}	Set point temperature for a thermostat	°C
ΔT_{db}	Temperature dead band for a thermostat	°C
UA_{hx}	Heat exchanger overall UA value	KJ/hm ² K
U_{tank}	Loss coefficient of the tank	KJ/hm ² K
$U\Delta$	Additional loss coefficient for the tank	KJ/hm ² K
Q_{load}	Energy removed for load (SH and DHW)	kJ/h
Q_{HX}	Energy supplied by heat exchanger (kJ/h)	kJ/h
Q_{AUX}	Auxiliary energy supplied by heater	kJ/h

Photovoltaic system

	Peak power	
	Incident solar radiation	
P_{max}	Incident solar radiation at STC	KW
G	Derating factor	KW
G_{STC}	Temperature coefficient of power	KW
F_{pv}	Module temperature	-
α	Module temperature at STC	(%/°C)
T_c	Array thermal loss coefficient	°C
$T_{c,STC}$	Electricity produced by the PV system	°C
U_{Ls}	Electricity purchased from the utility grid	kJ/hm ² K
E_{PV}	Electricity sold to the electricity grid	kWh
E_{GP}	Energy consumption	kWh
E_{GS}		kWh
E_C		kWh

General Introduction



The economic development in recent decades on the national and international level led to an enormous improvement in living conditions and population growth. This was accompanied by an explosion of energy demand in all sectors. Energy consumption in developed countries grows at a rate of approximately 1% per year, and that of developing countries, 5% per year [1]. Fossil fuels were the dominated energy sources used to meet this continuously increasing energy demand, resulting in global warming and climate change. World statistics show that in four years (2004–2008), while the world population increased by 5%, the gross energy production and annual CO₂ emissions increased by 10%, reaching 12 billion tons of oil equivalent of total primary world energy supply and 29.4 billion tons of CO₂ emissions in 2008 [2].

Find appropriate solutions to the dual problem of climate change and energy demand is a key challenge for the sustainable development. The sustainable development has been defined in many ways, but the most frequently definition is from the World Commission on Environment and Development (WCED), 1987. “Sustainable development is development that meets the needs of the present without compromising the ability of the future generations to meet their own needs” [3].

Building construction industry is a one of the most consuming energy sectors. Worldwide, buildings are responsible for a large share of the global energy consumption. According to the International Energy Agency (IEA), more than a third of the total final energy use is consumed by residential and tertiary sectors [4]. In Algeria, buildings, with about 35% in the residential sector and 6% in the tertiary sector, use approximately 42% of total energy consumption [5]. The reasons that led to the increase in energy demand are: (a) substantial increase of population and

housing, (b) low prices of conventional energy, (c) increase number of electrical equipment in each house, (d) use of non-economic electrical equipment such as incandescent lamps and cheap air conditioners, (e) absence of awareness and lack of culture on the energy control, (f) growing desire of people to comfort.

As a result, the building sector has a significant potential for energy savings. The reduction of energy consumption can be achieved on one hand by improving energy efficiency in building sector, and on the other hand by replacing the fossil fuels based energies by renewable energies. These actions may provide a great contribution to the achievement of the concept of sustainable development.

The Algerian thermal regulation of residential buildings was released in 1997. Within the framework of this thermal regulation, three Regulatory Technical Document were elaborated (DTR).

- The DTR.C3-2 which establishes the rules for calculating of winter heat losses for residential buildings [6].
- The DTR.C3-4 includes the rules for calculating of the summer heat input for residential buildings [7].
- The 3-31 DTR.C deals with the natural ventilation of residential premises [8]. The implementation of this regulation should allow a saving of 20 to 30% on energy consumption for heating homes.

Renewable energies integration in the building sector has the greatest potential for the reduction of end-use energy consumption. In this context, the **Algerian State**, has adopted a Renewable Energy and Energy Efficiency Program, published in 2011, including an ambitious energy efficiency program particularly in the residential sector [9]. Proposed measures to achieve energy efficiency in this sector include the introduction of thermal insulation of buildings, which will reduce energy consumption

related to home heating and cooling by about 40% [10]. Thus, a pilot project of 600 houses with High Energy Performance (HEP), as demonstrative operation, was launched. It incorporates the principle of energy conservation in the design and construction of buildings. The promotion and development of renewable energies including solar, enshrined in the Law on Renewable Energy 2004 [11]. By 2030, the Renewable Energy and Energy Efficiency Program expected to reach a 27% (22 GW) share of renewable energy in the balance of the national electricity [9]. The choice to use renewable energy is strengthened by its geographical location. Indeed, Algeria holds one of the largest solar potential in the world. Sunshine duration in almost all the country exceeds 2000 hours annually and can reach 3900 hours (highlands and Sahara). The energy received daily on a horizontal surface of 1 m² is about 5kWh on most territory of the country (1700 kWh/m²/year at North and 2263 kWh/m²/year in the South [12].

During the last few years, the Algerian authorities have made development of rural housing one of their priorities. Since 2005, Algeria has launched a programme for the construction of one million housing units. Nearly half of this programme (450000 units) is devoted to housing in rural areas in order to keep rural populations in place and to encourage their return from urban areas [13]. The construction of a rural house, benefited by a state subsidy (SS) of 7000\$, aimed to encourage families to build a self-construction with a decent house in rural environment.

However, the construction of these houses whose level of energy performance is very bad, surely leads to a significant increase in energy consumption, since the government has built them without taking into account the climatic conditions and the required thermal performance level. Whilst, solar energy can play an important role in the improvement of energy balance and the environmental protection.

This thesis proposes methods and solutions to improve energy performance of residential rural housing in order to converting them into a high-energy performance houses through the integration of passive and active solar energy systems and investigate their contribution in the sustainable development.

This thesis is organized as follows:

Chapter 1 gives a review of the previous works on improvement of building energy performance, including incorporating of passive solar design and active solar systems in building.

Chapter 2 presents the main information about energy production and energy consumption in Algeria particularly in residential sector followed by an analysis of renewable energy potential and applications.

Chapter 3 sets out some basics of integrating solar energy in residential sector. We focus on the architectural design of the house for the energy requirements reduction and the application of active solar systems for energy supply.

Chapter 4 is concerned with the development of multi-zone house model coupled with solar energy systems. Firstly, thermal modelling of a multi-zone house and mathematical description of the different components that constitutes the solar heating system was made. Then, a complete model of multi-zone house coupled solar heating system was performed under TRNSYS software. Finally, a grid-connected PV system was modelled in order to meet electrical energy loads of the house.

In Chapter 5, an experimental study was conducted on a bioclimatic house located in Algiers in order to study the contribution of the solar heating system in the improvement of the indoor comfort. The experimental study allows also to validate the main components of the solar heating system model.

Chapter 6 deals with the overall energy saving and CO₂ emission mitigation at the level of the energy balance of Chlef district results in the improvement of energy performance of rural houses built during the last rural housing construction programs. To achieve this goal, the model developed in Chapter 5 is applied on a case study of a single-family rural house located in Chlef district. A parametric study was performed in order to improve the energy performance of the reference house and reach the level of high-energy performance house. There are two ways to improve the energy performance of a typical rural house. First, a passive one through the integration of a set of solar passive design to reduce the need for heating and air conditioning. Second, an active one using solar heating system to produce heat for space heating and domestic hot water preparation and solar PV to supply the house with electricity. Furthermore, in order to get information about the profitability of EEM and solar systems on rural housing, an economic analysis is performed.

CHAPTER 1: Bibliographical study

1.1. Introduction

Solar energy is an alternative source of energy, mainly because it is free and does not cause environmental problems. There is a common consensus between academic scientists that renewable energy use is necessary to mitigate climate change and there is a deep connection between the use of renewable energy and the sustainable development. The exploitation of solar radiation resource to reduce energy consumption in buildings sector can be achieved by passive or active method. The passive method is related to many building aspects, such as its form and orientation, insulation of walls, roof and floor, windows-to-wall area, glazing type and shading device. The active solar system includes solar systems for domestic hot water preparation, space heating, space cooling and photovoltaic system for electricity generation. This Chapter gives a review of the main solutions proposed for energy performance improvement in building. The review starts with an analyze of previous works that deal with the reduction of energy requirements of building by passive mean. Then, the recent works that investigate the main benefit of application active solar systems in building in discussed.

1.2. Passive solar systems

Literature that focus on the integration of the ‘passive solar designs’, or also called “bioclimatic designs” or “energy efficiency measures” in the building envelope is increasing constantly. **Chesné et al. [14]** studied the relationship between the insulation thickness and the bioclimatic margin of a building, defined as the gap between the potential of passively using solar energy and the building heating energy needs. Parametric study of the influence of adding various thicknesses of insulation to a non-insulated case study building in Trappes, France, reveals that the

first few centimeters of insulation have most significant influence on both the decrease of the heating energy needs and the increase of the bioclimatic margin, and that these changes progressively become very small and fall below 1% after a certain insulation thickness. **Jinghua et al. [15]** studied the effect of the thickness and the position of building facade insulation on the total energy demand, among other things. By using a combined optimization strategy for insulation, window/wall ratio, glazing and shading system, they achieved a reduction of up to 25.92% in the total heating and cooling demand. However, after a certain insulation thickness threshold was surpassed, the energy reduction continued, but at a significantly lower rate. **Masoso and Grobler [16]** showed, through a parametric study of a case study building in Gaborone, Botswana, that a combination of high internal loads and cooling set point may lead to the anti-insulation behavior of a building during the cooling season, when higher insulation levels begin to also yield higher cooling loads. The design variables in the study are the cooling set point and the thickness of external wall insulation, while the cooling load has been estimated by EnergyPlus and validated on a physical model. **Oral and Yilmaz [17]** developed a theoretical argument for determining the maximal feasible U-values for walls which ensure thermal comfort, while minimizing the heating load. The limit U-value of each wall depends on the building's form, represented as the ratio of the total facade area to the building volume, glazing type, windows-to-wall ratio and the wall orientation. The case study is performed for three Turkish cities: Istanbul, Ankara and Erzurum, representing temperate humid, temperate dry and cold zones with long and intensive heating periods. **Lollini et al. [18]** determined the optimum roof, wall and floor insulation levels with respect to the net present value and the payback rate as the objective functions, first on the component level by theoretical argument, then on the

building level by parametric study. The case study includes a single family house and a tower building, as buildings with extreme envelope surface area/volume ratios, located in six Italian climatic zones (in Lampedusa, Palermo, Latina, Lucca, Arezzo, Milan, Sondrio, Bressanone), with heating energy loads estimated by EC501 software, based on the Italian legislative framework. They find critical transmittance values for each of the climate zones and also note that the optimal insulation configuration at the building level does not necessarily correspond to the optimal thermal transmittances calculated for the individual components.

Orientation is one of the most important parameters that intervene in the passive solar design [19]. South oriented windows constitute an effective passive solar heating system in heating season. However, windows and shading should be jointly considered, in hot season, in order to effectively control the heat gain. The use of shading systems is more beneficial in regards to natural illumination and to lower energy consumption [20]. **Leskovar and Premrov [21]** studied the optimal windows-to-wall ratios minimizing the total annual heating and cooling load for a case study of a two-storey house with prefabricated timber-frame structural system, located in Ljubljana, Slovenia. The house is well insulated with an opaque envelope elements having U-value between 0.102 and 0.135 $\text{Wm}^{-2} \text{K}^{-1}$, using triple low-e glazing, and overhangs on the south and external vertical shading devices on the west and the east facades. The parametric study is performed in PHPP with the design variables being the windows-to-wall ratios at each facade, three timber-frame macro-panel systems and the building orientation. The results indicate that the optimal windows-to-wall ratio for walls with very low U-values is smaller than in walls with higher U-values, and the authors derive a linear interpolation predicting approximate energy demand based on the wall U-value and the windows-to-wall ratio. **Inanici and**

Demirbilek [22] aimed to determine the optimum building aspect ratio and south window size which minimize the total annual heating and cooling load of apartments at intermediate floors in residential buildings, with no roof or ground contact, for five cities in Turkey: Erzurum, Ankara, Diyarbakir, Izmir and Antalya. The parametric study is performed using SUNCODE-PC software. The results show that the building aspect ratio has minor influence on energy performance (with differences at most 3%–6% for the same south window size), while the increase of south window size leads to the decrease of the total annual load in cool climates (Erzurum and Ankara) and its increase in warm climates (Diyarbakir, Izmir and Antalya). **Persson et al. [23]** evaluated the influence of the size and orientation of the triple glazed, low-e windows on the heating and cooling energy loads on a case study of 20 terraced passive houses built in Gothenburg, Sweden. The parametric study is performed with DEROB-LTH dynamic building simulation tool, and the design variables include windows size and orientation. The results show that the size of triple glazed, low-e windows does not have a major influence on the heating load, due to the extremely well insulated walls and the efficient ventilation system, but it is relevant for the cooling load. The optimal solution has smaller window area facing south and larger window area facing north when compared to the already built houses, showing that in passive houses, it is not necessary to keep down the window area facing north.

The individual performance of any of these energy efficiency measures can be considerably different when used in combination with others. The interaction between energy efficiency measures can reduce considerably the energy consumption. **Gratia and Herde [24]** aimed to develop guidelines for designing energy-efficient office buildings in the Belgian climate with respect to the building insulation level, airtightness, internal gains control, and the windows-to-wall ratios for

different external wall orientations, ventilation strategy and thermal mass use. Through the extensive discussion of the results of several parametric studies performed with OPTI and TAS on the case studies of two office buildings located in Uccle, Belgium. **Eskin and Türkmen [25]** in a parametric analysis investigated the effect of passive design strategies: insulation and thermal mass, building aspect ratio, external wall color, shading devices, window size and glazing type on the cooling and heating loads, estimated by EnergyPlus, of an office building in Turkey. The study is performed for cities in four major climatic zones in Turkey—hot summer and cold winter (Ankara), mild climate (Istanbul), hot summer and warm winter (Izmir) and hot and humid summer and warm winter (Antalya). **Gong et al. [26]** aimed to minimize energy consumption of a simple box model with a window and without internal heat sources for 25 representative cities in China by finding the optimal combinations of seven passive design measures: wall thickness, roof and external wall insulation thicknesses, window orientation, windows-to-wall ratio, glazing type and sunroom depth/overhang depth. The optimization process first employs the orthogonal method to analyze the significance of each parameter and their interactions on energy consumption, as estimated by THERB, and then uses the listing method to find optimal parameter combinations. As a result, the authors identify a total of seven passive design zones of China, within which the optimal combinations of passive design features are the same for each city. **Nathan et al. [27]** analyzed the effect of a set of measures energy efficiency for residential houses in a semi-arid climate. The energy efficiency measures include insulation panels for exterior walls, control of natural light (daylight), increase of windows surfaces, glazing effective, and various combinations of these. This model has determined that the energy consumption is reduced by 6.1% when several energy efficiency

measures are combined. **Danielle et al. [28]** studied the interaction between various measures of energy efficiency and thermal comfort in residential buildings in Salamanca (Mexico) using a detailed simulation and optimization procedures. The results show that a combination of efficient appliances, increased levels of roof and wall insulation, heating system water efficient is necessary to save about 52% of the annual energy for new homes. One of the most effective ways to reduce heat transmission rate and energy consumption for space cooling and heating is the use of an appropriate thermal insulation in the building envelope. **Cheung et al. [29]** discussed the effect of passive design strategies: insulation and thermal mass, external wall colour, shading devices, window size and glazing type on the annual cooling energy and peak cooling load, estimated by TRNSYS, through a parametric analysis of an apartment in a high-rise apartment building in a hot and humid climate of Hong Kong. **Porritt et al. [30]** compared the effects of a range of passive interventions for adapting the case study of a Victorian, late 19th century, terraced house in the south east of England in order to reduce the summertime overheating. The passive interventions include: adding one of three insulation options (loft, internal wall, external wall insulation), adding one of four solar gain control options (internal blinds, external shutters, fixed shading, low-e double glazing), painting external walls and roof in light colors to improve reflection of solar radiation, and natural ventilation strategies. The interventions, as well as a number of their combinations, are simulated using IES-VE software package for summer months (June to September). It is concluded that, for a predicted test reference weather year in the 2080s, the overheating problem could be addressed purely by passive means, and the most effective interventions are wall insulation, external window shutters and painting walls in light color. Note, however, that the study assumed the house to be

occupied during evenings and mornings only, and did not consider the reduction of peak daytime temperatures. **Florides et al. [31]** examined the measures reducing annual cooling load in the hot environment for a case study of a building located in Nicosia, Cyprus. The parametric study was performed with TRNSYS and the design variables include roof insulation, ventilation rate, glazing type, overhang shading depth, building orientation, aspect ratio and thermal mass. The lifecycle cost analysis of the optimal measures reveals that roof insulation and efficient window glazing are most cost effective measures. **Jaber and Ajib [32]** in a parametric study performed with TRNSYS, have determined the effects of the windows type, size and orientation on the annual heating and cooling energy demand of a case study of a single-story house located in three different climate zones: Amman and Aqaba in Jordan and Berlin in Germany. Optimal parameter combinations are identified for the lifecycle cost as the objective function. The results indicate that the heating load is highly sensitive to windows type and size as compared with the cooling load. About 27.59 % of the annual energy consumption can be saved by choosing optimal orientation, window sizes and use of sun protection during hot season, in addition to the insulation of walls and roof by 0.13 m and 0.20 m, respectively. **Bambook et al. [33]** coupled GenOpt with IDA ICE in order to optimize passive design of a detached, single-story house in Sydney with respect to the lifecycle heating and cooling energy cost. The design variables are the wall and roof insulation thicknesses, the window type, the shading depth, the internal thermal mass wall thickness and the night ventilation rate. Details of distinct Pareto solutions are discussed, and it is observed that the optimal solution can cost-effectively reduce the space heating and cooling energy requirement by up to 94%, compared to the current design practice in Sydney.

1.3. Active solar systems

The exploitation of solar energy resource can be achieved also by tracking solar radiation by solar systems such as solar heating or cooling system and photovoltaic system.

Solar combisystem is one the most efficient system for both domestic hot water preparation and space heating. **Viorel Badescu [34]** describe models for five components of an active solar heating system. The integrated model was implemented to Pirmasens Passive House (Rhineland Palatinate, Germany). Two series schemes of interconnection for the domestic hot water preparation system and the space heating system, respectively, are analyzed. The results show that most part of the collected solar energy is used for domestic hot water preparation and the series interconnection is unfavorable for the space heating system. **Mitchell Leckner and Radu Zmeureanu [35]** investigated the feasibility of a Net Zero Energy house with solar combisystem. The results show that the investment of embodied energy in the NZEH and combisystem gives important energy savings with relatively quick energy payback times of 8–11 years, and energy payback ratios of 3.6–4.8. The life cycle cost analysis has shown that it is unlikely at current solar technology and electricity prices that the average Montreal homeowner would accept the additional expenses for the construction of a NZEH as presented in this study. However, the analysis also showed that there are financial benefits to taking the first step and making a house more energy efficient with changes to items such as insulation, appliances and using domestic hot water saving devices. Depending on the design, the payback for these combined efficiency changes range from 39.3 years to as low as 6.1 years. **Jason Ng Cheng Hin, Radu Zmeureanu [36]** presented the optimization of a model of a solar combisystem in an energy efficient

house in Montreal (Qc), Canada. A hybrid particle swarm and Hook–Jeeves generalized pattern search algorithm is used to minimize the life cycle cost, energy use and exergy destroyed of the combisystem. Due to the high cost of the solar collector technologies and the low price of electricity in Quebec, none of the optimal configurations have acceptable financial payback periods. However, they all have energy payback times between 5.8 and 6.6 years. **A.Hugo et al. [37]** investigated the performance of a solar combisystem with a long-term thermal storage capacity for a typical one-storey detached house in Montreal. Simulation results from the TRNSYS program show that, starting with the second year, the system is able to cover fully the heating and domestic hot water thermal loads using the solar energy exclusively. The energy Payback time index shows that the embodied energy initially invested in the equipment is recovered in less than 6 years through the thermal energy savings. Furthermore, the solar combisystem can be used to provide space cooling, in addition to DHW and space heating. **S. Rasoul Asaee et al.[38]** conducted a study to evaluate the thermal performance of a solar combisystem with space heating, cooling, domestic hot water heating and thermal storage capability for houses in the four climate regions of Canada (Atlantic, Central, Prairies and Pacific) based on simulations conducted using models developed within the TRNSYS 17.1 energy simulation software. The results show that solar combisystems can provide a substantial fraction of the space heating, cooling and domestic hot water heating energy requirement of a simple house in all major climatic regions of Canada.

The integration of photovoltaic modules in the building envelope allow one to consider a multifunctional frame and then to reduce the cost by substitution of components. **G. Fraisse et al. [39]** investigated the energy performance of water hybrid Photovoltaic /Thermal (PV/T) collectors applied to combisystems of Direct

Solar Floor type. The recovered heat energy can be used for heating systems and domestic hot water. A combination with a Direct Solar Floor is studied. The results show that the research led on the hybrid solar collectors are interesting and promising. However, it is required that both photovoltaic and thermal field maintain a strong, partnership in order to conceive a unique industrial component which integrates the thermal absorber and the photovoltaic module.

The combination of passive with active solar systems lead to achieve different high-energy performance buildings concepts, from low-energy building through passive building and zero energy building to positive energy building and even autonomous building [40]. High-energy performance buildings involve two strategies, minimizing the need for energy use in buildings through energy efficient measures and adopting renewable energy and other technologies to meet the remaining energy needs.

Danny S. Parker [41] presented measured annual performance data from a dozen recent-vintage very low energy homes in North America. Many of the designs combines greater energy efficiency with solar electric photovoltaic power in an attempt to create Zero Energy Homes. The data indicate that very low energy use buildings can very readily be achieved in North America. In general, the better cost effectiveness seen from energy efficiency measures indicates that greater investment in conservation should be prerequisite to installation of solar water heating and solar electricity in Zero Energy homes.

Verbeeck and Hens [42] searched for the economically optimal balance of the energy-saving measures for retrofitting five reference buildings in Brussels, Belgium. The design variables include the insulation thicknesses of walls, roof and floor and glazing type, as well as investments in the space heating system, hot water production, solar collectors and photovoltaic panels. Using the calculation procedure

from the Flemish Energy Performance Regulation, based on EN 832, the study shows that roof insulation is the most effective measure, both energy-wise and economically, followed by better performing glazing. It also shows that it is better to invest in insulation first, then in more energy efficient heating system, while renewable energy systems are least profitable investment in this study. **L. Wang et al. [43]** discussed a possible solution for zero energy building in United Kingdom (UK). EnergyPlus software is employed to enabled façade design studies considering building materials, window sizes and orientation and TRNSYS is used for the investigation of the feasibility of zero energy houses with renewable electricity, solar hot water system and energy efficient heating systems. The results show that it is theoretically possible to achieve the zero energy homes in the UK.

1.4. Conclusion

Through this bibliographic study, it can be concluded that:

- The climate conditions has a very effect on the annual energy demand of building.
 - Integrating passive solar designs in early step of construction can provide an important energy saving;
 - Thermal insulation is the most critical parameter of the building;
 - The combined effect of passive and active solar systems is able to cover a significant part of energy demand for the entire year;
 - Energy demand should be reduced to a minimum through energy efficient building designs leaving just a very small amount of energy requirement to be covered by renewable energy generation.
-

Chapter 2: Energy situation in Algeria



2.1. Introduction

The energy consumption in Algeria is increasing at a faster rate due to urban and economic development in constant progression. Energy demand could double by the year 2020 (60 MTOE, even 70 MTOE) by increasing uses of energy and activities. Statistics expect energy consumption to increase at about annual growth are of about 3.5% [44]. The use of energy in buildings represents a large share of this energy consumption and it is still in expansion. The Algerian energy strategy is decidedly towards sustainable development. In order to reduce the total energy demand and provide sustainable solutions the environmental challenges and to problems regarding the conservation of the energy resources of fossil origin, the state gives priority to the development of renewable energy.

This chapter presents an analysis of Algeria's energy situation, and the potential of renewable energy including, solar, wind biomass, hydro and geothermal and their applications.

2.2. Conventional energy

2.2.1. Energy consumption

Algeria's total final consumption has steadily been increased in recent years. The evolution of energy consumption by sectors is shown in **Fig.2.1**. The total energy consumption in Algeria has increased significantly between 1980 and 2008. From 2008 to 2010, we noticed a decrease in energy demand in households and industrial sectors due to the substitution of the use of LPG in home by natural gas. It can be also seen from **Fig.2.1** that the households sector contributes over an important part to the energy demand.

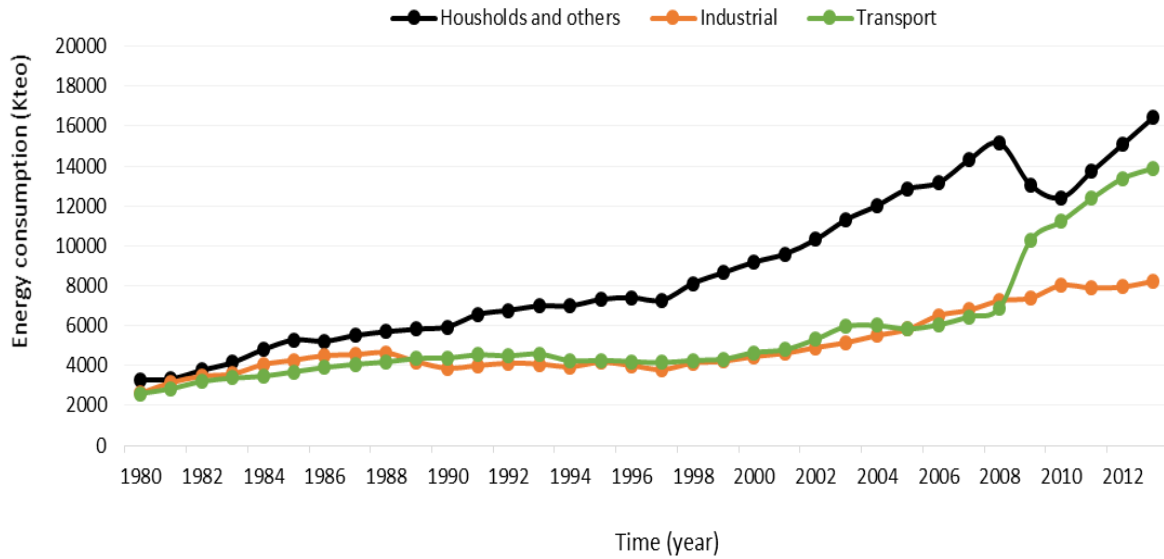


Fig.2.1 Evolution of final energy consumption by sectors between 1980 and 2013. (MEM source)

Fig.2.2 shows the evolution of energy consumption by category of sources. Like the national production, the petroleum products is the major source of energy in Algeria, followed by electricity and natural gas.

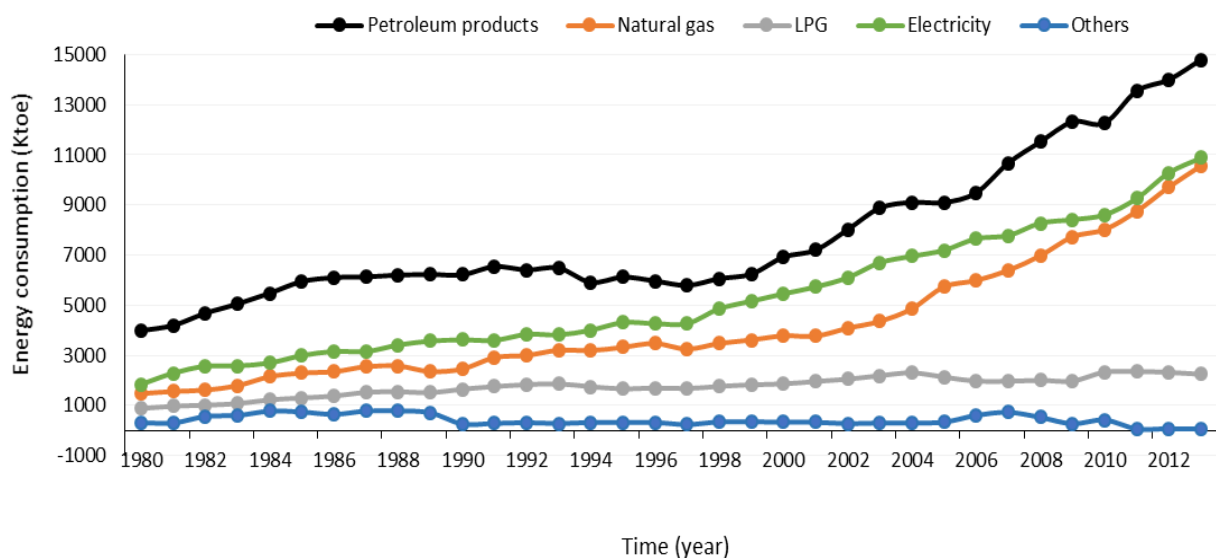


Fig.2.2 Evolution of final energy consumption by product between 1980 and 2013. (MEM source)

According to MEM statistics for energy balance for 2013 [45], the total final energy use accounts for 38500 Ktep.

In **Fig.2.3** is shown the distribution of the energy consumption in different sectors in 2013. The residential sector accounted for 35 % (12296 Ktoe) of all final energy used in Algeria and was the second largest energy-using sector, after the transport sector 13880 Ktoe (40%). The agriculture and industrial sectors account for respectively 284 Ktoe (1%) and 8229 Ktoe (24%).

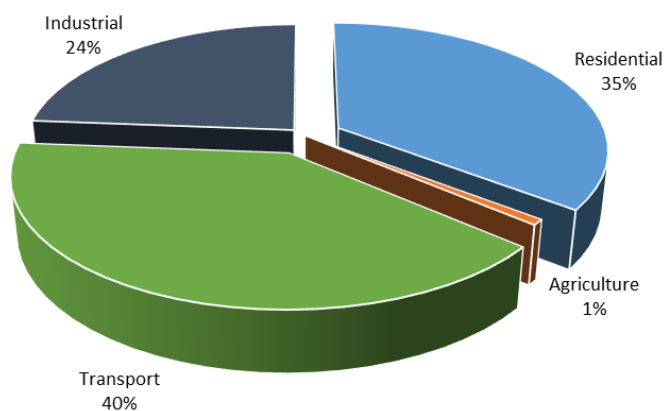


Fig.2.3 Distribution of final energy consumption by sector in 2013
(MEM source).

Fig.2.4 shows the distribution of the energy consumption by category of sources in 2013. The petroleum products is in the first place with 14791 Ktoe, which represents 39% of the total energy consumption. The natural gas and electricity account for 10562 Ktoe (27%) and 10778 Ktoe (28%), respectively.

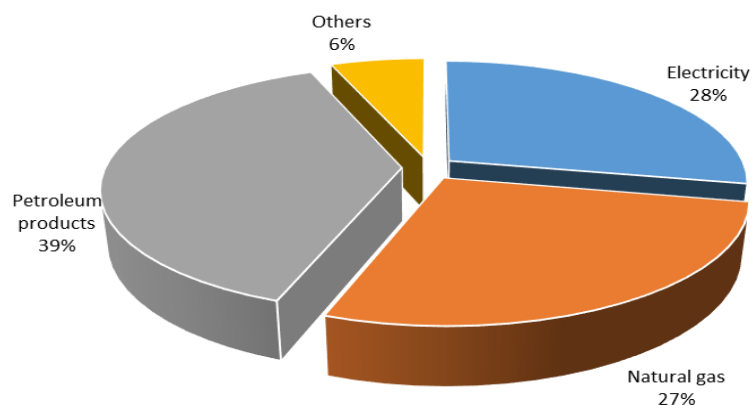


Fig.2.4 Distribution of final energy consumption by product in 2013 (MEM source).

2.2.2. Energy consumption in residential sector

The final energy consumption in the residential sector has reached 12269 Ktoe in 2013. From **Fig.2.5**, which represents the evolution of energy consumption in residential sector between 2010 and 2013, we can notice that the energy consumption in this sector is in constant growing from year to year. An increase of about 28% (3407 Ktoe) is recorded from 2010 to 2013.

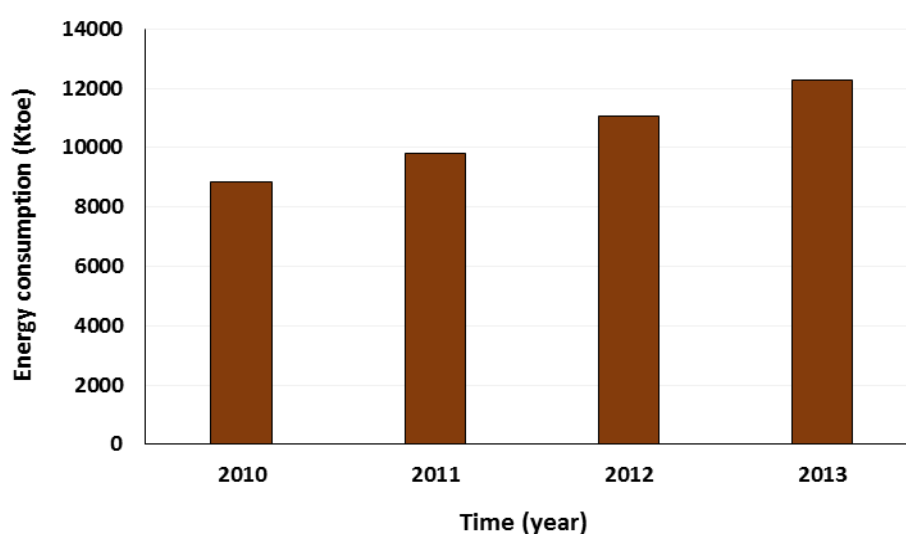


Fig.2.5 Energy consumption in the residential sector from 2010 to 2013.

However, the residential sector is the greatest consumer of electricity, which is the highest of all others sectors as shown in **Fig 2.6**. The electric consumption in the residential sector reach 770 Kteo, which represents 33% of the total electrical consumption.

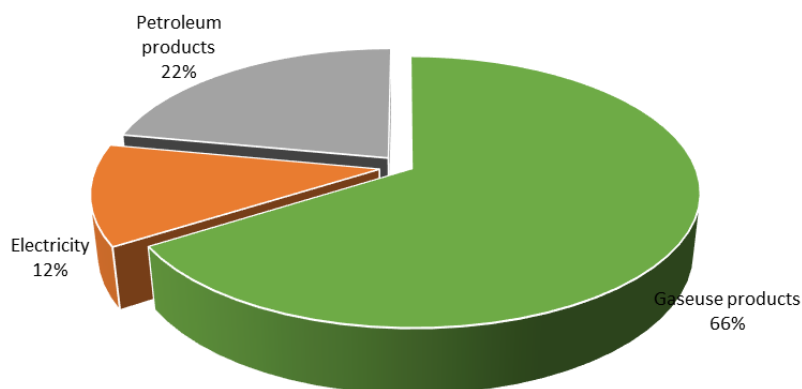


Fig.2.6 Distribution of energy consumption in residential sector in 2007 (MEM source).

2.3. Renewable energies

2.3.1. Potentials

Despite a range of efforts by the decision makers to increase access to modern energy sources in the country, the percentage of renewable energies in the national energy balance remains insignificant (0.006%) [46]. Energy policy advocates increasing the contribution of renewable energy in the national energy balance. The objective is to achieve a contribution of around 6% in the balance of power production by 2015 and 20 % by 2030.

However, Algeria has a rich potential of renewable energy. The distribution of these potentials are [44]:

- Thermal solar: 169,440 TWh/year.

- Photovoltaic: 13.9 TWh/year.

- Wind energy: 35 TWh/year.

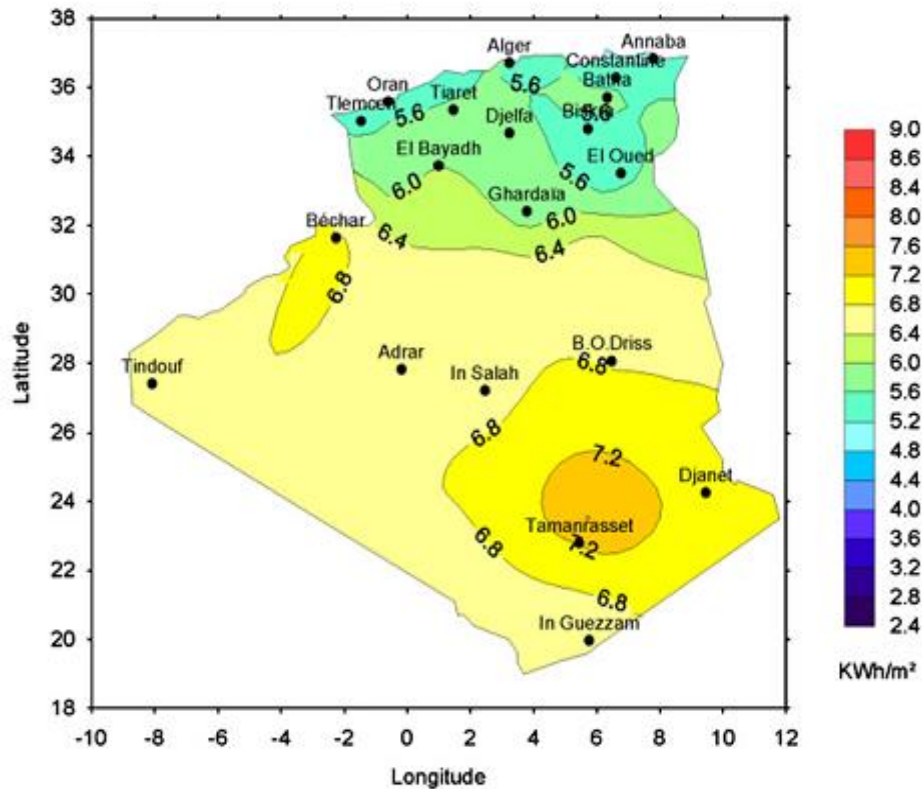


Fig.2.7 example of the overall exposure received in Algeria.

2.3.1.1 Solar energy

Solar energy is considered the potential source of renewable energy, the most of which is being naturally collected in the Sahara region. The insolation time over the quasi-totality of the national territory exceeds 2000 h annually and may reach 3900 h (high plains and Sahara) [1], as shown in **Table 2.1**.

Table2.1

Solar potential in Algeria

Areas	Coastal area	High plateau	Sahara
Surface (%)	4	10	86
Average duration of sunning (h/year)	2650	3000	3500
Received average energy(kWh/m ² /year)	1700	1900	2650

The daily obtained energy on a horizontal surface of 1m² is of 5 kWh over the major part of the national territory, or about 1700kWh/m²/year for the North and 2263 kWh/m²/year for the South of the country (**Fig.2.7**) [47].

2.3.1.2 Wind energy

Algeria has moderate wind speed (2 à 6 m/s), which is suitable for pumping water especially in high plateau. **Fig.2.8** shows the annual average wind velocities in Algeria.

The region of Adrar receives the most wind in the country judging from the results of the preliminary survey. Evaluations of powers recoverable at heights from 10 to 50 m could conclude in registering this region as a favorable site for the establishment of a windy farm. Other sites (North, High Plateaux) hide non-negligible energetic potentials.

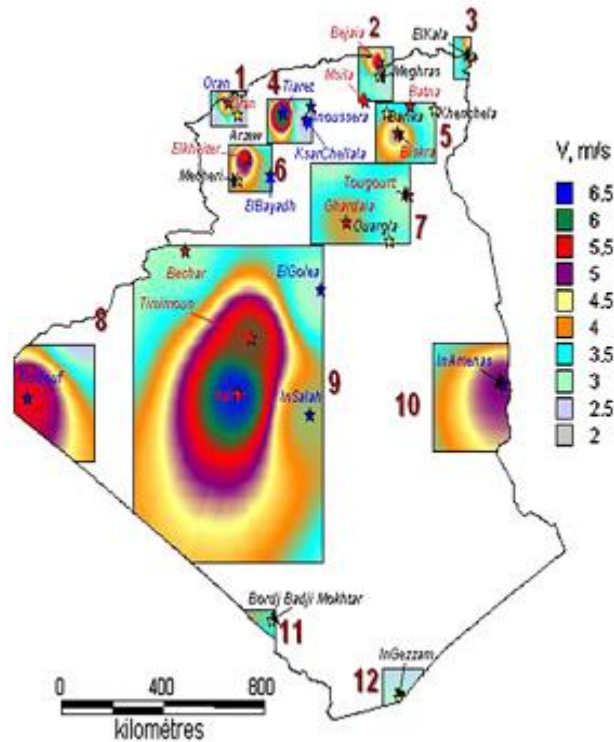


Fig.2.8 Wind chart in Algeria.

2.3.1.3 Hydroelectricity

The overall flows falling over the Algerian territory are important and estimated to 65 billion cubic meters but of little benefit to the country: restrained rainfall days, concentration on limited areas, high evaporation and quick evacuation to the sea.

In Algeria, more than 50 dams are currently operational, see **Table 2.2**.

2.3.1.4 Geothermal energy

According to the study conducted by CDER on the geothermal energy potential in Algeria, there are more than 200 hot springs in North-East and North-West part of the country. One-third's temperatures are superior to 45°C and the highest temperatures registered are 98 °C and 118 °C in Hamam El Maskhoutin and Biskra,

respectively [48]. The Jurassic limestone of North Africa, which constitutes great geothermal reservoirs, is at the origin of these geothermal sources. This reservoir commonly called “Albian platform”, is extended over several thousand m², as shown in Fig.2.9.

Table 2.2
Hydroelectric production park [MEM, 2014]

Plant	Installed power (MW)
Darguina	71.5
Ighil Emda	24
Mansouria	100
Erraguene	16
SoukEl DJEMAA	8.085
Tizi MEDEN	4.458
IGHZERNCHEBEL	2.712
GHRIB	7.000
GOURIET	6.425
BOUHANIFIA	5.700
BENI BEHDE	3.500
TESSALA	4.228

2.3.1.5 Biomass energy

The biomass potentially offers great promises with bearing of 3.7 millions of TEP coming from forests and 1.33 million of TEP per year coming from agricultural and urban wastes; however, this potential is not enhanced and consumed yet [12].

Biomass can be burnt directly or it can be converted into solid, gaseous and liquid fuels using conversion technologies such as fermentation to produce alcohols,

bacterial digestion to produce biogas and gasification to produce a natural gas substitute. Industrial, agricultural livestock and forest residues can be used as a biomass energy source [49].

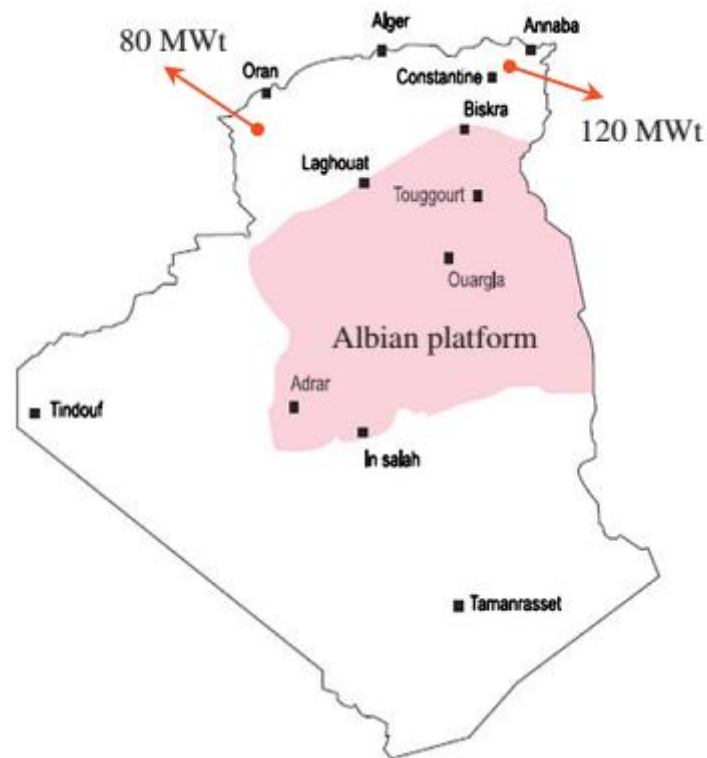


Fig.2.9. Albian platform situation [1]

In Algeria, the current biomass potential coming from forests is about 37 Mtoe, however only 10% of this potential is recovered. The potential coming from agricultural and urban wastes is about 1.33 1.33 Mtoe.

2.3.2 Renewable energies applications

The main renewable energy application are limited to electrification, pumping, telecommunication, public lighting and small refrigeration systems. The distribution of

installed power per resources is shown in **Table 2.3** and per application in **Table 2.4**.

The overall installed power is 2.353MW.

Table2.3

Distribution of installed power per resources.

Resources	Installed power (Watt)	Percentage (%)
Solar	2.279.960	70
Wind	73.300	30
Total	2.353.260	100

Recently, the photovoltaic panels have been utilized for various applications in Algeria [12]. Some of these applications include

_ Electrification with solar power of 20 villages spread out among the four wilayas of the south: Tamanrasset, Tindouf, Illizi and Adrar. The solar energy produced by these systems is above 1.5 GWh.

_ A solar hybrid (photovoltaic/diesel) power station of 13 kW in power station of 13 KW in Illizi, beaconing of 2300 km of roads.

_ Supplying electricity for more than 100 telecommunications stations (650 kW).

_ Electrification of more than 300 houses (550 kW), the total cost of this project was estimated at s115,000.

_ 10 kW photovoltaic power station connected to the national grid.

_ One oil station fed with solar energy (7 kW).

_ NEAL Company: 150MW hybrid power station (solar/gas), with 34MW solar.

_ Development of the market of solar energy water heater carried out by APRUE (Promotion of the Rational Use of Energy) to equip 5500 houses and 16,000 m² in the tertiary sector.

_ Rural electrification program: provide photovoltaic electricity to 16 villages with a total of 800 houses (0.5 MW).

Table 2.4

Distribution of installed power by application

Applications	Installed power (Watt) (Watt)	Percentage (%)
Electrification	1.352.800	57.48
Pumping	288.400	12.25
Public lighting	48.430	2.05
Telecommunication	498.000	21.16
Others	165.630	7.03
TOTAL	2.353.260	100

2.4. Conclusion

In this chapter, the energy situation of Algeria has been outlined and data for renewable energies are presented. Algeria is an energy producing-exporting country. The main energy sources is crude oil, followed by natural gas. However, domestic fossil reserves are limited and harm the environment.

In order to be less dependent on fossil fuel, meet the increasing energy demand and protect the environment, Algeria must diversify their energy resources. Indeed, government gives particular importance for promoting renewable energy and improving energy efficiency, with the aim to produce 40% of electricity from renewable energy by 2030.

Solar energy is considered as a promising source in the improvement of the energy balance and the protection of the environment. In fact, it is clear that Algeria is endowed with good solar energy potentials. There is also optimism for wind and geothermal, but further work is required for comprehensive determination of geothermal and wind resources. Despite the huge potential of renewable resources, the share of energy from renewable sources in energy balance is not significant.

***Chapter 3: Solar energy applications in
rural housing***

3.1 Introduction

One of the most abundant and environmental friendly energy sources is indisputably the sun. It is proved and recognized today that the solar energy reaching the terrestrial surface any year exceed amply the global annual energy consumption [50]. Indeed, according to the European Renewable Energy Council (EREC) (2010), the constant flux of energy coming from the sun, during one year, is the equivalent of more than 2000 times the total energy consumed by humans since the beginning of their history [51]. Algeria has an abundant potential for using solar energy resource, particularly in the rural areas. As a result, solar systems can play an important role in improving energy efficiency of rural housing. Solar energy may be used directly using solar passive or active systems. Shape and orientation of the house, thermal insulation of the envelope, thermal mass, etc. can be categorized as passive system, whereas, active heating systems with solar collectors and photovoltaic systems for electrical power generation can be classified under active systems.

Rural housing are more energy efficient than urban housing. However, the vast majority of new rural houses still ignore a lot of energy saving opportunities, which is available in the sunlight falling on the house and other natural elements of the site and opportunities in the structure and materials of the house itself, which, with thoughtful design could be used to collect and use free energy. The objective of this Chapter is to show how we can benefit from this free energy to improve energy efficiency of rural housing in Algeria. The basic principles of passive solar design and application of active solar systems are discussed.

3.2 Passive solar designs

Passive solar design is the use of the form and fabric of the building to admit, store and distribute primarily solar energy for heating and lighting [52]. The term 'passive solar design' encompasses a variety of techniques used to trap heat within a building during the winter months while avoiding overheating during the summer months. It integrates a combination of building features, which can markedly reduce the need for mechanical heating and electric lighting [53].

3.2.1 Principal of passive solar design

A room with a window facing south represents a simple passive solar system [54], as shown in **Fig.3.1** Sunlight enters the house through the aperture (collector) usually south-facing windows with a glazing material made of transparent glass. Radiation is then absorbed at the surfaces of internal walls. Absorbed radiation increases the internal energy of the material of the surface of a wall and is converted into heat.

The heat is stored for shorter or longer period within the element, depending on its thermal capacity. At night, as the room cools, the heat is exchanged between media (elements) of different temperatures. As a result, air temperature within the room increases. Flow of energy supplied to the room's interior through glazing may be reduced by using roof overhangs, blinds, shutters, etc., or increased by enlarging glazed areas.

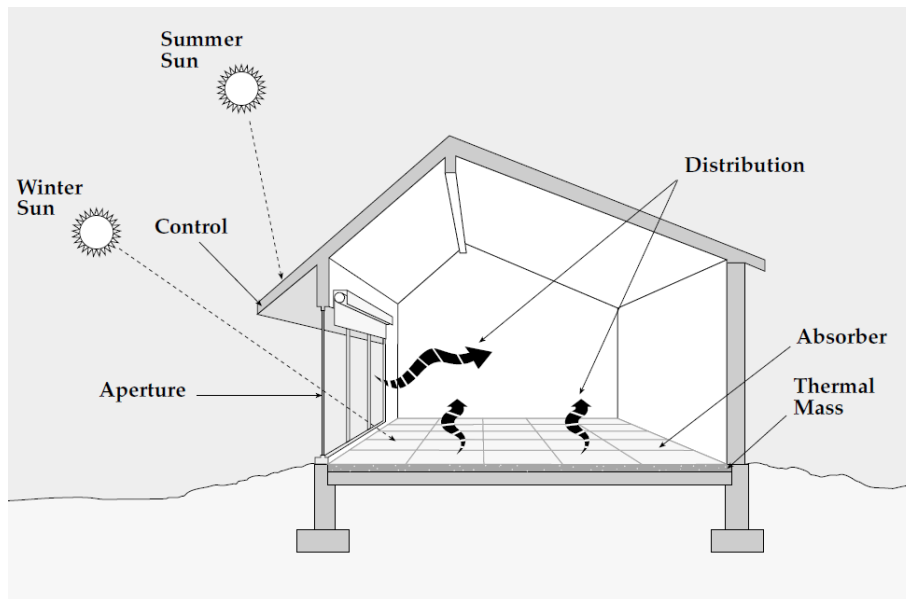


Fig.3.1 Concept for application of a passive solar system.

3.2.2 Elements of passive solar designs

Elements of passive solar design include house's orientation and shape, thermal insulation, internal room arrangements, thermal mass, windows size and location, shading devices, etc.

3.2.2.1 Orientation of the house

Shape and orientation

Shape and orientation of a house influences the energy demand for heating and cooling. Two variables are related to house shape: the compactness index and the shape factor. The compactness index C_f is the ratio between the volume V and the outer surface S of the building facade [55].

$$C_f = S/V$$

A very compact building is one that has a high volume/surface ratio, where the surface exposed to possible heat losses or gains is as small as possible. The shape factor is the ratio of building length to building depth. It was determined that the best orientation for rectangular buildings was when the longest walls were oriented toward the south. As shown in **Fig.3.2**, in square buildings, the lower heating demand values were obtained when one of the façades of the building began to face south [56].

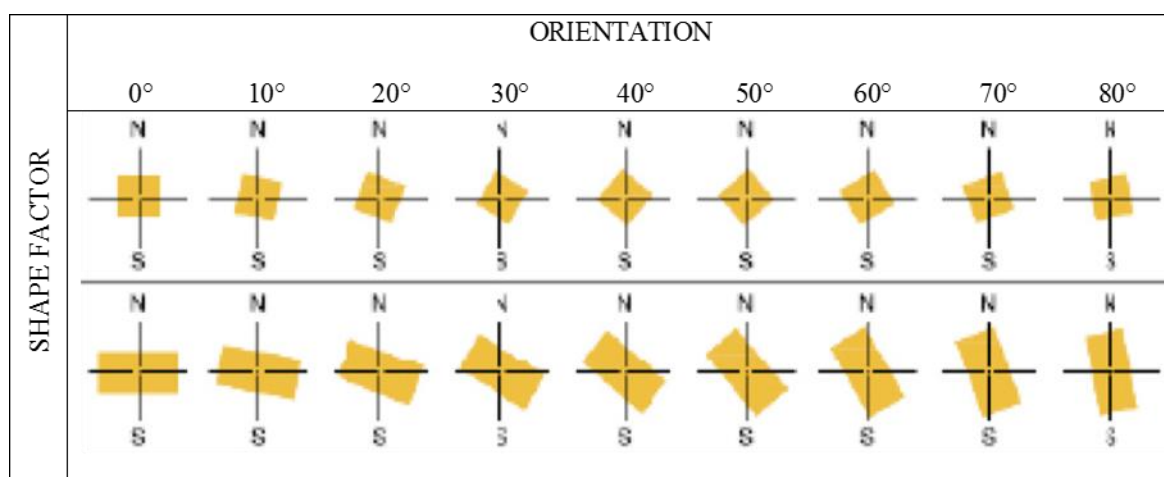


Fig.3.2 heating energy saving, depending on shape factor and orientation [56].

Orientation and shading devices

In winter, the sun entering through south-facing windows can positively contribute to solar passive heating, but increase the cooling demand in summer. The use of shading devices is an important passive solar design and can dramatically reduce these energy requirements. There are many different ways to control the amount of sunlight that is admitted into a house. From a passive solar viewpoint, the most effective method of shading is on the outside of the building using overhangs, fins, or louvers...etc.

The design of effective shading devices will depend on the orientation of the house. For south-facing window, the sun is high in summer, making it easy to block the sun with shading devices and it is naturally low in winter, allowing the radiation to penetrate below the shading devices and enter the house.

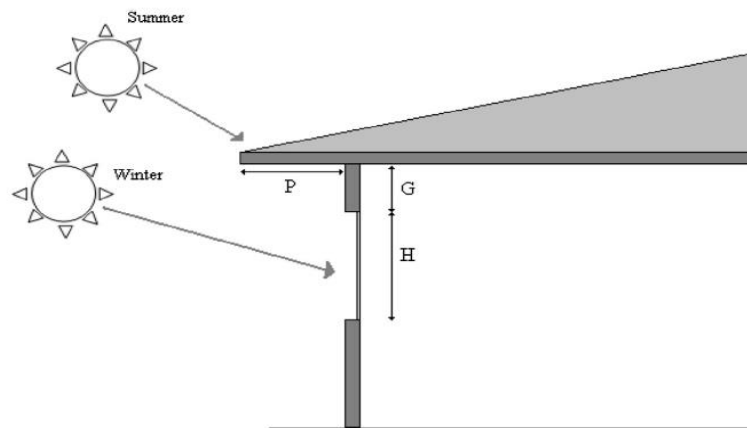


Fig.3.3 Effect of overhang on incident radiation through window.

For example, a simple fixed overhang can easily shade the south-facing windows in the cooling season, when sun angles are high, as shown in **Fig.3.3**. West windows may be the most problematic and there are few shading systems that will be effective enough to offset the potential for overheating from a large west-facing window. East windows catch the morning sun. Not enough to provide significant energy, but, unfortunately, usually enough to cause potential overheating problems in summer.

In rural housing, shading can be provided by natural landscaping as a mature tree, as shown in **Fig.3.4**. The deciduous trees allow sun to warm house in winter and provide shade in summer.

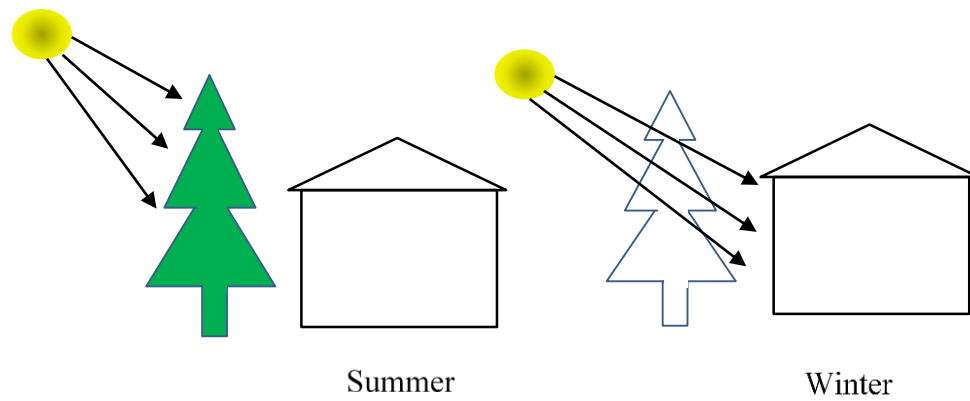


Fig.3.4. effect of deciduous trees

Orientation and window size

South-facing window is a key component of any passive solar system. Large area of glazing allows as much sunlight as possible into the house in winter. North windows in almost every climate lose significant heat energy and gain very little useful sunlight in the winter. In general, north-facing windows should not be large. Very large north-facing windows should have high insulation value.

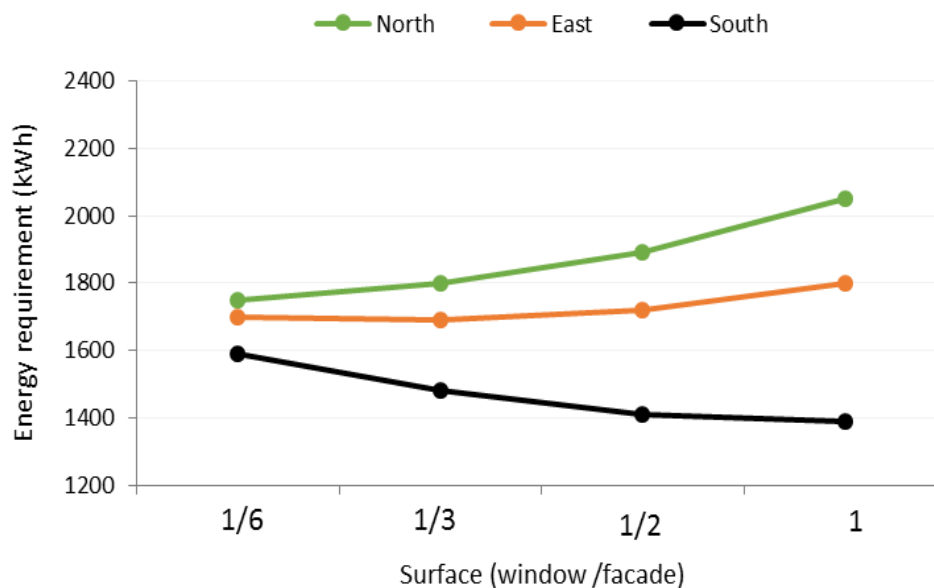


Fig.3.5. evolution of the heating requirement with window size [57].

As shown in **Fig.3.5**, the heating demand decreases significantly with the increase of the size of south-facing window. However, the increase of the size of the north-facing window increases the energy requirements.

3.2.2.2 Room placement inside building

A room layout was planned according to its function. **Fig.3.6** shows the placement of rooms in an efficient energy house. In general, living areas and other high-activity rooms should be located on the south side to benefit from the solar heat. The closets, storage areas, garage and other less-used rooms can act as buffers along the north side, but entryways should be located away from the wind. Kitchens should ideally be located within the house in such a way as to avoid over-heating. An ideal location for a kitchen is on the eastern side of the house. This catches the morning sun but not the warmer, late afternoon sun.

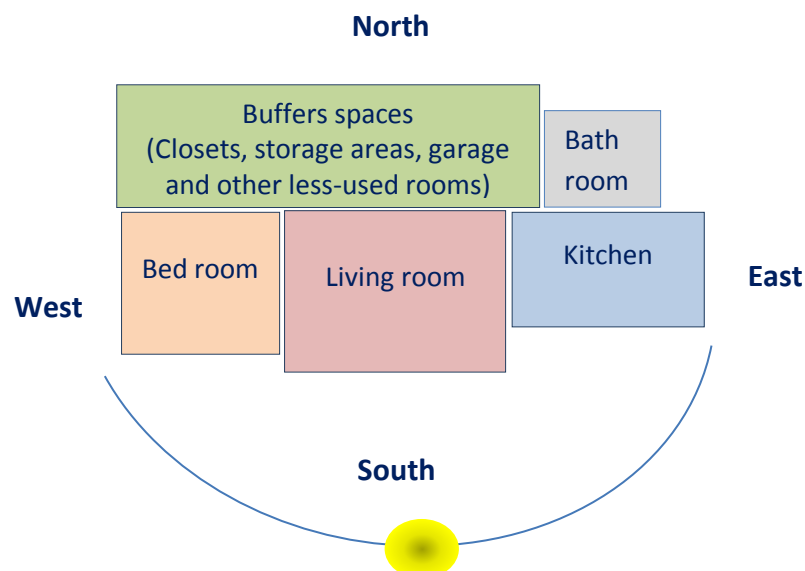


Fig.3.6. placement of rooms inside a house

3.2.2.3 Thermal mass

The amount of thermal mass determines how much of heat collected by south-facing window can be stored. The thermal mass in a passive solar system is usually a conventional construction material such as brick, cast concrete, concrete masonry, concrete slabs, or tile, and is usually placed in the floor or interior walls. The thermal storage capabilities of a given material depend on the material's conductivity, specific heat and density. Conductivity tends to increase with increasing density. Therefore, the major factor affecting performance is density. Generally, the higher the density the better.

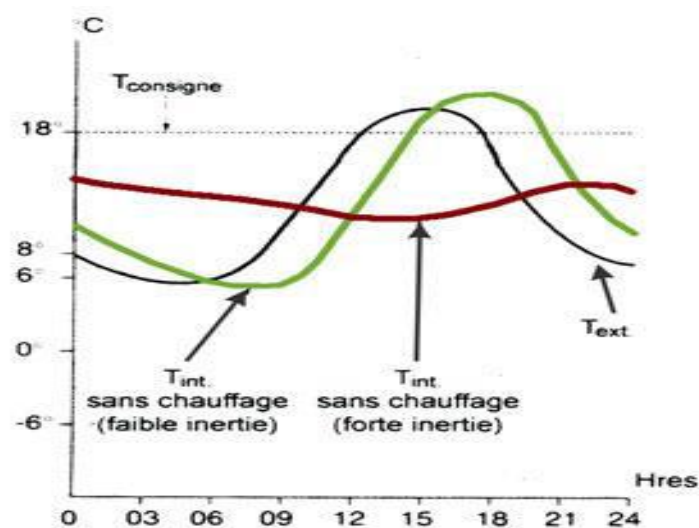


Fig.3.7. effect of the thermal mass on energy requirement in winter [58].

Fig.3.7 shows the effect of thermal mass of the house on the energy requirement for a sunny day in summer and **fig.3.8** for a sunny day in winter. As shown, in winter, high thermal mass stores the solar gains and shifting the peak of the indoor temperature later in the day, when the outside temperature is lower. A good thermal mass in summer is used to store the heat received during the day and release it at

night, when the outdoor temperature has cooled. This heat can be dissipated by night cooling.

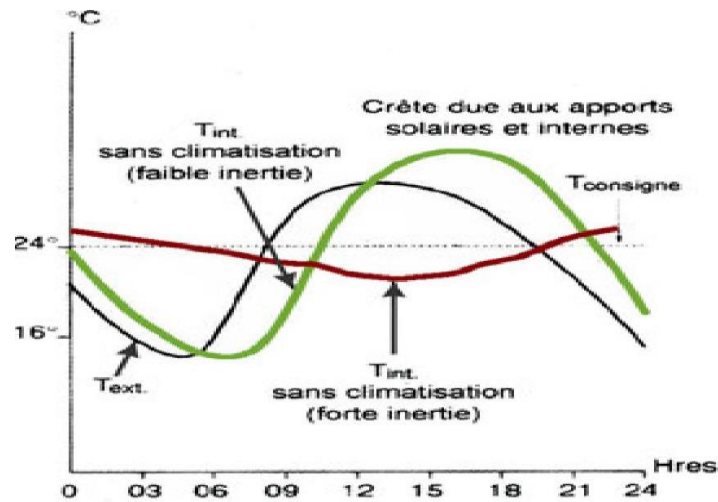


Fig.3.8. effect of the thermal mass on energy requirement in summer [58].

3.2.2.4 Thermal insulation

For an effective thermal mass, the house envelope must be insulated from the outside temperature. Appropriate insulation can mitigate heat loss in winter or gain in summer. As shown in **Fig.3.9** heat exits a non-insulated house quickly thus requiring more heating resource to keep a room comfortable.

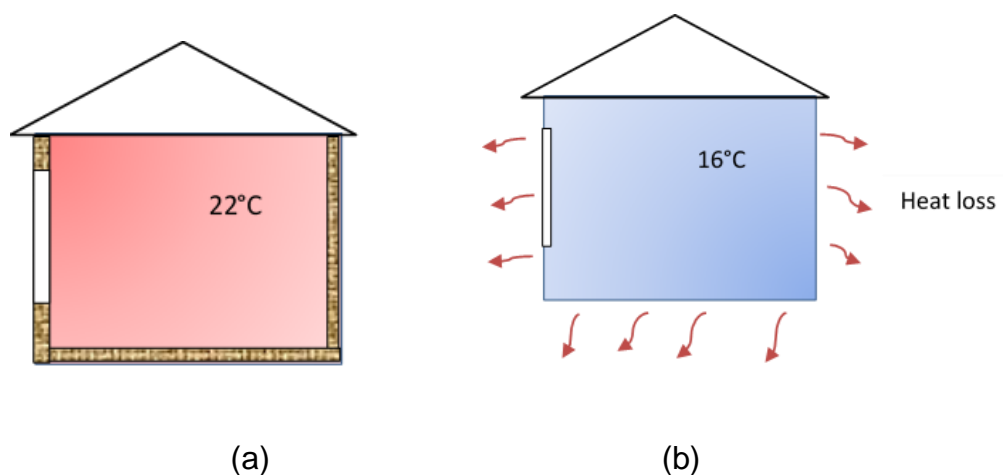


Fig.3.9. Difference between an insulated room (a) and no insulated room (b).

Adding thermal insulation to walls, floor, roof and foundation improves their thermal resistance (R-value). The types of insulation can be classified into four categories and respective subcategories depending on their material type as shown in **Fig.3.10**.

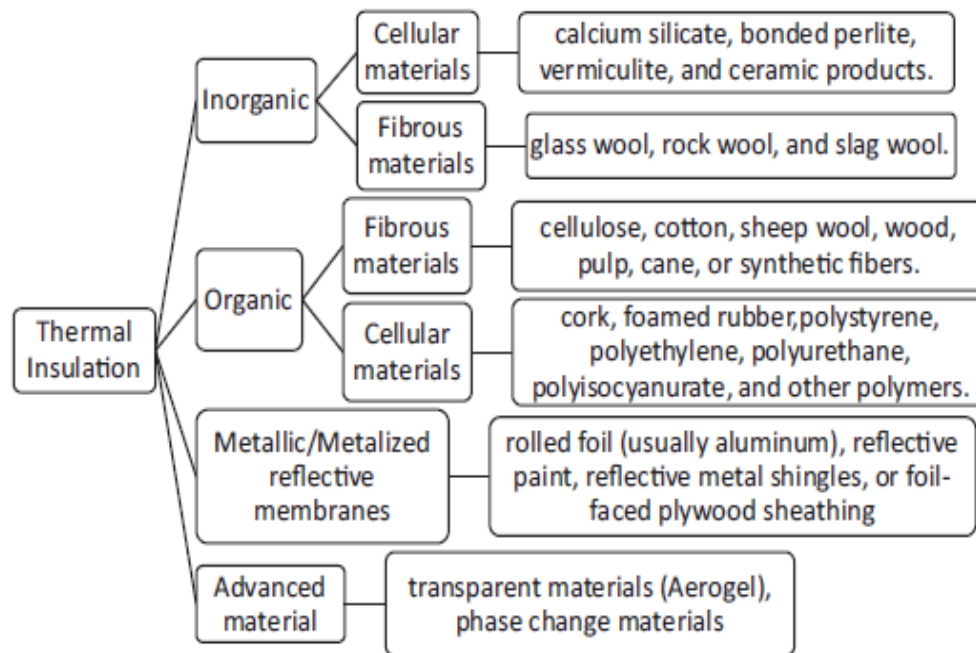


Fig.3.10. different types of thermal insulation [59].

Resent years, extrusion polystyrene (EPS) has been widely used and developed as thermal insulation material for exterior wall because of its choiceness characteristic, such as very low density of 28.8 kg/m³, high specific heat of 1213 J/kg K, and the extremely low thermal conductivity of 0.03 W/m K [60].

3.2.2.5 Glazing type

In winter, the transmittance for solar radiation should be as high as possible, but at the same time, they should provide relatively good thermal insulation. Triple glazing or double glazing with a low-e coating is recommended. A window's heat

transmittance is measured by U-factor. A smaller U-factor provides more insulating value than a larger one. The smaller the number, the better, as shown in **Fig.3.11**.

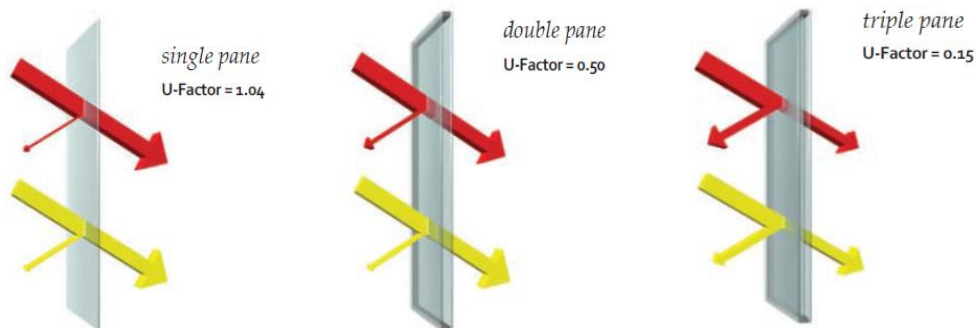


Fig.3.11. thermal quality of glass

3.2.2.6 Nocturnal ventilation

Sealing the house carefully to reduce air infiltration – air leakage - is as necessary to energy conservation as adding insulation. Air will flow rapidly through cracks and crevices in the wall, so even a small opening can allow heat to bypass the insulation and lead to big energy losses. The tightness of houses is generally measured in the number of air changes per hour (ACH). A good comfortable energy-efficient house will have approximately 0.35 to 0.50 air changes per hour under normal winter conditions [61]. In summer, increased ventilation at night can help remove heat that is stored in the house structure during the daytime to avoid high summer temperatures. This ventilation is applicable only in regions with high daytime temperature, and where the minimum night temperature in summer is lower than 20°C. The simplest passive strategies generally relies on good window design to allow ventilation at night.

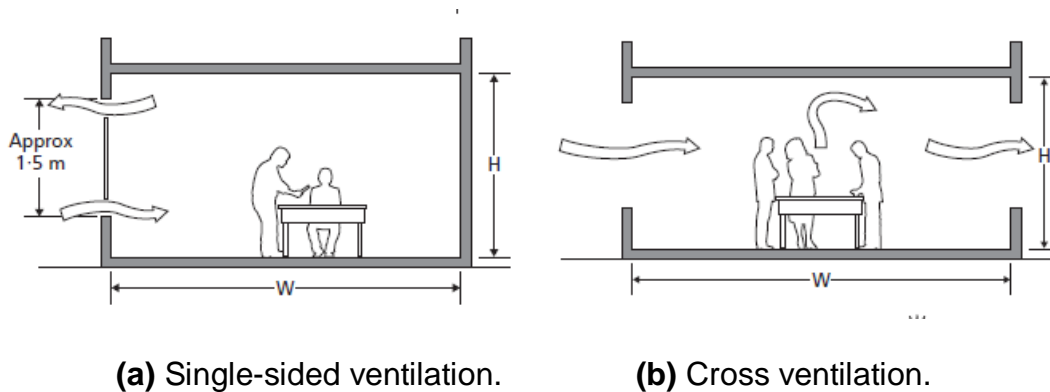


Fig.3.12. Nocturnal ventilation strategies.

Single-sided ventilation occurs when large windows are situated on only one external wall, (see **Fig.3.12 (a)**). Exchange of air takes place by wind turbulence, by outward openings interacting with the local external air streams and by stack effects driven by temperature difference. However, cross ventilation occurs when inflow and outflow openings in external walls have a clear internal flow path between them, as shown in **Fig.3.12 (b)**. Flow characteristics are determined by the combined effect of wind and temperature difference. Night ventilation in insulated buildings with high thermal response factors can reduce the maximum daytime temperatures by 2–3 °C [62].

3.3 Active solar systems

3.3.1. Solar heating systems

The most common use of thermal solar energy is for heating domestic hot water and it can also be used to heat water for both domestic hot water and space heating. These later called “Solar combisystem”. One of the most comprehensive studies on solar combisystem was performed within the frame of IEA-SHC-Task 13 and 26 (IEA 2007) by comparing 21 different configurations [63]. The optimization of nine selected systems under the same climatic reference conditions were performed by

computer simulations using TRNSYS program. A solar combisystem can be represented globally, as shown in **Fig.3.13**.

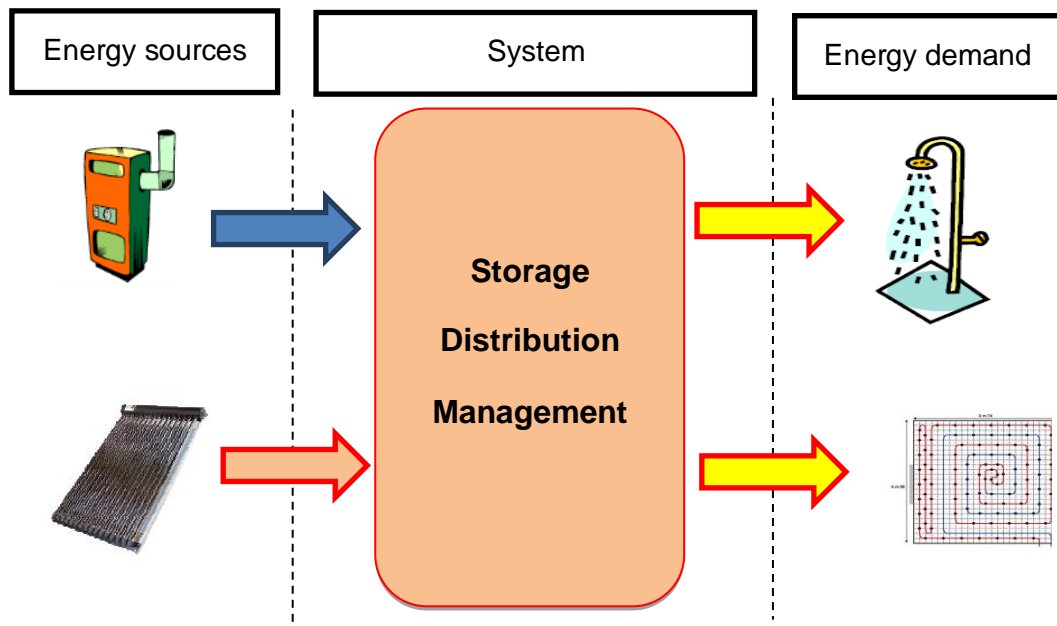


Fig.3.13. Main components of a solar combisystem [64].

3.3.1.1 Solar thermal collectors

Thermal collectors used in building are classified into two main types of thermal collector, flat-plate and evacuated collectors. The key element of both flat plate and evacuated tube collectors is the absorber. This is the surface, usually flat, on which the solar radiation falls and which incorporates tubes or channels through which the heat transfer fluid can circulate.

Flat-plate collector

Fig.3.14 shows the main components of a flat-plate collector. The flat-plate collectors applications are heating, domestic hot water (dwellings and commercial

buildings) and indoor swimming pools (temperature between 20°C and 70°C and low efficiency under low irradiation).

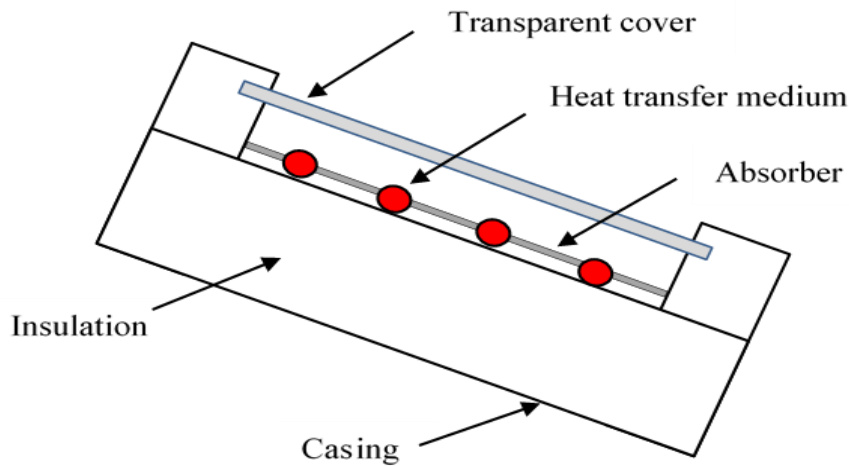


Fig.3.14. flat-plate collector

Evacuated tube collectors

Fig. 3.15 shows the main components of an evacuated tube collector. Evacuated tube collectors are generally more efficient than flat plate collectors, but are also more expensive as they are more sophisticated devices. Their increased efficiency results from mounting the absorber in an evacuated and pressure-proof glass tube, which reduces conductive and convective losses. They work efficiently at low radiation levels and with high absorber, temperatures and can provide higher output temperatures than flat plate collectors. Evacuated tube collectors can be used in applications where the demand temperature is 60–150 °C (DHW heating, domestic and commercial, swimming pool heating, cooling (using absorption chillers or desiccants)).

3.3.1.2. Storage tank

The aim of the water tank is to store the thermal energy provided by the solar collectors. Also, thermal energy is extracted when needed from the tank and

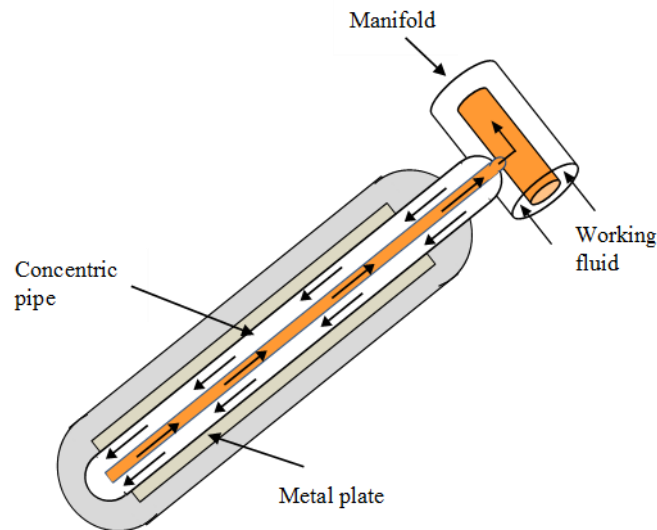


Fig.3.15. Evacuated tube collector.

transported as hot water to the user. There are two types of solar storage tanks based on the thermal stratification, fully stratified water tanks and fully mixed water tanks.

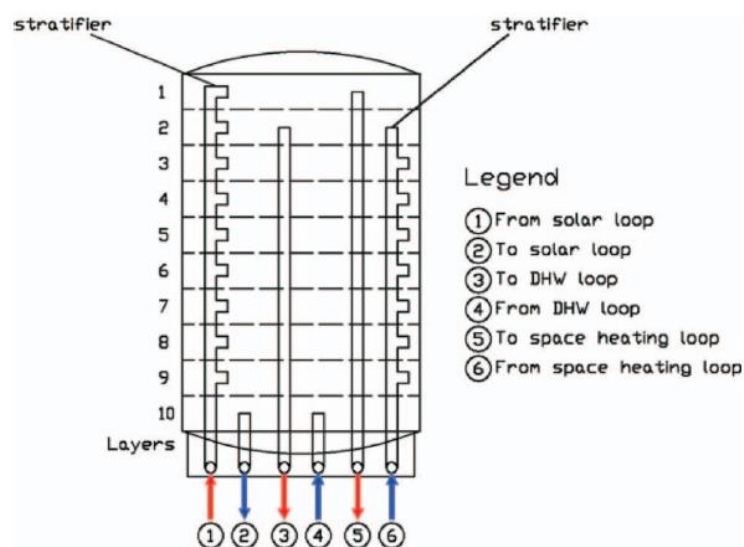


Fig.3.16. schematic of the stratified storage tank [63]

The fully mixed storage tank is very popular than the stratified tank. **Fig.3.16.** shows an example of a stratified tank with two inlet stratification devices, one for the solar loop and one for the return loop. The task of these devices is to feed the incoming water in a layer with a temperature approximately similar to the one of the incoming water [65]. The degree of thermal stratification in the storage tank is a critical element for achieving high performance.

3.3.1.3 Heating floor system

Heating floor system are widely used to provide low temperature heating in houses. The concrete floor slabs store heating by means of hot circulating through the embedded water tubing inside the slab, as shown in **Fig 3.17.** Thus, the building structure is utilized for storing thermal energy in order to release it when required. The large heat transferring surface of the slab makes it possible to transfer considerable amounts of heat to the occupied spaces. The water supply temperature needs to be around 5°C above the desired indoor air temperature. The heat stored in the concrete core is transferred to the room during several hours - 60% via radiation and 40% via convection [66].

The water, which is supplied in slab, is in the beginning at its maximum temperature and as it travels through the circuit in slab the temperature is reduced due to conduction from the water to the concrete slab and eventually to the heated space through convection and radiation. Supply water temperature, water flow rate, span of the slab, circuit or tubing length within slab affect the temperature drop.

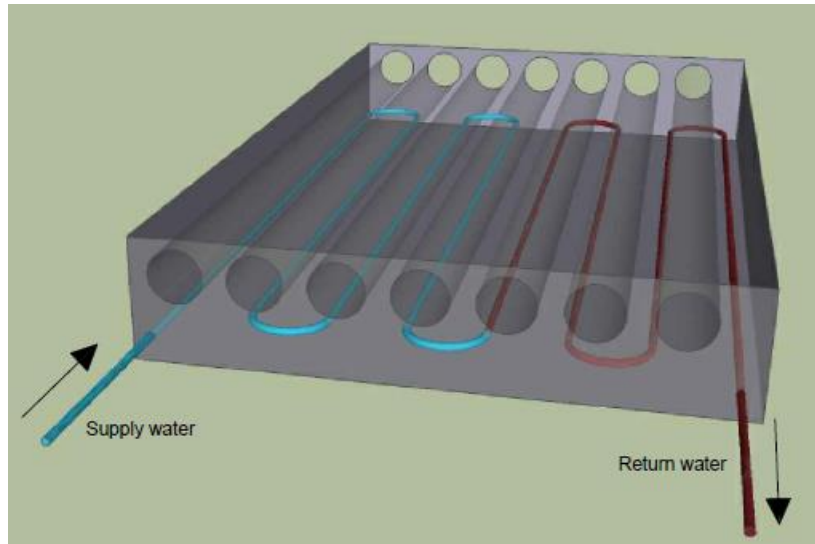


Fig.3.17. Tubing configuration in a concrete floor slabs.

3.3.2. Photovoltaic systems

Photovoltaic systems are solar energy supply systems, which convert sunlight directly to electricity. The main component in PV systems is the solar panel. Putting together several PV cells forms a PV module; several modules form arrays and several arrays form panels. Solar cells are usually made of semiconductor materials such as silicon, gallium arsenide, cadmium telluride or copper indium diselenide. The power output of a PV system depends on the irradiance on the PV cells, the efficiency of PV cells used and its effective area. Photovoltaic systems can be grouped into two main groups; namely off-grid systems and grid-connected systems.

3.3.2.1 Off-grid PV system

Off-grid systems are systems that are not connected to the public electricity grid. These systems require an energy storage system for the energy generated because the energy generated is not usually required at the same time as it is generated.

These systems are used in areas where it is not possible to install an electricity supply from the mains utility grid, as shown in **Fig.3.18**.

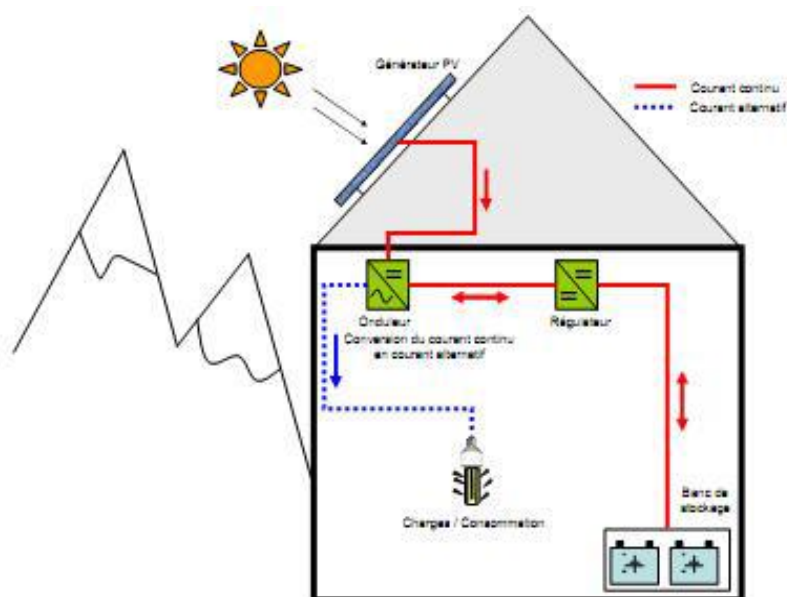


Fig.3.18 Stand-alone PV system [67]

A typical off-grid system comprises the following main components:

- Solar PV Modules: these convert sunlight directly to electricity.
- Charge Controllers: manage the charging and discharging of the batteries in order to maximize their lifetimes and minimize operational problems
- Battery or Battery Bank: Stores the energy generated by the PV modules
- Inverter: converts the DC current generated by the solar PV modules to AC current for AC consumer load.

3.3.2.2 Grid-connected PV system

A grid-connected PV system is an electricity generating solar PV system that is connected to the utility grid. In this case, the generated electrical energy is

consumed in the house, excess electrical energy can be sent to the electricity grid. When there is electrical energy shortage in the house, the electricity grid supplies the house with electrical energy, as shown in **Fig 3.18**.

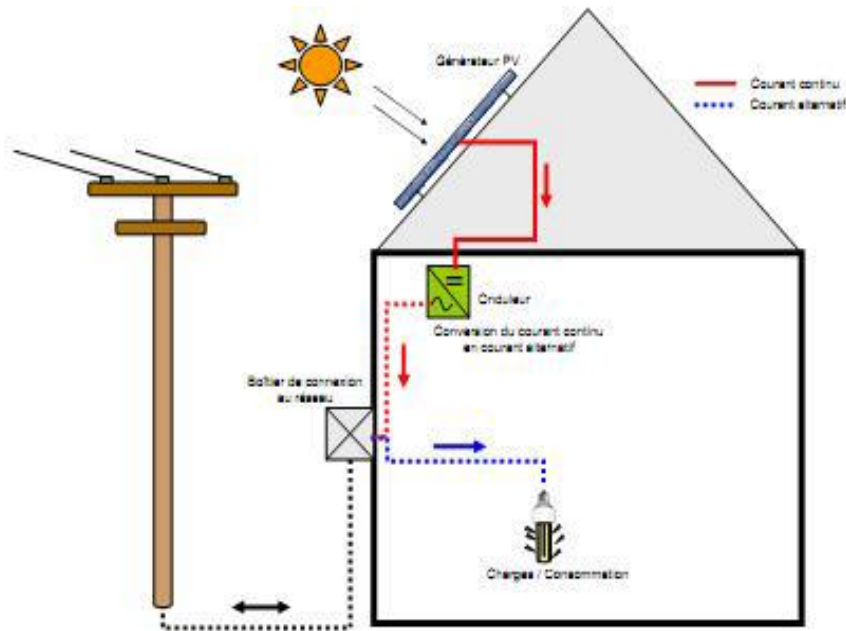


Fig.3.18 Grid-connected PV system [67]

A typical grid-connected PV system comprises the following components:

- Solar PV Modules: these convert sunlight directly to electricity.
- Inverter: converts the DC current generated by the solar PV modules to AC current for the utility grid.
- Main disconnect/isolator Switch
- Utility Grid

3.4 Conclusion

In the present chapter, passive and active solar applications in rural housing in Algeria has been discussed. Through this study, it can be detected that the intention behind incorporating passive solar design is to reduce the need for energy consumption for heating and cooling. The basic elements of passive solar design are optimal shape and orientation of the house, use of an efficient window type and large window size toward south, insulation of the house envelope and use of shading device and application of nocturnal ventilation in cooling season.

Furthermore, the use of active solar systems can contribute significantly in energy supply of the house. A thermal solar system for produce heat for DHW and space heating and a grid-connected PV system for the electrical energy.

***Chapter 4: Modelling of a residential house
coupled with solar systems***

4.1. Introduction

A large number of simulation softwares concerning thermal building simulation exist today. It's a powerful tool for studying the thermal performance of building and its HVAC system and predicting the thermal comfort of its occupants. The most applicable in the building thermal performance simulation are DPV (Design Performance Viewer), Design Builder, Ecotect, EnergyPlus, eQUEST, EcoDesigner, ESP-r, Green Building Studio, Lesosai, IDA ICE, IES VE, TRACE700, TRNSYS and Riuska [68]. The building geometry, including the layout and configuration of the space (surfaces, volumes, building orientation, building construction (thermal characteristics of components), internal loads and schedules for lighting, occupants, and equipment, heating, ventilating, and air conditioning (HVAC) system type and whether data (solar radiation, temperature, speed air) constitute the basic input for thermal simulation. The output data or simulation result may include overall estimate of the energy performance of the building and an overall estimate of the energy cost. The main aim of this chapter is to give a concise overview of the model used in this work. We start with a short presentation of TRNSYS simulation environment. Then, a detail mathematical description of the components that constitute the complete model is performed. The model includes a multi-zone house coupled with solar heating system and a grid-connected PV system.

4.2. Presentation of TRNSYS software

TRNSYS is an acronym that stands for TRAnSient SYstem Simulation program, which is a transient simulation package developed by the Solar Energy Laboratory, University of Wisconsin and it is written in ANSI standard Fortran-77. It is one of the most known and widely used software in thermal building simulation [69-74]. It is a

software package designed to simulate the transient behavior of thermal energy systems. Users simulate complex systems in TRNSYS by selecting system components and linking together their inputs and outputs. It has been used for more than 30 years for heating, ventilation, and air conditioning (HVAC) analysis and sizing, multi-zone airflow analyses, electric power simulation, solar design, building thermal performance, and analysis of home control schemes. It is based on the black box model (see **Fig. 4.1**), the user only needs to define the static and the input parameters, and can obtain the required results through the TRNSYS program.

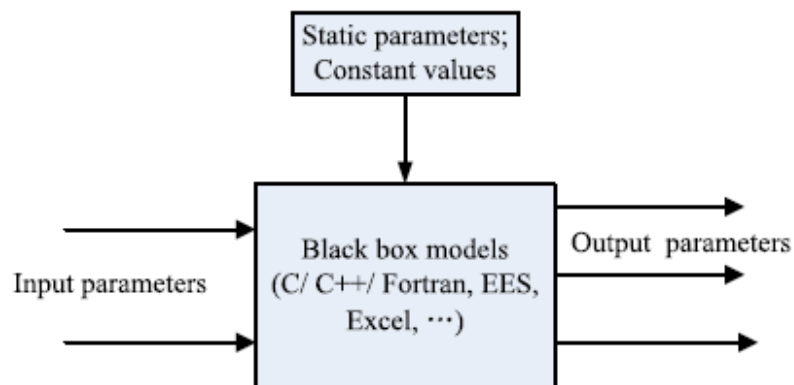


Fig.4.1. the black box model in the TRNSYS program [70]

In TRNSYS each component of the solar thermal system is described by an algorithm which is programmed in FORTRAN (in the standard Library), called Type. The user has access to the code of each type. New algorithms characterizing new system components can be developed and constitute users own Types.

4.3. Description of the model

A single-family residential house coupled with solar systems is modeled in this study, as shown in **Fig.4.2**. The solar systems include a solar heating system, using a flat-

plat collector and fully mixed thermal storage tank, for domestic hot water (DHW) and space heating requirements, and a grid-connected photovoltaic system for electricity supply. The solar heating system is coupled with the house through a floor heating.

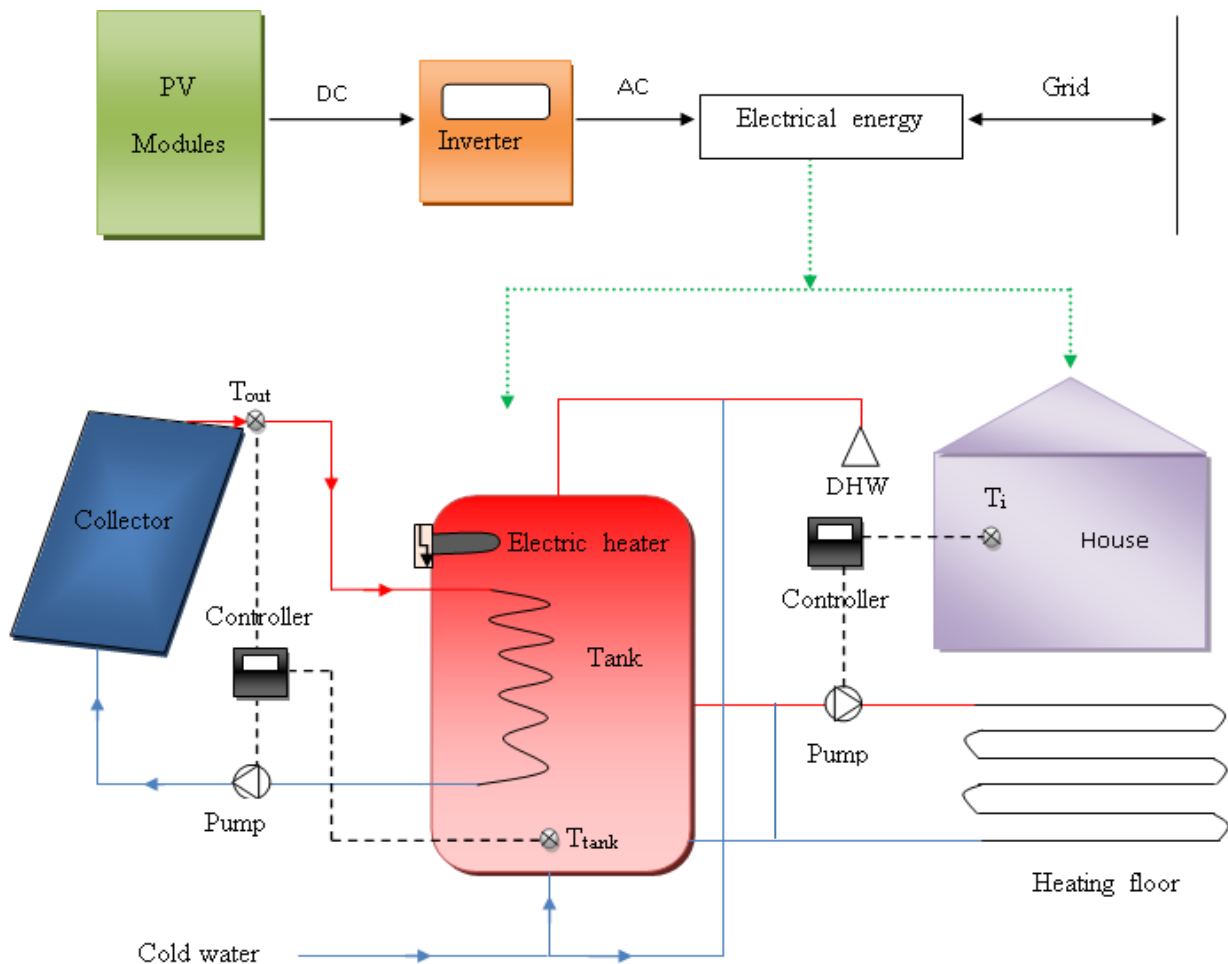


Fig.4.2. the house, its heating system, and PV system under investigation

TRNSYS simulation process is shown in **Fig. 4.3.** Numbers of inputs are required such as; solar radiation, sky and ground temperatures, wind speed...etc.

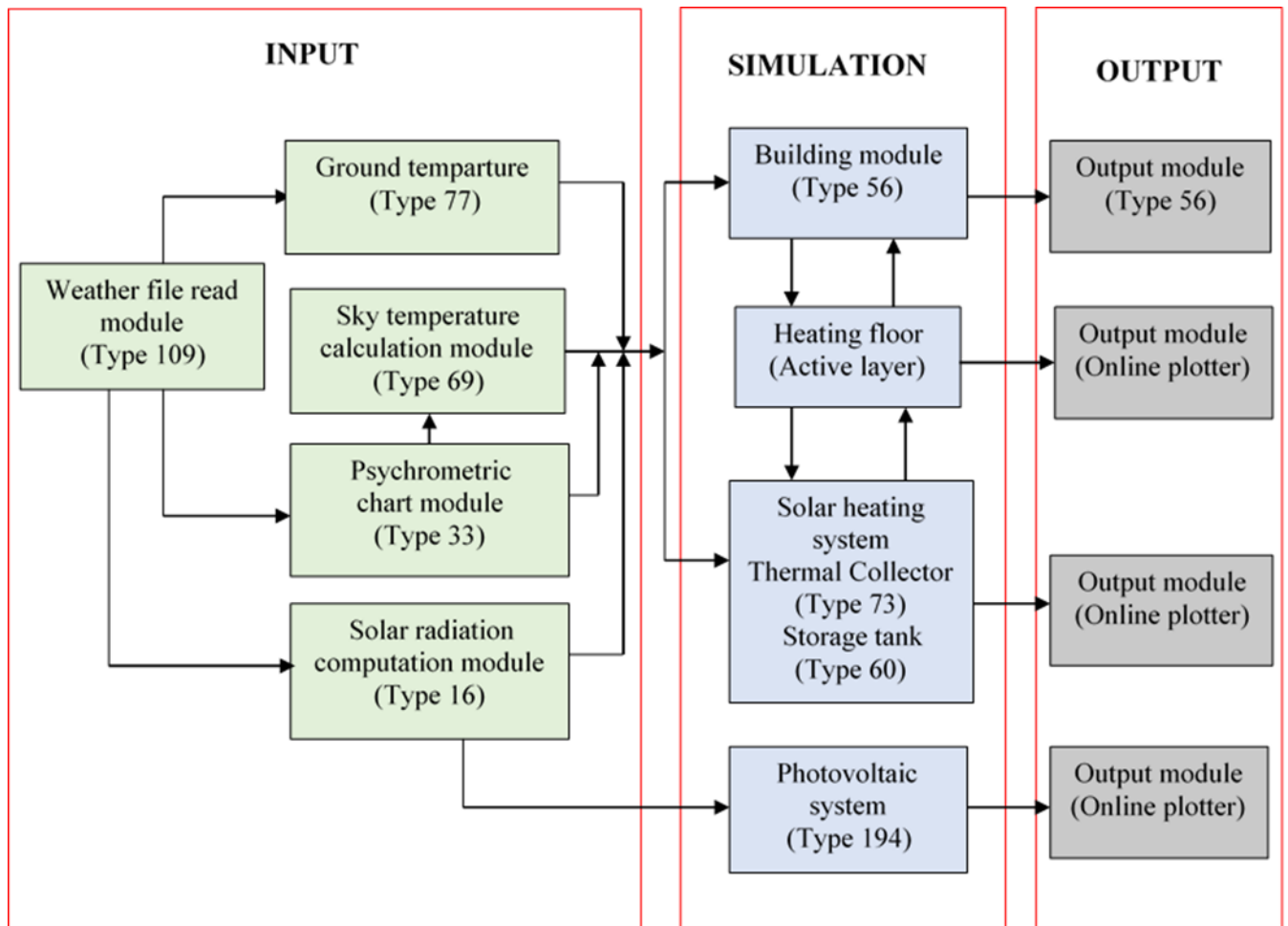


Fig.4.3. TRNSYS simulation process

4.4. Modelling of solar radiation

Estimation of solar radiation on a tilted surface is usually required for building modelling and solar energy systems simulations.

4.4.1. Solar angles

Solar declination

The solar declination, δ , in degrees for any day of the year (n) can be calculated approximately by following equation

$$\delta = 23.45 \times \sin \left[\frac{360}{365} \times (284 + n) \right] \quad (4.1)$$

Hour angle

The hour angle is the angular displacement of the sun east or west of the local meridian due to rotation of the earth on its axis at 15° per hour; morning negative, afternoon positive. The hour angle can also be obtained from the apparent solar time (AST):

$$\omega = (AST - 12) \times 15^\circ \quad (4.2)$$

Solar zenith angle

The zenith angle is the angle between the vertical and the line of sight of the sun. This is 90 minus the angle between the sun and the horizontal .

$$\cos\theta_z = \sin \alpha = \sin\phi \times \cos\delta + \cos\phi \times \cos\delta \times \cos\omega \quad (4.3)$$

Solar azimuth angle

The solar azimuth angle is the angle between the local meridian and the projection of the line of sight of the sun onto the horizontal plane. Zero solar azimuth is facing the equator, west is positive, while east is negative.

$$\sin\gamma_s = \frac{\cos\delta \times \sin\omega}{\sin\theta_z} \quad (4.4)$$

Angle of incidence

The solar incidence angle is the angle between the sun's rays and the normal on a surface. The angle of incidence is given by the following general expression:

$$\cos\theta = \cos\theta_z \times \cos\beta + \sin\theta_z \times \cos(\gamma_s - \gamma) \times \sin\beta \quad (4.5)$$

In the above equation:

β is the slope of the surface defined as the angle between the surface and the horizontal.

γ is the azimuth angle or the angle between the projection of the normal to the surface into the horizontal plane and the local meridian. The azimuth angle is 0° for south façade, 90° for west façade, -90° for east façade and 180° for north façade.

4.4.2. Solar radiation on horizontal surface

There are several methods for obtaining beam and diffuse radiation on a horizontal surface from total radiation on a horizontal surface data. The model used in this study to estimate the total tilted surface radiation require knowing the division of total horizontal radiation into its beam and diffuse components.

In Type 19, the estimation of horizontal radiation is based on the relationships developed by Reindl [75]. Two methods are presented. In the first method, the relationship uses the clearness index and the solar altitude angle to estimate the diffuse fraction.

The correlation is given by the following equations:

$$\begin{aligned} &\text{--For } 0 \leq K_T \leq 0.3 \text{ and } I_d/I \leq 1.0 \\ \frac{I_d}{I} &= 1.020 - 0.254 K_T + 0.0123 \sin(h) \end{aligned} \quad (4.6)$$

$$\begin{aligned} &\text{--For } 0.3 < K_T < 0.78 \text{ and } 1.0 \leq I_d/I \leq 0.97 \\ \frac{I_d}{I} &= 1.400 - 1.749 K_T + 0.177 \sin(h) \end{aligned} \quad (4.7)$$

$$\begin{aligned} &\text{--For } 0.78 < K_T \text{ and } 1.0 \leq I_d/I \\ \frac{I_d}{I} &= 0.486 K_T - 0.182 \sin(h) \end{aligned} \quad (4.8)$$

An hourly clearness can be defined:

$$K_T = \frac{I}{I_0} \quad (4.9)$$

The extraterrestrial radiation on horizontal surface by an hour period (between hour angles h_1 and h_2) is given by the following equation:

$$I_0 = \frac{12 \times 3600 G_{sc}}{\pi} \left[1 + 0.033 \cos \left(\frac{360N}{365} \right) \right] \\ \times \left[\cos(L) \cos(\delta) \sin(h_2 - h_1) + \left(\frac{\pi(h_2 - h_1)}{180} \right) \sin(L) \sin(\delta) \right] \quad (4.10)$$

Where, G_{sc} is the solar constant (W/m^2) and h_2 is larger than h_1 .

For the above horizontal radiation relationships, beam radiation on a horizontal surface is calculated by the difference between the total radiation and the diffuse component.

$$I_b = I - I_d \quad (4.11)$$

4.4.3. Solar radiation on tilted surface

The ratio of beam radiation on a tilted surface to that on a horizontal surface is calculated by:

$$R_b = \frac{\cos \theta}{\cos \theta_z} \quad (4.12)$$

Once R_b is found, the beam radiation on a titled surface is given by:

$$I_{bT} = I_b \times R_b \quad (4.13)$$

The contribution of reflected radiation on a tilted surface is calculated by assuming the ground acts as an isotropic reflector and defining R_r as the ratio of reflected radiation on a tilted surface to the total radiation on a horizontal surface is:

$$R_r = 0.5(1 - \cos\beta)\rho_g \quad (4.14)$$

Thus,

$$I_{gT} = IR_r \quad (4.15)$$

The contribution of diffuse radiation on a tilted surface is determined by using the isotropic sky model.

The isotropic sky model assumes that the diffuse radiation is uniformly distributed over the complete sky dome. A factor R_d , the ratio of diffuse radiation on a tilted surface to that on a horizontal, is given by:

$$R_d = 0.5 \times (1 + \cos\beta) \quad (4.16)$$

Thus the diffuse radiation on a tilted surface assuming isotropic sky is:

$$I_{dT} = I_d \times R_d \quad (4.17)$$

Thus, the total radiation on tilted surface is given by the following equation:

$$I_T = I_{dT} + I_{bT} + I_{gT} \quad (4.18)$$

The solar radiation incident on the house envelope is calculated using the following angles:

The slope angle $\beta=0^\circ$ for horizontal surface and $\beta=90^\circ$ for vertical surface.

The azimuth angle is 0° for south façade, 90° for west façade, -90° for east façade and 180° for north façade.

4.5. Mathematical description of the house model

A multi-zone house model, Type 65, is used to simulate the heating and cooling demand of the house. Detailed theories about this component is presented in TRNSYS user manual [76]. The building model in Type 56 is a non-geometrical balance model with one air node per zone, representing the thermal capacity of the zone air volume and capacities that are closely connected with the air node. AS shown in **Fig.4.4** house characteristics (orientation, thermal characteristics of components etc.), air infiltration and internal thermal gains, are the main inputs of type 56.

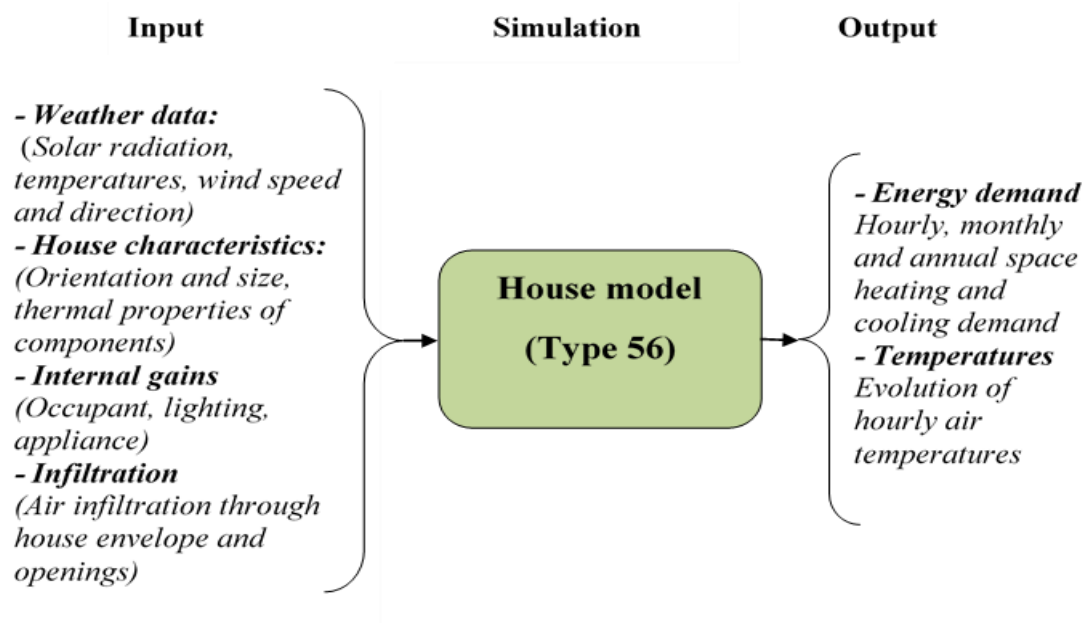


Fig.4.4. input and output of house model (Type 56)

4.5.1. Energy balance of a thermal zone

Considering that, the rate of change of internal energy for thermal zone is equal to the net heat gain; the overall energy balance can be illustrated as follows:

$$\dot{Q} = \dot{Q}_{surf} + \dot{Q}_{inf} + \dot{Q}_{vent} + \dot{Q}_{gain} + \dot{Q}_{cplg} \quad (4.19)$$

Where

Q_{surf} – convective heat flow from all inside surface

$$Q_{surf} = h_c \rho_a c_a (T_{s,i} - T_i) \quad (4.20)$$

Q_{inf} – infiltration gain from outside air flow

$$Q_{inf} = \dot{m}_{inf} \rho_a c_a (T_o - T_i) \quad (4.21)$$

Q_{vent} – ventilation gains from HVAC system

$$Q_{vent} = \dot{m}_{vent} \rho_a c_a (T_{vent,i} - T_i) \quad (4.22)$$

Q_{gain} – internal convective gains (occupancy, lighting and appliance)

$$Q_{gain} = h_c \rho_a c_a (T_s - T_i) \quad (4.23)$$

Q_{cplg} – gains due to convective air flow from zone or boundary condition

$$Q_{cplg} = \dot{m}_{j \rightarrow i} \rho_a c_a (T_{zone,i} - T_i) \quad (4.24)$$

4.5.2. Modelling of heat conduction through house envelope

Conduction heat transfer through the building envelope is one of the principal components of space cooling/heating loads and energy requirements.

The equation that governs the heat transfer through a homogeneous material can be expressed by:

$$\rho c \frac{\partial T}{\partial t} - \nabla \cdot k \nabla T - \dot{q} = 0 \quad (4.25)$$

Where ρ , c and k are respectively the density (kg m^{-3}), specific heat ($\text{kJ kg}^{-1}\text{K}^{-1}$) and thermal conductivity ($\text{kWm}^{-1} \text{K}^{-1}$) of the material; T is the temperature (K) and q the net rate of heat gain from the internal source or sink within the material (kWm^{-3}); and t is time (s).

In building simulation, conduction heat transfer is usually modeled as a one dimensional, transient process with constant material properties. **Eq. (25)** can be simplified to a one-dimensional partial differential equation (PDE) governing the transient heat conduction in a homogeneous slab with no internal heat source or sink.

$$\frac{\partial T(x,t)}{\partial t} = a \frac{\partial^2 T(x,t)}{\partial x^2} \quad (4.26)$$

Where: $a=k/pc$ is the thermal diffusivity of material.

Eq. (26) is usually solved numerically, often by means of conduction transfer function methods. TRNSYS heat transfer calculations are based on the transfer function methodology that has been introduced by Stephenson and Mitalas (1971) [77]. The walls, roofs and floors are modeled according to the transfer function relationships of Mitalas and Arseneault [78] defined from surface to surface. The transfer function links the present heat flux to the past and present surface temperature. For any wall, the heat conduction at the surfaces are:

For internal surface:

$$q_{s,i} = \sum_{k=0}^{n_{b_s}} b_s^k \cdot T_{s,0}^k - \sum_{k=0}^{n_{c_s}} c_s^k \cdot T_{s,i}^k - \sum_{k=0}^{n_{d_s}} d_s^k \cdot q_{s,i}^k \quad (4.27)$$

For external surface

$$q_{s,o} = \sum_{k=0}^{n_{a_s}} a_s^k \cdot T_{s,o}^k - \sum_{k=0}^{n_{b_s}} b_s^k \cdot T_{s,i}^k - \sum_{k=0}^{n_{d_s}} d_s^k \cdot q_{s,o}^k \quad (4.28)$$

These time series equations in terms of surface temperatures and heat fluxes are evaluated at equal time intervals. K refers to the term in time series (current time $k=0$, previous time $k=1$, etc.). The time-base on which these calculations are based is specified by the user. The coefficients of the time series (a's, b's, c's, and d's) are determined from the material layers properties of the wall (i.e. thermal conductivity, capacity, density and thickness) using the z-transfer function algorithm of reference [78]. A detailed example for the calculation method of these coefficients is performed.

4.5.3. Heat fluxes at surfaces of an exterior wall

Fig.4.5 shows the heat fluxes and temperatures that characterize the thermal behavior of any wall or window.

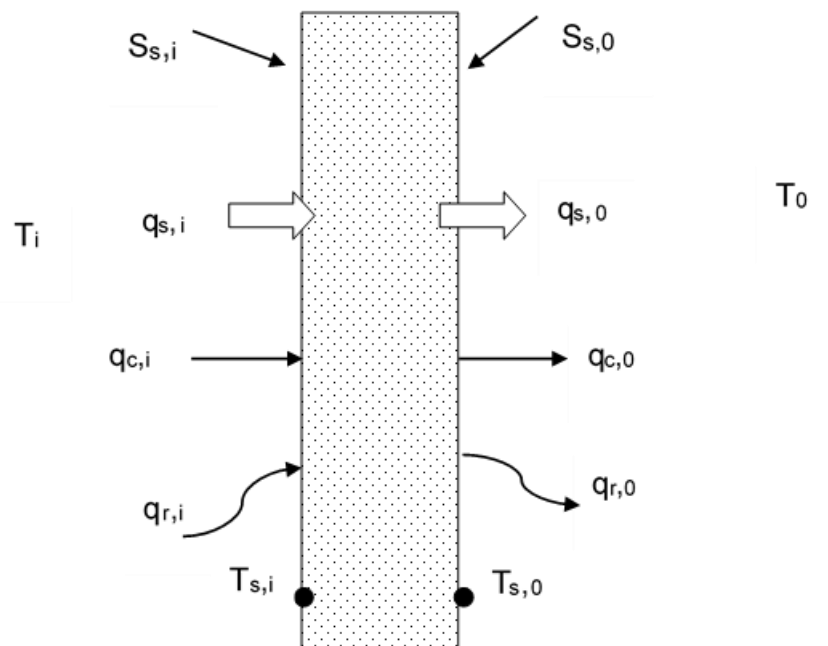


Fig.4.5 Heat transfer at an external wall

The long-wave radiation exchange between the surfaces within the zone and the convective heat flux from the inside surfaces to the zone air are approximated using the star network given by Seem [79]. This method uses an artificial temperature node (T_{star}) to consider the parallel energy flow from a wall surface by convection to the air node and by radiation to other wall and window elements, as shown in Fig.4.6. Detail of this method can be found in (see Annex A).

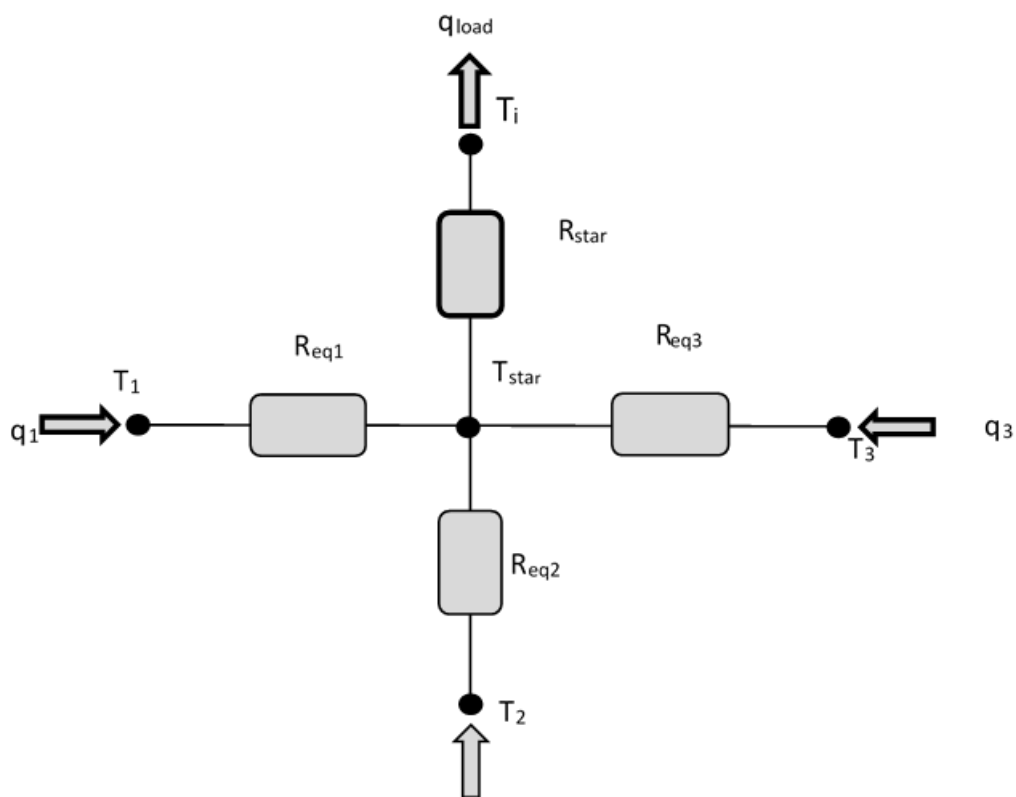


Fig.4.6. star network for a zone with three surfaces.

Using of the concept of the star temperature, the convective heat flux to the zone air can be expressed as follows:

$$\dot{Q}_{surf,i} = \frac{1}{R_{star,i}} (T_{star} - T_i) \quad (4.29)$$

The energy balance at the internal surface give

$$q_{s,i} = q_{comb,s,i} + S_{s,i} \quad (4.30)$$

The star temperature can be used to calculate the combined radiative and convective heat flux from the inside wall surface as follows:

$$q_{comb,s,i} = q_{r,i} + q_{c,i} \quad (4.31)$$

Then,

$$q_{comb,i} = \frac{1}{R_{eq,i} A_i} (T_{s,i} - T_{star}) \quad (4.32)$$

Where, A_i is the inside surface area.

The energy balance at the external surface gives :

$$q_{s,o} = q_{comb,s,o} + S_{s,o} \quad (4.33)$$

For external surfaces, the long-wave radiation exchange at the outside surface is considered explicitly using a fictive sky temperature, T_{sky} , and a view factor to the sky, f_{sky} , for each external surface. The total heat transfer is given as the sum of convective and radiative heat transfer:

$$q_{comb,s,o} = q_{r,o} + q_{c,o} \quad (4.34)$$

The convection heat flux to the outside surface from the boundary/ambient,

$$q_{c,o} = h_{c,o} (T_{sa} - T_{s,o}) \quad (4.35)$$

The net radiative heat transfer with all surfaces in view of the outside surface,

$$q_{r,o} = \varepsilon_{s,o} (T_{s,o}^4 - T_{fsky}^4) \quad (4.36)$$

$$T_{fsky} = (1 - f_{sky})T_o + f_{sky}T_{sky} \quad (4.37)$$

4.5.4. Heat gain from inside surface of an exterior wall

The inside surface heat flux for an external wall as a function of the boundary air temperatures can be expressed according to the following transfer function relationship. This is the combination of equations from (27) to (37).

$$\dot{q}_{s,i} = B_s T_{a,s} - C_s T_{a,s} - D_s \quad (4.38)$$

Where

$$B_s = \frac{e_s h_{s,o}}{(1 - f_s)}$$

$$C_s = \frac{f_s}{(f_s - 1)} \left(\frac{1}{R_{eq,i} A_{s,i}} \right)$$

$$D_s = \frac{f_s S_{s,i} + e_s (S_{s,o} - K_{s,o}) + K_{s,i}}{(1 - f_s)}$$

$$e_s = \frac{b_s^0}{a_s^0 + h_{s,o}}$$

$$f_s = (b_s^0 e_s - c_s^0) R_{eq,i} A_{s,i}$$

The values for $K_{s,i}$ and $K_{s,o}$ are defined by the transfer function equations (27) and (28).

The sol-air temperature, $T_{a,s}$, is the temperature of the outdoor air which, in the absence of all radiation exchanges, would give the same heat transfer at the outside surface as actually occurs. For a vertical wall, it is generally expressed as:

$$T_{sa,i} = T_o + \frac{(\alpha I_T)}{h_{c,o}} \quad (4.39)$$

4.5.5. Heat gains from internal and adjacent walls

For walls adjacent to another zone, internal walls, **Eq.38** applies, but with: $T_{a,s} = T_{star,j}$ for adjacent wall and $T_{a,s} = T_{star,i}$ for internal wall.

And

$$B_s = \frac{e_s}{(1 - f_s)} \left(\frac{1}{R_{eq,j} A_{s,j}} \right)$$

$$e_s = \frac{b_s^0}{a_s^0 + \frac{1}{R_{eq,j} A_{s,j}}}$$

4.5.6. Total gains from surfaces in a Zone

The total gain to zone i from all surfaces is the sum of the combined heat transfers:

$$\begin{aligned} \dot{Q}_{surf,i} = \sum A_s \dot{q}_{comb,i} = & \sum_{j=1}^{Adj.Zones} \sum_{i=1}^{surface\ i\ to\ j} A_s B_s T_{star,j} + \sum_{surfaces}^{ext.} A_s B_s T_a + \\ & \sum_{int.walls} A_s B_s T_{star} + \sum_{bound}^{known.} A_s B_s T_{b,s} - \sum_{in\ zone\ i}^{surface} A_s (C_s T_{star,i} - D_s - S_{s,i}) \quad (4.40) \end{aligned}$$

4.5.7. Infiltration and convective coupling

Infiltration rate are given in terms of air changes per hour for each zone. The mass flow rate is the product of the zone air volume, air density, and air change rate.

Infiltration occurs always from outdoor conditions. Equal amounts of air are assumed to leave the zone at the zone temperature. The energy gains to any zone i due to infiltration is:

$$\dot{Q}_{inf,i} = \dot{m}_{inf,i} C_p (T_a - T_i) \quad (4.41)$$

In order to solve the basic equations modeling the heat transfer through and between all elements in the zone, the problem is reduced to the following matrix equation.

For each wall or window separating zones of floating temperature or each wall having a known boundary condition, it is possible to specify a convective coupling. This coupling is the mass flow rate that enters the zone across the surface. An equal quantity of air is assumed to leave the zone at the zone temperature. The energy gain due to the convective coupling is the sum of all such gains for all walls or windows in the zone.

$$\dot{Q}_{cplg,s} = \sum_{adj,zones} \sum_{surfaces\ i\ to\ j} \dot{m}_{cplg,s} C_p (T_j - T_i) \quad (4.42)$$

Where $\dot{m}_{cplg,s}$ is the mass flow rate of air entering zone i across walls or windows.

4.5.8. Free-floating temperature

The rate of change of internal energy for any free floating zone is equal to the net heat gain or

$$C_i \frac{d}{dt} T_i = \dot{Q}_i \quad (4.43)$$

Where C_i is the thermal capacitance of zone i . The net heat gain, \dot{Q}_i , is a function of T_i and the temperatures of all other zones adjacent to zone i .

$$T_{\tau,i} = T_{i,\tau-\Delta t} + \frac{\bar{Q}_i \Delta t}{C_i} \quad (4.44)$$

Where Δt is the simulation time-step. $T_{i,\tau-\Delta t}$ is the zone temperature at the beginning of the time-step.

The average temperature is linear, such that the average is:

$$T_i = \frac{T_{i,\tau} + T_{i,\tau-\Delta t}}{2} \quad (4.45)$$

If **Eq.45** is solved for $T_{i,\tau}$ and the result substituted into **Eq.44**, along with the individual expressions representing the net heat gain, the following is obtained:

$$\begin{aligned} \frac{2C_i(\bar{T}_i - \bar{T}_{i,\tau-\Delta t})}{\Delta t} = \sum_{zones} adj, \sum_{surfaces} \dot{m}_{cplg,s} C_p \bar{T}_j + \dot{m}_{inf,i} C_p T_a - \left(\frac{1}{R_{star,i}} + \right. \\ \left. \left(\sum_{zones} adj, \sum_{surfaces} \dot{m}_{cplg,s} + \dot{m}_{inf,i} \right) C_p \right) \bar{T}_i + \left(\frac{1}{R_{star,i}} \bar{T}_{star,i} + Q_{g,c,i} \right) \end{aligned} \quad (4.46)$$

Eq.29 and **Eq.40** can be equated and regrouped to find:

$$\begin{aligned} \left(\frac{1}{R_{star,i}} - \sum_{int.wall} A_s B_s + \sum_{surface} A_s C_s \right) \bar{T}_{star,i} - \left(\sum_{adj,zone} \sum_{walls} A_s B_s \right) \bar{T}_{star,j} - \\ \frac{1}{R_{star,i}} \bar{T}_i = \left(\sum_{exterior} A_s B_s \right) T_a + \sum_{boundaries} known A_s B_s T_{b,s} + \sum_{surface} A_s (D_s + S_{s,i}) \end{aligned} \quad (4.47)$$

The set of energy balances given by **Eq.46** and **Eq.47**, written for all zones, results in a linear set of equations in average zone temperatures and average star temperatures. In matrix form,

$$[X] \cdot [\bar{T}] = [Z] \quad (4.48)$$

This matrix can be partitioned such that

$$[X] = \begin{bmatrix} X_{11} & X_{12} \\ X_{21} & X_{22} \end{bmatrix}$$

$$[T] = \begin{bmatrix} \bar{T} \\ \bar{T}_{star} \end{bmatrix}$$

$$[Z] = \begin{bmatrix} Z_1 \\ Z_2 \end{bmatrix}$$

Where

$$X_{11,ii} = \left(\sum_{\substack{\text{surfaces} \\ i \text{ to } j}} \dot{m}_{cplg,s} + \dot{m}_{inf,i} \right) C_p + \frac{2C_i}{\Delta t} + \frac{1}{R_{star,i}}$$

$$X_{11,ij} = \sum_{\substack{\text{adj.} \\ \text{zones}}} \sum_{\substack{\text{surfaces} \\ i \text{ to } j}} \dot{m}_{cplg,s} C_p \quad \text{for } i \neq j$$

$$X_{12,ii} = \frac{-1}{R_{star,i}}$$

$$X_{12,ij} = 0 \quad \text{for } i \neq j$$

$$X_{21,ii} = \frac{-1}{R_{star,i}}$$

$$X_{21,ij} = 0 \quad \text{for } i \neq j$$

$$X_{22,ii} = - \sum_{\text{int.wall}} A_s B_s + \sum_{\substack{\text{surface} \\ \text{in zone } i}} A_s C_s + \frac{1}{R_{star,i}}$$

$$X_{22,ij} = - \sum_{\text{adj.zone}} \sum_{\text{walls } i \text{ to } j} A_s B_s$$

$$Z_{1,i} = \dot{m}_{inf,i} C_p T_a + \frac{2C_i \bar{T}_{i,\tau-\Delta t}}{\Delta t} + Q_{g,e,i}$$

$$Z_{2,i} = \left(\sum_{\substack{\text{exterior} \\ \text{surfaces}}} A_s B_s \right) T_a + \sum_{\substack{\text{known} \\ \text{boundaries}}} A_s B_s T_{b,s} + \sum_{\substack{\text{surface} \\ \text{in zone } i}} A_s (D_s + S_{s,i})$$

For the case of all zones in floating temperature,

$$[\bar{T}] = [X]^{-1}[Z] \quad (4.49)$$

The final temperature for each zone i is

$$T_{\tau,i} = 2\bar{T}_i - T_{i,\tau-\Delta t} \quad (4.50)$$

4.5.9. Heating and cooling loads

It is possible to determine the energy requirement for zones controlled in an idealized way. Therefore, the heating and cooling energy flow is directly connected to the zone air temperature. The output of the heating and/or cooling equipment is a function of the zone temperature as shown in **Fig.4.7**, where

P_i – Power output for zone i (negative for heating, positive for cooling)

$P_{\max,i}$ – Absolute value of the maximum power for zone i

$T_{\text{set},i}$ – Set temperatures for heating or cooling in zone i

The zone temperature is free floating in the comfort region where the power is zero. If the temperature of a free-floating zone is within the heating or cooling regions at the end of a timestep, power is applied throughout the timestep so that the final zone temperature just reaches T_{set} . If the power required is greater than the maximum specified, then the maximum power is applied throughout the timestep and the zone temperature is again free floating.

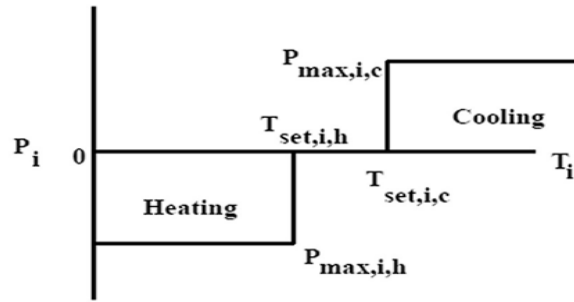


Fig.4.7. Power output versus temperature

The temperature change of the zone air, when power is supplied, is assumed to be linear. If power is required and enough is available to maintain the final zone temperature at $T_{set,i}$, then the final and average zone temperatures are known.

$$T_{req,i} = \frac{T_{\tau-\Delta t} + T_{set,i}}{2} \tag{4.51}$$

Where, $T_{req,i}$ is the average zone temperature over the time-step if less than maximum power is required.

For the zones that have floating temperatures, the solution for average zone temperatures and star temperatures is again of the form

$$[\bar{T}] = [X']^{-1}[Z'] \tag{4.52}$$

The coefficients of the X' matrix and Z' vector depend upon the control region. In the comfort zone, with no energy requirement:

$$X'_{ij} = X_{ij} \quad \text{for all } i \text{ and } j \tag{4.53}$$

$$Z'_i = Z_i \tag{4.54}$$

For zones whose temperature falls below the point for maximum heating or above that for maximum cooling

$$X'_{ij} = X_{ij} \quad \text{for all } i \text{ and } j \quad (4.55)$$

$$Z'_i = Z_i + P_{max,i,h} \text{ or } Z'_i = Z_i - P_{max,i,c}, \quad (4.56)$$

For zones that fall within the heating or cooling regions and require less than maximum power, the final temperature is assumed to be equal to the heating or cooling set temperature and the average room temperature is the $T_{req,i}$. **Eq.43** can be rewritten to include the power requirements.

$$C_i \frac{d}{dt} T_i = \dot{Q}_i - P_i \quad (4.57)$$

P_i and Q_i are considered constant over the time-step and Q_i is evaluated at the average zone temperature. Substituting into **Eq.57** yields:

$$\bar{P}_i - \frac{1}{R_{star,i}} T_{star,i} - \sum_{j=1}^{adj.zones} \sum_{i \text{ to } j}^{surfaces} m_{cplg} \cdot C_p \cdot \bar{T}_j = - \left[\frac{1}{T_{star,i}} + \left(\dot{m}_{inf,i} + \sum_{j=1}^{adj.zones} \sum_{i \text{ to } j}^{surfaces} m_{cplg} \right) C_p \right] \bar{T}_{req,i} - \frac{C_i}{\Delta t} (T_{set,i} - T_{\tau-\Delta t}) + \dot{m}_{inf,i} \cdot C_p \cdot T_a + Q_{g,c,i} \quad (4.58)$$

Eq.58 is substituted into the set of energy balances on all zones for any zone that is in the less than maximum heating or cooling region. The solution given by **Eq.49** is valid with the following substitutions for zones evaluated with **Eq.58**.

$$X'_{11,ij} = X_{11,ij} \quad \text{for } i \neq j$$

$$X'_{11,ii} = 1.0$$

$$X'_{12,ij} = X_{12,ij}$$

$$X'_{22,ii} = X_{22,ii}$$

$$X'_{21,ii} = 0$$

$$Z'_{2,i} = Z_{2,i} - X'_{11,ii} T_{req,i}$$

4.5.10. Thermal window model

Windows may consist of more than one pane of glass with different gas fillings between them. Every window pane has its own temperature node and the inner window pane is coupled via the star network to the star node temperature of the building zone as described in the previous section. The outer window pane is coupled via convective heat transfer to the temperature of the ambient air and via long-wave radiative exchange with the fictive sky temperature, T_{fsky} , as described above. The heat capacity of the frame, the window panes and the gas fillings are neglected.

In **Fig.4.8** is shown a glazing system as an assembly of two glazing layers separated by gas layers.

For each glazing of the window, the resulting temperature is calculated considering transmission; absorption and reflection of incoming direct and diffuse solar radiation diffuse short-wave radiation being reflected from the walls of the zone or an internal shading device, convective, conductive and long-wave radiative heat transfer between the individual panes and with the inner and outer environment.

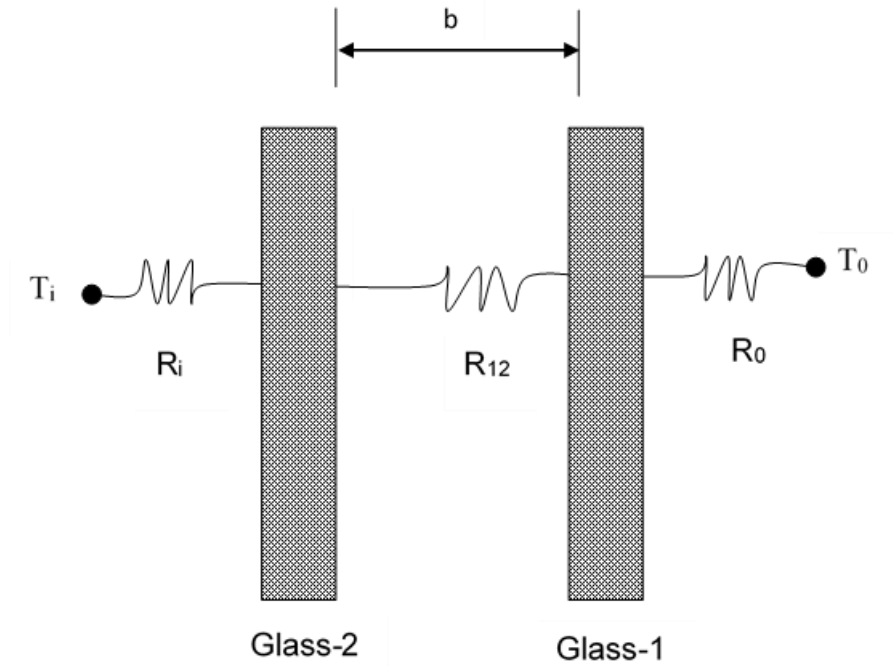


Fig.4.8 Resistance network between window panes

The heat flux from the inner pane of the window to the ambient is calculated as:

$$\dot{Q}_{2-0} = U_{2-0}A(T_2 - T_0) \quad (4.59)$$

With

$$U_{2-0} = \frac{1}{R_{12} + R_0}$$

$$R_0 = \frac{1}{h_{c,0} + h_{r,0}}$$

$$R_i = \frac{1}{h_{c,i} + h_{r,i}}$$

$$R_{12} = \frac{1}{h_{12}}$$

$$h_{12} = h_{conv} + h_{rad} + h_{cond}$$

The radiative heat exchange coefficient between glazing's is calculated using

$$h_{rad} = \frac{4\sigma T_{mean}^3}{\frac{1}{\varepsilon_1} + \frac{1}{\varepsilon_2} + 1} \quad (4.60)$$

The convective heat exchange coefficient between the individual glazings is calculated considering the slope of the window using:

$$h_{conv} = \frac{Nu\lambda}{b} \quad (4.61)$$

Where

$$Nu = 1 + 1.44 \left(1 - \frac{1708(\sin(1.8\beta))^{1.6}}{Ra \cos\beta} \right)^+ \left(1 - \frac{1708}{Ra \cos\beta} \right)^+ + \left(\left(\frac{Ra \cos\beta}{5830} \right)^{1/3} - 1 \right)^+$$

$$Ra = \frac{g\Delta TL^3}{T\mu\alpha}$$

4.6. Model of the heating floor

For modelling the radiant heating floor, an 'active layer' is added to the floor definition in Type 56 (multizone building). A typical cross-section of a radiant slab is shown in **Fig.4.9**. Due to the finite distance between pipes, a two-dimensional temperature field develops in the plane of the heating floor element cross-section. Thermal input or output along piping loops causes a change in the water temperature within the pipe. This change affects the construction element temperature in the z direction. This means that all three dimensions have to be taken into account for the calculation of a thermos active construction element system.

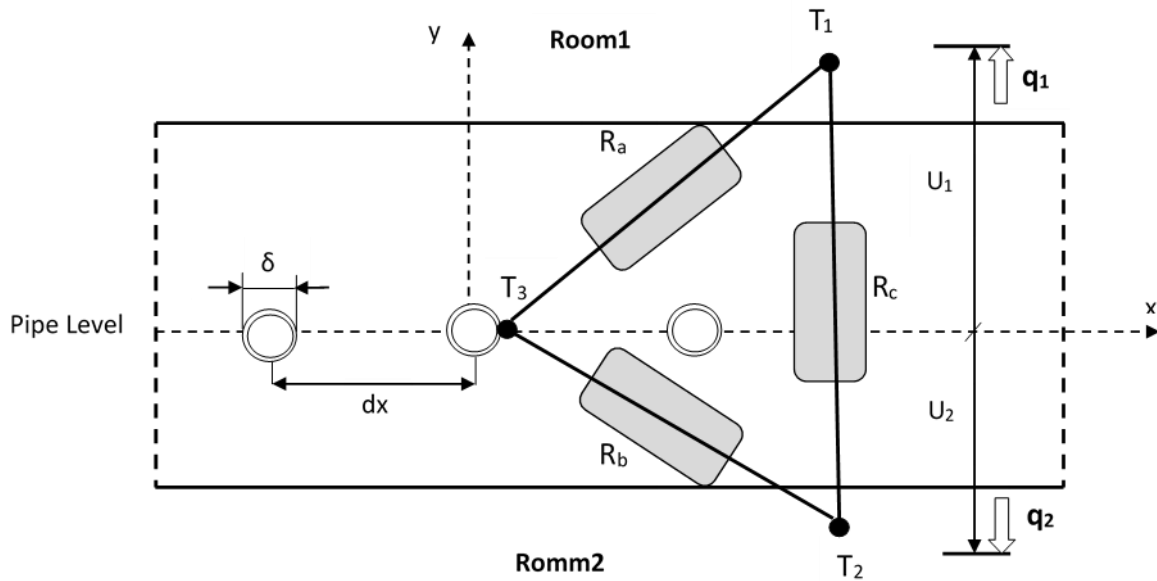


Fig.4.9. Heat flow in a cross section of a thermos-active construction element and network of resistances, triangular arrangement.

The calculation of thermos-active construction element systems is calculated by a powerful method [80].

4.6.1. Heats flow on the slab surfaces

The stationary solution for temperature distribution in the x - y plane results in the following formula, for heat flow on the surface towards room 1.

$$q_1 = \Phi \cdot U_1 (T_3 - T_1) + (1 - \Phi) \frac{U_1 \cdot U_2}{U_1 + U_2} (T_2 - T_1) \quad (4.62)$$

The first term to the right of the equation sign in **Eq.62** describes the heat flow between temperature T_3 on the outside surface of the pipe and temperature T_1 within room. The temperature difference is multiplied by the proportionality factor Φ . U_1 which represents the coefficient of thermal transmittance for the pipe configuration. The physical variable Φ is used as correction factor. This variable resembles the

shape factor and can be derived from the partial differential equation for thermal conduction. For the configuration of pipes, Φ becomes [81].

$$\Phi = \frac{2 \cdot \pi \cdot \lambda_b \cdot \Gamma}{d_x \cdot (U_1 + U_2)} \quad (4.63)$$

Where

$$\Gamma = \left[\ln \left(\frac{d_x}{\pi \cdot \delta} \right) + \frac{2 \cdot \pi \cdot \lambda_b}{d_x \cdot (U_1 + U_1)} + \sum_{s=1}^{\infty} \frac{g_{1(s)} - g_{2(s)}}{s} \right]^{-1}$$

The heat flow for the side of the room2 can be determined in a similar way:

$$q_1 = \Phi \cdot U_2 (T_3 - T_2) + (1 - \Phi) \frac{U_1 \cdot U_2}{U_1 + U_2} (T_1 - T_2) \quad (4.64)$$

4.6.2. The Resistance R_x

Equation (63) and (64) can be represented by a network of resistances in a triangular arrangement (see Fig.4.9). The three resistances can be described as follows:

$$R_a = \frac{1}{\Phi \cdot U_1} \quad (4.65)$$

$$R_b = \frac{1}{\Phi \cdot U_2} \quad (4.66)$$

$$R_c = \frac{U_1 + U_2}{U_1 \cdot U_2 \cdot (1 - \Phi)} \quad (4.67)$$

As shown in Fig.4.10, the triangular network can be transformed into an equivalent star network using the following relations:

$$R_1 = \frac{R_a \cdot R_c}{R_a + R_b + R_c} \quad (4.68)$$

$$R_2 = \frac{R_b \cdot R_c}{R_a + R_b + R_c} \quad (4.69)$$

$$R_x = \frac{R_a \cdot R_b}{R_a + R_b + R_c} \quad (4.70)$$

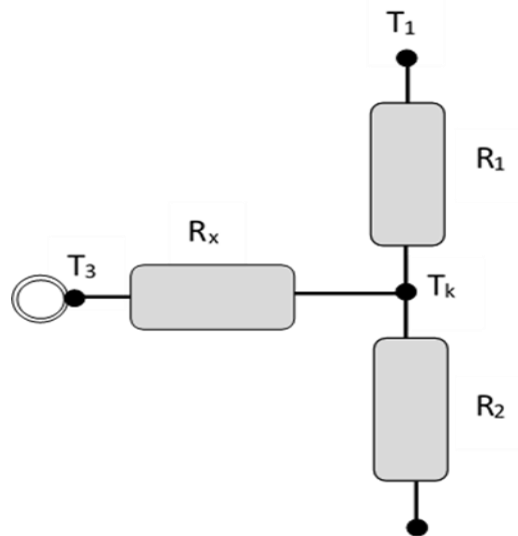


Fig.4.10. Network of resistances, star arrangement

Inserting the **Eq. (65)** to **Eq. (67)** into the equations **Eq. (68)** to **Eq. (70)** the following results are achieved for the star resistances:

$$R_1 = \frac{1}{U_1} \quad (4.71)$$

$$R_2 = \frac{1}{U_2} \quad (4.72)$$

$$R_x = \frac{(1-\phi)}{\phi \cdot (U_1 + U_2)} \quad (4.73)$$

Thus, the resistance R_x depends only on two geometric variables, i.e., the distance between pipes d_x and the pipe diameter δ , and on the thermal conductivity of the material layer λ_b in the pipe plane. The transformation from triangular to star-shaped network results in the additional temperature T_k for the center point of the star-network. This temperature equals the mean temperature in the pipe plane when $y=0$ (see **Fig.4.9**). This temperature is called core temperature. Under the assumption that $d/d_x > 0.3$ and $\delta/d_x < 0.2$, the resistance R_x can be given as follows:

$$R_x = \frac{d_x \left[\ln\left(\frac{d_x}{\pi \delta}\right) + \sum_{s=1}^{\infty} \frac{g_1(s) + g_2(s)}{s} \right]}{2 \pi \lambda_b} \quad (4.74)$$

The summation term is negligible for practical applications. Therefore, Eq. 6.4.4-15 can be simplified to the following:

$$R_x = \frac{d_x \ln\left(\frac{d_x}{\pi \delta}\right)}{2 \pi \lambda_b} \quad (4.75)$$

4.6.3. Thermal transmittance through pipe

The thermal transmittance is the heat transfer from the fluid within the tube with the temperature T_w through the pipe shell to the concrete with the temperature T_3 . As shown in **Fig.4.11**, there is two thermal resistances. The thermal resistance for heat transfer from the fluid to the pipe shell in proportion to the surface area of the construction element by ($d_x \cdot l$) can be determined by the formula.

$$R_w = \frac{d_x^{0.13}}{0.8 \pi} \left(\frac{\delta - 2d_r}{m l} \right)^{0.87} \quad (4.76)$$

The resistance for heat transfer through the pipe shell by thermal conduction in proportion to the surface area of the construction element by $(d_x \cdot l)$ can be determined in a similar way.

$$R_r = \frac{d_x \ln\left(\frac{\delta}{\delta - 2d_r}\right)}{2 \lambda_r \pi} \quad (4.77)$$

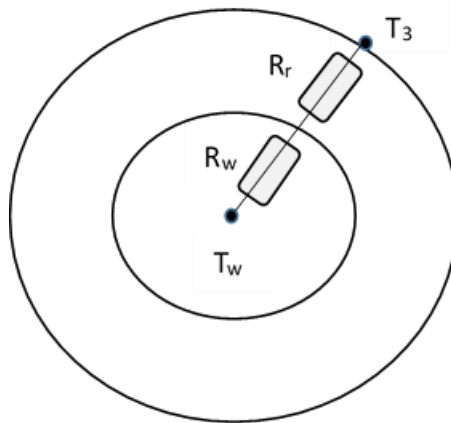


Fig.4.11. Thermal resistances inside a water tube

4.6.4. Mean water temperature in a pipe coil

The temperature of the fluid inside the pipe T_w is not constant, but changes along the pipe coil, as showing in **Fig.4.12**. The thermal resistance in z direction can be expressed by the following formula:

$$R_z = \frac{1}{\dot{m}_{sp} \cdot c \left\{ 1 - \exp \left[- \left(\dot{m}_{sp} \cdot c \cdot \left(R_w + R_r + R_x + \frac{1}{U_1 + U_2} \right) \right)^{-1} \right] \right\}} - R_w + R_r + R_x + \frac{1}{U_1 + U_2} \quad (4.78)$$

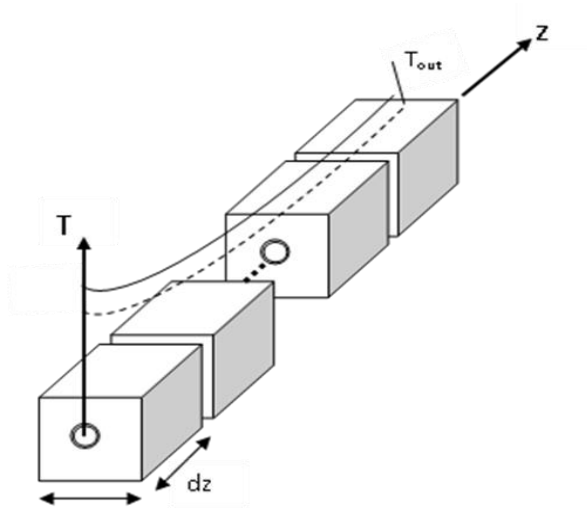


Fig.4.12. Change in temperature along the pipe coil

4.6.5. Total resistance R_t

When placed in series, as shown in **Fig.4.13**, all of the single resistances can be summed up to form a total resistance:

$$R_t = R_z + R_w + R_r + R_x \tag{4.79}$$

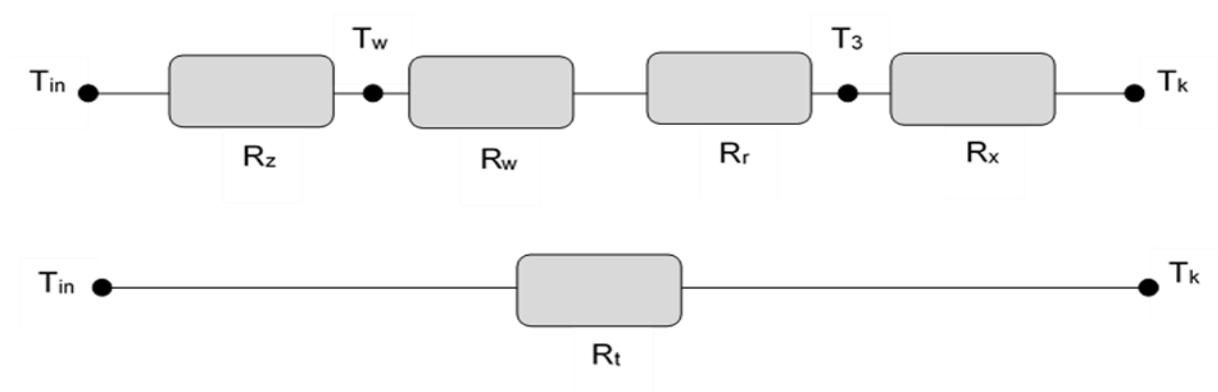


Fig.4.13. Resistance between water inlet temperature and core temperature

The pipe coil has to be split up into several sections. The total resistance can be given for each of the n sections by the following formula.

It is demonstrated that for a specific mass flow rate of 15 kg/hm^2 , the sum of the coefficients of thermal transmittance U_1+U_2 can be decreased without significant change in the total resistance R_t . Thus, the total resistance is simplified to:

$$R_t = \frac{1}{2 \dot{m}_{sp.c}} + R_w + R_r + R_x \quad (4.80)$$

The criterion in **Eq.78** can be specified as the boundary condition.

$$\dot{m}_{sp.c} \cdot (R_w + R_r + R_x) \geq \frac{1}{2}$$

If this boundary condition cannot be met by the selected configuration, the pipe coil has to be split up into several sections. In a similar way as described above, the total resistance can be derived for each of the n sections from

$$R_{t,i} = \frac{1}{2 \dot{m}_{sp.n.c}} + R_w + R_r + R_x \quad (4.81)$$

The boundary condition of each section is expressed by

$$\dot{m}_{sp.c} \cdot n \cdot (R_w + R_r + R_x) \geq \frac{1}{2}$$

Inserting the equations for each single resistance **Eq.75**, **Eq.76** and **Eq.77** into **Eq.81**, for a turbulent current in the pipe results in the following formula for the total resistance:

$$R_{t,i} = \frac{1}{2 \dot{m} n c} + \frac{d_x^{0.13} \left(\frac{\delta - 2d_r}{\dot{m} l} \right)^{0.87}}{0.8 \pi} + \frac{d_x \ln \left(\frac{\delta}{\delta - 2d_r} \right)}{2 \pi \lambda_r} + \frac{d_x \ln \left(\frac{d_x}{\pi \delta} \right)}{2 \pi \lambda_b} \quad (4.82)$$

Where

$$\frac{d_i}{d_x} > 0.3 \quad \text{and} \quad \frac{\delta}{d_x} < 0.2$$

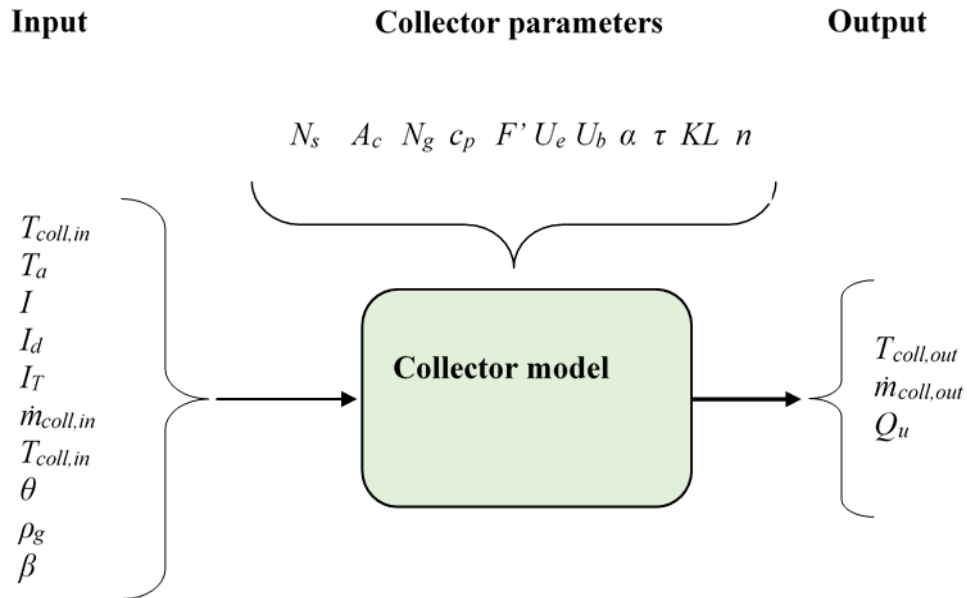


Fig.4.14. parameters, input and output of the thermal collector

4.7. Model of solar collector

Type 73 is the theoretical flat plate solar collector model adopted to model the performance of solar collectors. The main parameters input and output of the thermal solar collector is shown in **Fig.4.14**. The total collector array may consist of collectors connected in series and in parallel. The thermal performance of the total collector array is determined by, the number of modules in series and the characteristics of each module. The Hottel-Whillier steady-state model is used for estimating its thermal performance within each simulation time step.

4.7.1. Absorbed solar radiation

Using an isotropic radiation model on an hourly basis, the following relation can be used to estimate the absorbed radiation [82]:

$$S = I_{bT}(\tau\alpha)_b + I_d(\tau\alpha)_d \left[\frac{1+\cos(\beta)}{2} \right] + \rho I \left[\frac{1-\cos(\beta)}{2} \right] (\tau\alpha)_g \quad (4.83)$$

In other hand, when the total incident solar radiation on the solar collector plane is determined, the absorbed solar radiation can be given by:

$$S = (\tau\alpha) \times I_T \quad (4.84)$$

Inserting **Eq.83**.into **Eq.84.**, the overall transmittance-absorptance product is determined as:

$$(\tau\alpha) = \frac{I_{bT}(\tau\alpha)_b + I_d(\tau\alpha)_d \left[\frac{1+\cos(\beta)}{2} \right] + \rho I \left[\frac{1-\cos(\beta)}{2} \right] (\tau\alpha)_g}{I_T} \quad (4.85)$$

As shown in **Fig.4.15**, the incident energy falling on the collector, $\tau\alpha$ is absorbed by the absorber plate and $(1-\alpha)\tau$ is reflected back to the glass cover. The reflection from the absorber plate is assumed to be diffuse, so the fraction $(1-\alpha)\tau$ that strikes the glass cover is diffuse radiation and $(1-\alpha)\tau\rho_D$ is reflected back to the absorber plate.

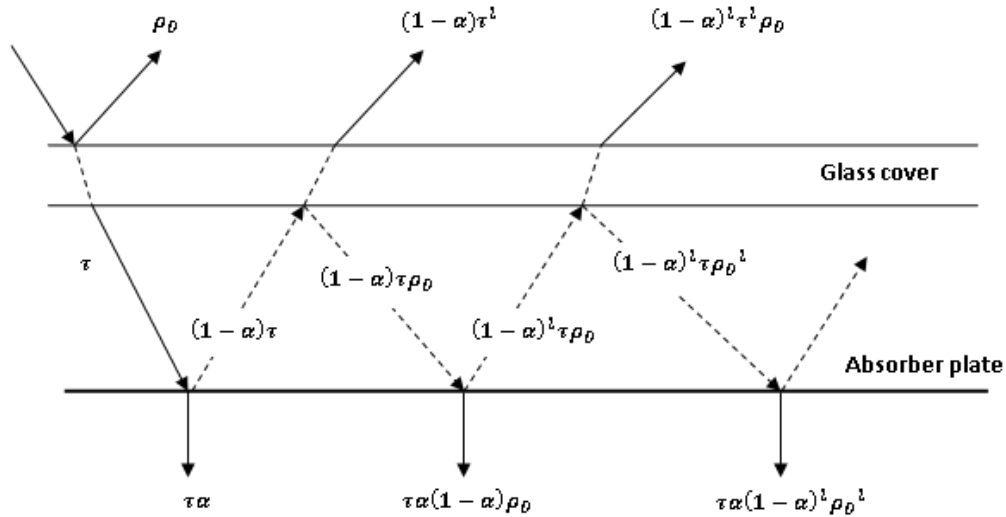


Fig.4.15. Multiple reflections between the solar collector cover and absorber plate.

The multiple reflection of diffuse radiation continues so that the fraction of the incident solar energy ultimately absorbed is

$$(\tau\alpha) = \tau\alpha \cdot \sum_{n=1}^{\infty} [(1-\alpha) \cdot \rho_D]^n = \frac{\tau\alpha}{1-(1-\alpha) \cdot \rho_D} \tag{4.86}$$

A reasonable approximation of (Eq.86) for most practical solar collectors is

$$(\tau\alpha) = 0.01\tau\alpha \tag{4.87}$$

The effective incidence angle for diffuse radiation from sky and ground reflected radiation, for a given collector tilt angle, are given by (Brandemuehl and Bekman, 1980) [83]:

$$\theta_{e,D} = 59.68 - 0.1388\beta + 0.001497\beta^2 \tag{4.88}$$

$$\theta_{e,G} = 90 - 0.5788\beta + 0.002693\beta^2 \tag{4.89}$$

The absorptance can be obtained from (Bekman et al.) [84]:

$$\frac{\alpha}{\alpha_n} = 1 + 2.0345 \times 10^{-3} \times \theta_e - 1.99 \times 10^{-4} \times \theta_e^2 + 5.324 \times 10^{-6} \times \theta_e^3 - 4.799 \times 10^{-8} \times \theta_e^4 \quad (4.90)$$

Where α_n is the absorptance at normal incident angle, which can be found from the properties of the absorber.

The incidence angle, θ , of beam radiation required to estimate R_B can be used to find $(\tau\alpha)_B$ and **Eq.(4.88)** and **Eq.(4.89)** to calculate $(\tau\alpha)_D$ and $(\tau\alpha)_G$, respectively.

For the calculation of the transmittance τ we need to calculate τ_α and τ_r .

$$\tau = \tau_\alpha \times \tau_r \quad (4.91)$$

For smooth transparent surfaces, the reflection of polarized radiation on passing from medium 1 with a refractive index n_1 to medium 2 with refractive index n_2 is (Duffie and Beckman, 2006) **[85]**:

$$\tau_r = \frac{1}{2} \times \left(\frac{1-r_{\parallel}}{1+r_{\parallel}} + \frac{1-r_{\perp}}{1+r_{\perp}} \right) \quad (4.92)$$

Where r_{\perp} is the perpendicular component of unpolarized irradiation and r_{\parallel} is the parallel component of unpolarized radiation, which could be expressed as:

$$r_{\perp} = \frac{\sin^2(\theta_2 - \theta_1)}{\sin^2(\theta_2 + \theta_1)} \quad (4.93)$$

$$r_{\parallel} = \frac{\tan^2(\theta_2 - \theta_1)}{\tan^2(\theta_2 + \theta_1)} \quad (4.94)$$

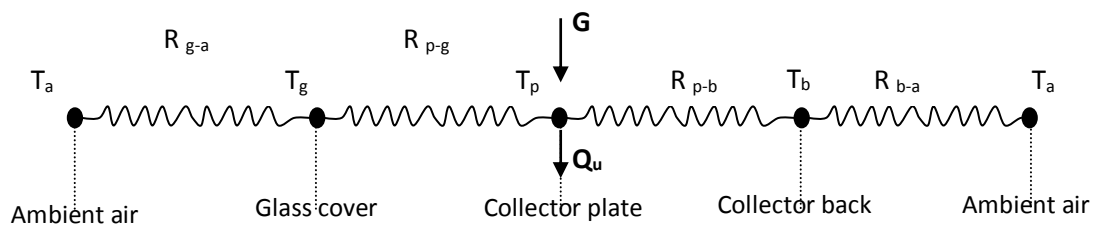
Where θ_1 and θ_2 are the angles of incidence and refraction, respectively, and they are related by the following expression:

$$n = \frac{n_1}{n_2} = \frac{\sin\theta_1}{\sin\theta_2} \tag{4.95}$$

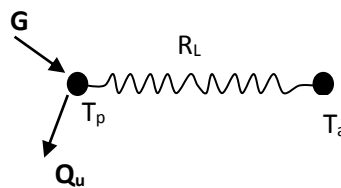
The transmitted radiation, when only considering the absorption losses, can be calculated from:

$$\tau_\alpha = e^{\left(\frac{-KL}{\cos\theta_2}\right)} \tag{4.96}$$

Where k is the extinction coefficient, which can vary from 4m^{-1} (for low-quality glass) to 32m^{-1} (for high-quality glass), and L is the thickness of the glass cover.



(a). Resistance network



(b). Simple collector network

Fig.4.16. Thermal network for a single cover collector in term of resistance between plates

4.7.2. Collector energy losses

The thermal network for a single-cover, flat-plate collector in terms of the resistance between plates is shown in **Fig.4.16 (a)**. The temperature of the plate is T_p , the collector back temperature T_b , and absorbed solar radiation is S . In a simplified way, the various thermal losses from the collector can be combined into a simple resistance, R_L , as shown in **Fig.4.16 (b)**.

The energy losses from the collector can be written as:

$$Q_{loss} = U_{L \times A_c} \times (T_p - T_a) \quad (4.97)$$

The overall heat loss coefficient is a complicated function of the collector construction and its operating conditions, given by the following expression:

$$U_{L,j} = U_t + U_b + U_e \quad (4.98)$$

The coefficient U_t is given by the following empirical equation (Klein, 1975) **[86]**:

$$U_t = \frac{1}{\frac{N_g}{\frac{C}{T_p} \left[\frac{T_p - T_a}{N_g + f} \right]^{0.33} + \frac{1}{h_w}}} + \frac{\sigma \times (T_p^2 - T_a^2) \times (T_p - T_a)}{\frac{1}{\varepsilon_p + 0.05 \times N_g \times (1 - \varepsilon_p)} + \frac{2 \times N_g + f - 1}{\varepsilon_g} - N_g} \quad (4.99)$$

Where

$$f = (1 - 0.04 \times h_w + 0.0005 \times h_w^2) \times (1 + 0.091 \times N_g)$$

$$C = 365.9 \times (1 - 0.00883 \times \beta + 0.001298 \times \beta^2)$$

$$h_w = 5.7 + 3.8W$$

The energy loss from the bottom of the collector can be practically eliminated by providing sufficiently good insulation. This heat loss is first conducted through the insulation and then by a combined convection and infrared radiation transfer to the surrounding ambient air. Because the temperature of the bottom part of the casing is low, exchange by radiation is neglected; thus, the energy loss is given by

$$U_b = \frac{1}{\frac{t_b}{k_b} + \frac{1}{h_{c,b-a}}} \quad (4.100)$$

Typical values of the back surface heat loss coefficient are 0.3-0.6 (W/m²-K).

In a similar way, the heat transfer coefficient for the heat loss from the collector edges can be obtained from

$$U_e = \frac{1}{\frac{t_e}{k_e} + \frac{1}{h_{c,e-a}}} \quad (4.101)$$

Typical values of the edges heat loss coefficient are 1.5-2.0 (W/m²-K).

4.7.3. Useful energy

The energy collection of each module in an array of N_s modules in series is modeled according to the Hottel-Whiller equation [87].

$$Q_u = \frac{A_c}{N_s} \sum_{j=1}^{N_s} F_{R,j} [I_T(\tau\alpha) - U_{L,j}(T_{i,j} - T_a)] \quad (4.102)$$

Where j is the number of module and F_R is the heat removal factor, expressed symbolically by:

$$F_R = \frac{N_s \dot{m} c_p}{A_c U_L} \left[1 - \exp\left(-\frac{U_L F' A_c}{N_s \dot{m} c_p}\right) \right] \quad (4.103)$$

F' is fin collector's efficiency, given by:

$$F' = \frac{\frac{1}{U_L}}{W \left[\frac{1}{U_L [D + (W-D) \times F]} + \frac{1}{C_b} + \frac{1}{\pi D_i h_{fi}} \right]} \quad (4.104)$$

F is standard fin efficiency factor, obtained from:

$$F = \frac{\tanh[m \times (W-D)/2]}{m \times (W-D)/2} \quad (4.105)$$

The variable m is defined as follows:

$$m = \sqrt{\frac{U_L}{k_p \times \delta_p}} \quad (4.106)$$

The following empirical formula was used to evaluate the heat transfer coefficient between the working fluid and the tube wall.

$$h_{fi} = 1430 + 23.3t - 0.048t^2) w_{water}^{0.8} D_i^{-0.2} \quad (4.105)$$

Where $t = T_{fi} - 273.15$ with T_{fi} is the average working fluid temperature inside the tube and w_{water} is the water speed.

The outlet fluid temperature of one module is used as the inlet to the next and given as:

$$T_{coll,j} = \frac{AF_{R,j} (I_T(\tau\alpha) - U_{L,j}(T_{i,j} - T_a))}{N_s \dot{m} C_p} + T_i \quad (4.108)$$

4.8. Modelling of the water storage tank

A fully mixed storage tank, with immersed serpentine heat exchangers, is modeled by Type 60 from the standard TRNSYS library. A fully mixed tank is heated up by the serpentine with the inner fluid at a constant inlet temperature. The model includes

one electric resistance-heating element, subject to temperature and /or time control. Both heaters may be on simultaneously.

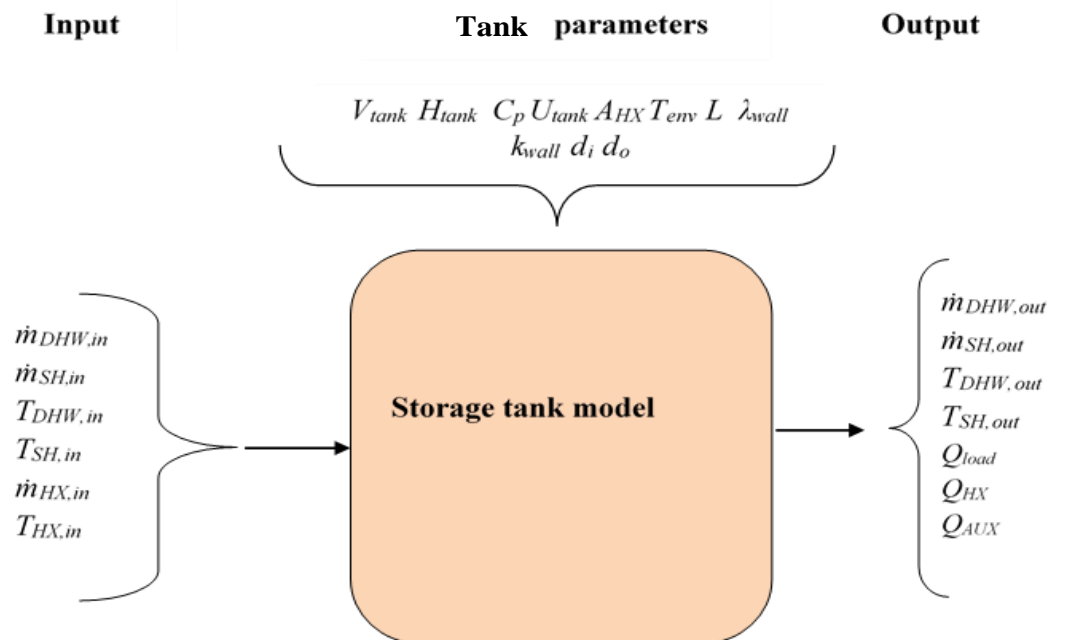


Fig.1.17. parameters, input and output of the storage tank.

The auxiliary heaters employ a temperature dead band. The heater is enabled if the temperature of the tank is less than $(T_{set} - \Delta T_{db})$.

The main parameters, input and output of the thermal storage tank is shown in **Fig.4.17**.

As showing in **Fig.4.18**, there is one internal heat exchanger. Hot water from heat source enter the heat exchanger at temperature $T_{HX,in}$ and exit at temperature $T_{HX,out}$. Hot water for DHW preparation leave the tank at temperature $T_{DHW,out}$ The hot water used for space heating leave at temperature $T_{SH,out}$ and return to tank at temperature $T_{SH,in}$. Cold water enter the tank at temperature $T_{DHW,in}$.

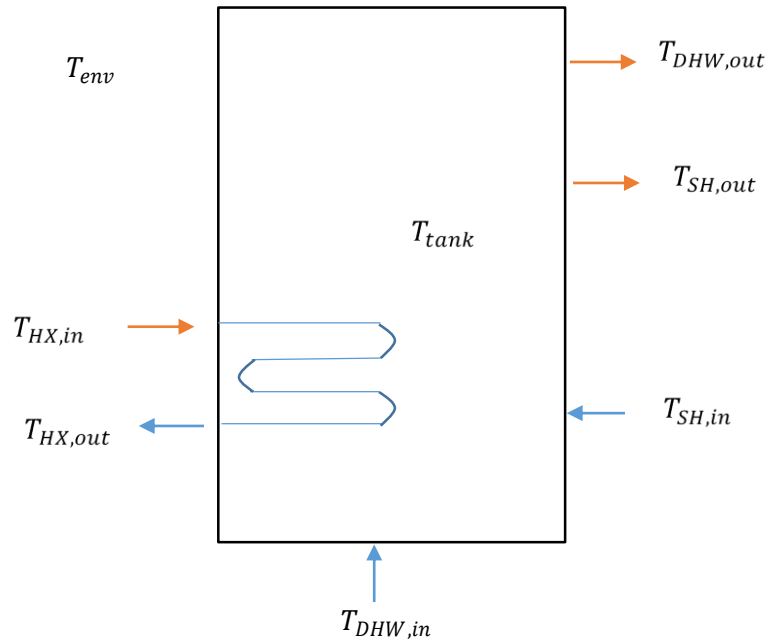


Fig.4.18. Fully mixed storage tank

4.8.1. Energy balance of the tank

The energy balance of the fully mixed storage tank is as follows:

$$\dot{Q}_{acum} = \dot{Q}_{hx} - \dot{Q}_{load} + \dot{Q}_{aux} - \dot{Q}_{loss} \quad (4.109)$$

The term \dot{Q}_{acum} is the accumulated heat at the tank in kJ. Using a first order scheme for the time derivatives, and a time increment of Δt , this term is evaluated as a function of the temperature of the tank at the current time step T_{tank-n} and the temperature of the tank at the previous time step T_{tank} as:

$$\dot{Q}_{acum} = \rho C_p V_{tank} \frac{T_{tank-n} - T_{tank}}{\Delta t} \quad (4.110)$$

Where c_p and ρ are the storage fluid heat capacity and density, and V_{tank} the volume of the tank.

The heat loss from the storage tank to ambient \dot{Q}_{loss} can be computed in terms of the ambient temperature T_a and the tank to ambient overall heat transfer coefficient UA_{loss} .

The tank to ambient heat transfer coefficient can be obtained by multiplying the overall tank heat loss coefficient, $(U_{tank} + \Delta U)$, by the tank external area.

$$\dot{Q}_{loss} = (U_{tank} + \Delta U) \times A_{tank} \times (T_{env} - T_{tank}) \quad (4.111)$$

The energy removed by the load includes the thermal energy for DHW preparation and space heating demand.

$$\dot{Q}_{load} = \dot{m}_{DHW} C_p (T_{DHW,in} - T_{DHW,out}) + \dot{m}_{SH} C_p (T_{SH,in} - T_{SH,out}) \quad (4.112)$$

Where, $T_{DHW,in}$ and $T_{DHW,out}$ are the cold water temperature from main and the required hot water temperature, respectively. $T_{SH,in}$ and $T_{SH,out}$ are the return hot water temperature from heating floor system and the required temperature for space heating, respectively.

The energy provided by the solar collectors and input to tank through a heat exchanger \dot{Q}_{HX} is calculated by multiplying the logarithmic mean temperature $LMTD$ by the overall heat transfer coefficient of the heat exchanger UA_{hx} .

$$\dot{Q}_{HX} = UA_{HX} \times (LMTD) \quad (4.113)$$

The overall heat transfer coefficient UA_{HX} and logarithmic mean temperature difference ($LMTD$) of heat exchanger is determined iteratively by assuming the heat exchanger effectiveness, $(T_{HX,in} - T_{HX,out}) / (T_{HX,in} - T_{HX,tank})$, is 0.9. Then, the logarithmic mean temperature $LMTD$ is found as:

$$LMDT = \frac{T_{HX,in} - T_{HX,out}}{\ln \frac{T_{HX,in} - T_{tank}}{T_{HX,out} - T_{tank}}} \quad (4.114)$$

Where $T_{HX,in}$ and $T_{HX,out}$ refer to inlet and outlet temperature in the immersed heat exchanger and T_{tank} the temperature of the fully mixed tank.

The UA value of heat exchanger is computed as:

$$\frac{1}{AU_{HX}} = \frac{1}{h_i A_i} + \frac{1}{k_{wall}} + \frac{1}{h_o A_o}$$

Finally, the temperature at the outlet of the heat exchanger is given by:

$$T_{HX,out} = T_{HX,in} - \frac{Q_{HX}}{\dot{m}_{HX} \cdot c_{pHX}} \quad (4.115)$$

A fully mixed tank, heated up by the serpentine with the inner fluid at a constant inlet temperature, was tested by **Farrington and Bingham (1986) [88]**. The test starts with the storage tank with an initial temperature of $T_{tank} = 25 \text{ }^\circ\text{C}$. Then, fluid at $T_{HX,in} = 70 \text{ }^\circ\text{C}$ is circulated through the serpentine (inlet temperature), until the temperature difference between the inlet and outlet of the serpentine is below $0.1 \text{ }^\circ\text{C}$. The serpentine effectiveness ϵ , the overall heat transfer coefficient UA_{HX} and the heat exchanger power Q_{HX} are analysed as a function of the logarithmic mean temperature difference LMTD during the whole test period. Numerical results are in very good agreement with experimental data over all the LMTD range. Differences observed between experimental and numerical curves of ϵ ; UA_{HX} and Q_{HX} for a specific LMTD value are always kept below 5% **[89]**.

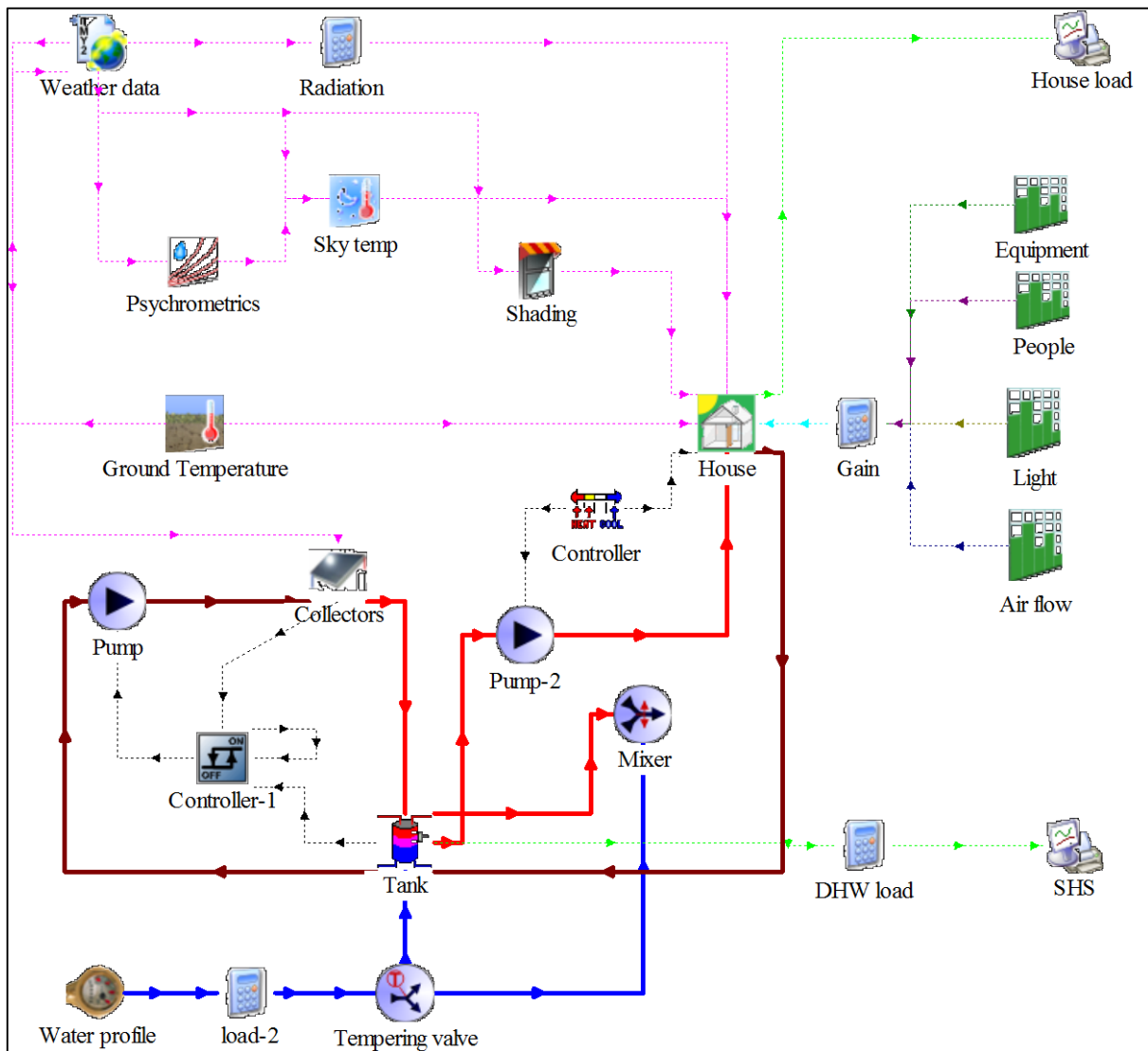


Fig.4.19. Overview of a house with solar heating system and grid-connected PV system in the TRNSYS studio

4.8.2. Average tank temperature

Substituting **Eq.110** to **Eq.113.** in **Eq.109,** the energy balance of the fully mixed storage tank becomes.

$$\rho C_p V_{tank} \frac{T_{tank-n} - T_{tank}}{\Delta t} = \dot{m}_{DHW} C_p (T_{DHW,in} - T_{DHW,out}) + \dot{m}_{SH} C_p (T_{SH,in} - T_{SH,out}) + UA_{HX} \times (LMDT) + (U_{tank} + \Delta U) \times A_{tank} \times (T_{env} - T_{tank}) \quad (4.116)$$

Therefore, **Eq. (4.116)** can be expressed as a change in storage tank temperature for the time step required as:

$$T_{tank-n} = T_{tank} + \dot{m}_{DHW} C_p (T_{DHW,in} - T_{DHW,out}) + \dot{m}_{SH} C_p (T_{SH,in} - T_{SH,out}) + UA_{HX} \times (LMDT) + (U_{tank} + \Delta U) \times A_{tank} \times (T_{env} - T_{tank}) \quad (4.117)$$

4.9 TRNSYS model of a solar heating system

After the mathematical description of different components models, a complete model of the solar heating system was built in TRNSYS, as shown in **Fig.4.19**. The model consists of components that interact with each other.

Other minors TRNSYS components used in the construction of the model are as follows:

4.9.1. Valves

Type11 includes pipe or duct 'tee piece', mixers, and diverters, which are subject to external control, is often necessary in thermal system.

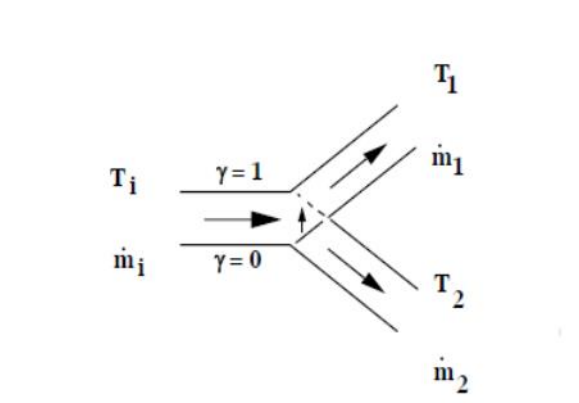


Fig 4.20. Flow diverter

Diverting Valve

Fig (4.20) describes the operation of a flow diverter with one inlet which is proportionally split between two possible outlets, depending on the Input control function.

The mathematical description of a flow diverter is as follows:

$$T_1 = T_i \quad (4.118)$$

$$\dot{m}_1 = \dot{m}_i(1 - \gamma) \quad (4.119)$$

$$T_2 = T_i \quad (4.120)$$

$$\dot{m}_2 = \dot{m}_i\gamma \quad (4.121)$$

Tee piece

Fig (4.21). describes the function of a tee piece that completely mixes two inlet streams of the same fluid at different temperatures. The mathematical description of a tee piece is as follows:

$$T_0 = \frac{\dot{m}_1 T_1 + \dot{m}_2 T_2}{\dot{m}_1 + \dot{m}_2} \quad (4.122)$$

$$\dot{m}_0 = \dot{m}_1 + \dot{m}_2 \quad (4.123)$$

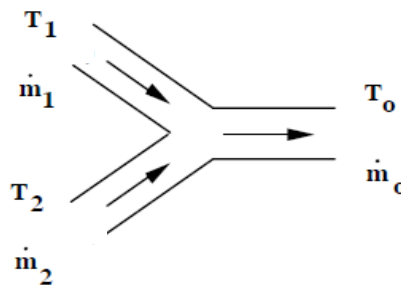


Fig 4.21. Tee piece

Tempering valve

A tempering valve is used to mix hot and cold water in such a way as to maintain the set temperature of the mixed water at the outlet, as shown in **Fig (4.22)**. The mathematical description of the function of a tempering valve is shown in **Table (4.1)**.

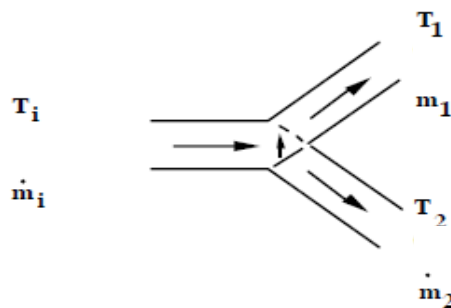


Fig 4.22. Tempering valve

Table (4.1)

Mathematical description of Tempering Valve

$T_1 = T_i$	$\gamma = (T_{set} - T_i)/(T_h - T_i)$	If $T_h > T_{set}$
$\dot{m}_1 = \dot{m}_i(\gamma)$	$\gamma = 1$	If $T_h \leq T_i$
$T_2 = T_i$	$\gamma = 0$	If $T_h \leq T_i$
$\dot{m}_2 = \dot{m}_i(1 - \gamma)$	T_{set} must be $\geq T_i$ at all times	

Where \dot{m}_i mass flow rate of inlet fluid, \dot{m}_o mass flow rate of outlet fluid, \dot{m}_1 mass flow rate at position 1, \dot{m}_2 mass flow rate at position 2, T_h heat source fluid temperature, T_i Temperature of inlet fluid, T_o temperature of outlet fluid, T_{set} maximum temperature of fluid supplied to load, T_1 temperature at position 1, T_2 temperature at position 2, Y control function having value between 0 and 1.

4.9.2. Controllers

Differential Controller

Type 2b is used in the modelling of on/off differential controller. This controller generates a control function γ_o that can have values of 0 or 1. The value of γ_o is chosen as a function of the difference between upper and lower temperatures, T_H and T_L , compared with two dead band temperature differences, ΔT_H and ΔT_L . Mathematically, the control function is expressed as follows: We consider that the controller was previously ON.

$$\text{If } \gamma_i = 1 \text{ and } \Delta T_L \leq (T_H - T_L), \gamma_o = 1 \quad (4.124)$$

$$\text{If } \gamma_i = 1 \text{ and } \Delta T_L > (T_H - T_L), \gamma_o = 0 \quad (4.125)$$

However, the control function is set to zero, regardless of the upper and lower dead band conditions, if $T_{IN} > T_{MAX}$. This situation is often encountered in domestic hot water systems where the pump is not allowed to run if the tank temperature is above some prescribed limit.

Where, ΔT_H [C] upper dead band temperature difference, ΔT_L [C] lower dead band temperature difference, T_H [C] upper Input temperature, T_{IN} [C] temperature for high limit monitoring, T_L [C] lower Input temperature, T_{MAX} [C] maximum Input temperature, γ_i [0..1] Input control function, γ_o [0..1] output control function.

Room Thermostat

Type 8 is used in the modelling of Three Stage Room Thermostat. A three-stage room thermostat is modeled to output three on/off control functions that can be used to control a system having a solar heat source, an auxiliary heater, and a cooling system. In this Room Thermostat is used to keep the room temperature at set point temperature.

$$T_{H'} = T_H + \gamma \times \Delta T_{db} \quad (4.126)$$

Where, ΔT_{db} is the "dead band" temperature difference.

4.9.3. Temperatures

Effective Sky Temperature

Type 69 is used to calculate an effective sky temperature for use in determining long wave radiative exchange with external building surfaces. The building model treats the sky as a black body, thus an effective temperature is calculated based on the ambient temperature, a calculated emittance of a clear sky, and a calculated cloudiness factor. The emittance, ε , of the sky is calculated according to the following:

$$\varepsilon = 0.711 + 0.005T_{sat} + 7.3 \times 10^{-5}T_{sat}^2 + 0.013 \cos \left[2\pi \frac{time}{24} \right] + 12 \times 10^{-5}(p_{atm} - p_0) \quad (4.127)$$

Where T_{sat} is the ambient saturation temperature, p_{atm} is the ambient pressure, p_0 is the pressure at sea level, and time is the hour of the year. The cloudiness factor, C , can be calculated using the diffuse solar radiation on a horizontal surface (I_d) and the total radiation on a horizontal surface (I):

$$C = \left(1.4286 \frac{I_d}{I} - 0.3\right)^{0.5} \quad (4.128)$$

The effective sky temperature, T_{sky} , is then calculated as:

$$T_{sky} = T_{amb}(\varepsilon + 0.8(1 - \varepsilon)C)^{0.25} \quad (4.129)$$

Ground Temperature

The ground temperature is performed using Type 77. The temperature of the undisturbed ground is a function of the time of year and the depth below the surface and could be described by the following correlation:

$$T_{ground} = T_{mean} - T_{amp} \times \exp\left[-depth \times \left(\frac{\pi}{365\alpha}\right)^{0.5}\right] \times \cos\left\{\frac{2\pi}{365} \times \left[t_{now} - t_{shift} - \frac{depth}{2} \times \left(\frac{365}{\pi\alpha}\right)^{0.5}\right]\right\} \quad (4.130)$$

T_{mean} : Mean surface temperature (average air temperature) [°C].

T_{amp} : Amplitude of surface temperature (maximum air temperature minus mean air temperature) [°C].

Depth: Depth below surface [m].

α : Thermal diffusivity of the soil [m²/day].

t_{now} : Current day of the year [day].

t_{shift} : Day of the year corresponding to the minimum surface temperature [day].

4.9.4. Pump

In TRNSYS type 3, the pump's maximum flow rate, the fluid specific heat, the maximum power and the power coefficient that enter the fluid stream are set as parameters. Type 3 also requires inputs of fluid inlet temperature, inlet mass flow rate and control signal. The control signal is set to one or zero ($0 \leq Y \leq 1$).

The outlet temperature is calculated as:

$$T_0 = T_i + \frac{P \times f_{par}}{\dot{m} \times C_p} \quad (4.131)$$

The outlet mass flow rate is simply

$$\dot{m}_0 = \gamma \dot{m}_{max} \quad (4.132)$$

A linear relationship between flow rate and power consumption is assumed:

$$P = \gamma P_{max} \quad (4.133)$$

Where F_{par} fraction of pump power converted to fluid thermal energy, \dot{m} pump mass flow rate, \dot{m}_{max} maximum mass flow rate (when $Y = 1$) P power consumption of pump, P_{max} maximum power consumption (when $Y = 1$), T_i inlet fluid temperature, T_0 outlet fluid temperature, Y control function ($0 \leq Y \leq 1$).

The model is finally connected to the environmental module to simulate its performance under Chlef's TMY (typical meteorological year (Type 54)) data. Temperatures, wind speeds and solar radiations at regular time intervals are read in by a data processor to generate direct and diffuse radiation outputs for a number of surfaces with arbitrary orientation and inclination.

4.10. Modelling of grid-connected photovoltaic system

A schematic of the grid-connected photovoltaic system is presented in **Fig 4.20**. The main components of a typical grid-connected PV system comprises a solar PV modules (PV array) which convert sunlight directly to electricity and an inverter to convert the DC current generated by the solar PV modules to AC current. The electricity demand of the building is served by the PV system and the excess is fed into the grid.

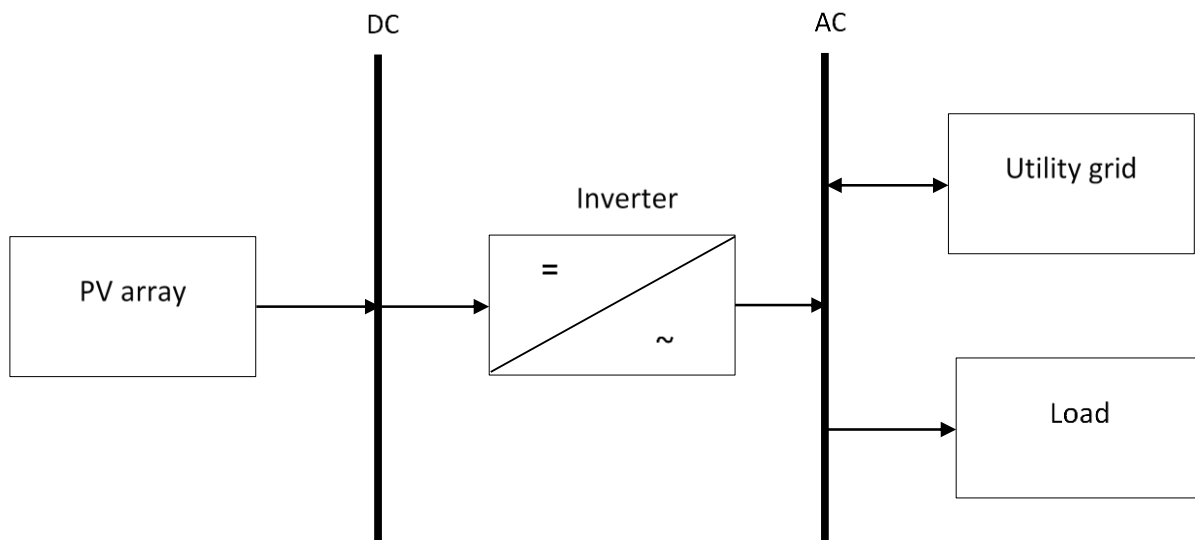


Fig.4.23. Grid-connected PV system

4.10.1. PV array output

The power produced by the PV system is calculated using the following formula [90]:

$$P_{pv} = P_{max} F_{pv} \left(\frac{G}{G_{STC}} \right) (1 + \alpha (T_c - T_{c,STC})) \quad (4.134)$$

Where, P_{\max} is the peak power output (kW), F_{pv} is the derating factor, G is the solar radiation incident on the PV modules in the current hour (kW/m^2), G_{STC} is the incident radiation at standard test conditions ($1\text{kW}/\text{m}^2$), α is the temperature coefficient of power ($\%/^{\circ}\text{C}$), T_c is the PV cell temperature in the current hour ($^{\circ}\text{C}$), and $T_{c,\text{STC}}$ is the PV cell temperature under standard test conditions (25°C).

4.10.3. Module operating temperature

The operating temperature of the PV module is calculated from the energy balance equation. Part of the absorbed radiation is used to generate electricity and the remainder is converted into thermal energy. The energy balance equation for a module with unit area can be written as [91]:

$$\tau\alpha I_T = \eta_c I_T + U_{LS}(T_c - T_a) \quad (4.135)$$

Where τ is the transmittance of the cover of the solar cells, α is the fraction of the incident solar radiation absorbed by the cells, and η_c is the efficiency of the solar cell. T_c and T_a are PV cell and ambient temperature, respectively. U_{LS} denotes the loss coefficient, which includes convection and radiation loss from top and bottom as well as conduction loss.

The ratio of the module transmittance-reflectance product to the module loss coefficient from NOCT value is given by:

$$\frac{\tau\alpha}{U_{LS}} = \frac{(T_{c,\text{NOCT}} - T_{a,\text{NOCT}})}{I_{T,\text{NOCT}}} \quad (4.136)$$

Assuming that this ratio is constant, the module temperature at any time step is:

$$T_c = T_a + \left(\frac{I_T \tau \alpha}{U_{Ls}} \right) \left(1 - \frac{\eta_c}{\tau \alpha} \right) \quad (4.137)$$

The NOCT value is calculate that is calculated at irradiance of 800Wm^{-2} , wind speed of 1 ms^{-1} , ambient temperature of 293 K and no load operation.

It is assumed that the PV module and inverter system operates at the maximum power point for the given radiation conditions.

4.10.4. Energy interchange between PV system and grid

The annual energy balance is obtained by summing the energy interchanges between a grid-connected PV system and utility grid at each hour. The energy balance at any hour of year is given by:

$$E_{PV} + E_{GP} - E_C - E_{GS} = 0 \quad (4.138)$$

Where E_{PV} is electricity produced by the PV system, E_{GP} is electricity purchased from the utility grid, E_C is energy consumption of the house and E_{GS} is electricity sold to the electricity grid.

As mentioned previously, the electricity produced by the PV system at each hour of the entire year is calculated by Type 119. The electricity output from the PV system for a specific hour is compared with the corresponding hourly electrical load. If the hourly electrical output exceeds the hourly load, the power is used to satisfy the electrical demand in this hour, and the surplus power is exported to the grid. Thus, the electrical energy purchased from the utility grid in this hour is zero ($E_{GP}=0$) and the electricity exported to utility grid is by:

$$E_{GS} = E_{PV} - E_c \quad (4.139)$$

If the hourly electricity output is less than the hourly electrical load, the grid is used to supply the additional power to satisfy the electrical demand in the hour, and no electrical energy is exported ($E_{GS}=0$). The electricity imported from the grid in this hour is given by:

$$E_{Gp} = E_c - E_{PV} \quad (4.140)$$

4.11. Conclusion

The aim of this chapter was to perform a dynamic model of a multi-zone house coupled with active solar systems under TRNSYS software. Solar systems include a solar heating system and a grid-connected PV system. We started with a mathematical description of a multi-zone house incorporating a floor heating system. Then, a flat-plate collector and a fully mixed storage tank was modeled and the TRNSYS model of the solar heating system was presented. The heating system is coupled to building through the heating floor system. Finally, a grid connected PV system was modeled using a specific "Type" from the library of the TRNSYS tool. The energy balance between the PV system and the grid has been modeled using a new TRNSYS component.

The model developed in this chapter will be used later in this work for the assessment of the energy demand (heating, cooling and electricity) of case studies houses.

***Chapter 5: Experimental study and
validation of the solar heating system
model***

5.1. Introduction

In the present chapter, the model of solar heating system supplying a multi-zone house, developed in the last chapter, was applied on case study of a single-family low-energy house located in Algiers. First, an experimental study was performed to investigate the effect of the passive and active solar systems on the indoor air temperature of the house. Then, the TRNSYS model of solar heating systems coupled with a low energy house has been validated by registering the indoor air temperature evolution of the different zones of the studied house. Different days during cold period were chosen to perform these experimental studies.

5.2. Description of the model

5.2.1. Bioclimatic house characteristics

The prototype is a rural low-energy house with 90-m² net floor area (**Fig 5.1**). It was realized in the framework of MED-ENEC Project and the partnership of two research centers (CDER & CNERIB) and in accordance with Algerian building code [92].

The house is oriented along East-West axis to collect more solar radiation in winter. There are four thermal zones: living room, two bedroom and kitchen, as shown in **Fig.5.2**. The living room and bedroom1 had a largest windows area due south which allows for the most passive solar thermal heating of the home in the winter. The walls of the house are with stabilized earth blocs and the external walls and floor are well insulated, in addition to PVC double glazed windows and shading devices. Construction properties for the house are listed in **Table 5.1**. A roof overhang is used for south-facing windows in order to prevent direct solar radiation during summer

period. The house is equipped with a solar heating system for Domestic Hot Water (DHW) and space heating.



Fig.5.1. the prototype bioclimatic house.

5.2.2. Description of the solar heating system

The main components of the solar heating system are shown in **Fig 5.3.**: solar collectors (1) installed on the top of the pitched roof (45°) and in accordance with the local latitude of the site, hot water tank (2), under heating floor (7). The operation of the solar heating system is as follows: The three-way valve (5) is under the control of a differential controller (6) in the pumping station. Priority is given to the load (space heating). Thus, the system operates as a Direct Solar Floor. The collector array is directly connected to the heating floor; the concrete slabs combine the functions of space heating storage and heat exchanger. The water heated in the solar collector, flows through the heating floor and then flows back to the solar collector. If the

temperature of the unfavorable zone of the house, which is controlled by a thermostat (3) located on the ground floor, is higher than the set-point temperature, the hot water is oriented toward the storage tank for DHW preparation.

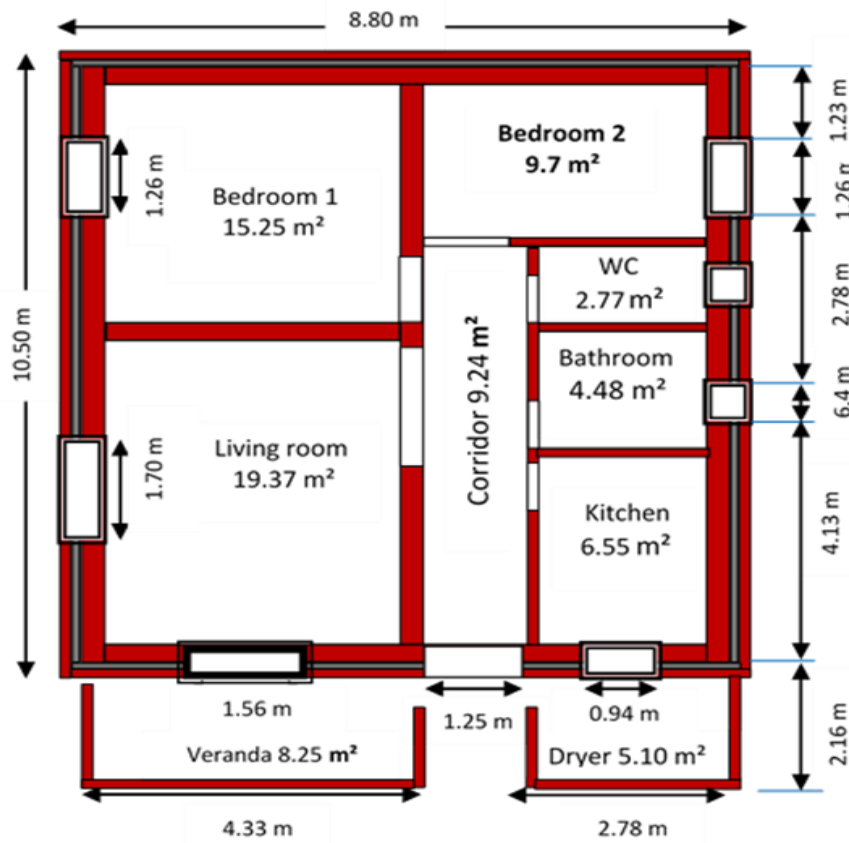
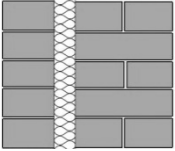
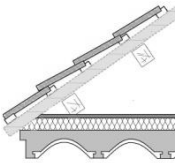
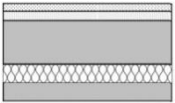



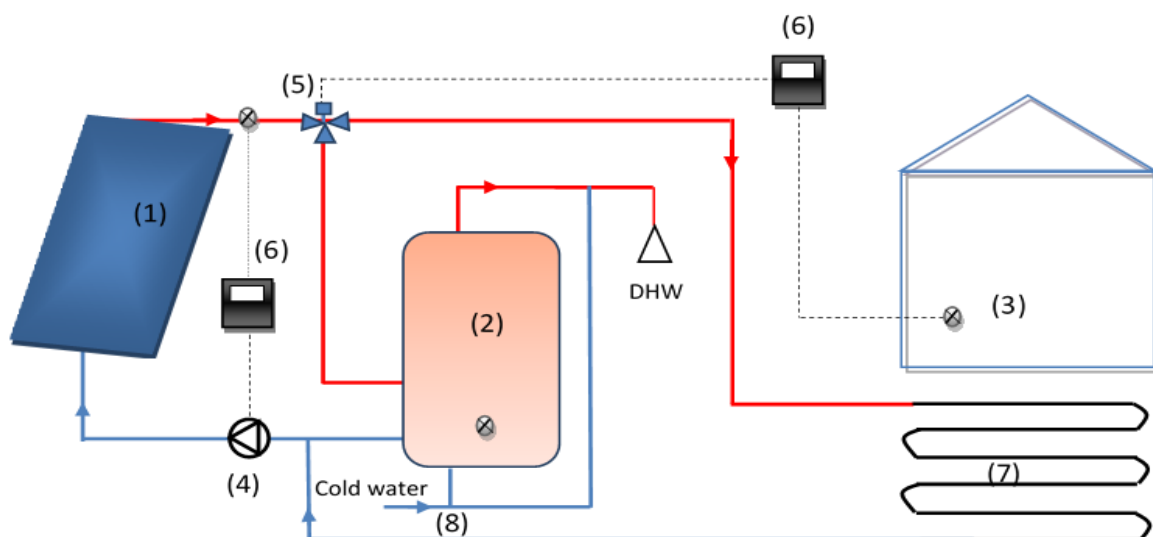
Fig.5.2. Plan view of the prototype house

The cold water from the city main enters at the bottom of the storage tank. A tempering valve (8) is used to enable the control of DHW temperature at around 45°C at the user-end. An auxiliary water heater are used to ensure a correct water temperature for DHW.

Table 5.1

U values of the building envelope

Layers	Composition	Thickness	U value (W/m ² .K)
	Stabilized earth blocs	0.14	0.36
	Polystyrene	0.09	
	Stabilized earth brick	0.29	
	Concrete	0.05	0.23
	Polystyrene	0.06	
	Concrete	0.15	
	Mortar	0.03	
	Tiling	0.02	
	Mortar	0.03	0.54
	Polystyrene	0.16	
	Concrete	0.8	
	Plaster	0.3	
	Double glazing		2.22

**Fig. 5.3.** Scheme of the solar heating system.

Tables (5.2), (5.3) and (5.4) give the characteristics of the thermal collector, the heating floor system and the storage tank, respectively.

Table 5.2

Characteristics of the thermal collector

Parameter	Value	Unit
Collector area	8	m ²
Fluid specific heat	4.19	kJ/kg.K
Collector fin efficiency factor	0.7	
Bottom, edge loss coefficient	3	
Absorber plate emittance	0.7	
Absorptance of absorber plate	0.8	
Number of covers	1	
Index of refraction of cover	1.526	

Table 5.3

Characteristics of the heating floor system

Parameter	Value	Unit
Specific heat of water	4.19	KJ/kg.K
Pipe spacing	0.2	M
Pipe outside diameter	0.02	M
Pipe wall thickness	0.002	M
Pipe wall conductivity	1.26	(W/m ² . °C)

Table 5.4
Characteristics of the storage tank

Parameter	Value	Unit
Tank volume	0.3	m ³
Tank high	1.25	M
Fluid specific heat	4.19	KJ/kg.K
Fluid density	1000	Kg/m ³
Tank loss coefficient	0.9	KJ/hr.m ² .K
Fluid thermal conductivity	1.40	KJ/hr.m.K
Heat exchanger inside diameter	0.01	M
Heat exchanger outside diameter	0.012	M
Heat exchanger length	2	M
Heat exchanger wall conductivity	1.40	KJ/hr.m.K
Heat exchanger material conductivity	1.40	KJ/hr.m.K

5.3. TRNSYS model

The solar heating system coupled with the studied house is reproduced as a virtual model in the TRNSYS software, as shown in **Fig 5.4**.

In order to explain the control strategy of the solar heating system, an example is given in **Fig. 5.5**. As shown, when the temperature at the outlet thermal collector is higher than 20°C, the hot water is supplied to heating floor and the air temperature in the controlled zone starts to increase. When the temperature reaches 20°C, the flow rate is oriented toward the storage tank. Therefore, the average temperature in the storage starts to increase.

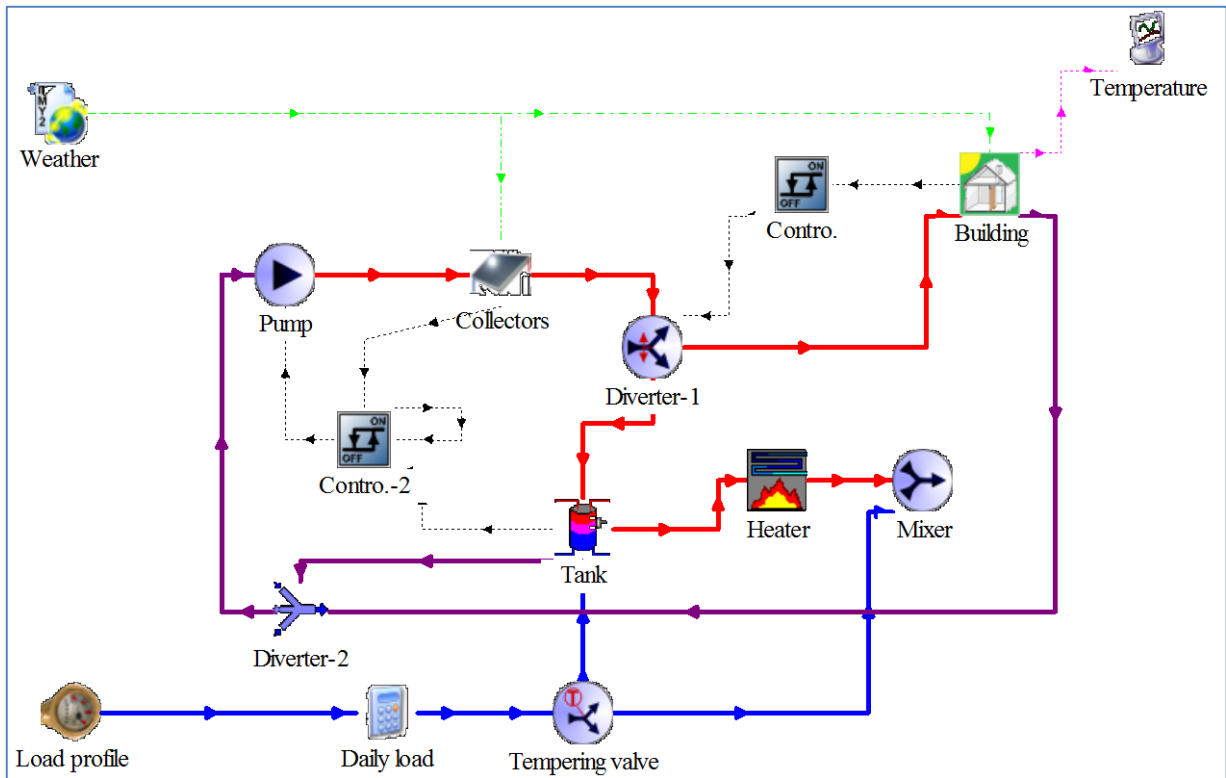


Fig.5.4. TRNSYS model of the direct solar floor system

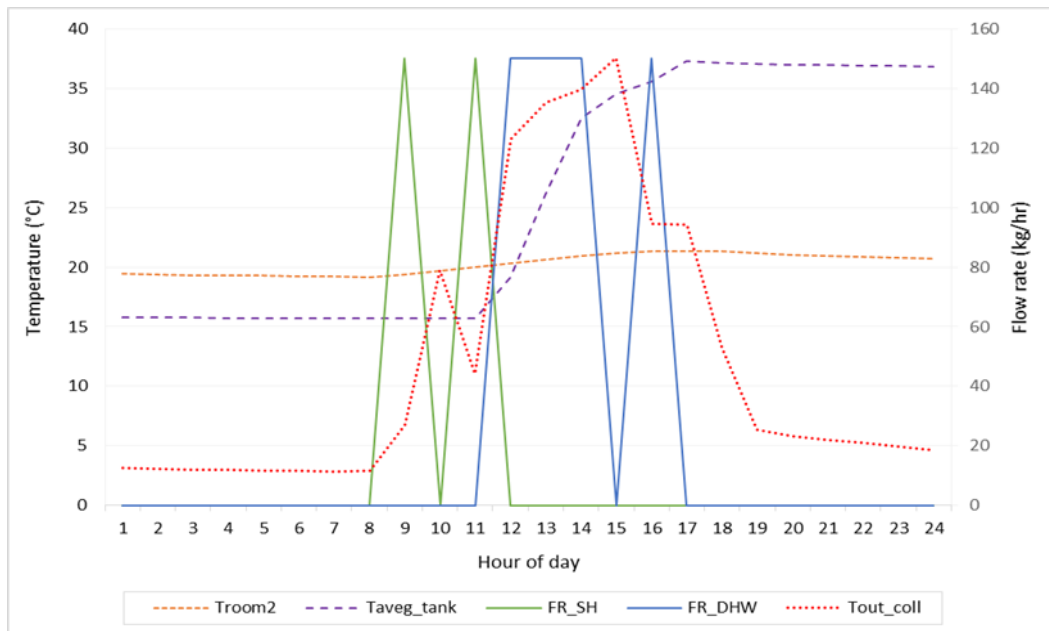


Fig.5.5. Control strategy of the solar heating system

5.4. Experimental study

5.4.1. Data acquisition system

A data-acquisition system was set up to register the experimental variables. This system consists of a computer and a Keithley digital multi-meter2700 (see Fig.5.7). A set of type-K thermocouples is used to measure temperatures at several locations.

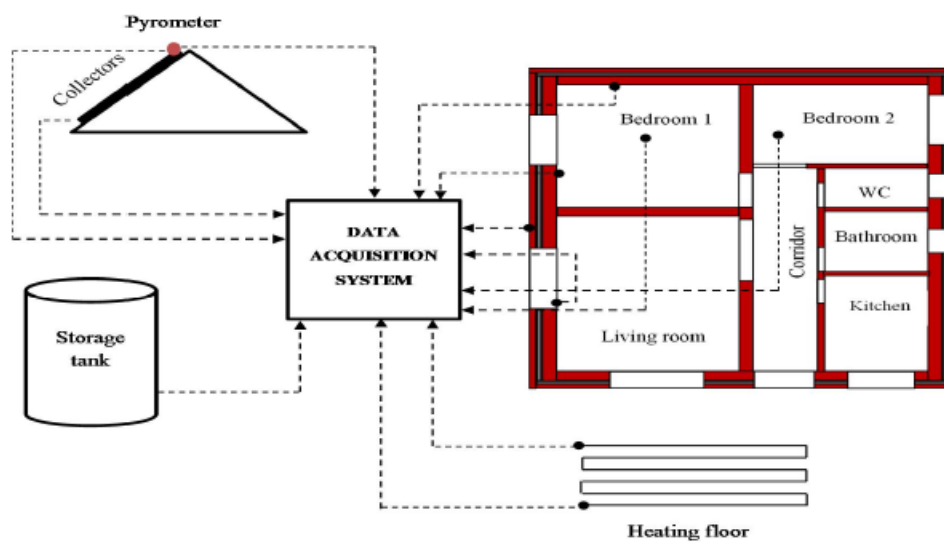


Fig.5.6 Scheme of data acquisition system

Global Solar irradiation data measured using a pyrometer mounted in accordance with the position of the slope of the collector (45°), as shown in Fig.5.8. The indoor air temperature in the different zone of the house is measured using a Testo (Fig.5.9).



Fig.5.7 computer and a digital multi-meter



Fig.5.8. pyrometer



Fig.5.9. Testo

The solar radiation and the outdoor temperature are registered at 30 min intervals during the experimental period.

5.4.2. Experimental results

Fig.5.10 shows the evolution of the outdoor air temperature and the solar radiation on the thermal collector slope (45°) during four days in December. December is one of the coldest months of the year in Algeria. It can be noticed that the last day is less sunny than the three first days. The average outside temperature measured during the monitored period is 13.78°C , with a minimum value of 9°C and a maximum of 24°C . A great daily fluctuation can be noticed externally, reaching up to 13°C . The maximum solar radiation during the monitoring period vary between 980 W/m^2 in the first day and 600 W/m^2 in the last day.

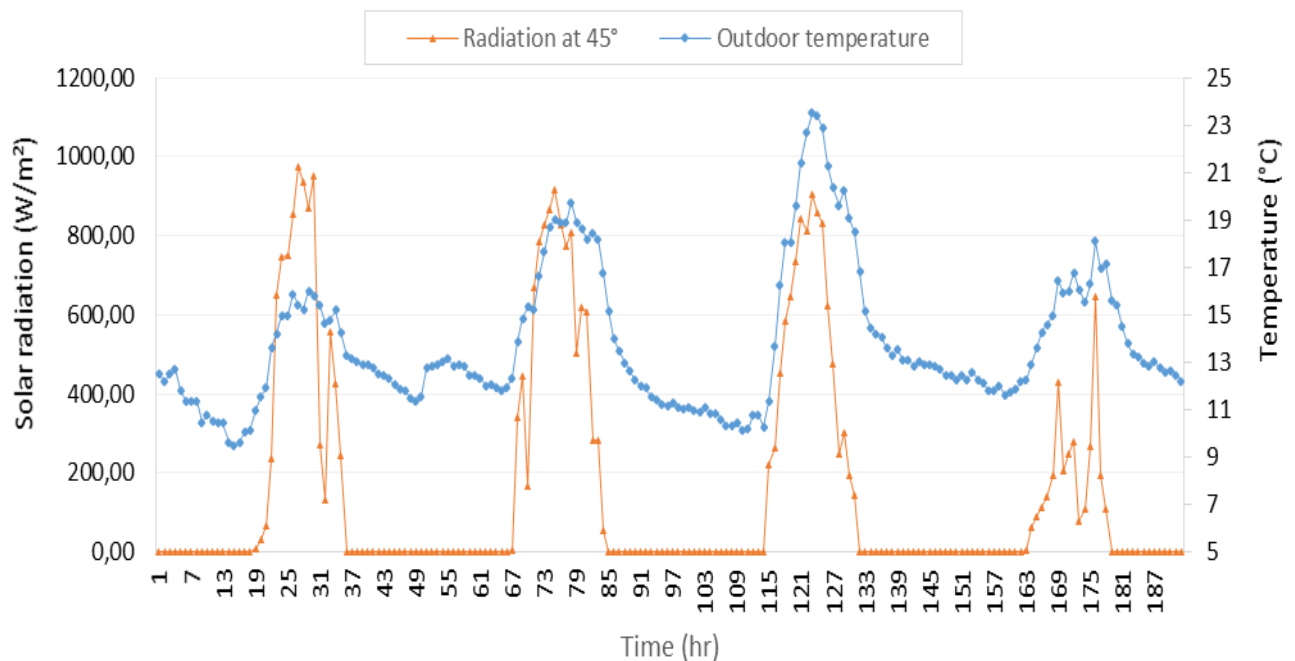


Fig.5.10. Evolution of the outdoor temperature and solar radiation during the mentored period.

Indoor air temperature conditions may have large daily variations depending on the level of thermal insulation and thermal mass of building envelope. In order to investigate the effectiveness of the passive solar system, a large window facing south and thermal insulation, a field measurement was carried out on the prototype house during the monitored period. **Fig.5.11** shows the evolution of internal and external surfaces temperatures of south-wall during the four days. It can be seen that the thermal insulation and thermal mass are effective in stabilizing the daily temperature fluctuations of inside wall surface and reducing consequently the temperature fluctuations of indoor air, which improves the indoor air quality.

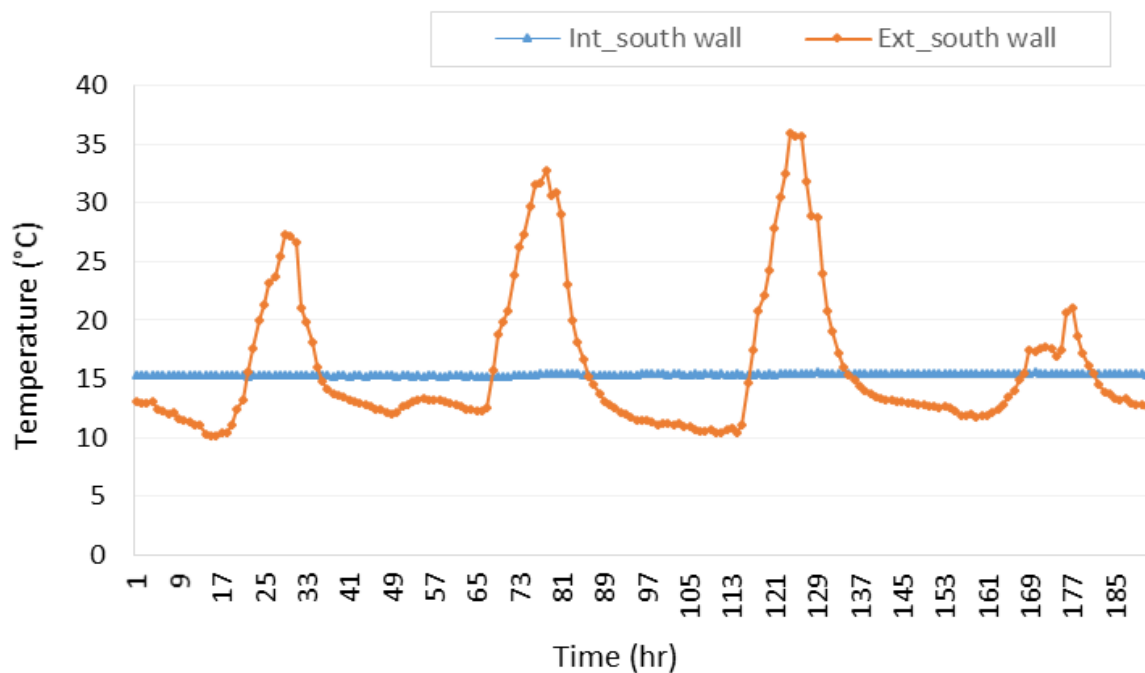


Fig.5.11. Wall surfaces temperatures

Fig.5.12 shows the effect of the room placement inside the house and windows oriented due south on the indoor thermal comfort. The living room, due to its placement in the south side of the house and a large glass area facing south, has a temperature slightly higher than the room2. Therefore, the indoor air temperature in

the living room reach 17.5 °C in daytime and stay upper than 16°C in nighttime. For the room 2, as the solar gain is absent it located in the north side of the house, the indoor temperature decreases from day to day (from 15°C to 13.5°C).

In order to investigate the effectiveness of active solar thermal system, a field experiment was carried out in the prototype house during the monitored period. During this period, the heating floor is activated during the first two days in the room2 and during the last two days in the room1.

Fig.5.13 shows that the contribution of the solar heating system in improvement of the indoor air temperature is very important. For room2, the maximum indoor temperature increased from 16.5°C in first day to 18°C in second day. For room1, the maximum temperature reached 19.5°C in the second day due to the combination of active and passive solar gain.

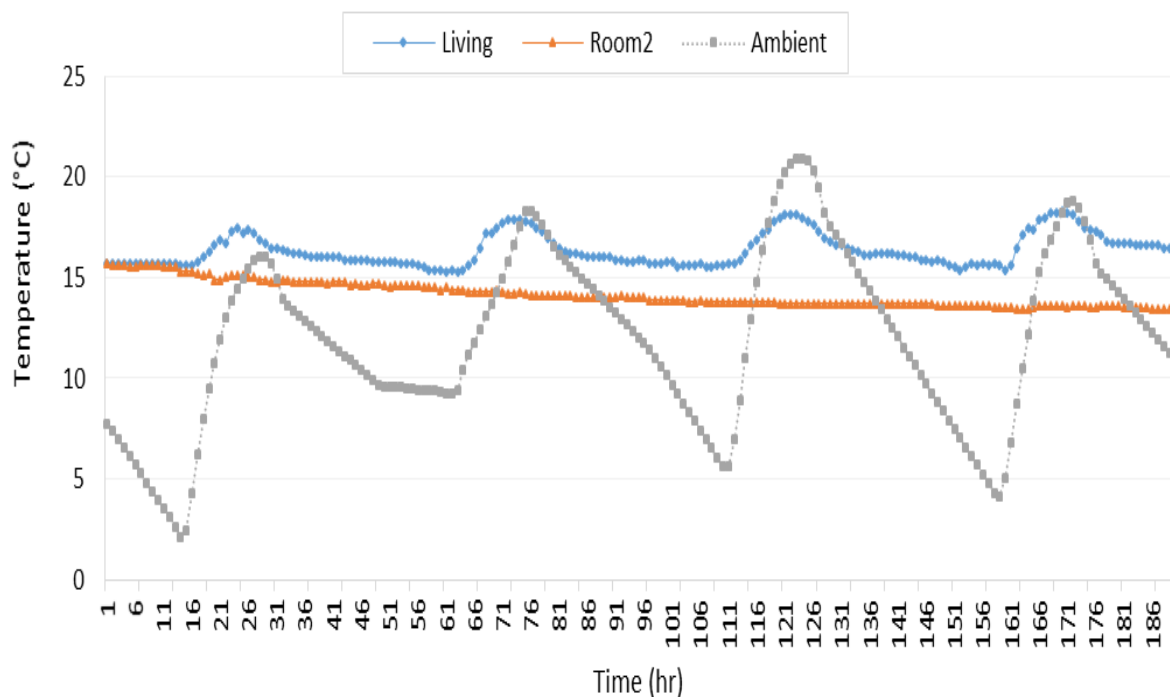


Fig.5.12. measured temperature of interior air of the house

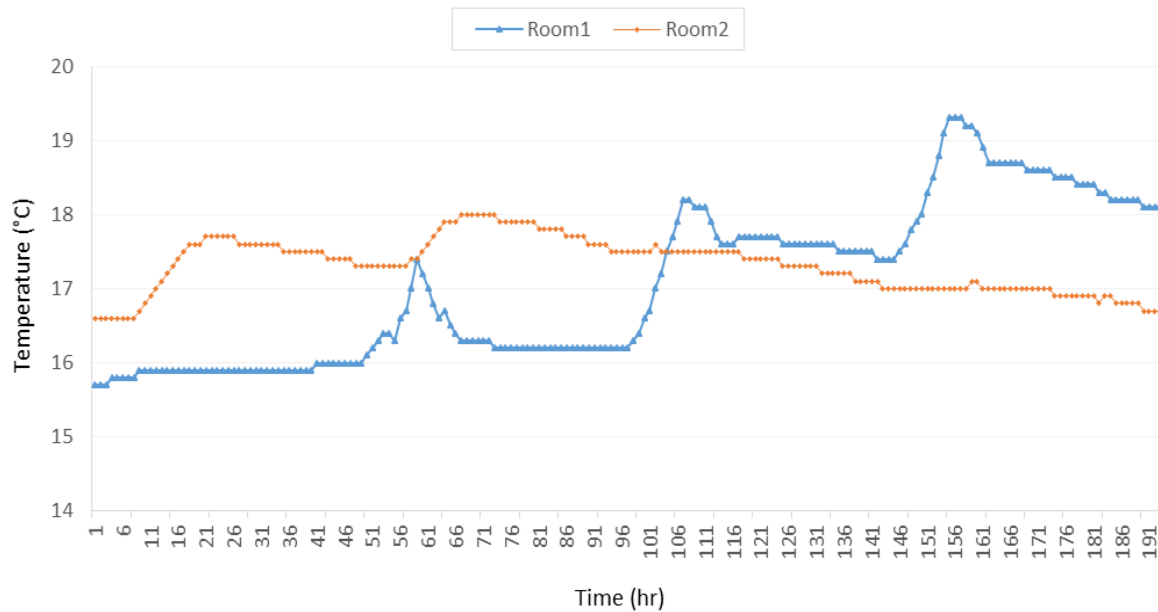


Fig.5.13. effect of the heating floor on the interior air temperature

Fig.5.14 shows the evolution of the average tank temperature during the monitored period. It can be seen that the temperature in the storage tank not exceed 16°C . As the interior air temperature of the unfavorable zone remain less than 20°C , all the collected heat from the thermal collector is oriented toward the floor heating to meet the space heating demand.

5.4.3. Validation of the model

In order to calibrate the multi-zone house model with heating floor system, a field measurement was performed. In this case, we consider that the floor heating system is activated only in the Room1 (active solar gain), the Living-room benefited from only the passive solar through a large window facing south and in the Room2, there is any

solar gain. The registered meteorological data were used as inputs to the TRNSYS solar system model. The simulation results are compared with the experimental data.

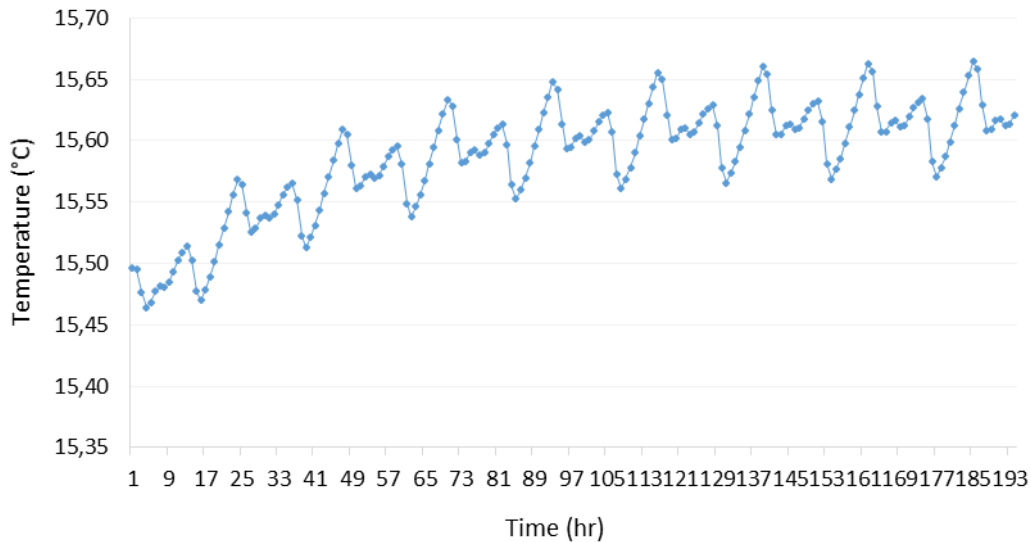


Fig.5.14. Average tank temperature during the monitored period

To test the accuracy of the model, the mean relative error (MRE) and root mean square error (RMSE) are used to analyze the simulated and the measured values [93].

$$MRE = \left| \frac{\sum_{i=1}^n (C_i - M_i)}{N \times M_i} \right| \times 100\%$$

Where M_i and C_i are i th values, respectively, measured and calculated, N is the number of measurements. The measured and simulated hourly temperatures at the output of the thermal collector is shown in **Fig.5.15**.

Table.5.5 shows that the MRE between the simulated and the measured values are less than, 1%, the minimum absolute temperature difference 0°C and the maximum absolute temperature difference 0.46°C,

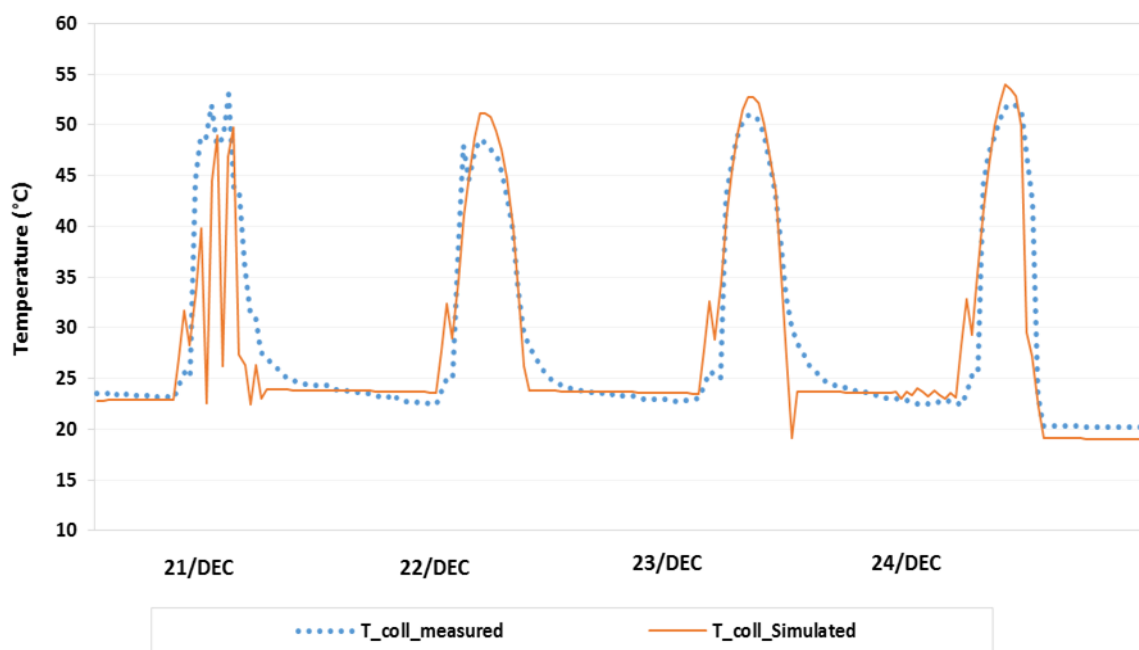


Fig.5.15. Measured and simulated temperatures of the fluid output from the thermal collector.

Table 5.5

Mean relative error

	T_{\min} (°C)	T_{mean}	T_{\max} (°C)	MRE (%)
Collector	0.00	0.08	0.46	1%
Room1	0.03	0.44	1.55	2.30%
Room2	0.01	0.20	0.82	1.61%
Living room	0.05	0.53	1.48	3.14%

The hourly indoor temperatures (simulated and measured) in the Room1, Room2 and Living-room are shown in **Fig.5.16** and **Fig.5.17**. We can noticed that there is a similar change trend between the simulated and the measured values. The MRE is 2.30%, 1.61% and 3.14 % in the Room1, Room2 and Living-room, respectively.

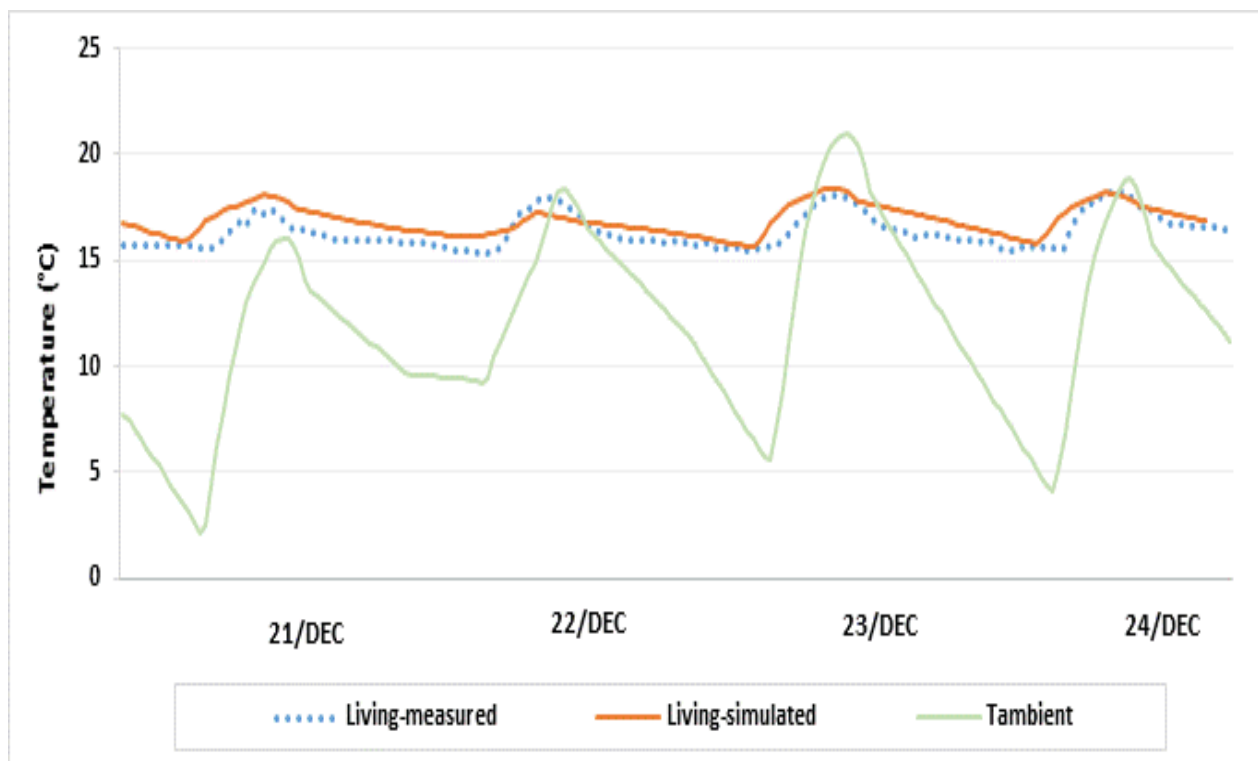


Fig.5.16. Measured and simulated temperatures
of the interior air of the living room

The minimum and the maximum absolute temperatures differences are 0.03°C and 1.55°C, in the Room1, 0.03°C and 0.82°C in the Room2 and 0.05°C and 1.48°C in Living-room, respectively. In general, the simulated results agreed well with the experiment results.

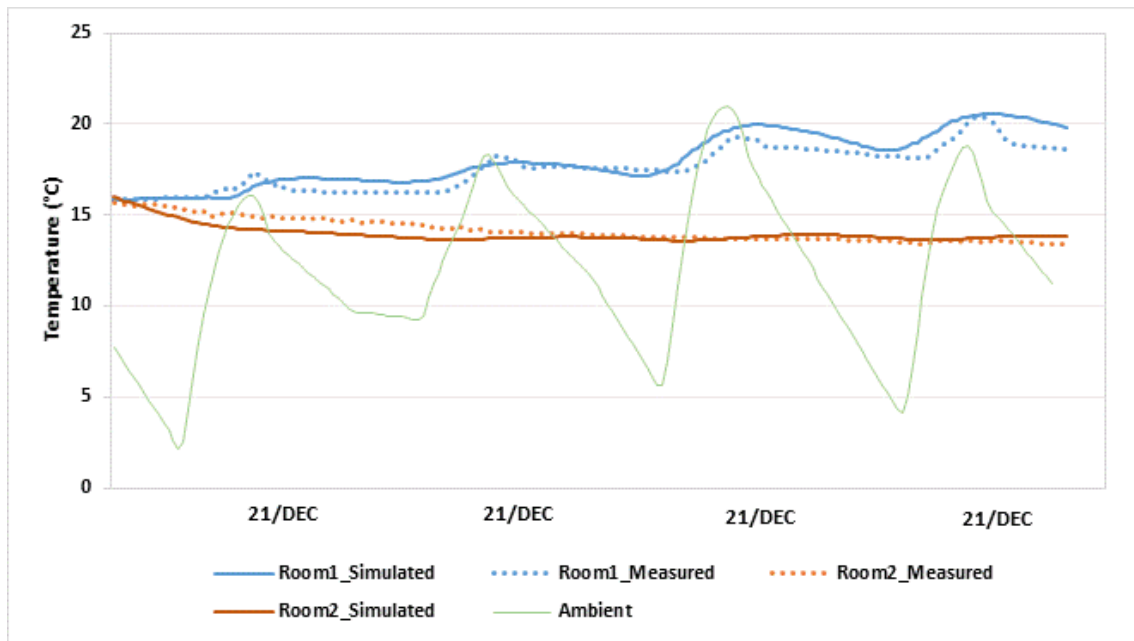


Fig.5.17. Measured and simulated temperatures of the interior air of t Room1 and Room2

5.5. Conclusion

The aim of this chapter was to perform an experimental study to investigate the effect of passive and active solar systems on the indoor air temperature of a single-family low-energy house. The results show that the solar gain through a large window facing south in combination with thermal insulation represent a powerful system to improve indoor air temperature of the house. The results show also that the solar heating system operating as a direct solar floor can contribute significantly in the improvement of the indoor thermal comfort of the house during cold season.

Before been used the model for others energetic analysis, the solar heating system is reproduced in TRNSYS software and validated with experimental data under Algiers climate conditions. The results show a good agreement between measured and simulated data.

***Chapter 6: Solar energy integration in rural
housing and their impact on the
sustainable development of Chlef district***

6.1. Introduction

In the present chapter, the impact of solar energy integration in rural housing on the sustainable development of the Chlef district is considered. To reach this goal, an energetic and environmental analysis are made.

For energetic analysis, the model developed and validated in the previous chapters is applied on case study of a single-family typical rural house located in Chlef district. As mentioned before, the model includes a multi-zone house coupled with solar systems. Energy balances are calculated for the case study house. Scenarios for a house redesign are then proposed, with the aim of reaching a high-energy performance rural house.

The energy requirements for the reference house are reduced first by passive mean through the integration of a set of energy efficiency measures (EEMs). Then, by active mean, with the use of a solar heating system to provide heat for space heating demand in winter season and DHW preparation over all the year. A grid-connected PV system is designed to produce electricity for household need and electrical energy required for electrical heater (auxiliary energy for solar heating system). In all cases, a parametric study is conducted to optimize the energy efficiency measures and determine the optimum sizes of solar systems.

Then, based on the energy balance of the reference house, the overall energy saving and the reduction of CO₂ emissions at the energy balance of chlef district due to this energy conservation are investigated.

Finally, in order to get information about the profitability of EEM and solar systems on rural housing, an economic analysis is performed. In this direction, we investigate yearly revenue, investment cost and return on investment due to the installation of a

grid connected PV system, a solar heating system and EEM in rural housing of Chlef district.

6.2. Energy situation of Chlef district

The district of Chlef is located in the Northwestern region of Algeria. It is 208 km far from the capital Algiers, at latitude 36.13°, longitude of 1.20° and an altitude of 133 m. It extends over an area of 4791 km² and a population of around one million inhabitants with a density of 194 inhabitants/km². It occupies a strategic place due to its geographical location. It is characterized by a Mediterranean climate: sub-humid in the North and continental in the South, cold in winter and hot in summer.

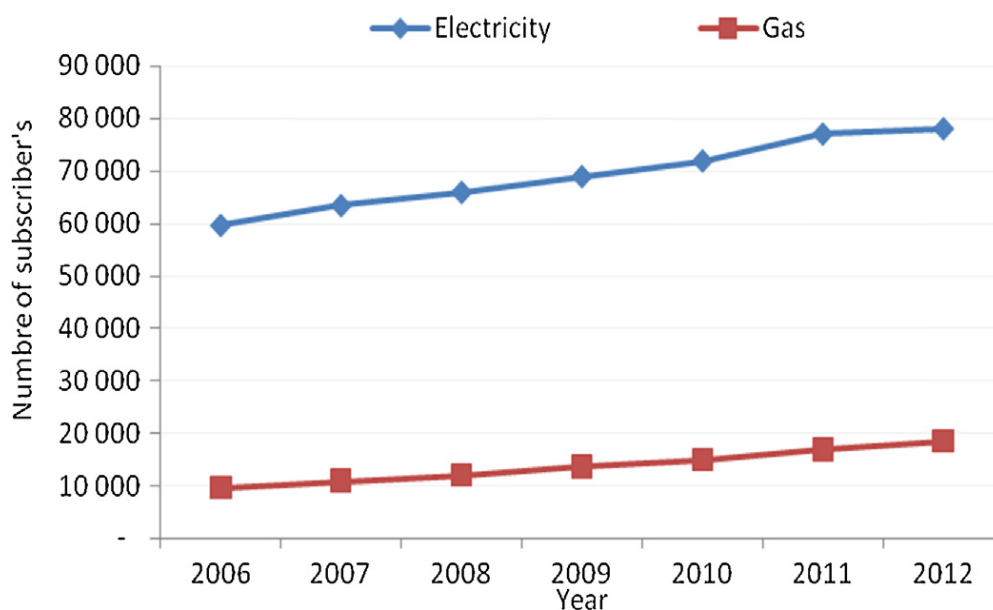


Fig. 6.1. Evolution of the number of electricity and natural gas subscribers in Chlef [SONELGAZ, Chlef].

Electricity and natural gas are the most common energy sources used by the households in the region. The electricity is used for lighting, household appliances running and space cooling, while natural gas is used for cooking, space heating and

production of sanitary hot water. In the zones where houses are not connected to natural gas, especially those in rural areas, the gas supply is provided by butane gas cylinders. Previously, rural inhabitants used the wood and its derivatives for cooking and heating. But in recent years, the development of the road network and the availability of butane gas cylinders decreased the use of wood.

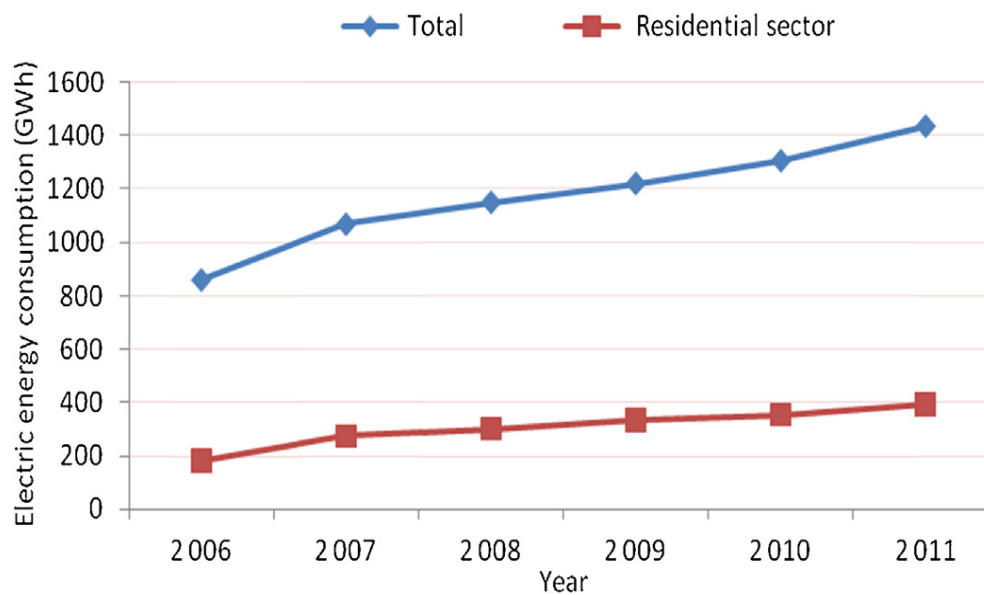


Fig. 6.2. Evolution of the overall electricity consumption and of the residential sector, in Chlef [SONELGAZ, Chlef].

The number of subscribers connected to the low voltage (LV) electricity grid and low pressure (LP) natural gas are continually increasing from year to year, as shown in **Fig. 6.1**. These data are provided by the “Société Nationale de Distribution d’Electricité et du Gaz” (Sonelgaz) of the district of Chlef. According to the assessment made in 2011 by the Department of Energy and Mines, the subscribers number connected to the low voltage network (LV) is 78,562 subscribers representing a coverage rate of 94.56%. The rate of the district is near the national average rate which is around 95%. For natural gas, the current rate has increased from 26% in

2004 to 36.03% in 20. However, the rate is one of the lowest in Algeria. This increase of the subscriber's number is mainly due to connection of new buildings to the electricity grid and gas, which will surely lead to new consumption scenario. In **Fig. 6.2** are represented the evolution of the overall electricity consumption in the residential sector, of the district of Chlef. It is noticed that the electric energy demand is growing sharply from one year to another. An increase of approximately 30% is recorded from 2006 to 2011 due mainly to the increase in housing stock, estimated at 189,708 units at the end of 2011. This trend of increase was experienced in recent years. The evolution of butane gas consumption shows that the demand on the butane gas is decreasing significantly from 2006 to 2009 (Fig. 4). This evolution is due to an increase in the number of subscribers to the natural gas network, as shown in **Fig.6.3**.

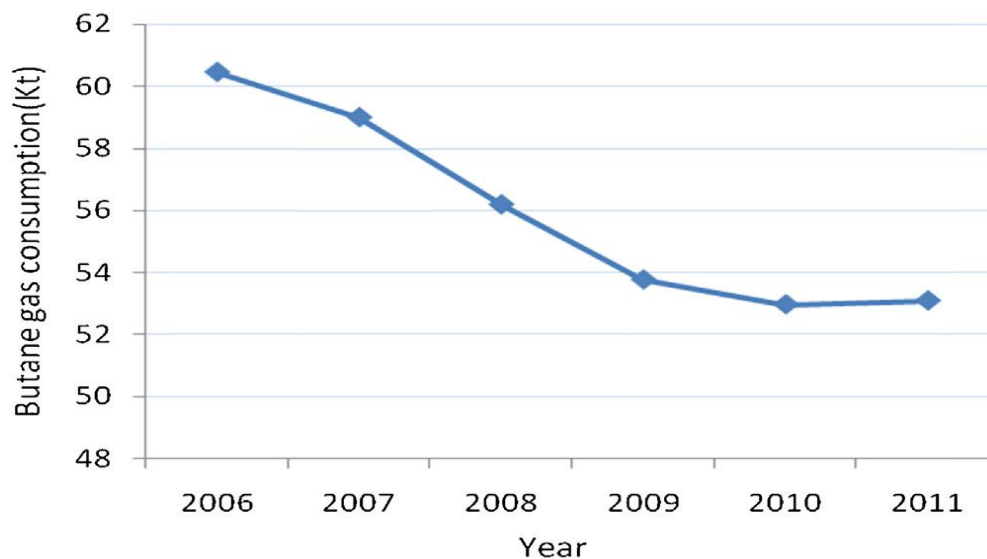


Fig. 6.3. Evolution of the butane gas consumption in Chlef ,[SONELGAZ, Chlef].

6.3. Rural housing programs

According to the direction of housing and public facilities of the district of Chlef, the rural housing program has practically tripled in the last ten years, rising from 7350 to

23 700 rural house for the program 2010-2014., From **Fig.6.4**, it can be seen that rural housing had the lion's share of the construction programs compared to others programs. The construction plan of rural housing (2010 to 2014) has experienced greater increase compared with the one of (1999 to 2004). For the construction of a rural house, state Subsidy (SS = 7000\$) is given to help local people to start building a new house in rural areas. This program generates a positive impact on the stability plan, living conditions improvement of the rural areas population and the eradication of precarious housing. Except the town of Chlef, all the other municipalities, 34 in number, have been hit by this program for obvious reasons. Indeed, according to official data, rural areas are home of 50% of the population, whose house is characterized for a large part by precarious constructions where living conditions are deplorable. The majority of houses are scattered, whereas the rest is concentrated around the towns of the municipalities.

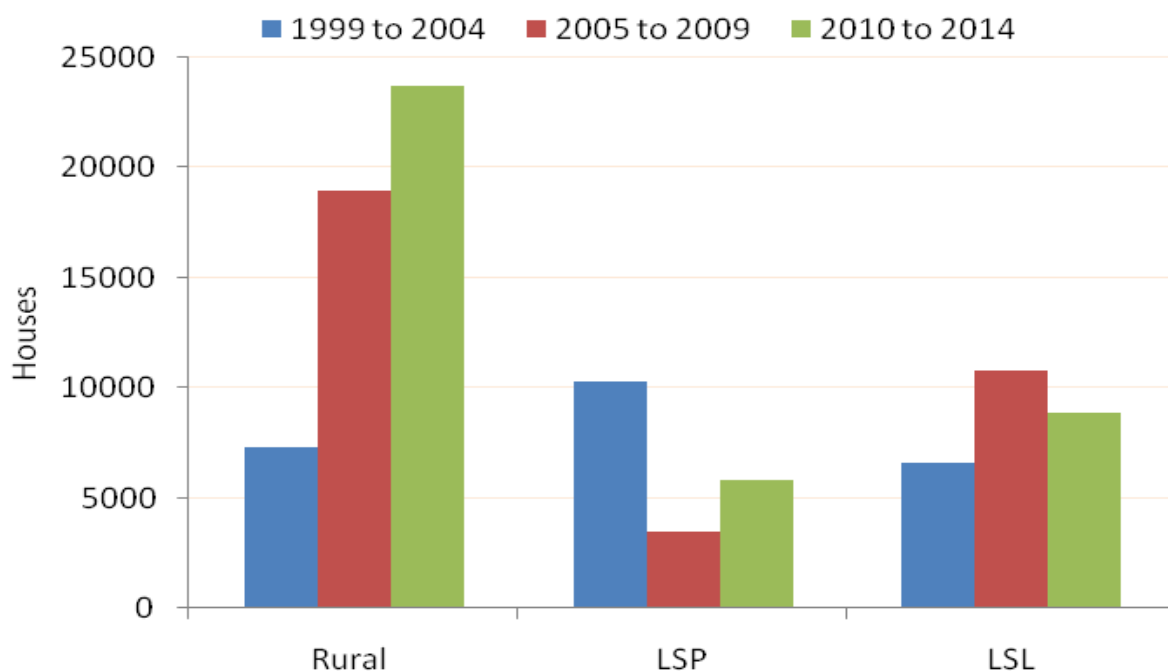


Fig.6.4. Housing construction programs in Chlef district

6.4. Improvement of energy performance of a rural house

6.4.1. Reference house characteristics

It was intended to build rural houses with tiles (with pitched roof) but people prefer flat-roof houses made of concrete, since they offer them alternatives for parts under roof. For this purpose, we have proposed a typical representative rural house with a flat roof, as shown in **Fig.6.5**. This type of housing is the most widely built in district of Chlef with 80 m² floor area [94]. The house has a simple rectangular layout with floor dimensions of 10 × 8 m and the long axis of the house running east–west while its height is about 3 m. The interior of the house consists of a living room, two bedrooms, a kitchen, a bathroom and a toilet and occupied by an average of four people per habitat. The floor plan for the reference house is shown in **Fig.6.6**.



Fig.6.5. Typical rural houses in Chlef with flat roof

This house is connected to the electricity grid, but the gas supply is provided by butane gas cylinders. Since the house is located in a rural area where district heating

is not available, a mobile heating system operating with propane gas or butane gas is used for space heating. During the warmer months, no air conditioning is used, in addition to natural night ventilation; inhabitants use mechanical ventilation such as ceiling fans for cooling. Construction properties for the house are listed in **Table 6.1**.

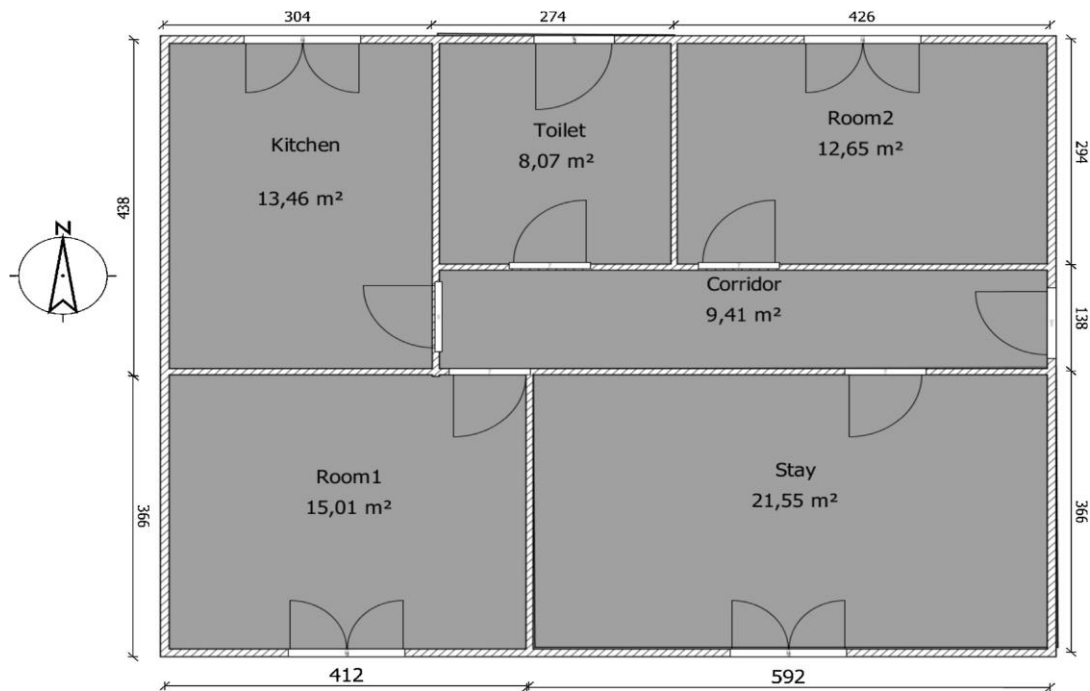


Fig.6.6. Typical rural house plan with a living area of 80 m².

In the majority of housings in this district, the construction materials are also very similar, the roof is in heavy concrete and slabs, the wall in hollow clay brick, the floor is in cement. Facades containing windows are oriented towards the south and north. The windows are all clear, single pane glazing with a wood frame. It was assumed that four people, each contributing 115 W (75 W sensible and 40 W latent) to the internal gains, would occupy the house during hours from 5:00 pm to 8:00am, and one person is present from 8:00 am to 5:00 pm. Fridays and Saturdays, four persons presence is assumed throughout the day. The total internal gains were calculated from a load profile of typical household electrical loads and occupancy to be 3

W/m² of floor area averaged over a 24 h period. The temperature set points for the zone were set to 20–26°C from 7:00 am to 10:00 pm and during sleeping hours a wider thermal comfort range of 18–26°C was implemented as a lower temperature can be tolerated in bedrooms.

Table 6.1

Wall characteristics of the reference house

Construction	Material	Thermal transmittance (W m ⁻² K ⁻¹)
Exterior wall	Cement plaster (2.5cm) hollow brick (15cm) plaster coating (2.5cm)	2.303
Interior wall	Cement plaster (1.5cm) hollow brick (10cm) plaster coating (1.5cm)	3.395
Roof	heavy concrete (10cm) slabs (15cm) plaster coating (1.5cm)	2.338
Floor	Heavy concrete (5cm) mortar (4cm) tiling (2cm)	3.466
Window	single glazing	5.68

6.4.2. Weather data

Representative Chlef weather data are analyzed in the aspect of solar radiation and average monthly temperatures, as shown in **Fig.6.7**. Based on data from the hourly global irradiation on horizontal surface, we can see that the Chlef region has a higher average annual daily to 4.61 kWh/m²/day. It can be noticed that the winter has less solar potential whose average daily monthly global radiation varies between 2

kWh/m²/day and 3 kWh/m²/day. Solar radiation becomes very important between March and October when the average daily monthly global radiation varies from 5 kWh/m²/day to 7 kWh/m²/day. The average monthly temperature varies between 10.5°C in January and 30.5°C in July.

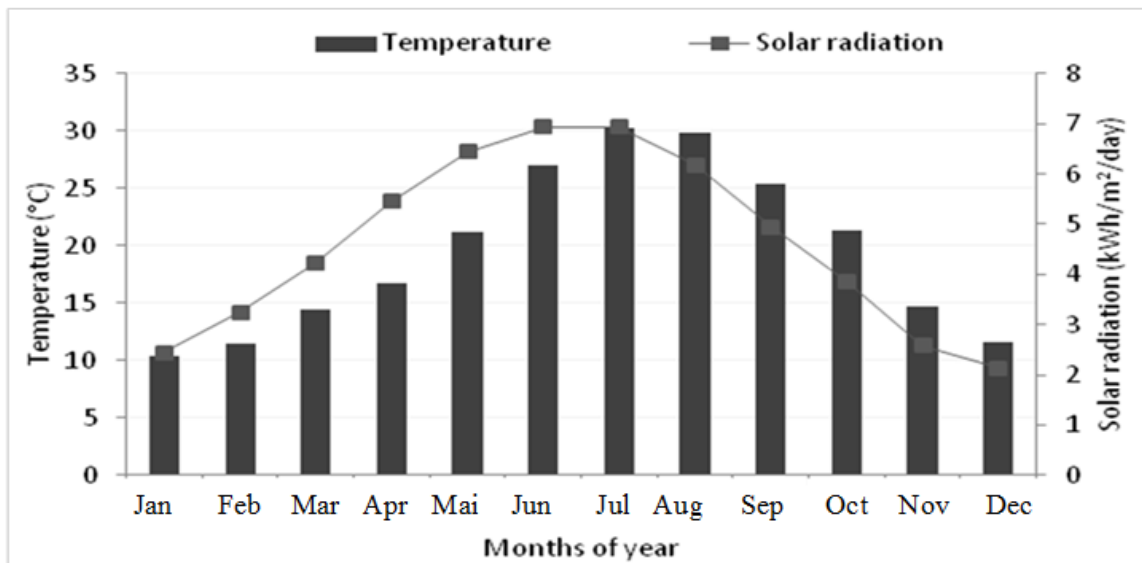


Fig.6.7. Average daily monthly irradiance and temperature of Chlef district

6.4.3. Energy efficiency measures

In this analysis, in order to reduce the heating and cooling needs and improve consequently the energy efficiency of the reference house, a parametric study is conducted to determine the optimum energy efficiency measures (EEMs). The energy need of the house is taken as the criteria for the optimal EEMs. The effect of this optimum EEMs is examined, individually and in combination, as shown in **Table 6.2**. These energy efficiency measures include [95]:

- Optimal orientation of the house: As the reference house presents a rectangular form, two orientations of house are considered in this analysis. First, the house is oriented on the East/West axis with longest walls facing south and north. Second, the house is oriented on the North/South axis with longest walls facing East and West. Note that windows are oriented with longest walls of house.
- Optimal thermal insulation thickness: In order to determine an optimum insulation thickness, the annual heating and cooling requirement for the reference house is estimated for different thermal insulation thickness (from 0.02 to 0.20 m) of external walls and roof. The thermal insulation used is the expanded polystyrene (1.4 W/m K).
- Glazing type: The glazing type is a parameter to be considered in order to reduce heating and cooling requirements. For this reason, single glazing (5.47 W/m K) is replaced by double glazing (1.4 W/m K). Interaction between glazing type and thermal insulation is also investigated.

Table 6.2

Energy saving measures and their combination

Configuration	Description
1	Baseline (construction characteristics described in Table 2)
2	Orientation (east/west axis)
3	Increasing of windows size
4	Use of efficient glazing (1.4 m ⁻² K ⁻¹)
5	Thermal insulation of wall and roof
6	Combination: insulation of exterior walls and roof with use of efficient glazing and increasing of windows size with use of shading device

- Optimal windows size: the windows size of the reference house represents only 12% of the facade facing south. This minimizes direct solar gain and daylight through windows of the house. Different windows sizes (from 10 to 90%), with the use of

external shading device in summer, are studied to determine an optimum windows size. The minimum windows size is 10% from the façade area in order to reach human comfort.

6.4.4. Impact of energy efficiency measures

6.4.4.1 Effect of house orientation

The optimal house orientation increases the quantity of daylight and reduces the energy demand for artificial light. **Fig.6.8** shows that the total energy needed to provide comfort throughout the year is about 12438 kWh when the house is oriented on a North/South axis and about 12065 kWh when the house is oriented on an East/West axis.

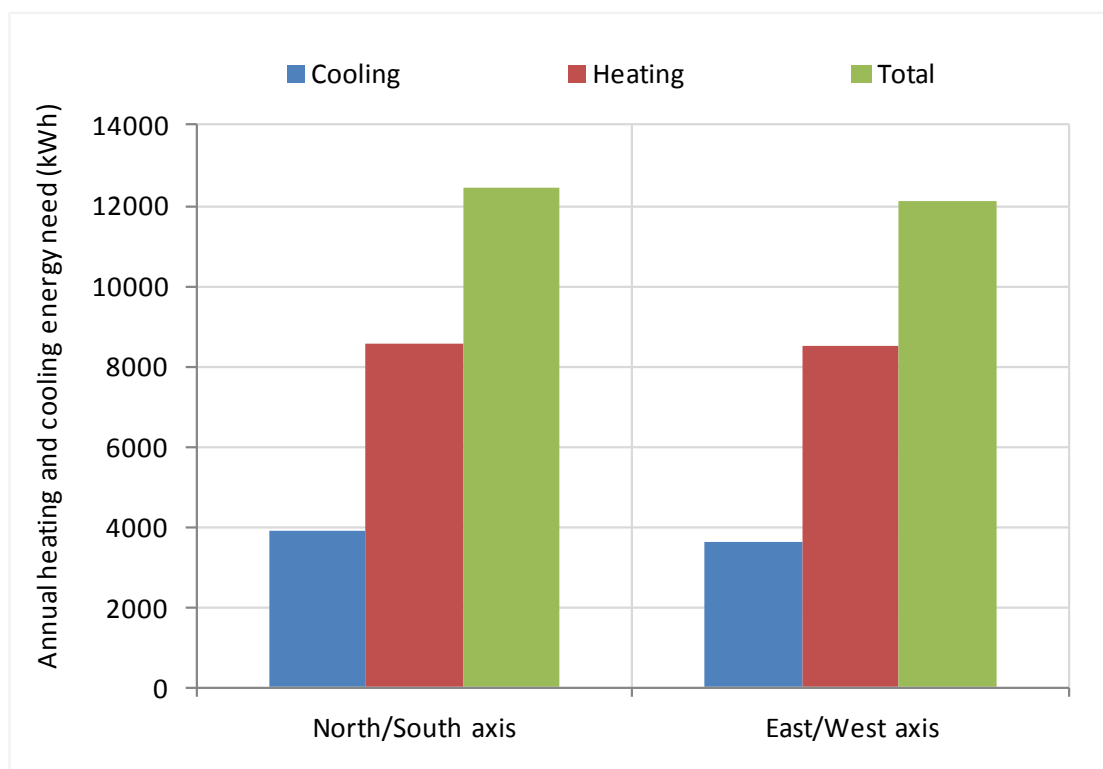


Fig.6.8. Annual heating and cooling needs at different orientations

The greatest energy saving was obtained when the rectangular house is oriented on an East/West axis with the longest walls facing south and north. The simple fact of house orientation on an East/West axis in the design step, with the longest side facing south can save 2.99 % of energy. It can be found that buildings with a small ground plan were less sensitive to changes in orientation.

6.4.4.2. Effect of windows size and shading device

The effect of windows size on heating need is estimated for different windows size from the total façade area. **Fig.6.9** shows that for the south façade, increasing windows size from 10% to 40% decreases annual heating requirement from 8569 to 8260 kWh. This is due mainly to the large amount of useful solar heat gains obtained through south facing windows. However, beyond this size (50% to 90%), heating needs of south face tend to increase with the increase of window size. This can be attributed to the fact that the increase of solar heat gain with large window areas is offset by increased heat losses with large windows due to their relatively low insulation. For the north façade, heating requirement of the house increases from 8569 to 9527 kWh with an increasing windows size (from 10% to 90%).

As can be seen in **Fig.6.10**, for both façades (north and south) annual cooling needs increases (from 3551 to 5317 kWh for south façade and from 3551 to 4511 kWh for north façade) with an increasing windows area (from 10% to 90%). However, thanks to external shading device, the increasing of cooling needs result in the increasing of windows size of the southern façade can be avoided. Since, shading device plays an important role in modulating heat gain of the house and blocking out unwanted radiant heat gain. As a result, the optimum windows size is 10% for North façade and 40% South façade.

Increasing the windows size of the southern facade by 40% (11.2 m²) compared to the originally windows size (12%) with the use of external shading device in summer provides significant energy savings by reducing the total energy needs of 5.40%.

It is noticed also that in addition to gain maximum benefit from solar radiation in heating season, increased window area facing south enhances a house natural lighting especially in rural area where sunscreens are absent. While, the minimum windows size on north façade (10%) minimizes heat loss by conduction in heating season. However, it represents a good way to bring in daylight and avoid solar heat gains by improving night cooling in cooling season.

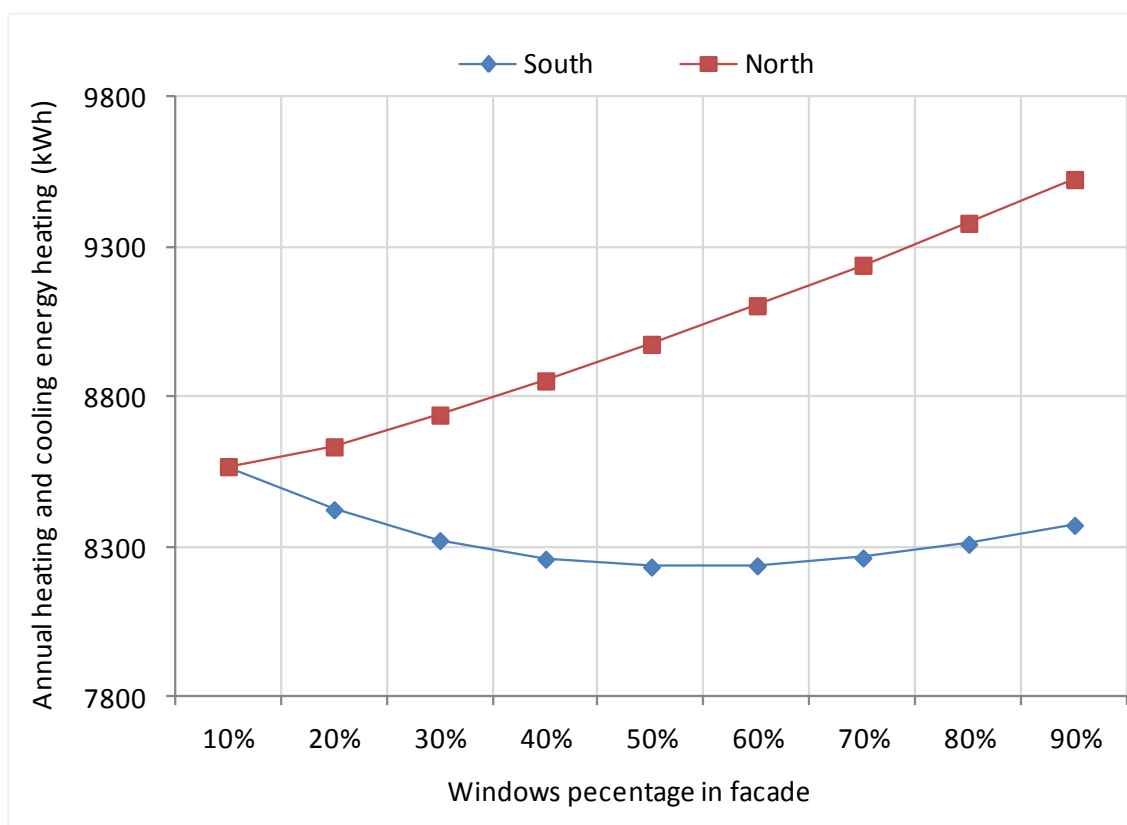


Fig.6.9. Annual heating energy at different windows sizes

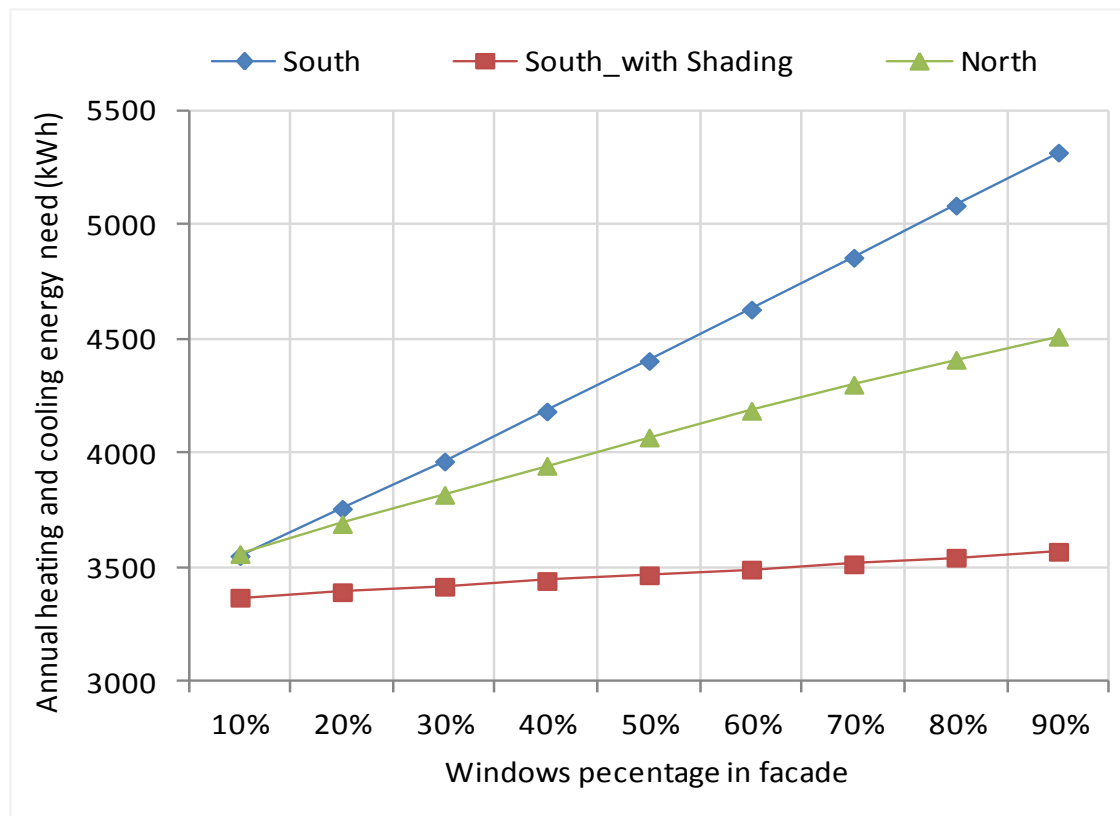


Fig.6.10. Annual cooling energy at different windows size

6.4.4.3. Effect of thermal insulation

In order to determine an optimum insulation thickness, the annual heating and cooling needs for the reference house is estimated for different thermal insulation thickness for walls and roof. As can be seen from the results shown in **Fig.6.11**, the increase in the thickness of the thermal insulation leads to a significant reduction in the energy need of house. The annual energy need diminishes (from 12090 kWh to 5384 kWh) as the insulation level increases (from 0.02 m to 0.2 m). A reduction of 49.40% in annual energy need is recorded when increasing the thermal insulation thickness of only (0.08 m). However, beyond this thickness, the impact on annual energy need strongly attenuates with a reduction of about 6%, for an increase of the insulation thickness of 0.08 to 0.2 m. Consequently, the effectiveness of increasing

the insulation as a method for reducing energy need is effective only up to a certain point, after which a massive increase in insulation continues to produce a reduction in the heating demand, but at a lower rate. In our case study, the optimum insulation thickness is 0.08 m for both walls and roof.

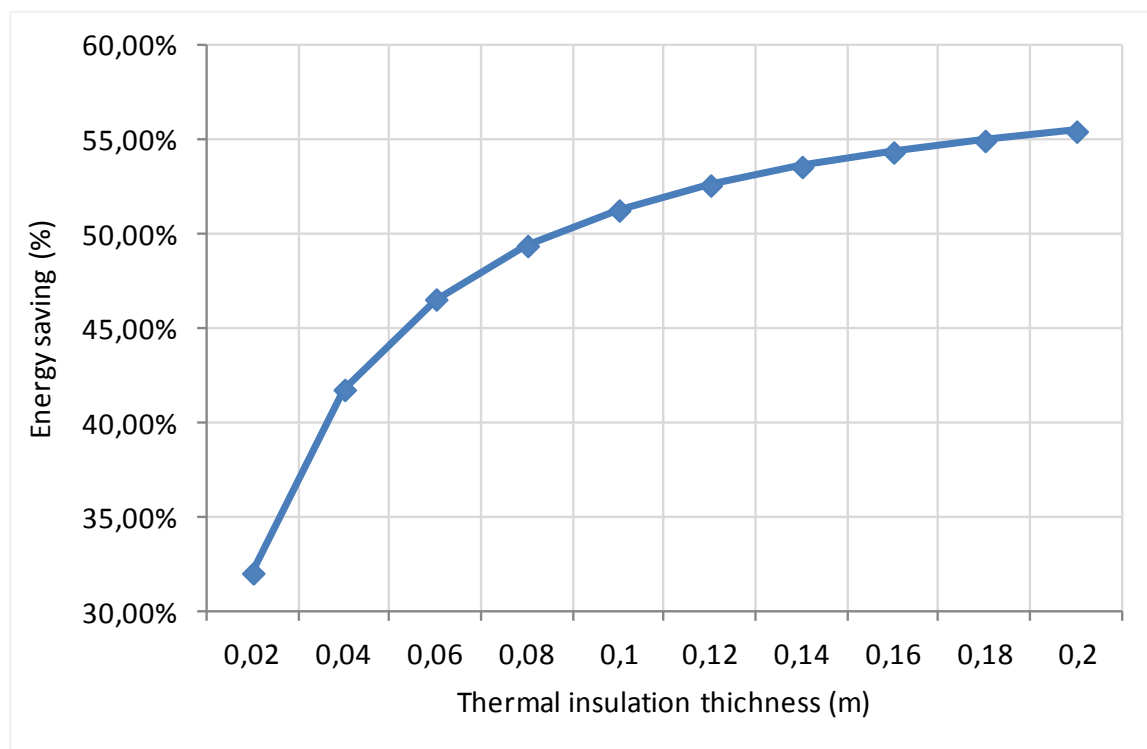


Fig.6.11. Energy saving at different insulation thickness for ceiling and walls

6.4.4.4. Effect of glazing type

In this section, an analysis of the impact of the glazing type on the house energy needs is presented. The interaction between the glazing type and insulation level is also illustrated through the simulation of two configurations. The simulation results of the case studies are presented in **Table 6.3**.

For the reference house, the impact of double glazing windows on the annual energy needs is low. The total annual energy needs decrease (from 12065 kWh to 11485

kWh); a reduction of only 4.80% is achieved. While, in the case of an insulated house, the impact is significant. The annual energy needs are decreased (from 6118 kWh to 5326 kWh), with a reduction of 12.94%.

Table 6.3

Effect of the glazing type

	Reference house	Insulated house
Single glazing	12065	6118
Double glazing	11485	5326
Energy saving rate	4.8%	12.94%

6.4.4.5. Effect of the combination

The individual performance of any of these energy efficiency measures can be considerably different when used in combination with others. The optimum energy efficiency measures to minimize the requirements of energy have been identified are presented in **Table 6.4** and the energy savings achieved by these optimum energy efficiency measures (EEM) individually and in combination in **Fig.6.12**

The orientation of the house on an East/West axis with longest walls facing south and north reduces the annual energy need of 2.99 %. The Increase of the existing window area of the south façade, measured as a percentage of total wall area, to 40 % leads to a reduction of 5.40 % in annual energy need.

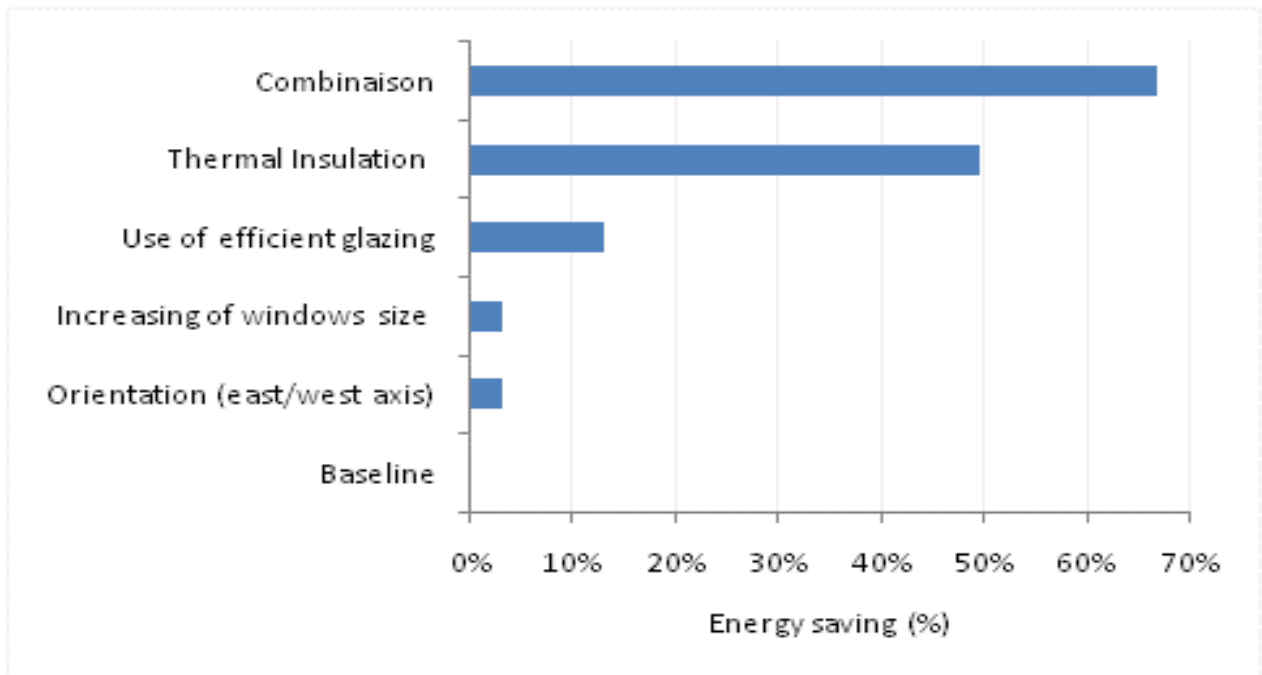


Fig.6.12. Annual energy reduction rate

The U value for external walls is improved from $1.77 \text{ W/m}^2 \text{ K}$ to $0.38 \text{ W/m}^2 \text{ K}$ and the U value for roof from $2.55 \text{ W/m}^2 \text{ K}$ to $0.4 \text{ W/m}^2 \text{ K}$ resulting in annual energy need reduction of 49.40%. This makes the thermal insulation the best measure of energy efficiency.

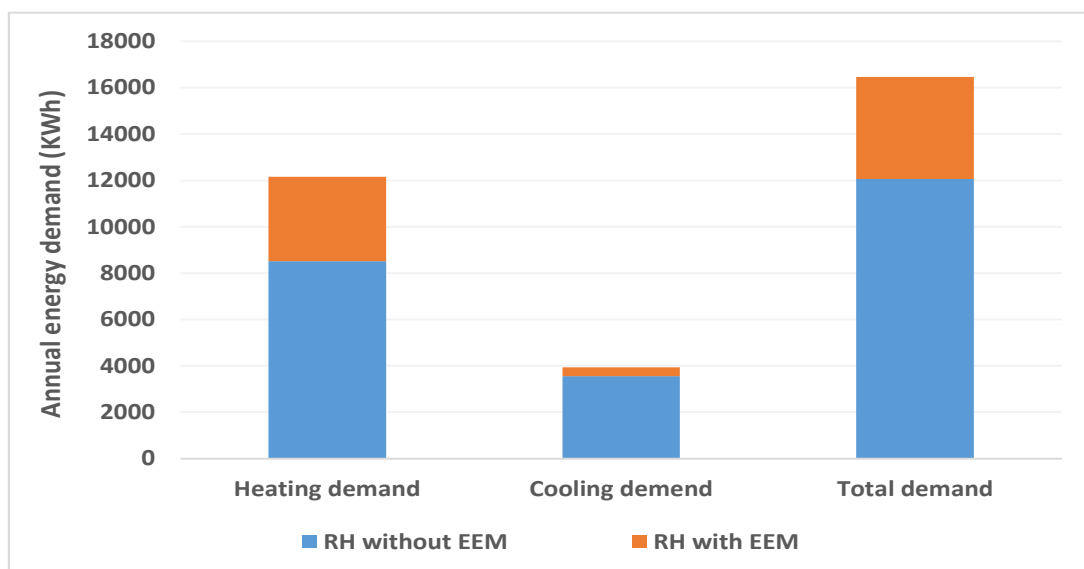


Fig.6.13. Annually energy requirement comparisons between two houses with and without EEM

The improvement of the U value of glazing from $5.74 \text{ W/m}^2 \text{ K}$ to $1.4 \text{ W/m}^2 \text{ K}$ leads to a further energy need reduction of 12.94%.

As shown in **fig.6.13**, compared with reference house design, the energy saving in energy with optimum EEM is about 63.51% reduction of the original annual energy need (from 12065 kWh/y to 4402 kWh/y). There is a reduction in annual heating energy need from 8514 kWh/y to 3641 kWh/y (57.23%) and a reduction in annual cooling energy need from 3551 kWh/y to 382 kWh/y (89.24%).

A comparison between the monthly energy demand of the RH with and without EEM is shown in **Fig.6.14**. As shown, the integration of EEM in combination in the RH envelope constitute a powerful mean of decreasing energy demand, especially in inter season.

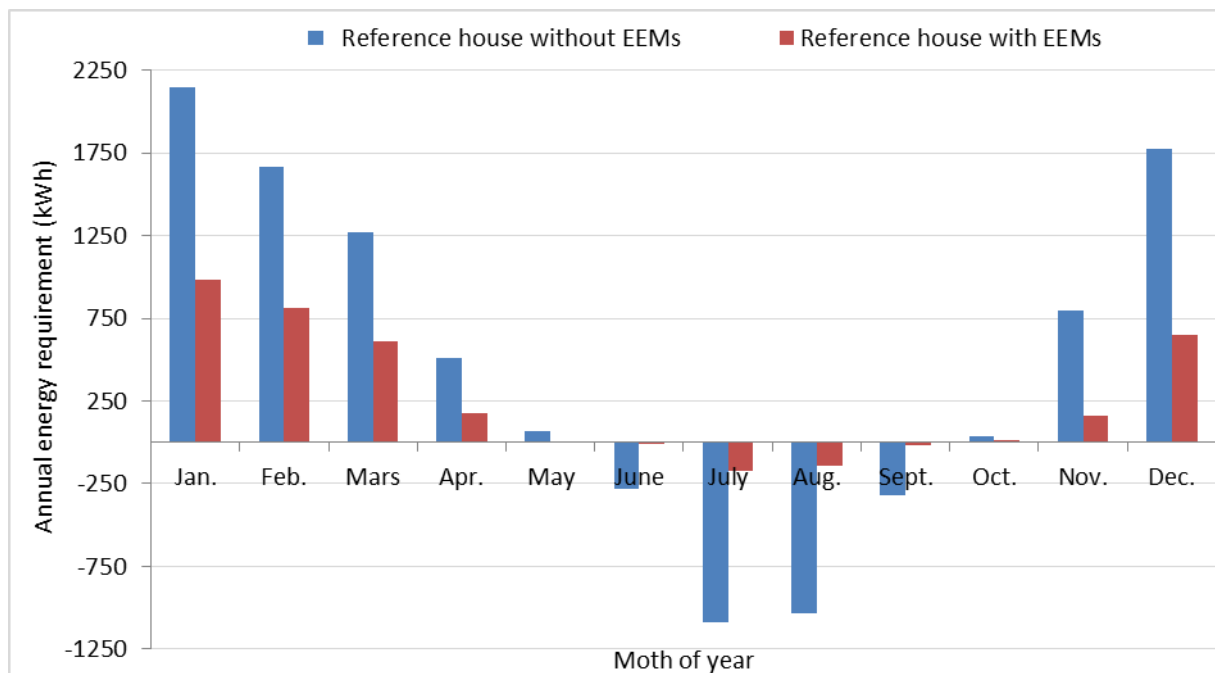


Fig.6.14. Monthly energy requirement comparisons between two houses without and with EEM

Table 6.4

Difference between RH with and without EEM

	RH without EEM	RH with EEM
Orientation	Unspecified orientation	South
External walls (U-value)	1.77	0.38
Roof (U-value)	2.55	0.4
Window glazing (U-value)	5.74	1.4
Window distribution of Facades	14%-S/14%-N	40%-S/10%-N

6.4.5. Thermal comfort

Thermal comfort has been evaluated, based on the computed hourly indoor temperatures. A temperature frequency plot of the resulting indoor temperatures of the house with and without applying EEM is presented in **Fig.6.15**.

Table 6.5

Indoor thermal comfort in the RH with and without EEM

Temperature range	RH without EEM	RH with EEM
Annual hours in 20–26°C	35.39 %	54.31 %
Annual hours under 20°C	31.89 %	25.04 %
Annual hours above 26°C	21.42 %	0.24 %
Annual hours above 28°C	11.42 %	0 %

The thermal comfort range is between 20°C and 26°C. There is a clearly difference between these two cases. The large spread of temperatures in the case without EEM

illustrates the higher energy need to maintain the house within the thermal comfort range. In this case, the number of hours outside the thermal comfort range is significantly higher. As shown in **Table 6.5**, the indoor temperatures are above 26°C for 1877 hrs (21.42%) of the year and below 20°C for 3640 hrs (31.89%) of the year. In the case with EEM, the indoor temperatures are above 26°C for only 217 hrs (0.24%) of the year. Indeed, the indoor temperature for this house does not exceed 28°C in summer. Overheating period is very limited essentially thanks to night ventilation. C, Tantasavasdi [96] have shown that in addition to natural night ventilation, a ceiling fan can be an interesting solution to achieve a comfortable indoor environment in warm time. Since, the ceiling fan increases the indoor air velocity. In winter, it was found that comfortable indoor temperatures were more difficult to achieve with the integration of EEM. In fact, the indoor temperatures are below 20°C for 2858 hrs (25.04%) of the year.

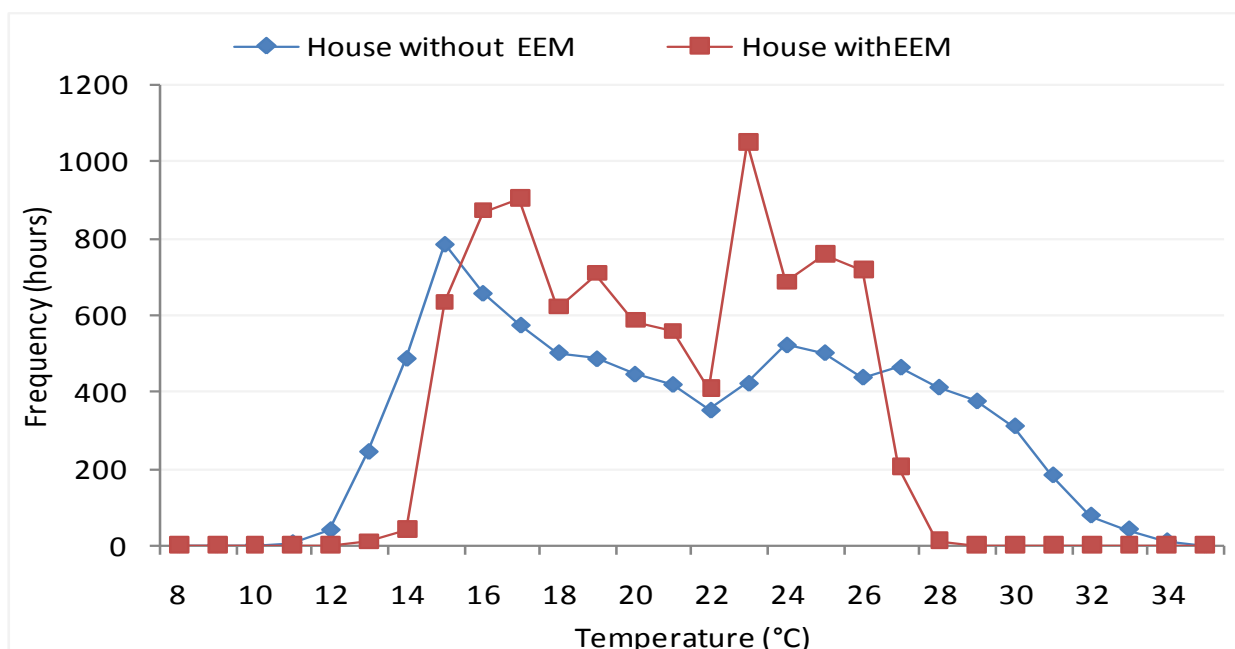


Fig.6.15. Frequency of indoor temperatures without and without EEM.

6.4.6. Solar heating system

6.4.6.1. Description of the system

Currently, the vast majority of the domestic hot water systems in Algeria is supplied by gas or electricity, consuming large amounts of conventional energy [97]. In this chapter, a solar heating system is designed to supply hot water for both DHW and space heating. The main components of this system are schematically shown in **Fig.6.16**.

The solar collector (1) covers the energy of the incident solar radiation into thermal energy of the working fluid. The hot working fluid leaving the collectors is transported to the storage tank (2) where it delivers heat to the water inside and returns cooler to the solar collectors.

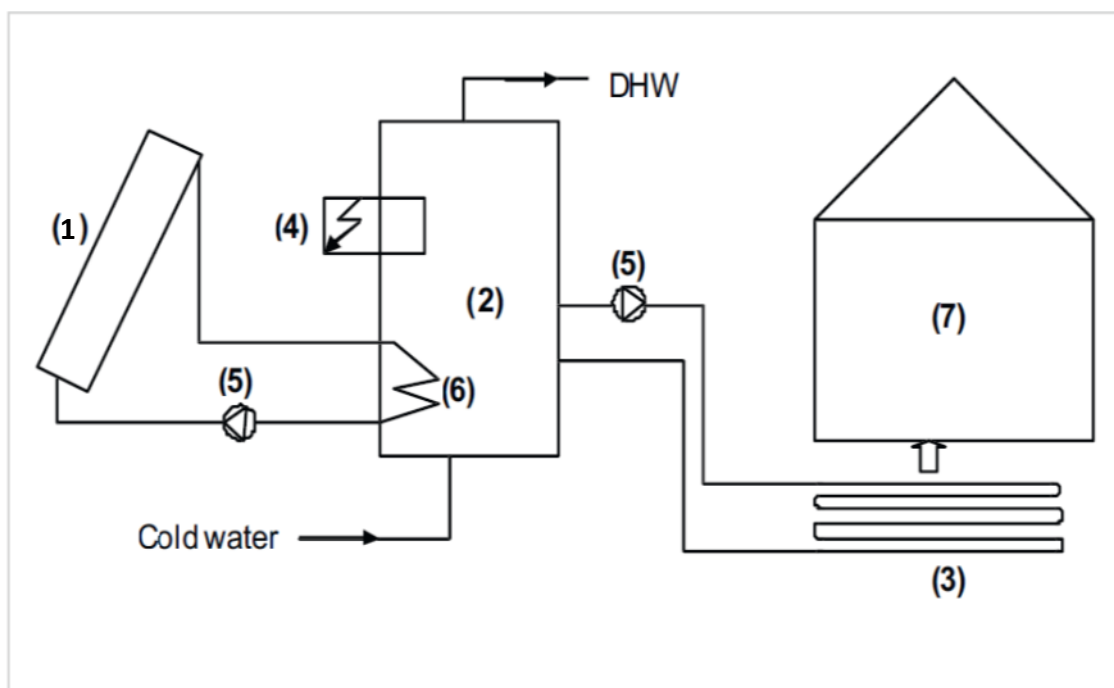


Fig.6.16. Scheme of the solar heating system under study

The water leaving the storage tank, with temperature between 35°C and 55°C is pumped independently through the zones of the house (7). When indoor air temperature is higher than 20°C, the pump (5) is turned off.

6.4.6. 2. Household hot water consumption

The current total average Algerian individual domestic hot water usage is taken to be 50 L/day [98]. Four occupants are assumed in a typical rural house in Chlef district. Therefore, the total domestic hot water consumption is 200 L/day. Hourly DHW profile is illustrated in **Fig.6.17**. The mains water is assumed to be constant 15°C and the set point for DHW is 45°C.

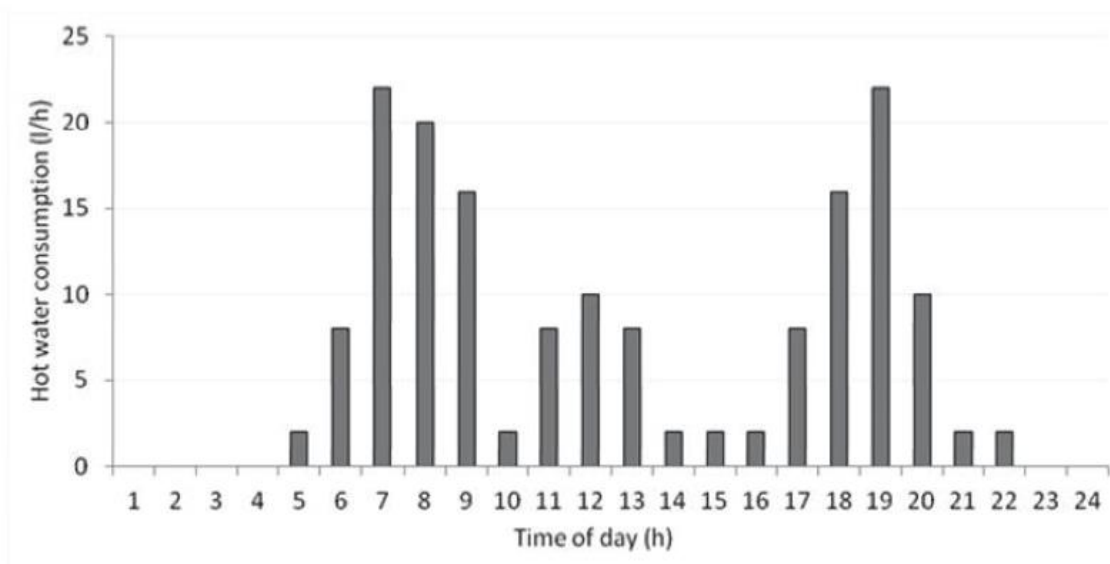


Fig.6.17 Daily hot water consumption profile (200 l/day).

6.4.6.3 Optimization of system parameters

The solar fraction is an optimization parameter that manifests the overall performance of the entire system. Thus, compared to other parameters, which indicate the performance of a single component, the solar fraction is the better indicator of the system performance [99]. The solar fraction is the fraction of the total

hot water energy that is supplied by solar system, is calculated using the equation [100].

$$SF = \frac{(Q_{load} - Q_{aux})}{Q_{load}} \quad (6.1)$$

Effect of collector area

In order to determine the adequate collector area, five collector areas that 2, 4, 6, 8, 10, 12 m² are considered, as shown in **Fig.6.18**. The initial value of the hot water tank volume-to-collector area ratio is set equal to 75 l/m², which is the base value for the f-chart method [101]. The recommended range of the collector mass flow rate-to-collector area ratio in the literature [102,103] is initially set equal to 40 kg/hm². The results show that increasing the collector area from 2 to 6 m² increases sharply the annual solar fraction of the system. It reaches a maximum of 71.62% at 6 m². A little increasing in solar fraction is recorded between 6 and 8 m². For this work, the optimal collector area is 6 m².

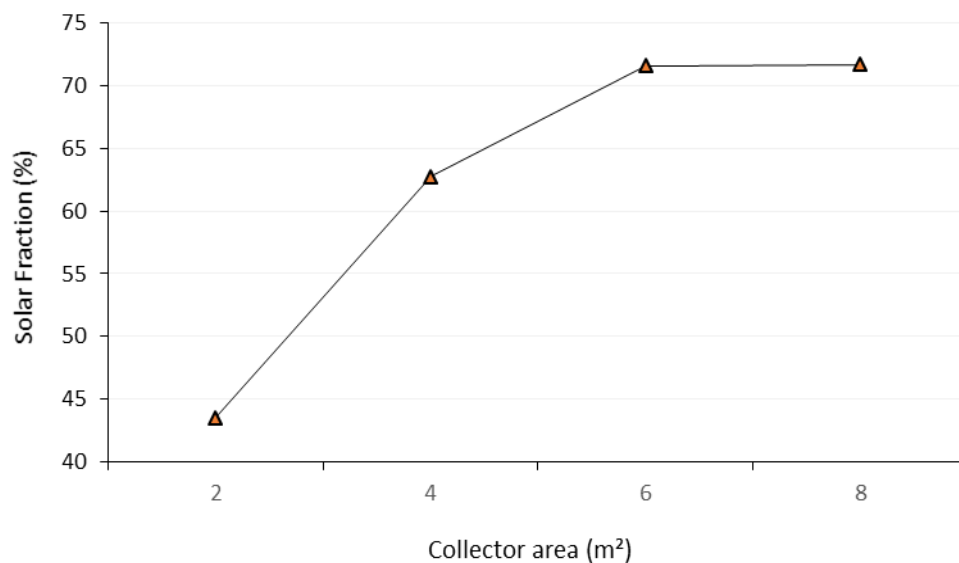


Fig 6.18 Variation of the annual solar fraction for different collector areas.

Effect of collector mass flow rate

The effect of collector's mass flow rate on the annual solar fraction was simulated for a collector area 6 m^2 and a tank volume equal to 450 l . Different mass flow rate ranging from 40 to 300 kg/h . are considered, as shown in **Fig.6.19**. The results show that the solar fraction increases rapidly as the mass flow rate increase from 40 to 120 kg/h . It increases from 71.86% at 40 kg/h to a maximum value of approximately 72.16% at 120 kg/h . from this value, the solar fraction starts to decrease with further increase in mass flow rate and become 69.23% at 300 kg/h .

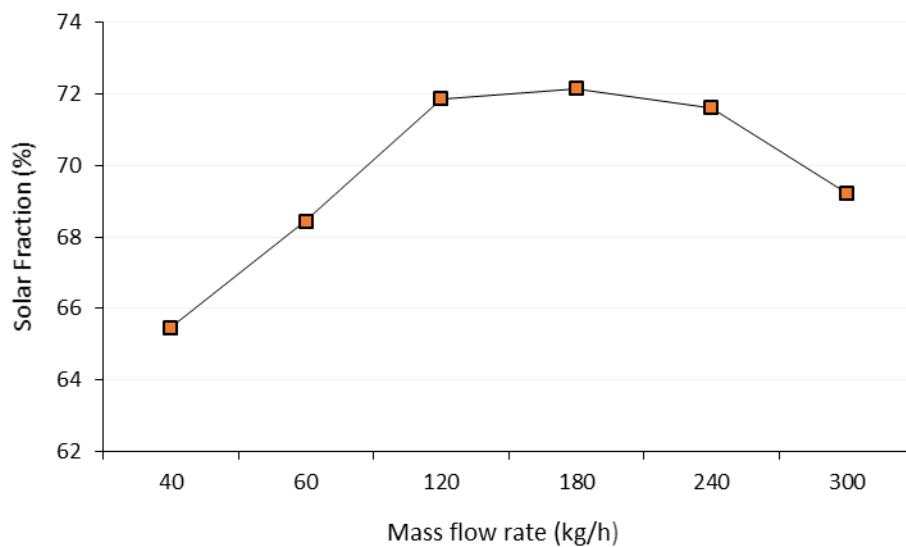


Fig.6.19. Variation of the annual solar fraction for different collector's mass flow rate.

Effect of tank volume

The effect of the tank volume on the solar fraction of the system is studied for various tank volume for 6 m^2 collector and 20 kg/hm^2 flow rate. The impact of the tank volume on the performance of the solar system is shown in **Fig.6.20**. As shown, the solar fraction increases rapidly as the tank volume increases, from 100 to 200 kg/h . for the tank volume values between 200 and 300 liter , the increase in solar fraction is

gradual with a maximum value of solar fraction of 69.03% at 300 liter. After this value, the annual solar fraction starts to descent, which is likely due to an increase in heat losses form the storage tank.

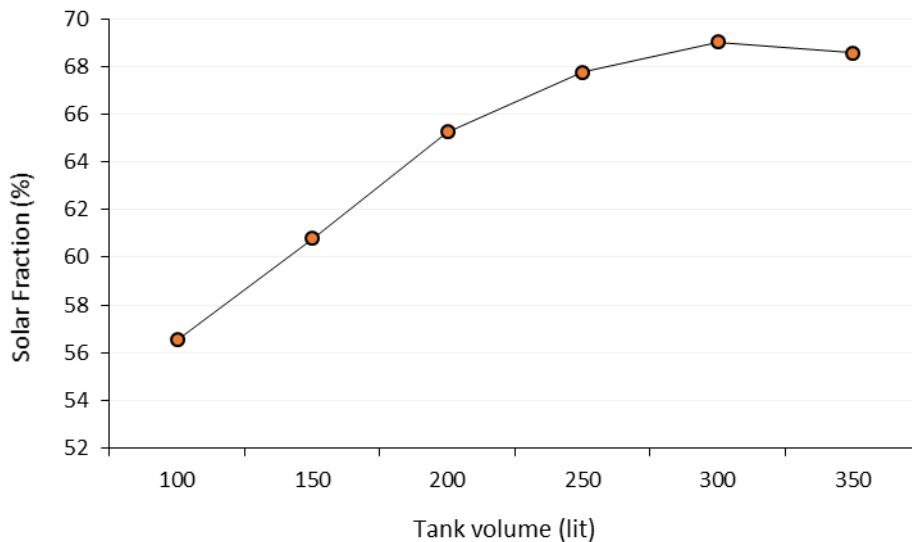


Fig 6.20. Variation of the annual solar fraction for different tank volume.

6.4.6.4. Performance of optimized solar heating system

The monthly and annual energy performance of the optimized solar heating system is presented and analyzed in this section. As shown in **Fig.6.21**, there are four loads to be covered by the solar heating system, the amounts of the thermal energy supplied for space heating “SH load” and for DHW “, in addition to the heat loss of the storage tank and energy consumed by the electrical pumps.

The heat demand for space heating is absent from May to November and important during cold season. The space heating demand increases from December to January and decreases from January to April. However, the heat demand for DHW is very similar for all the months of the year (about 228 kWh/month).

The increase of the heat demand increases the energy consumed by the electrical pumps. This later is important during the colds months. The maximum is 325.7 kWh in January. The heat loss from the heating system is proportional to solar heat gain, as the later increases, as the heat loss increases.

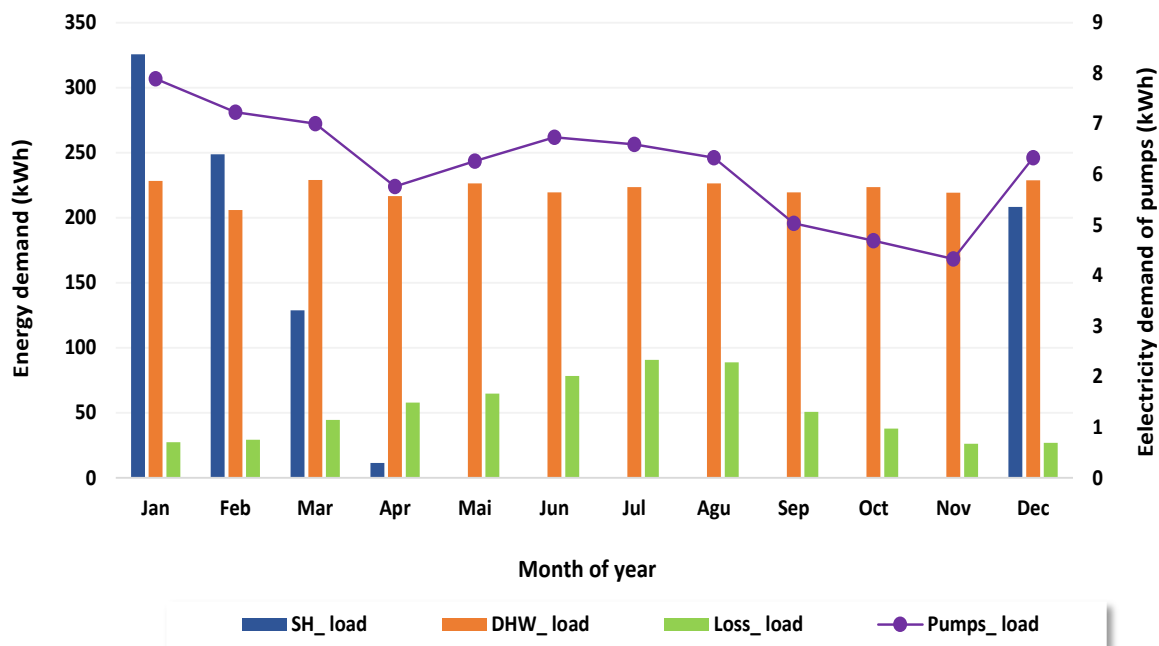


Fig.6.21. Monthly thermal energy loads.

The annual heat loads is shown in **Fig.6.22** We can notice that the heat required for the preparation of the DHW represents the great fraction (62%), due to the fact that the DHW is used over all the year. Thanks to the passive mean of decreasing energy demand, discussed in the Chapter II, heat demand for space heating represents only (21%) of the total heat demand. Despite the use of well insulation storage tank, the heat loss is important, which represents 15% of the total load. In comparison to the others loads, the electrical energy needed to operate the electrical pumps is lower (2%), but not negligible.

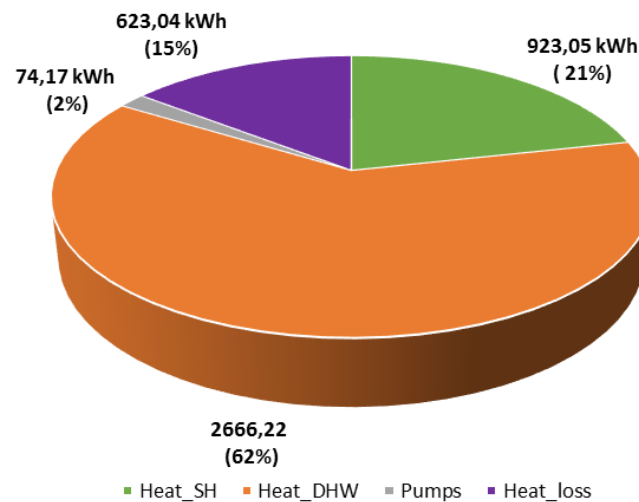


Fig.6.22 Annual thermal energy loads.

The monthly heat output from the solar heating system, heat supplied by the classical heater and solar fraction are shown in **Fig.6.23**. As the space heating demand is absent, the solar heating system is able to provide the total heat energy requirements in summer, where the solar fraction reaches 100%. During autumn and spring (offseason), the most energy demand is covered by the heating system. For example, a solar fraction of 94.95% and 81.49 can be achieved in April and November, respectively.

During cold months, as the solar collectors could be used to provide heat demand for space heating and DHW, the heat output from the heating system is insufficient to cover these loads. The use of classical heater is required. The minimum solar fraction is 30.56 in January. We can notice also that as the month is cold, as the heat supplied by the classical heater is high. Contrarily, the heat gain from heating system decreases during the cold months.

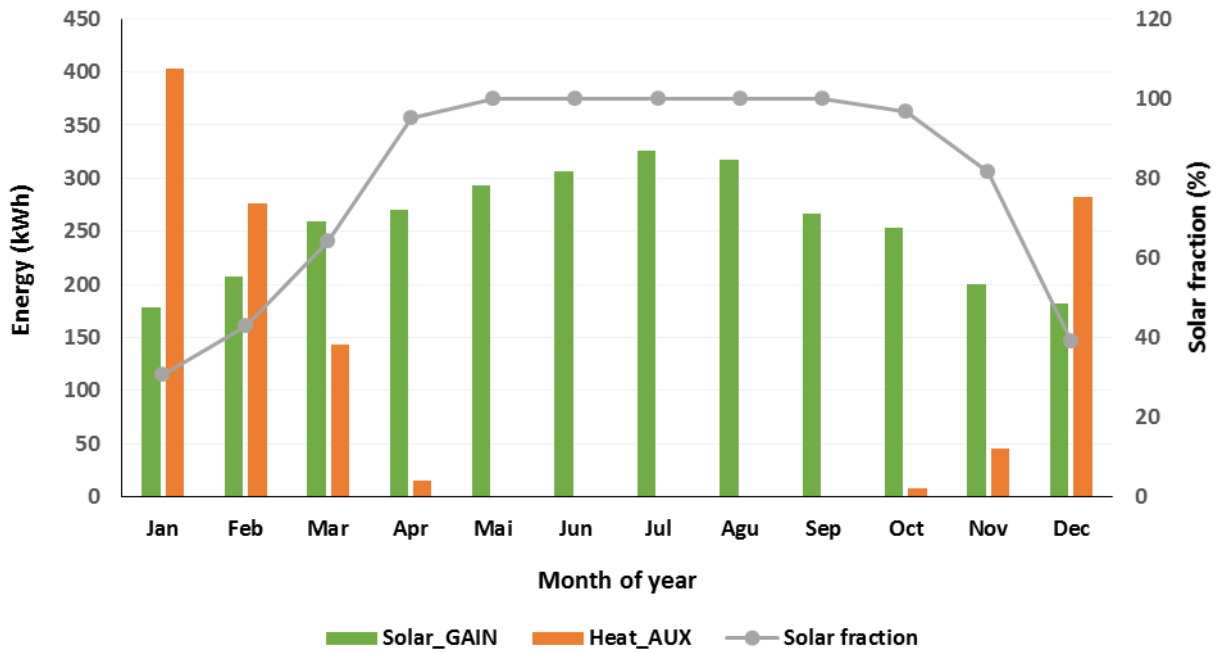


Fig.5.23. Monthly heat production of the solar heating system

The annual heat produced by the solar heating system and classical heater are shown in **Fig.6.24**. It can be noticed that the most annual heat demand can be covered by solar heat gain output from the heating system, which represents 72% of the total energy supplied. The annual heat supplied by the classical heater when the heat provided by the heating system is insufficient represents only 28%.

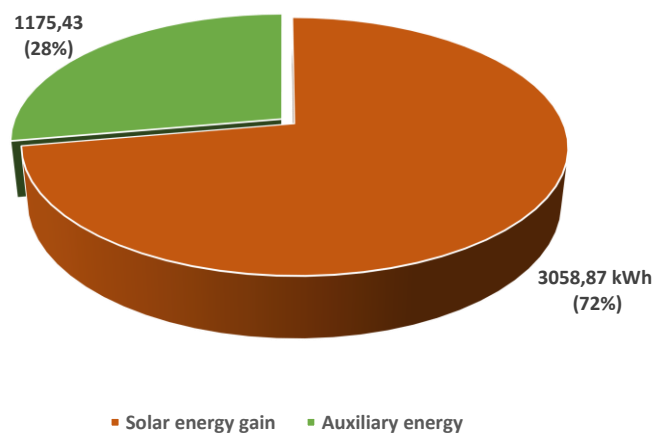


Fig.6.24. Annual heat production of the solar heating system

6.4.7. Grid-connected PV system

The PV system would produce electrical energy to satisfy needs for electrical energy of the house. The house uses the utility power grid for storage-delivering energy to the grid when the PV system produces more energy than the home uses and draws from the grid when the PV system produces less energy than the house needs. The scheme of a grid-connected PV system chosen in this study was presented in chapter 4 (**Fig.4.20**). It is comprised of a PV array, an inverter, a meter to measure the energy exported to the grid and the energy imported from the grid. The array slope is set to 35° in accordance with local latitude (36.13 N) and can be installed on the flat roof or beside the house, far from the sunscreens. PV module parameters are listed in **Table 6.6**. This PV module is available in Chlef market. New solar energy Omniksol-1.0k-TL inverter is used to convert DC current produced by the PV panels into alternating current (AC).

Table 6.6

Electrical specifications of module ET-M660250WW

Characteristics	Value
Maximum power (W)	230
Module efficiency (%)	15.37
Nominal operating cell temperature (°C)	45.3
Open Circuit Voltage (V)	37.70
Short Circuit Current (A)	8.69
Maximum power current (A)	8.22
Maximum power voltage (V)	30.43

6.4.7.1 Electrical consumption profile

Rural houses are characterized by their average level of electrical equipment [104]. Generally, the energy source for space heating and for sanitary hot water (DHW) production is gas, which is available and less expensive in the region. Cooling is absent due to the high cost of air conditioners. Consequently, electricity consumption in the house provides only services of lighting, refrigeration and general power (e.g. dishwasher, washing machine, computers, telecommunications etc.).

Before being able to calculate the energy production of our PV system, we need to establish reference electrical consumption for an individual family located in rural area based on the power consumption of a rural households sample in different areas of the district, and the use of electrical equipment by the inhabitants. According to data provided by Sonelgaz of Chlef District, the annual electricity consumption of selected homes is given as a sample in **Table 6.7**. We can notice that the rural houses in the region have a very similar annual electrical consumption which varies from 1300 kWh and 1400 kWh. Based on this electrical consumption, we propose an annual profile established from conventional electrical equipment identified, their conditions of use and their annual consumption, see **Table 6.8**.

Table 6.7

Electricity consumption of the sample

N° house	Number of occupants	Number of rooms	Electrical consumption (kWh / year)
1	5	4	1963
2	5	4	1954
3	4	4	1940
4	6	4	1990
5	4	4	1933

The average annual electricity load is calculated using Eq.4.

$$load = \sum_1^n P_i \times N_i \times f_i \quad (6.2)$$

P is the power of equipment (e.g. refrigerator, television ...), N_i is the number of equipment and f is the usage frequency of the equipment. n indicates the total number of equipment (in our case 8 equipments). Using data in Table 6, the average yearly electrical consumption EC_y is 1991kWh. The average daily electrical consumption EC_d is given by.

$$EC_d = \frac{EC_y}{365} \quad (6.3)$$

It can be noted that for a single family household where electricity is used only for lighting and electrical appliances, the average daily electrical consumption of 5.45 is very high. This is mainly due to the use of inefficient electrical equipments which consumes a lot of energy.

To design an efficient PV system with the less cost of investing in house, it is important to use an efficient electrical equipment [105]. Thus, a second annual profile is estimated by replacing incandescent lamps, which are commonly used by Algerian homes, with low consumption lamps and conventional appliances by other efficient. From **Table 6.8**, we can detect that the use of efficient electrical equipment helps to reduce the annual electrical needs of the reference house from 1991 kWh to 1350 kWh, with a reduction of 47.91%. From the annual domestic electrical consumption, the average daily electric load is 3.69 kWh, which is valid from April to November. However, during the heating season (from December to March), in addition to the 1350 kWh for domestic electrical load, the 1249 kWh required for SH and DHW are

taken into account. Therefore, the average daily electrical load during these months is 13.91 kWh.

Table 6.8

Annual electrical equipment consumption of the reference house

Device type	Power (W)		Number	Usage Frequency	Average annual consumption (kWh)	
	Conventional	Efficient			Conventional	Efficient
Refrigerator	120	80	1	continuously	416	312
Washing machine	1.35 kWh/cycle	0.94 kWh/cycle	1	2 cycles /week	227	236
Television	120	100	1	5h/day	247	234
Sat. receiver	40	40	1	5h/day	53	59
Ironing amenities	300	300	1	1h / day	109	105
Lighting	75	40	6	5h/day	823	350
Computer	120	80	1	1h/day	44	27
Ceiling fan	75	28.5	4	4h/day (60 days)	72	27
Total					1991	1350
Auxiliary heat load						1249

Based on these two daily electricity consumption, we perform two hourly domestic electrical load profiles (hour by hour) for these two different periods, which are shown in **Fig.6.25**. We can notice that electricity consumption is significantly higher in winter than summer due to heating requirements and additional lighting.

6.4.7.2 Optimization of the PV system size

In order to design a PV system according to the electricity load required (2.1kWh/day) for the reference house, we have studied the energy performance of different PV array sizes (from 0.46 to 2.3 kW_p). As shown in **Fig.6.26**, a PV array of 1.84 kW_p may produce more than the annual electrical consumption of the reference house (2599 kWh). As a result, a 1.84 kW_p PV system is selected for analysis in this study. The designed PV array is composed of nine PV panels, each panel produces 30.34 V and 230 W_p (8.22 A). PV panels are connected in series to gives required input voltage of inverter (80 V).

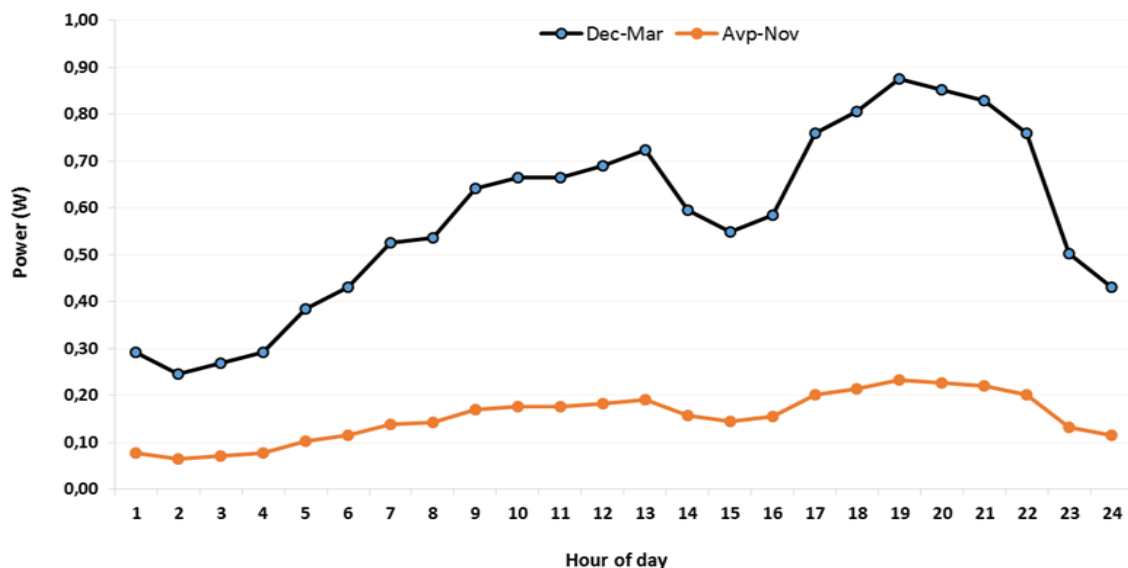


Fig.6.25. Daily home electricity consumption profile

6.4.7.3 Contribution of PV energy

The annual electrical simulations results for a 1.84 kW_p PV system are given in

Fig.6.27.

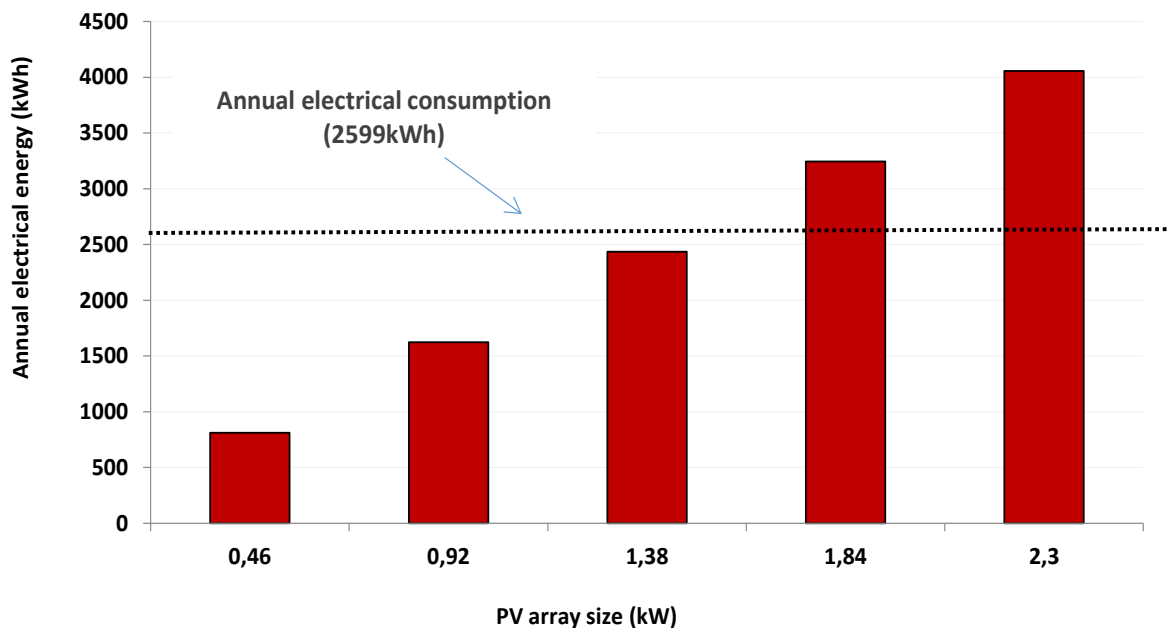


Fig. 6.26. Annual electricity production with different PV array sizes.

The total electricity consumption in the home from all sources “AC primary load”, supplied in parallel from the inverter and the network is $EC = 2599$ kWh and the total annual kWh exported to the electricity network per annum which occurs when the PV inverter generates excess electricity relative to the home electricity demand “grid sales” is $ES = 2200$ kWh. The total annual kWh imported from the electricity network per annum which occurs when the PV inverter generates less electricity relative to the home electricity demand “Grid purchases” is $EP = 1407$ kWh and the total annual kWh produced by the PV system “PV array” is $EPV = 3384$ kWh. The PV system produced the equivalent of 70% of the total electricity consumed in the home. The

annual electricity purchased from the grid represents 30% of the total electricity consumption in the home.

The monthly electrical simulation results for the 1.84 kWp PV system are shown in **Fig.6.28**. The maximal production of the PV system is 429 kWh in April and the minimal production is 318 kWh in December.

However, the monthly electricity imported from the grid is very important in winter (275 kWh in December) due to heat required for heating and minimal in summer (74 kWh in June).

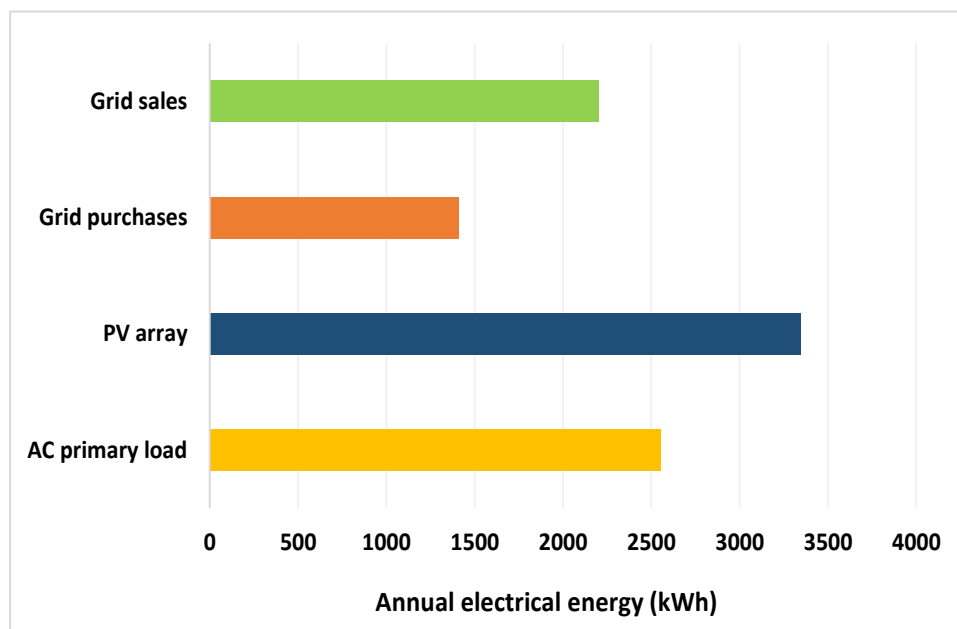


Fig.6.27. Electrical simulation results.

The monthly net electricity imported from the grid “Net purchases” is calculated by subtracting the electricity exported to the grid “energy sold” from the electricity imported from the grid “energy purchased”. As shown in **Fig. 6.29**, we can note that the monthly net electricity purchased from the grid is negative during the summer, since the monthly electricity fed to the grid is higher than the electricity purchased

from grid with a maximum in January (-199 kWh). However, during the heating season, the net electricity purchased from the grid is positive. This mean that the electricity fed to the grid is lower than the electricity purchased from grid.

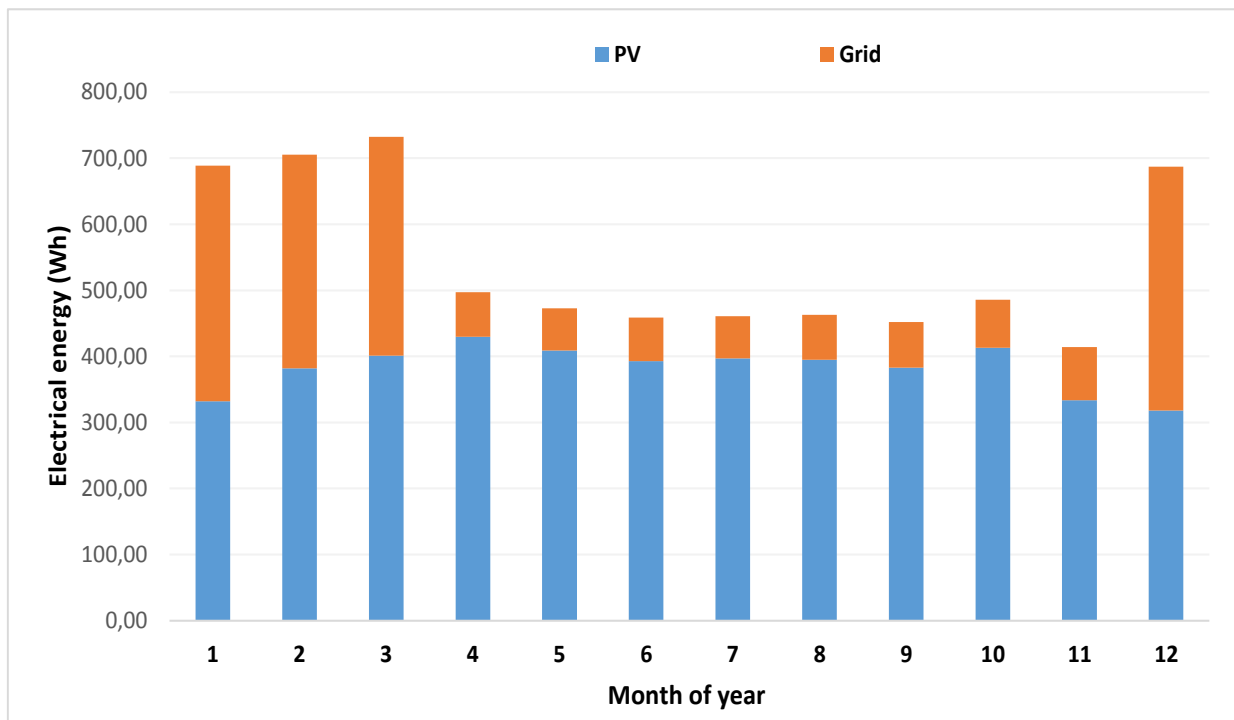


Fig.6.28. Monthly average electrical produced by the grid and PV system.

The daily electrical simulation results for the 1.84 kWp PV system for two days (a sunny and a cloudy day) are shown in **Fig.6.30** and **6.31**. The presented results are consumed electricity, the purchased electricity, the generated PV electricity, and the PV electricity exported to the electricity grid for each one hour of the day. We can note that the PV system can still produce electricity on cloudy days, but not as much as on a sunny day.

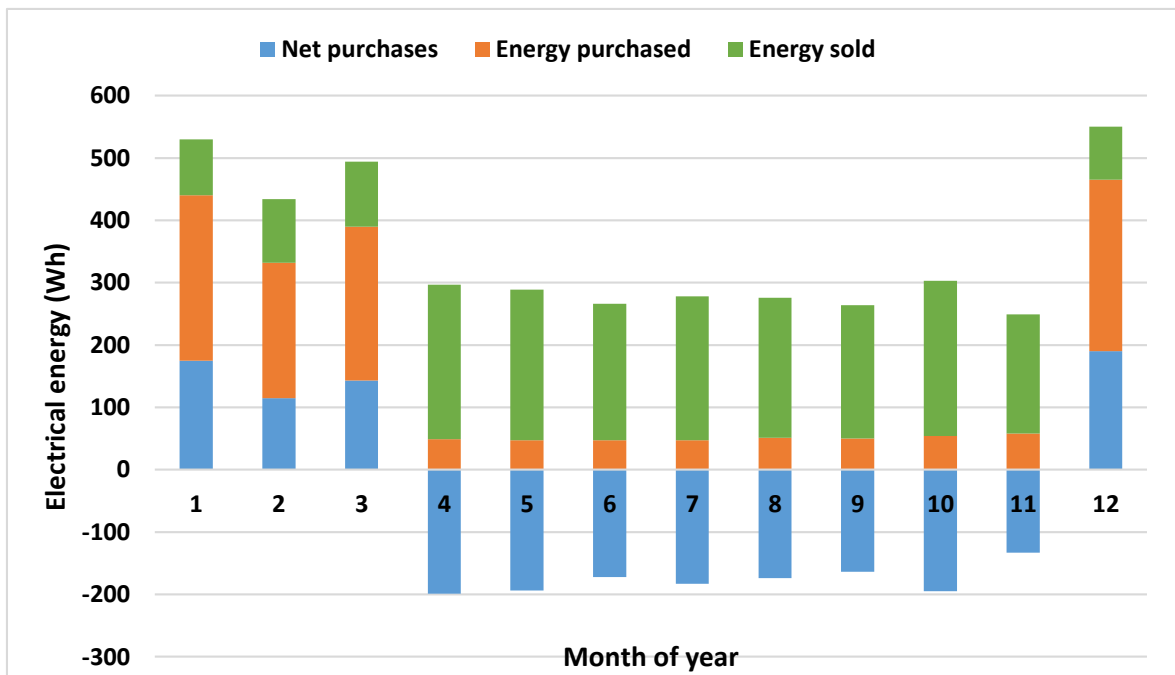


Fig.6.29. Monthly net electricity purchases from the grid.

Fig.6.30 shows for a sunny day, that the PV- origin electricity between 6:00 am and 8:00 am does not cover the energy consumption, as the sun did not generate any electrical energy. The PV electricity starts to be generated from 8:00 am to 19:00 pm. When the electricity is generated from the sun, it easily covers the house energy consumption. The excess electricity produced by the PV system, relative to the home electricity demand, is exported to the electricity network. After 19:00 pm the energy consumption is not covered as the PV electricity is not generated. Then, all electricity is purchased from the electricity grid. **Fig.6.31** shows for a cloudy day that the electricity generated by the PV system cannot cover the energy consumption between 8:00 am and 19:00 pm. In this case (cloudy day), the energy consumption is entirely or partially purchased from the electricity grid.

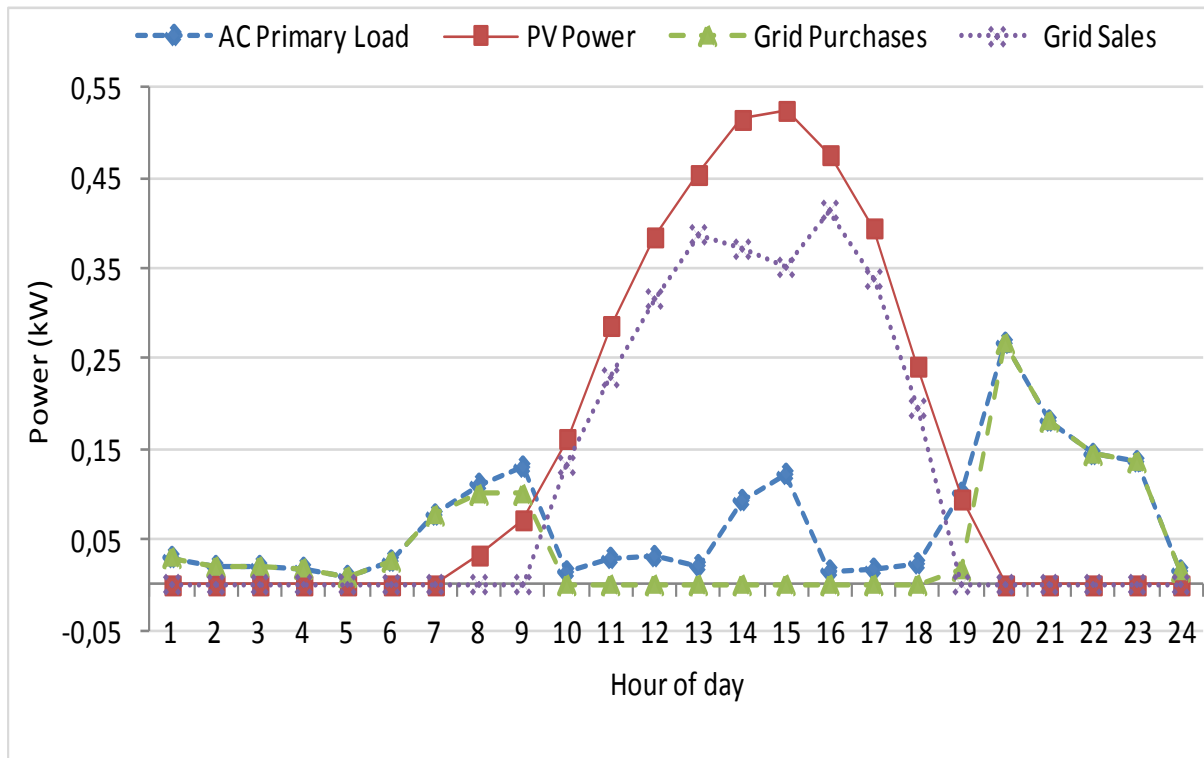


Fig.6.30. Hourly electrical simulation results of a sunny day

In conclusion, the PV system may entirely cover consumption of electrical energy in the house using the grid electricity as storage to overcome parts of day without solar energy. In addition, it is clear that part of the day when several appliances such as lighting starts to operate at the same time is critical part of the day for the electricity grid as there is the highest electricity demand and no solar electricity is available.

6.4.8. Energy balance of the HEP house

Installing energy efficiency measures and solar energy systems in rural house lead to reach the level of HEP house. The annual energy demand and generation is summarized in **Fig.6.32** and **Table 6.9**. As shown, the total energy demand for domestic electricity, DHW, and space heating and cooling can be completely

produced by EEM and solar systems, in addition to use efficient appliance and ceiling fan to provide comfort in summer.

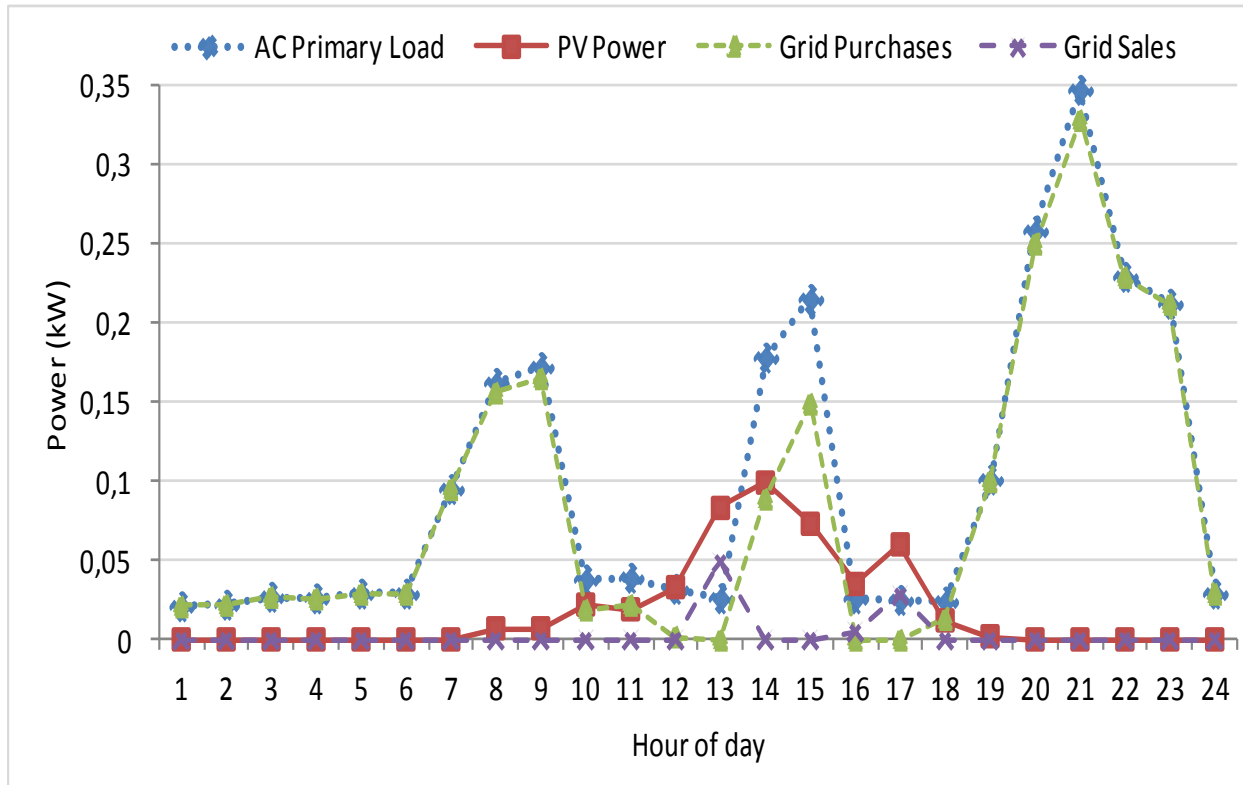


Fig.6.31. Hourly electrical simulation results of a cloudy day.

Table 6.9

Energy production and energy demand of HEP

Energy demand		Energy production	
Electricity domestic	1991	EEM	8042
DHW	2666	SH system	5058
Space heating	8514	PV system	3384
Space cooling	3551	Efficient appliance	641
Total	16722	Total	17125

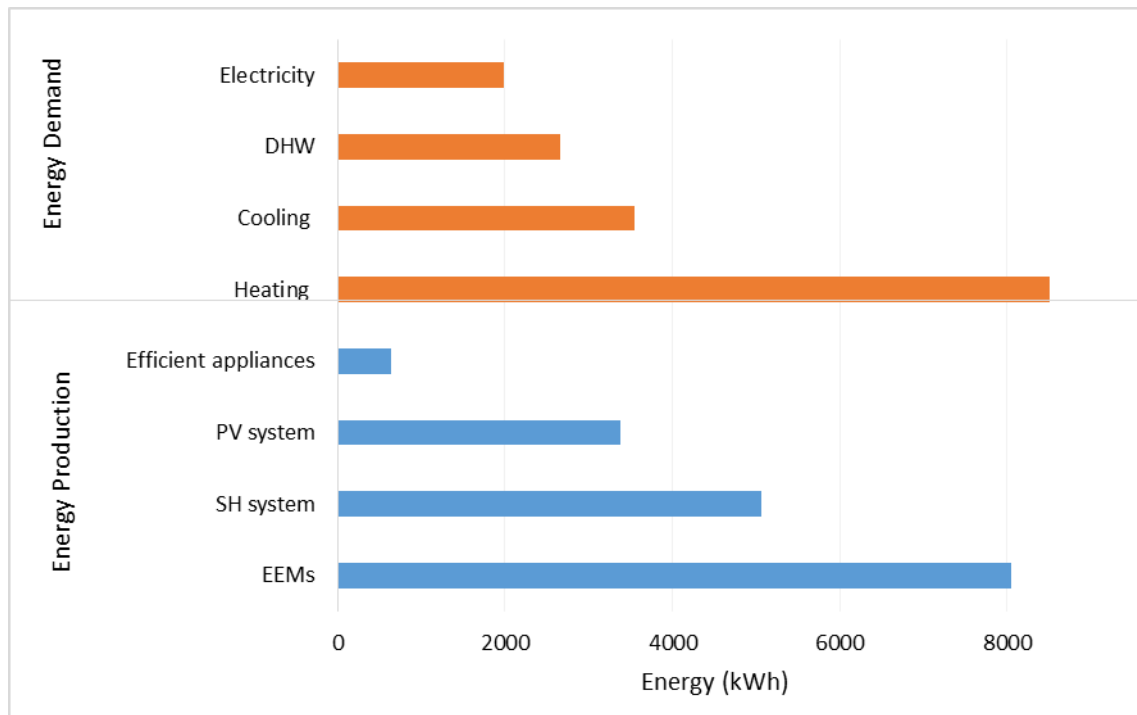


Fig.6.32 Comparison between annual energy demand and energy production

6.5. Overall energy saving and CO₂ mitigation

Reducing the energy consumption of a building by installing more energy-efficient fixtures or onsite renewable energy systems will reduce its GHG emissions due to the reduction in its energy demand [106]. In order to evaluate the reduction of negative environmental impact due to the use of solar energy in rural housing, the GHG emissions reduction needs to be calculated.

The primary GHG emissions from building operation include carbon dioxide (CO₂), nitrous oxides (N₂O), methane (CH₄), and ozone (O₃) [107]. These gases can be represented in equivalent quantities of CO₂ emissions using their global warming potential factors that are developed by the Intergovernmental Panel of Climate Change (IPCC) [108]. The following average Algerian conversion factors from electricity to CO₂ emissions and from gas to CO₂ emissions are used.

- 0.65 kg of CO₂/kWh of electricity consumed.
- 0.27 kg of CO₂/kWh of gas consumed.

In order to estimate the global annual GHG reduction due to improvement of energy performance of all rural houses built during last rural housing programs, it is necessary to calculate the global energy saving. This can be achieved from the results of electrical energy and gas saving due to improvement of energy performance of a rural house, as shown in **Table 6.10**.

The electrical energy saving (difference between the yearly electrical energy need of the house before and after installing EEM and SS) includes electricity saving due to domestic electricity reduction and space cooling reduction and can be calculated as follows:

$$ES_{elec} = [(EN_{elec,1} + EN_{sc,1}) - (EN_{elec,2} + EN_{sc,2})] \times N_t \quad (6.4)$$

Where, EN_{elec} represents the yearly electrical energy need for lighting and appliance. EN_{sc} is the yearly electricity need for space cooling.

Knowing that the energy capacity of a cylinder of 13 kg is 179 kWh, the number of butane gas cylinders could be saved due to the energy reduction for DHW and space heating demand can be expressed as follows:

$$ES_g = \frac{1}{179} \times [(EN_{sh,1} + EN_{DHW,1}) - (EN_{sh,2} + EN_{DHW,2})] \times N_t \quad (6.5)$$

Where, EN_{sh} is the annual energy needed for space heating. EN_{DHW} is the annual energy needed for domestic hot water. N_t is the total number of rural houses.

As shown in **Table 6.11**, the overall energy saving and the reduction of CO₂ emissions due to the integration EEM and use solar energy system in rural housing are significant. It is observed that more than 131 GWh of electricity and 1480257

butane gas cylinders will be saved. The total associated CO₂ reduction is 156.913 MTonnes.

Table 6.10

Electrical energy and gas butane saving

	Heat demand (kWh)			Electrical demand (kWh)		
	Space Heating	DHW	Gas saving	Space Cooling	Electricity domestic	Electricity saving (kWh)
RH without EEM and SS	8514	2666	0	3551	1991	0
RH with EEM	3641	2666	4873	382	1350	3810
RH with EEM and SHS	1249		9931	382	1350	3810
RH with EEM and PVS	3641	2666	4873	0	0	5542
RH with EEE and SS	0	0	11180	0	0	5542

The savings in annual energy and CO₂ emissions for various combination of EEMs and solar systems are shown in **Fig.6.33** The contribution of SHS and PVS in combination with EEM in energy saving and CO₂ reduction. As shown, EEM can reduce the energy demand by 51, 91% and CO₂ emissions by 57.27%. Thus, the reduction of energy consumption through the integration of EEM is necessary before installing solar energy systems.

From the energetic point of view, the contribution of the SHS with EEM in the energy saving is important compared to the contribution of PVS with EEM. A difference of 19.89 % is recorded. However, from CO₂ reduction point of view, this difference is

only 3.63% due mainly to the high conversion factor of electricity. We can conclude that both SHS and PVS are necessary for sustainable development.

Table 6.11

Overall CO₂ emissions reduction

	Electricity Saving (GWh)	CO ₂ reduction (tons)	Gas Saving (GWh)	CO ₂ reduction (tons)
EEM	90.2970	58693	115.4900	31182
EEM with SHS	90.2970	58693	235.3647	635.48
EEM with PVS	131.3454	85374	115.4900	311.82
EEM and SS	131.3454	85374	264,9660 (1480257 cylinders)	71540

6.6. Economic analysis

In order to carry out economic analysis due to the integration of energy efficiency measures (passive system) and active solar systems application in rural housing of Chlef district, the estimation of the yearly income and the cost of each component of the systems must be set out. In the analysis, the time value of money, the effective interest rate or rising energy prices, or the replacement cost where not considered. The life cycle of the solar systems components is estimated to be 25 years and thermal insulation of the house envelope 35 years. To compile the most accurate and realistic prices for the case study house, every effort was made to get up-to-date pricing from local vendor for the buildings materials and solar components.

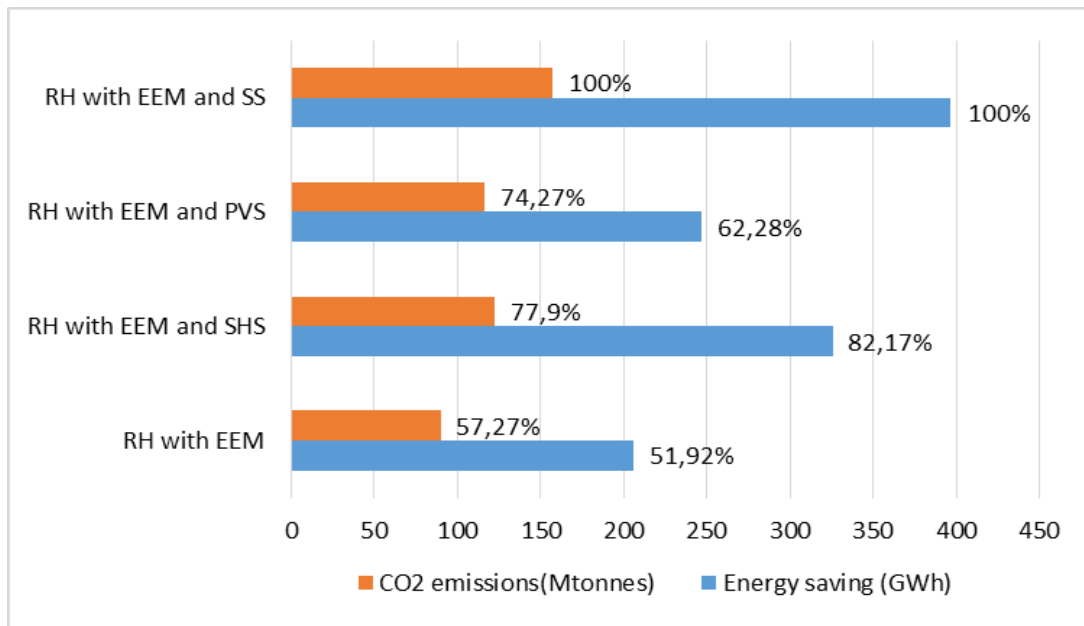


Fig.6.33 Overall energy saving and CO₂ reduction

5.6.1. Yearly income

The yearly income for the case of the existing rural house in Chlef district when the thermal insulation and the PV system are additionally installed was calculated using data from **Table 6.12**. The total yearly income by house is given as

$$YI = YI_{el} + YI_g \quad (6.6)$$

The yearly income due to butane gas saving is given as

$$YI_g = C_g \times ES_g \quad (6.7)$$

Where, C_g stands for the price of gas (1.11 DZA/kWh).

The yearly income due to electricity saving is given as

$$YI_{elec} = C_{el} \times ES_{el} \quad (6.8)$$

Here, C_{el} , stands for the price of electricity purchased from the electricity grid assumed to be 4.179 DZA/kWh €/kWh.

6.6.2. Investment cost

The initial investment cost includes the cost of the grid connected PV system, solar heating system and the cost due to integrating EEM in the house envelope (cost of thermal insulation and double glazing window) as given by **Eq.13**.

$$IC = IC_{PV} + IC_{SHS} + IC_{EEM} \quad (6.9)$$

PV system cost

Market cost of the PV system IC_{PV} includes the cost of the PV array, the inverter. The costs for mounting the PV system and the inverter are assumed to be 10% of the investment cost for the PV system. Hence,

$$IC_{PV} = 1.1 \times (P_{ar} \times C_{ar} + P_{inv} \times C_{inv}) \quad (6.10)$$

Where, P_{ar} represents the array rated power, C_{ar} represents the average price of the array per the unit of its rated power and C_{inv} represents the average price for the inverter per the unit of the rated power. P_{inv} represents the inverter rated power.

Solar heating system cost

Market cost of the solar heating system includes cost of thermal collector, cost of thermal storage, and cost of heating floor, two solar pumps and other accessories. The cost of installation and accessories (pipes, controller, thermostat...) is assumed to be 15% of the total investment costs of the system.

$$IC_{SHS} = 1.5 \times (N_{coll} \times C_{coll} + C_{tank} + C_{floor} + 2 \times C_{pump}) \quad (6.11)$$

Where, N_{coll} is the collector number, C_{coll} represents the cost of single collector, C_{tank} is the cost of the tank, C_{floor} is the cost of the heating floor and C_{pump} is the cost of the pump.

Table 6.12

Cost of thermal insulation and SS components

EEMs	Cost (DZD/m²)	Area (m²)	Total cost (DZD)
Insulation	450	168.8	75960
Double glazing	12	29000	348000
Installation			42396
PV system	Cost DZD/Watt	Power (Watt)	Total cost (DZA)
PV array	100	1840	184000
Inverter	80	1000	80000
Installation and accessories			26400
Heating system	Cost DZD/m²	Area (m²)	
Collector	10000	8	80000
Tank			15000
installation and accessories			35175

Thermal insulation cost

The cost of integrating EEM include the cost of thermal insulation and the cost of double-glazing windows. The cost of installation is assumed to be 10% of the total investment costs for integration of EEM. Hence,

$$IC_{EEM} = 1.1 \times (S_{ins} \times C_{ins} + S_w \times C_w) \quad (6.12)$$

Where, S_{ins} represents the total area of the house envelope without windows area, C_{ins} represents the cost of thermal insulation per m^2 , S_w represents the total windows area of the house and C_w represents the cost of windows glazing per m^2 .

6.6.3. Return on investment

The return on investment is defined as the initial investment cost divided by the annual cost savings due to the installation of EEM and PV system.

$$RI = \frac{IC}{YI} \quad (6.13)$$

Fig 6.34 represents the investment cost in EEM, SHS and PVS and their corresponding return on investment.

As shown, the investment in EEM requires a high cost. It was estimated at 466.356 DZD. This is due mainly to the high cost of double-glazing (29000 DZD/ m^2) compared to the thermal insulation material (450 DZD/ m^2). However, thanks' to the high annual cost of 18.623 DZA, the return on investment is estimated to 25 years, far less than the assumed life cycle of 35 years.

Compared to the cost investment in EEM, the cost investment in a grid PV system is lower (290.400 DZD), but for limited annual cost saving abilities (8.320DZA) result in

a return on investment (24 years) that is only a little lower than its guaranteed life cycle of 25 years.

The SHS has the lowest capital investment cost (DZD) in comparison of the cost of EEM and PVS. However, as the most part of space heating demand is reduced by integration of EEM and the auxiliary energy for DHW is provided by the PVS, the cost saving in the case of SHS is lower (5058 DZA) leading to a return on investment of 30 years, which is higher than its life cycle.

When all investments in EEM and SHS and PVS are considered, the capital cost is about with a yearly income of 886.931 DZD. The return investment is about 24 years.

Thus, the investment in EEM and PV and SHS can be paid back during their service.

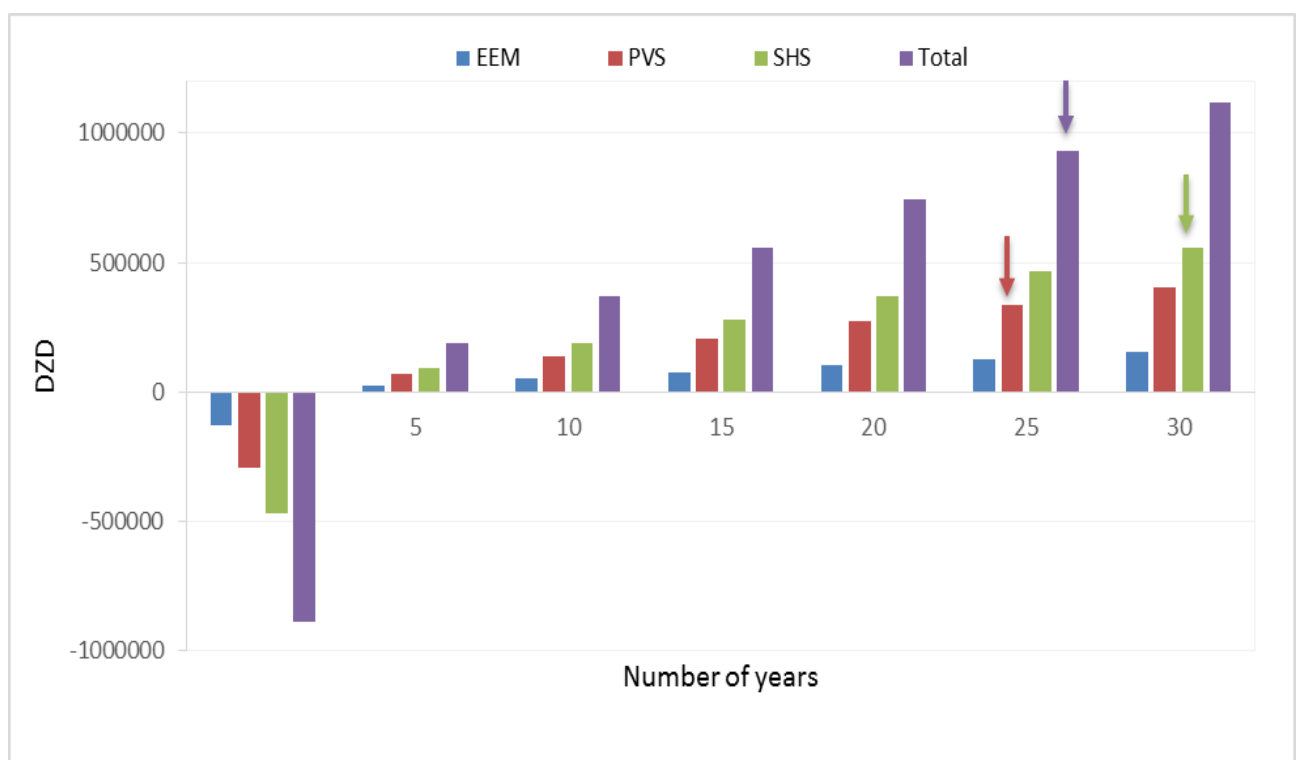


Fig.6.34 the capital cost of the grid-connected PV system and EEM and the yearly income

6.7. Conclusion

The present chapter aimed to study the contribution of HEP rural housing in the sustainable development of the Chlef district. Electricity and gas are the most consumed energy sources in the district, particularly in residential sector. The results indicate that the integration of EEM and application of solar systems in residential rural housing embodies the concepts of energy conservation, environmental protection and sustainable development. These solutions could play a very important role in residential sector energy saving, as well as CO₂ mitigation.

First, a single-family typical rural house was chosen as a reference house. The energy performance of this house was improved by passive and active means. The results for the passive mean show that the space heating and cooling energy requirements of a typical rural house can be reduced by 67%. This goal can be achieved through the adequate house orientation to the true south and increasing windows size of façade facing south, in addition to insulate the roof and wall by 0.08 m and using double glazing. Thanks to nocturnal cooling and shading device, the energy requirement for space cooling is reduced to the point of eliminating the need for an auxiliary cooling system, as the indoor temperatures fall largely within the thermal comfort zone.

For the active mean, a solar heating system with a 6 m² flat-plate collector and 300 litter storage tank that provides hot water requirements for both DHW and space heating of a single-family house is appropriate for this application. Therefore, an annual solar fraction of 72% can achieved. A solar PV system with a PV array of 1.84 kWp connected to the grid utility is suitable for rural application. This may produce in parallel with the grid the total electricity consumption in the home. The annual

contribution of the PV system is the equivalent of 70% of the total energy consumption.

Then, the model of the optimized reference house was applied on the all rural houses built during last rural housing construction programs. The results indicate that more than 131 GWh of electricity and 1480257 butane gas cylinders can be saved annually if all rural houses are converted into HEP houses. The energy saving led to an annually reduction of 71540 tons of butane gas and at 85374 tons of electricity.

Finally, the economic analysis indicates that due to high cost of solar energy systems, the investment in EEM and solar energy systems in combination may paid back in 24 years.

General conclusion

The aim of this work was to study the contribution of high-energy performance rural housing using solar energy on the sustainable development.

We started with the review of recent studies on improving building energy performance using solar energy, including energy efficiency measures (passive system) and active solar system. From these studies, we concluded that reducing the total energy load in residential housing, heat and electrical load, by passive means should be considered before designing active solar systems. The energy situation in Algeria has been then analyzed in the aspect of energy production, energy consumption. Furthermore, the potential of renewable energy and their application in country has been investigated. It has been concluded that in one hand, the energy consumption is still expansion particularly in residential sector and in other hand, Algeria enjoy by a great solar energy potential, which is suitable for solar energy systems applications. In addition, an analysis of solar energy integration in residential housing has been provided in order to explain the optimal methods used in the building design and solar systems sizing.

This study focused on the development a useful dynamic model of a multi-zone house coupled active solar systems using TRNSYS software to evaluate the impact of the integration of energy efficiency measures and active solar energy systems in rural housing built within the framework of the rural housing programs during recent years in Chlef district on its sustainable development. A typical rural house has been chosen as a reference house for the application of the dynamic model.

The developed model is calibrated with measured data. A series of experimental measurements were carried out on the building prototype located in Souidania (20 km southwest of Algiers). Very high prediction accuracy was achieved.

The results for the reference house indicates that the annual heating and cooling needs and electrical consumption of the reference house are very higher. Based on the validated thermal model, dynamic analysis were performed to determine the optimum house design and solar systems sizes. Thus, the energy performance of the reference house was improved. In one hand, the integration energy efficiency measures using passive method allowed a reduction of 63.5% of energy needs with a minimum of comfort for the reference house. In this case, as the space cooling need was reduced of 89%, the use of air conditioning in summer is not necessary and in wintertime; the space heating needs is reduced by 57.23%. In the other hand, through an active manner, a solar heating system with a 6-m² flat-plate collector and 300 litter, storage tank that provides hot water requirements for both DHW and space heating of a single-family house is appropriate for this application. Therefore, an annual solar fraction of 72% can be achieved. The use of grid-connected PV system allowed the production of electrical energy to feed appliances, lighting and the remaining energy for DHW preparation and space heating. Thus, with an important solar potential, which the region holds, the electricity production from solar PV, can contribute up to 72% of the annual electricity consumption.

The results at the level of the district show that rural electrification of houses using active solar systems and improving energy efficiency can generate significant energy savings at the level of the energy balance of the region. We can note that if the energy performance of all 23700 rural houses, carried out during various construction programs were improved, more than 131.34 GWh and 1480257 cylinders of butane gas can be saved annually. In addition, the annual CO₂ reduction associated to these energy savings was estimated at 71540 tons for butane gas and at 85374 tons for electricity.

The results from the economic analysis show that the investment in EEM and solar energy systems in combination may be paid back in 24 years.

The use of solar energy in the residential sector is no longer a choice, but a matter of urgency to ensure climate stability. In fact, the overall energy savings achieved make the residential sector in the Chlef district more energy efficient. On one hand, to reduce the problems of electricity cuts, which are frequent in the region in summer due to the use of air conditioners for cooling, and on the other hand, limiting the shortage of butane gas, which is highly consumed in winter to cope with the cold.

In this research, we believe that we have contributed to the achievement of an original work that can be utilized as a reference guide for decision-makers and related engineering designers and architects with inspiration for the use of solar energy systems in the residential sector, especially the construction of high-energy performance houses in rural areas where the conditions are very adequate.

Bibliography



-
- [1] Amine Boudghene Stambouli, Promotion of renewable energies in Algeria: Strategies and perspectives. *Renewable and Sustainable Energy Reviews* 15 (2011) 1169 – 1181.
 - [2] M. El Fadel et al. Emissions reduction and economic implications of renewable energy market penetration of power generation for residential consumption in the MENA region. *Energy policy* 52 (2013) 618-627.
 - [3] World Commission on Environment and Development (WCED). *Our common future*. Oxford: Oxford University Press, 1987 p. 43.
 - [4] Lon HAZYUK. *Dynamical optimization of renewable energies energy flux in buildings*. Lyon, France 2011.
 - [5] MEM, Ministère de l'énergie et des mines. Agence Nationale pour la Promotion et Rationalisation de l'Utilisation de l'énergie (APRUE). *Consommation Énergétique Finale de l'Algérie, 2009*. WWW.aprue.org.dz
 - [6] Rapport Technique, 'Document Technique Règlementaire, "Règlement Thermique des Bâtiments d'Habitation - Règles de Calcul des Déperditions Calorifiques", DTR C3-2', Fascicule 1, CNERIB, Alger, 1998.
 - [7] Rapport Technique, 'Document Technique Règlementaire, "Règlement Thermique des Bâtiments d'Habitation - Règles de Calcul des Apports Calorifiques des Bâtiments", DTR C3-4', Fascicule 2, CNERIB, Alger, 1998.
 - [8] Rapport Technique, 'Document Technique Règlementaire, "Règlement Thermique des Bâtiments d'Habitation - Ventilation naturelle des locaux à usage d'habitation', DTR.C 3-31', fascicule 3, CNERIB, Alger, 1998.
 - [9] MEM, Ministère de l'énergie et des mines. Agence Nationale pour la Promotion et Rationalisation de l'Utilisation de l'énergie (APRUE). *Bulletin trimestriel de l'APRUE n°10*. Algérie 2006. WWW.aprue.org.dz
 - [10] MEM, Ministère de l'Énergie et des Mines. *Programme des Énergies Renouvelables et de l'Efficacité Énergétique*. Algérie, 2011.
-

-
- [11] JORADP, Journal officiel de la République Algérienne Démocratique et Populaire. Loi n°04-09 du 27 Jomada Ethania 1425 correspondant au 14 août 2004 relative à la promotion des énergies renouvelables dans le cadre du développement durable. <http://www.joradp.dz>
- [12] Y. Himri et al. Review and use of the Algerian renewable energy for sustainable development. *Renewable and Sustainable Energy Reviews* 13 (2009) 1584–1591.
- [13] MED-ENEC- Energy Efficiency in the Construction Sector, Project for energy efficiency in the building sector, FEATURE STORY No12-2008. <http://www.med-enec.com/>
- [14] L. Chesné, T. Duforestel, J.J. Roux, G. Rusaouën. Energy saving and environmental resources potentials: toward new methods of building design. *Building and Environment*, 58 (2012), pp.199–207.
- [15] Y. Jinghua, Y. Changzhi, T. Liwei, Low-energy envelope design of residential building in hot summer and cold winter zone in China. *Energy and Buildings* 40 (2008) 1536–1546.
- [16] O.T. Masoso, L.J. Grobler. A new and innovative look at anti-insulation behaviour in building energy consumption. *Energy and Buildings*, 40 (2008), pp. 1889–1894.
- [17] G.K. Oral, Z. Yilmaz. The limit U values for building envelope related to building form in temperate and cold climatic zones. *Building and Environment*, 37 (2002), pp. 1173–1180.
- [18] S. Lollini, S. Barozzi, S. Fasano, S. Meroni, S. Zinzi. Optimisation of opaque components of the building envelope. *Energy, economic and environmental issues. Building and Environment*, 41 (2006), pp. 1001–1013.
- [19] Morrissey J, Moore T, Horne RE. Affordable passive solar design in a temperate climate:
- [20] An experiment in residential building orientation. *Renewable Energy* 2011;36:568–77.
Tzempelikos A, Athienitis AK. The impact of shading design and control on building cooling and lighting demand. *Solar Energy* 2007;81:369–82.
-

-
- [21] V.Ž. Leskovar, M. Premrov. An approach in architectural design of energy-efficient timber buildings with a focus on the optimal glazing size in the south-oriented façade. *Energy and Buildings*, 43 (2011), pp. 3410–3418
- [22] M.N. Inanici, F.N. Demirbilek. Thermal performance optimization of building aspect ratio and south window size in five cities having different climatic characteristics of Turkey. *Building and Environment*, 35 (2000), pp. 41–52.
- [23] M.-L. Persson, A. Roos, M. Wall. Influence of window size on the energy balance of low energy Houses. *Energy and Buildings*, 38 (2006), pp. 181–188.
- [24] E. Gratia, A.D. Herde. Design of low energy office buildings. *Energy and Buildings*, 35 (2003), pp. 473–491.
- [25] N. Eskin, H. Türkmen. Analysis of annual heating and cooling energy requirements for office buildings in different climates in Turkey. *Energy and Buildings*, 40 (2008), pp. 763–773.
- [26] X. Gong, Y. Akashi, D. Sumiyoshi. Optimization of passive design measures for residential buildings in different Chinese areas. *Building and Environment*, 58 (2012), pp. 46–57.
- [27] H. Nathan, et al., Dynamic modeling of potentially conflicting energy reduction strategies for residential structures in semi-arid climates, *Journal of Environmental Management* 97 (2012) 148–153.
- [28] G. Danielle, et al., Optimization of energy efficiency and thermal comfort measures for residential buildings in Salamanca, Mexico, *Energy and Buildings* 54(2012) 540–549.
- [29] C.K. Cheung, R.J. Fuller, M.B. Luther. Energy-efficient envelope design for high-rise apartments. *Energy and Buildings*, 37 (2005), pp. 37–48.
- [30] S. Porritt, L. Shao, P. Cropper, C. Goodier. Adapting dwellings for heat waves. *Sustainable Cities and Society*, 1 (2011), pp. 81–90.
- [31] G.A. Florides, S.A. Tassou, S.A. Kalogirou, L.C. Wrobel. Measures used to lower building energy consumption and their cost effectiveness. *Applied Energy*, 73 (2002),
-

- pp. 299–328.
- [32] S. Jaber, S. Ajib. Thermal and economic windows design for different climate zones. *Energy and Buildings*, 43 (2011), pp. 3208–3215.
- [33] S.M. Bambrook, A.B. Sproul, D. Jacob. Design optimisation for a low energy home in Sydney. *Energy and Buildings*, 43 (2011), pp. 1702–1711.
- [34] V. Badescu. Case study for active solar space heating and domestic hot water preparation in a passive house. *JOURNAL OF RENEWABLE ENERGY AND SUSTAINABLE ENERGY* 3, 023102(2011). <http://dx.do.org/10.1063/1.3558868>
- [35] Mitchell Leckner and Radu Zmeureanu. Life cycle cost and energy analysis of a Net Zero Energy House with solar combisystem. *Applied Energy* 88 (2011) 232–241. <http://dx.doi:10.1016/j.apenergy.2010.07.031>
- [36] J- N-C. Hin and R. Zmeureanu. Optimization of a residential solar combisystem for minimum life cycle cost, energy use and exergy destroyed. *Solar Energy* 100 (2014) 102–113. <http://dx.doi.org/10.1016/j.solener.2013.12.001>
- [37] A. Hugo et al. Solar combisystem with seasonal thermal storage. *Journal of building Performance Simulation*. Vol. 3, No. 4, December 2010, 255-268. <http://dx.org.doi:10.1080/19401491003653603>
- [38] S. Rasoul Asaee et al. Preliminary study for solar combisystem potential in Canadian houses. *Applied Energy* 130 (2014) 510–518. <http://dx.doi.org/10.1016/j.apenergy.2013.12.048>
- [39] G. Fraisse et al. Energy performance of water hybrid PV/T collectors applied to combisystems of Direct Solar Floor type. *Solar Energy* 81 (2007) 1426–1438. <http://dx.doi.org/10.1016/j.solener.2006.11.017>
- [40] S. Thiers and B. Peuportier. Energy and environmental assessment of two high energy performance residential buildings. *Building and environment* 51(2012)276-284. <http://dx.org.doi:10.1016/j.buildenv.2011.11.018>
- [41] Danny S. Parker. Very low energy homes in the United States: Perspectives on
-

- performance from measured data. *Energy and building* 41(2009)512-520.
- [42] G. Verbeeck, H. Hens. Energy savings in retrofitted dwellings: economically viable? *Energy and Buildings*, 37 (2005), pp. 747–754.
- [43] L. Wang et al. Case study of zero energy house design in UK. *Energy and building* 41 (2009) 1215-1222. <http://dx.org.doi:10.1016/j.enbuild.2009.07.001>
- [44] A. Boudghene Stambouli, et al. Review on the renewable energy development in Algeria: Current perspective, energy scenario and sustainability issues. *Renewable and Sustainable Energy Reviews* 16(2012) 4445-4460.
- [45] BP Statistical Review of World Energy. June 2013. www.bp.com/statisticalreview.
- [46] Ministère de l'Énergie et des Mines. Agence Nationale pour la Promotion et la Rationalisation de l'Utilisation de l'Énergie. Consommation Énergétique Finale de l'Algérie. Chiffres clés Année 2012.
- [47] Hattabi S. Algeria in pole position. Published in *Energy and Mines sector*. Periodic review of the Energy and Mines sector no. 2; April 2004. p. 105. Link: http://www.memalgeria.org:80/larevue/the_mag/energie_2-eng.pdf.
- [48] Askri H, Belmecheri B, Boudjema A, Boumendjel K, Daoudi M, Drid M, et al. Geology of Algeria. Internal report Schlumberger-WEC, Sonatrach; 1991. 93 pp.
- [49] Mustafa Omer A. Renewable energy resources for electricity generation in Sudan. *Renewable and Sustainable Energy Reviews* 2007;11:1481–97.
- [50] Hasting, Robert et Wall, Maria (Eds). (2007). Vol. 2 Exemplary Buildings and Technologies of Sustainable Solar Housing. London: Earthscan, 257 p.
- [51] Shirley Gagnon. ENERGIE SOLAIRE ET ARCHITECTURE. Université Laval Québec, 2012.
- [52] Passive Solar Energy in Buildings. Watt Committee Report Number 17. Published on behalf of THE WATT COMMITTEE ON ENERGY by ELSEVIER APPLIED SCIENCE PUBLISHERS LONDON and NEW YORK.
- [53] Rosemary Rawlings. Capturing solar energy. The Chartered Institution of Building
-

-
- Services Engineers London October 2009. CIBSE Knowledge Series: KS15.
- [54] Passive Solar Design for the Home. U.S. Department of Energy (DOE), Energy Efficiency and Renewable Energy Clearinghouse (EREC), February 200.
- [55] Mingfang T. Solar control for buildings. *Building and Environment* 2002;37:659–64.
- [56] R. Pacheco et al. Energy efficient design of building: A review. *Renewable and Sustainable Energy Reviews* 16 (2012) 3559– 3573.
- [57] Gratia, Elisabeth, *Concevoir avec le climat : la maison individuelle*, Architecture et Climat et MRW, (édition 2002).
- [58] Adeline Guerriat. *Maisons passives*. L'Inédite, Paris, 2008.
- [59] Suresh B. Sadineni et al, Passive building energy savings: A review of building envelope components. *Renewable and Sustainable Energy Reviews* 15 (2011) 3617–3631.
- [60] Jinghua Yu et al. Low-energy envelope design of residential building in hot summer and cold winter zone in China. *Energy and Buildings* 40 (2008) 1536–1546.
- [61] *Passive Solar Design Strategies: Guidelines for Home Building*. U.S. Department of Energy.
- [62] CIBSE Guide F. *Energy efficiency in buildings*. Second edition January 2004. The Chartered Institution of Building Services Engineers London.
- [63] Alexandre Hugo et al. Solar combisystem with seasonal thermal storage. *Journal of Building Performance Simulation*. Vol. 3, No. 4, December 2010, 255–268.
- [64] Antoine Leconte. *Identification de caracteristiques reduites pour l'evaluation des performances des systemes solaires combines*. Architecture, space management. Universite de Grenoble, 2011. French. <NNT : 2011GRENA016>. <tel-00661209>.
- [65] Andersen, E., et al. 2008. Investigation on stratification devices for hot water heat stores. *International Journal of Energy Research*, 32, 255–263.
- [66] Master of Science Thesis. Athinodoros Tzoulis. Performance assessment of building energy modelling programs and control optimization of thermally activated building
-

- systems. Faculty of Civil Engineering & Geosciences (CiTG) • Delft University of Technology, April 15, 2014.
- [67] YANN RIFFONNEAU, Gestion des flux énergétiques dans un système photovoltaïque avec stockage connecté au réseau, Université Joseph Fourier 2009.
- [68] YUDI NUGRAHA BAHAR, Representation of Thermal Building Simulation in Virtual Reality for Sustainable Building, 15 Avril 2014, Bourgogne University.
- [69] Marshall L. et al. Numerical simulation of underground Seasonal Solar Thermal Energy Storage (SSTES) for a single family dwelling using TRNSYS. *Solar Energy* 86 (2012) 289–300.
- [70] Fei Cao et al. Design and simulation of the solar chimney power plants with TRNSYS. *Solar Energy* 98 (2013) 23–33.
- [71] P. Almeida et al. Dynamic testing of systems – Use of TRNSYS as an approach for parameter identification. *Solar Energy* 104 (2014) 60–70.
- [72] R. Chargui and, H. Sammouda. Modeling of a residential house coupled with a dual source heat pump using TRNSYS software. *Energy Conversion and Management* 81 (2014) 384–399.
- [73] Ming Liu et al. Computer simulation with TRNSYS for a mobile refrigeration system incorporating a phase change thermal storage unit. *Applied Energy* 132 (2014) 226–235.
- [74] E. Massaguer et al. Development and validation of a new TRNSYS type for the simulation of thermoelectric generators. *Applied Energy* 134 (2014) 65–74.
- [75] Reindl, D. T., Beckman, W. A., Duffie, J. A., "Diffuse Fraction Correlations", *Solar Energy*, Vol. 45, No. 1, 1990, pp. 1-7.
- [76] TRNSYS, User's Manual. A Transient System Simulation Program. Version 16, Solar Energy Laboratory, University of Wisconsin-Madison, Madison, WI, 2006.
- [77] Stephenson, D.G. and Mitalas, G.P., "Calculation of Heat Conduction Transfer Functions for Multi-Layer Slabs," ASHRAE Annual Meeting, Washington, D.C., August
-

- 22-25, 1971.
- [78] Mitalas, G.P. and Arseneault, J.G., "FORTRAN IV Program to Calculate z-Transfer Functions for the Calculation of Transient Heat Transfer Through Walls and Roofs", Division of National Research Council of Canada, Ottawa.
- [79] J-ERVIN SEEM, Modeling of heat transfer in Buildings. University of Wisconsin-Madison, 1987.
- [80] Koschenz, M. and Lehmann, B. (2000). Thermoaktive Bauteilsysteme tabs. EMPA Dübendorf, Eidgenössische Materialprüfungs- und Forschungsanstalt, Zentrum für Energie und Nachhaltigkeit ZEN.
- [81] Glück B., Strahlungsheizung – Theorie und Praxis, Verlag C. F. Müller, Karlsruhe 1982
Soteris A. Kalogirou. Solar Energy Engineering, 1st Edition from ISBN-9780080922874, Ebook , 2009.
- [82] MJ Brandemuehl, WA Beckman; Transmission of diffuse radiation through CPC and flat-plate collector glazings. Solar Energy, 24 (1980), pp. 511–513.
- [83] Beckman, S.A. Klein, J.A. Duffie. Solar Heating Design. John Wiley et Sons, New York.
- [84] Duffie, J.A., Beckman, W.A., 2006. Solar Engineering of Thermal Process. John Wiley & Sons, Hoboken.
- [85] Klein S.A., 1975. Calculation of flat-plate collector loss coefficients. Solar Energy, 17 (1). Pp. 79-80.
- [86] TRNSYS 16 a TRAnsient SYstem Simulation program. Volume 5. Mathematical Reference. Solar Energy Laboratory, Univ. of Wisconsin-Madison, 2006.
- [87] J.A. Duffie, W. Beckman, Solar Energy Thermal Processes, Wiley, New York, 1974.
- [88] Farrington, R.B., Bingham, C.E., 1986. Analysis of Immersed Heat Exchangers. Solar Energy Research Institute, Golden, CO.
- [89] J. Cadafalch et al., Modelling of storage tanks with immersed heat exchangers, Solar Energy 112 (2015) 154–162.
- [90] Zhe Li, F.Boyle, A. Reynolds. Domestic application of solar PV systems in Ireland: The
-

-
- reality of the their economic viability. *Energy* 36 (2011) 5865-5876.
- [91] Jayanta Deb Mondol et al. Optimising the economic viability of grid-connected photovoltaic systems. *Applied Energy* 86 (2009) 985–999.
- [92] K. Imessad et al. Impact of passive cooling techniques on energy demand for residential Buildings in a Mediterranean climate. *Renewable Energy* 71 (2014) 589-597.
- [93] Shilei Lua et al. Establishment and experimental verification of PCM room's TRNSYS heat transfer model based on latent heat utilization ratio. *Energy and Buildings* 84 (2014) 287–298.
- [94] M.Missoum,,A.Hamidat, L.Loukarfi. Effect of integrating bioclimatic designs in rural housing on energy consumption of Chlef district (north-west of Algeria). 3ème Séminaire International sur les Energies Nouvelles et Renouvelables. Unité de Recherche Appliquée en Energies Renouvelables, Octobre 13-14, 2014, Ghardaïa, Algérie.
- [95] M. Missoum, A. Hamidat, L. Loukarfi, K. Abdeladim. Impact of rural housing energy performance improvement on the energy balance in the North-West of Algeria, *Energy and Buildings*, Volume 85, December 2014, Pages 374-388, ISSN 0378-7788.
- [96] C. Tantasavasdi, Natural ventilation design for house in Thailand, *Energy and Buildings* 33 (2001) 815–824.
- [97] M.Missoum, A.Hamidat, L.Loukarfi. Energetic performance analysis of a solar combisystem. Application to a rural house in Chlef Region (Algeria). International Conference on Technologies and Materials for Renewable Energy, Environment and Sustainability, Février 15-17, 2013, Beirut, Liban.
- [98] F. Sahnoune, M. Belhamel, et M. Zelmat. Etude comparative des performances thermiques d'un prototype de chauffe-eau solaire pour deux sites algériens, *Revue des énergies renouvelables*, Vol. 14 N°3 (2011) 481-486
- [99] Alireza Hobbi , Kamran Siddiqui. Optimal design of a forced circulation solar water heating systemfor a residential unit in cold climate using TRNSYS. *Solar Energy* 83
-

- (2009) 700–714.
- [100] Buckles, W.E., Klein, S.A., 1980. Analysis of solar domestic hot water heaters. *Solar Energy* 25 (5), 417–424.
- [101] Klein, S.A., Beckman, W.A., Duffie, J.A., 1976. A design procedure for solar heating systems. *Solar Energy* 18, 113.
- [102] Beckman, W.A., Klein, S.A., Duffie, J.A., 1977. *Solar Heating Design by the F-Chart Method*. John Wiley, New York.
- [103] Baughn, J.W., Young, M.F., 1984. The calculated performance of a solar hot water system for a range of collector flow rates. *Solar Energy* 32 (2), 303–305.
- [104] M.Missoum, A.Hamidat, L.Loukarfi. Energy performance simulations of a grid-connected PV system supplying a residential house in the north-western of Algeria.
- [105] International Conference on Technologies and Materials for Renewable Energy, Environment and Sustainability, Février 15-17, 2013, Beirut, Liban.
- [106] M.Missoum, A.Hamidat, L.Loukarfi. Apports des équipements efficaces dans la Performance d'une habitation suburbaine en Algérie. The international conference on energy environment and sustainable development, Novembre 29-30, 2011 Adrar, Algeria.
- [107] Moatassem Abdallah, Khaled El-Rayes. Optimizing the selection of building upgrade measures to minimize the operational negative environmental impacts of existing buildings. *Building and Environment* 84 (2015) 32-43.
- [108] TranSystems E.H. Pechan. The emissions & generation resource integrated database for 2012 (eGRID2012) technical support document. Springfield, VA:U.S. Environmental Protection Agency; 2012.
http://www.epa.gov/cleanenergy/documents/egridzips/eGRID2012_year09_TechnicalSupportDocument.pdf [accessed 02.03.14]
- [109] Intergovernmental Panel on Climate Change. Fourth assessment report: climate change (AR4). Intergovernmental Panel on Climate Change; 2007.
-

-
- http://www.ipcc.ch/publications_and_data/publications_and_data_reports.shtml#UvBC
[C Ir6-0](#) [accessed 02.03.14].
- [110] Ministère de l'Énergie et des Mines. Bilan énergétique national 2013 (édition 2014).
http://www.memalgeria.org/fr/statistiques/Bilan_Energetique_National_2013_edition_2014.pdf
- [111] Ministère de l'énergie et des mines. Agence National pour la Promotion et la Rationalisation de l'Utilisation de l'Énergie, APRUE. Consommation Énergétique Finale de l'Algérie, Année 2007 (Edition 2009).
OECD/IEA. Statistics on the web; 2014.
<http://www.iea.org/statistics/statisticssearch/report/?country=ALGERIA&product=indicators&year=2011>.
-

Appendix



Appendix A

Appendix A explain the method of star network concept, which is used to estimate the long-wave radiation exchange between the surfaces within the zone and the convective heat flux from the inside surfaces to the zone air.

Fig. (A.1) shows a view factor network for an enclosure with three surfaces. The resistance to long-wave radiation exchange between surfaces is:

$$R_{i-j,rad} = \frac{1}{\epsilon_i A_i G_{i-j} \sigma 4 T^3} \quad (A.1)$$

The absorption factor is the fraction of energy emitted by surface i which is absorbed by surface j.

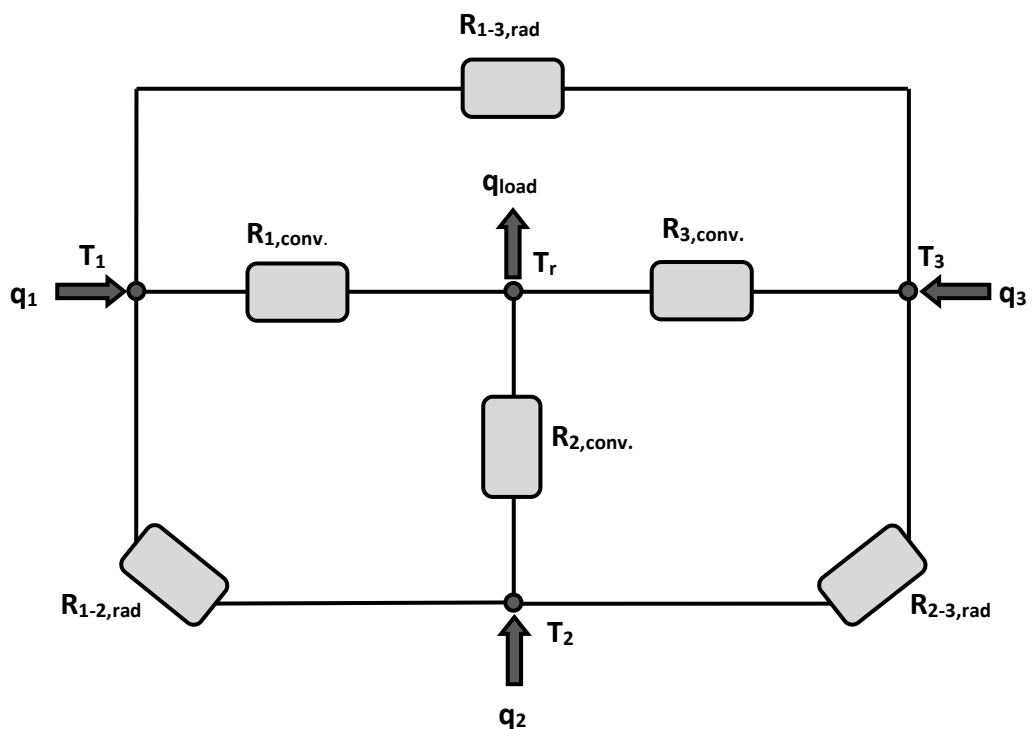


Fig.(A.1). view factor network

Fig. (A.2) shows a star network for an enclosure with three surfaces. An energy balance for every surface in an enclosure with three surfaces is

$$\frac{T_2 - T_1}{R_{2-1,rad}} + \frac{T_3 - T_1}{R_{3-1,rad}} + \frac{T_i - T_1}{R_{1,conv}} + q_1 = 0 \quad (\text{A.2})$$

$$\frac{T_1 - T_2}{R_{1-2,rad}} + \frac{T_3 - T_2}{R_{3-2,rad}} + \frac{T_i - T_2}{R_{2,conv}} + q_2 = 0 \quad (\text{A.3})$$

$$\frac{T_1 - T_3}{R_{1-3,rad}} + \frac{T_2 - T_3}{R_{2-3,rad}} + \frac{T_i - T_3}{R_{3,conv}} + q_3 = 0 \quad (\text{A.4})$$

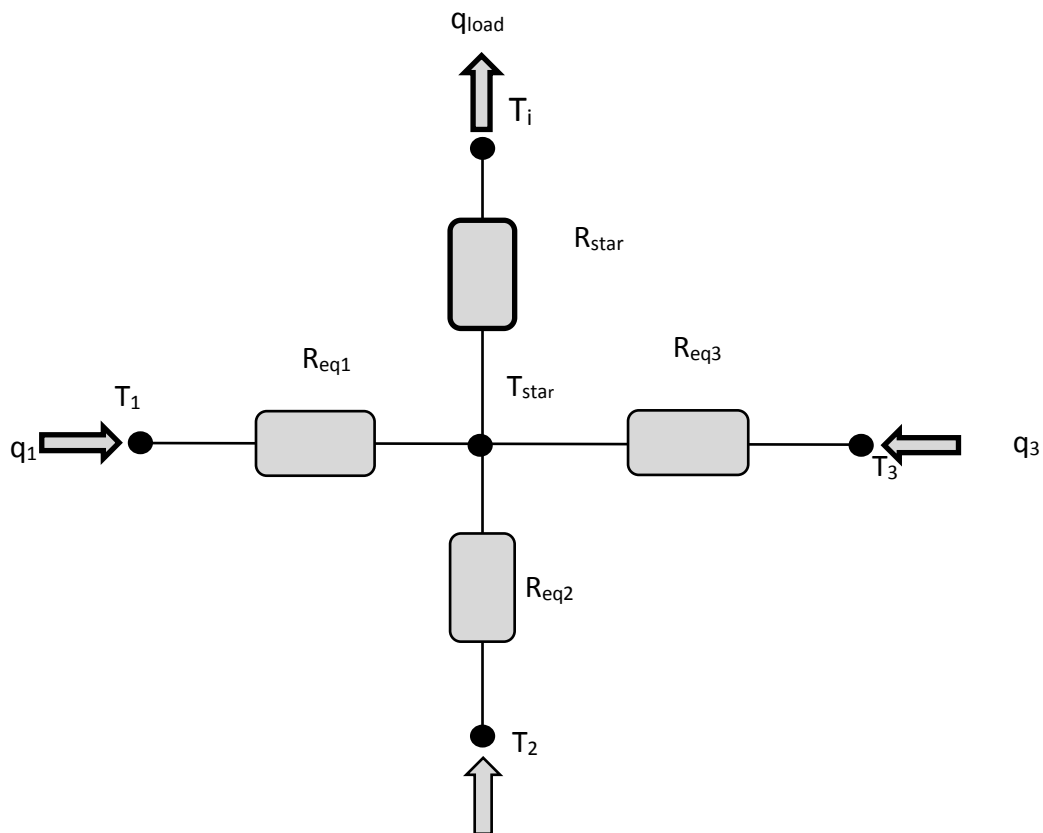


Fig. (A.2). star network for a zone with three surfaces.

Where

$R_{i-j,rad}$ – resistance to long-wave radiation between surfaces i and j .

$R_{i,conv}$ – resistance to convective heat transfer between surface i and room air.

q_i – energy input to surface i other than by convection with the room air or long-wave radiation exchange with other surfaces in the room.

An energy balance for the air in the room is

$$\frac{T_1 - T_i}{R_{1,conv}} + \frac{T_2 - T_i}{R_{2,conv}} + \frac{T_3 - T_i}{R_{3,conv}} = q_{load} \quad (\text{A.5})$$

Where

q_{load} – heating or cooling load.

The energy balances for every surface in the room and the energy balance on the room air can be combined into the matrix equations

$$XY = Z \quad (\text{A.6})$$

For three surface, **Eq. (A.5)** become

$$\begin{bmatrix} X_{11} & X_{12} & X_{13} & X_{14} \\ X_{21} & X_{22} & X_{23} & X_{24} \\ X_{31} & X_{32} & X_{33} & X_{34} \\ X_{41} & X_{42} & X_{43} & X_{44} \end{bmatrix} \begin{bmatrix} Y_1 \\ Y_2 \\ Y_3 \\ Y_4 \end{bmatrix} = \begin{bmatrix} Z_1 \\ Z_2 \\ Z_3 \\ Z_4 \end{bmatrix} \quad (\text{A.7})$$

Where

$$X_{11} = -\frac{1}{R_{1-2,rad}} - \frac{1}{R_{1-3,rad}} - \frac{1}{R_{1,conv}}$$

$$X_{22} = -\frac{1}{R_{1-2,rad}} - \frac{1}{R_{2-3,rad}} - \frac{1}{R_{2,conv}}$$

$$X_{33} = -\frac{1}{R_{1-3,rad}} - \frac{1}{R_{2-3,rad}} - \frac{1}{R_{3,conv}}$$

$$X_{12} = X_{21} = \frac{1}{R_{1-2,rad}}$$

$$X_{13} = X_{31} = \frac{1}{R_{1-3,rad}}$$

$$X_{23} = X_{32} = \frac{1}{R_{2-3,rad}}$$

$$X_{14} = X_{24} = X_{34} = 0$$

$$X_{41} = \frac{1}{R_{1,conv}}$$

$$X_{42} = \frac{1}{R_{2,conv}}$$

$$X_{43} = \frac{1}{R_{3,conv}}$$

$$X_{44} = -1$$

$$Y_1 = T_1 - T_i, Y_2 = T_2 - T_i, Y_3 = T_3 - T_i, Y_4 = q_{load}$$

$$Z_1 = -q_1, Z_2 = -q_2, Z_3 = -q_3, Z_4 = 0$$

Next, the inverse of X matrix is computed.

$$X^{-1} = \begin{bmatrix} X_{11,inv} & X_{12,inv} & X_{13,inv} & X_{14,inv} \\ X_{21,inv} & X_{22,inv} & X_{23,inv} & X_{24,inv} \\ X_{31,inv} & X_{32,inv} & X_{33,inv} & X_{34,inv} \\ X_{41,inv} & X_{42,inv} & X_{43,inv} & X_{44,inv} \end{bmatrix} \quad (A.8)$$

A floating node is defined as one in which heat transfer occurs only by convection to the air or by long-wave radiation exchange with other surfaces in the enclosure. As a result, conduction through building elements, solar radiation gains, and radiation

gains from people, equipment, and lights do not affect floating surface nodes, and infiltration or convection gains from people, equipment and lights do not affect the floating room air node. Thus, the resistance between surfaces when other nodes are floating can be computed as follow:

$$R_{1-2} = X_{12,inv} + X_{21,inv} - X_{11,inv} - X_{22,inv} \quad (A.9)$$

$$R_{1-3} = X_{13,inv} + X_{31,inv} - X_{11,inv} - X_{33,inv} \quad (A.10)$$

$$R_{2-3} = X_{23,inv} + X_{32,inv} - X_{22,inv} - X_{33,inv} \quad (A.11)$$

The resistances between the surfaces and the air node when other surface nodes are floating can be computed as follow:

$$R_{1-i} = -X_{11,inv} \quad (A.12)$$

$$R_{2-i} = -X_{22,inv} \quad (A.13)$$

$$R_{3-i} = -X_{33,inv} \quad (A.14)$$

The resistance between the star node and the air node is computed as follow:

$$R_{star} = \frac{\frac{R_{1-i}}{R_{1-2}^3} + \frac{R_{2-i}}{R_{1-3}^3} + \frac{R_{1-2}}{R_{2-3}^3}}{2 \left(\frac{1}{R_{1-2}^3} + \frac{1}{R_{1-3}^3} + \frac{1}{R_{2-3}^3} \right)} \quad (A.15)$$

The resistance between the surfaces and the star node can be computed as follow.

$$R_{eq1} = R_{1-i} - R_{star} \quad (A.16)$$

$$R_{eq2} = R_{2-i} - R_{star} \quad (A.17)$$

$$R_{eq3} = R_{3-i} - R_{star} \quad (A.18)$$

Appendix B

B.1. Energy production

Algeria has an important potential from the point of view of proved natural gas and oil reserves, 12.2 thousand million barrels of oil and 4.5 trillion cubic meters of natural gas at the end of 2012. In this year, Algeria produced approximately 1.667 million barrels per day of crude oil, of and 81.5 billion cubic meters of natural gas [109].

Algeria is one of the leading producer and exporter of oil and natural gas in the world. It is the fourth largest oil crude producer in Africa, and the sixth largest natural gas producer in the world.

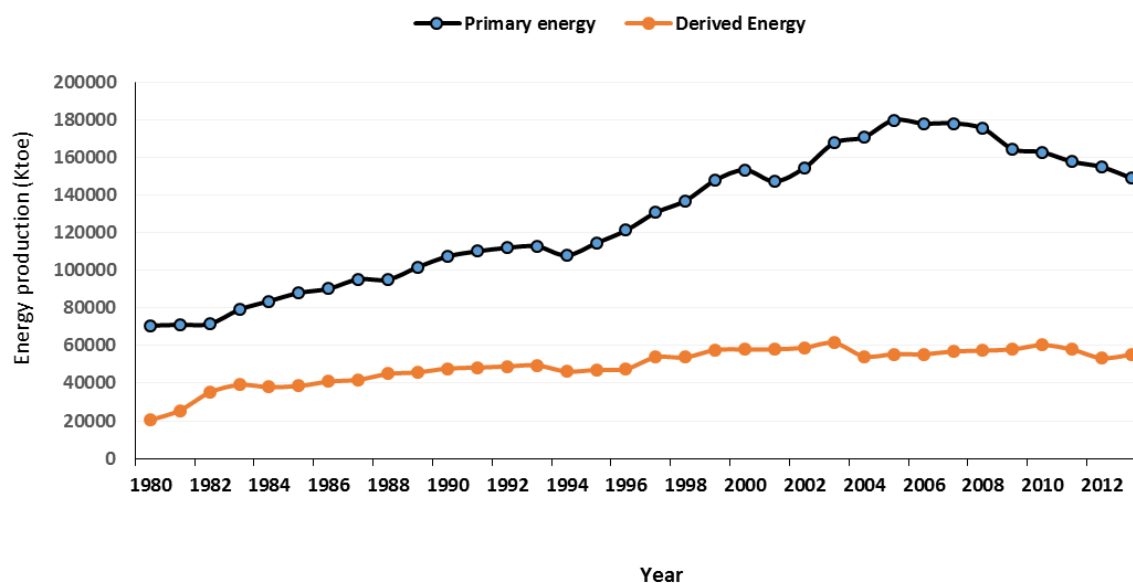


Fig.B.1. Evolution of energy production in Algeria between 1980 and 2013 (MEM source).

Fig.B.1 shows the evolution of primary and derived energy production between 1980 and 2013 in Algeria. It can be seen that the production of primary energy increased

substantially between 1980 and 2007. From 2007 to 2013, an important reduction in primary energy production is recorded (30864 Ktoe). According to MEM, this reduction due to the reduction of hydrocarbon production.

In 2010, by the implementation of the first 25MW solar power project at Hassi R'mel (150MW in total, CSP/natural gas), the production of primary electricity has increased sharply. This production of solar electricity was 124 GWh.

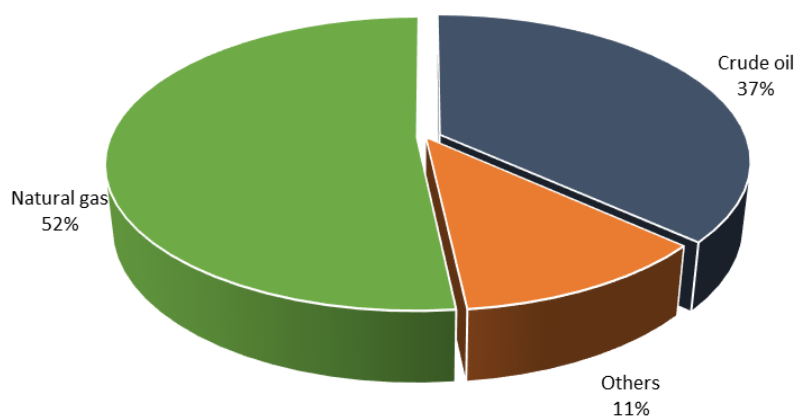


Fig.2.8 Distribution of primary energy production in 2013 (MEM source).

The production of derived energy increased between 1980 to 2010. From this year, the production of this energy begin to reduce. A reduction of 6909 Ktoe is recorded between 2010 and 2012 due to the reduction of the petroleum products and LNG production. The decrease of production of petroleum products can be explained by the reduction of treated petroleum volume, due to stopping induced by rehabilitation works of the refineries. Whilst, the fall of LNG production is due to the economic crisis in Europe.

Fig.B.2 shows the distribution of primary energy production in 2013 and **Fig.B.3** shows the distribution of derived energy production. Natural gas dominates the

production of primary energy (77058 Ktoe), which represents 52% of the total production. The production of crude oil is 54680 Ktoe (37%). Whilst, derived energy production is dominated by the petroleum products, 24515 Ktoe (44%). The production of LNG and electricity are 4660 Ktoe (26%) and 15012 Ktoe (27%), respectively.

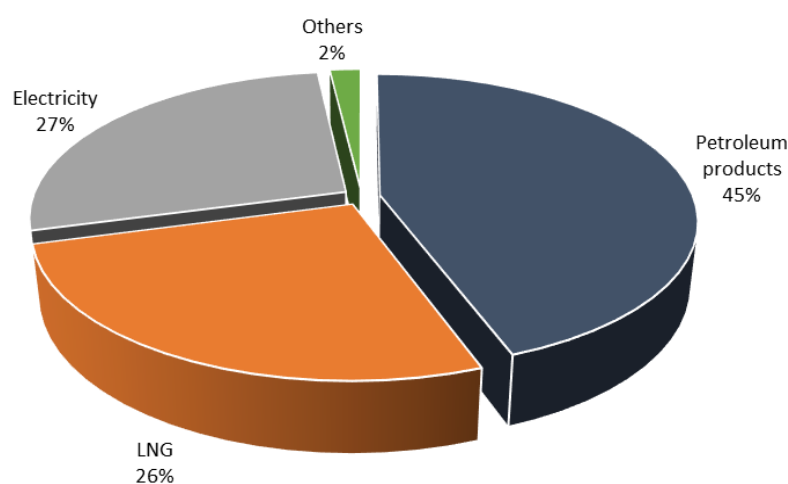


Fig.B.3. Distribution of derived energy production in 2013 (MEM source).

B.2. Greenhouse gas emissions

The main cause of CO₂ emissions in Algeria is fuel combustion. As shown in **Fig.B.4**, those emissions were just 52.73 Mt of CO₂ in 1990 and reached 114.35 Mt of CO₂ by 2012. Therefore, the CO₂ emissions are increasing continuously.

The GHG emissions due to the final energy consumption in 2012 are 90 MT CO₂, 2.357 TCO₂ per capita. The total GHG emissions from primary energy consumption are 152.6 MT of CO₂ [110]. These later are due mainly to petroleum products (60%) and gaseous products (40%).

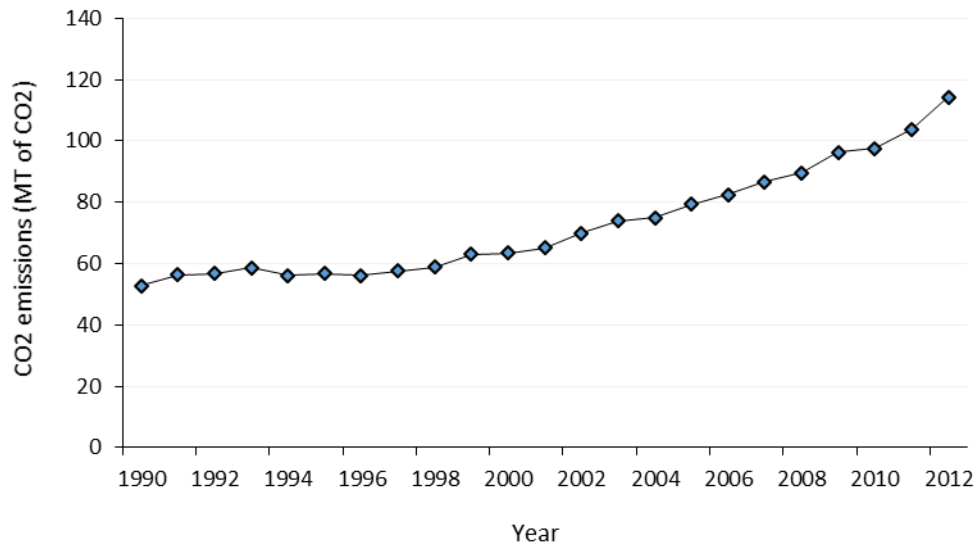


Fig.B.5. CO2 emissions from fuel combustion in Algeria. Source: data collected from Ref. [111].

As shown in **Fig.B.5**, the transport sector is the highest producer GHG (49%) followed by residential sector by 31% and industrial sector (12%) and agriculture sector (7%). It can be noticed that the residential sector has the most important potential for GHG mitigation.

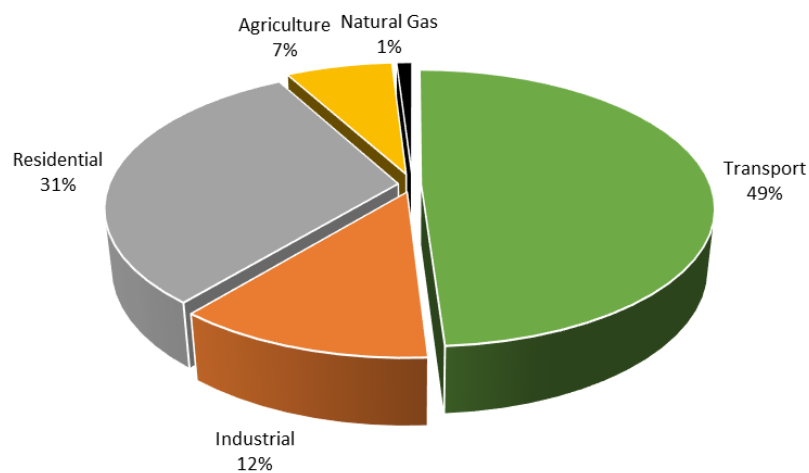


Fig.B.5. CO2 emissions from primary energy consumption by sectors

